# Development of Model Diblock Copolymer Surfactants for Mechanistic Investigations of Cell Membrane Stabilization

A DISSERTATION
SUBMITTED TO THE FACULTY OF
UNIVERSITY OF MINNESOTA
BY

Karen J. Haman

IN PARTIAL FULFILLMENT OF THE REQUIREMENTS
FOR THE DEGREE OF
DOCTOR OF PHILOSOPHY

Advisor: Frank S. Bates

August 2015

# Acknowledgments

As anyone who has known me throughout graduate school can attest, this work and my completion of it was in every respect a collaborative endeavor. It is impossible to name here every contributor to my progress, but I would like to thank a handful of key players by name and the rest by respective category. Even then, I fear I may be missing some. Like so many before me, I must resort to the common practice of struggling to find the words to express the depth and breadth of my gratitude. I offer here my humble, yet sincere thanks to those who have helped me along the way, especially in the last six years.

To my dad, Bill: you and I both know this degree happened as a direct result of your faithful support over the phone, in writing, and in person, not to mention your stubborn insistence that it could, in fact, be accomplished. Yours was the reassuring voice I heard on the darkest days, and yours also was the biggest smile in the arena at graduation. I am proud to be your daughter and proud to follow in your professional footsteps.

To my sister, confidante, best friend, and co-conspirator Patty: "well we've been together since I can't remember, we've been together all our lives." Few people get to experience the closeness that is having a twin, and those who do understand why it is so difficult to pin down exactly what I want to thank you for. You understand best of all what this degree has meant to the whole of me, and you were there all along, despite the miles between us. Thank you for cheering me on, delivering me well-timed swift kicks when I needed them, and enduring my endless sputtering about failed experiments with grace and dignity. I am grateful to God for you, for the gift you are and the gift it is to be known fully.

To my mom, Janet: thank you for your patient support throughout my Ph.D., especially when it came to listening. Your love for nature, nonfiction, and your willingness to try a

little kitchen chemistry (curds and whey) from the Mr. Wizard book are just a few of the ways you encouraged my budding interest in science as a child. I am beyond grateful for the sacrifices you made to ensure that Patty and I had every opportunity.

To Amy, Grandma Mary, and my aunts, uncles, and cousins: it has been so rewarding to receive your enthusiasm throughout this process. Thank you all for keeping up with me and with my degree progress – in that order. I am struck by the wisdom my Grandma Mary could offer that hit the mark time after time, and her hugs and care packages reminded me of her love continually. I am also thankful for the love and support my maternal grandparents gave me before they passed away. My Grandma Pat, the most naturally curious person I have ever known, inspired in me a love of writing by her encouragement that resonates with me even now, and I know Paka would be proud and overjoyed at the prospect of me heading to his beloved Iowa State.

It was still quite early in my graduate career when Trinity City Church launched in St. Paul, MN, and the friendships and relationships I have developed there have been instrumental to both my personal and professional growth. I will take what I have learned there about stewardship and how the gospel plays out in work with me, and TCC will always be "home" to me. I am grateful to Pastors Bryan Lair and Nick Wiesneski especially, for their leadership and faithful service to Jesus, to the glory of His name.

I would like to thank Chris and Kathleen Macosko, for their emotional and professional support over the last four years, not to mention the ways they have opened their home to dozens of students like myself over the years.

There are a handful of women just ahead of me in life who have poured into me over the last six years. They have freely offered their listening ears, thoughtful advice, and empathetic encouragement regarding all aspects of life, graduate school included. My heartfelt thanks go out to Rosanne Wood, Stef Wiesneski, Kelaine Haas, Sara Wright, Miranda Curzon, and Katie Vellabati. Each of you had an essential role in ushering me to this point, and I come away from Minneapolis much better for having known you.

I have countless colleagues to thank, who in their own ways have helped me stake out a path through the murk and mire of research. To the current and former members of the polymer group, the Bates group, and the now defunct Polymer Exiles office, thanks for

helping in thoughtful discussions, trainings, and camaraderie throughout the years. I am also indebted to members of the Zasadzinski and Kokkoli groups, support staff in CEMS, Chemistry, IBP, and the CharFac for a great deal of technical support and instrument access. Thanks to Michael Heinzer, whose no holds barred approach to synthesis gave me the courage to attempt synthesizing PPO. Thanks especially to a particular group of graduate students (Tessie Panthani, Jill Schmidt, Chris Thurber, and Yogesh Dhande), I learned the release of distance running, and these friends spent the better part of the last six years running the figurative race and numerous literal races with me. It was an honor and a delight, friends.

Importantly, I offer my sincere thanks to the collaborative research team which, much to my delight, has grown to include more members over the years. I gratefully acknowledge Evelyne Houang, who was there at the beginning, and who has turned into an invaluable cross-disciplinary colleague and friend. Without her enthusiasm and diligent *in vivo* and *in vitro* work, the polymers I synthesized would be no more interesting than any other surfactants. I will fondly remember our lengthy discussions over Lillihei coffee, and I wish her the best in her future career. Thanks also to collaborative PIs Joe Metzger and Demetris Yannopoulous, not only for helping to support my graduate work, but for thoughtful discussion and feedback at our group meetings.

Finally, I would like to thank my committee for their service and for the feedback they have provided. Thanks especially go to my adviser, Frank Bates, for his contributions to this work. Frank's exuberant enthusiasm for this peculiar bunch of block copolymers was my initial impression of the project, and its continuation served as a motivator all throughout my Ph.D. Thank you, Frank, for challenging me to find a way through some of the most difficult times, and for your support.

*To my family*

From him and through him and to him are all things. *To him be glory forever*. Amen.
(Romans 11:36 ESV)

# Abstract

Amphiphilic triblock copolymers of poly(ethylene oxide) and poly(propylene oxide), generically referred to as poloxamers, have been identified for therapeutic use in cell membrane stabilization applications since the early 1990s. Historically, mechanistic investigations of block copolymer facilitated membrane stabilization have nearly exclusively featured poloxamers, commercially available in a wide range of molecular weights and hydrophobic/hydrophilic compositions. This work instead considers diblock copolymers of poly(ethylene oxide) and poly(propylene oxide), for which molecular properties can be easily tuned by living anionic polymerization. The diblock architecture simplifies the structure-function understanding of block copolymer interactions with membranes by eliminating a redundant hydrophilic block (A) from the poloxamer A-B-A architecture.

Work presented here indicates that these diblock copolymers are capable of shielding liposome model membranes from harmful free radical-initiated peroxidation at lower loadings than analogous triblock copolymers. Besides the pharmacological advantages of lower required doses, the finding highlights the significance with respect to membrane interaction of differences in the chemical environments of the hydrophobic blocks between the triblock and diblock architectures. From this point, the roles of both hydrophobic block length and end-functionality were explored in liposome and in vitro model stresses, and the dependence of therapeutic benefit on each was established. Future systems to consider are discussed, and additional methods for investigation are detailed.

# Contents

**Acknowledgments** ..... **i**

**Abstract** ..... **v**

**Contents** ..... **vi**

**List of Tables** ..... **x**

**List of Figures** ..... **xi**

**Chapter 1 Introduction** ..... **1**
1.1 Block copolymer definition and structure ..... 1
1.2 Block copolymer self assembly ..... 3
*1.2.1 Assembly in the bulk* ..... *3*
*1.2.2 Assembly in selective solvents: micellization* ..... *3*
1.3 Poloxamers ..... 6
*1.3.1 Industrial origins and chemical make-up* ..... *7*
*1.3.2 Poloxamer micellization behavior* ..... *8*
*1.3.3 Medical uses of poloxamers* ..... *10*
1.4 Physiological background: muscle and membranes ..... 11
*1.4.1 Hierarchical structure of muscle* ..... *11*
*1.4.2 Sarcolemma* ..... *12*
*1.4.3 Duchenne muscular dystrophy pathogenesis and associated cell membrane damage* ..... *12*
*1.4.4 Membrane sealing by Poloxamer 188* ..... *13*
1.5 Biophysical investigations of membrane stabilization ..... 14
*1.5.1 Monolayer model membranes* ..... *14*
*1.5.2 Bilayered model membranes: liposomes* ..... *15*
*1.5.3 Liposome peroxidation as a model stress* ..... *17*
*1.5.4 Block copolymer protection against liposome peroxidation* ..... *17*
*1.5.5 Development of a model polymer system* ..... *19*
1.6 Objectives of this work ..... 22
*1.6.1 Diblock copolymer synthesis* ..... *22*
*1.6.2 Model membranes* ..... *22*
*1.6.3 Model membrane stress* ..... *23*
*1.6.4 Miscellaneous activities and collaborations* ..... *24*

**Chapter 2 Methods and Materials** ..... **25**
2.1 Polymer synthesis ..... 25
*2.1.1 Hydrophobic block synthesis* ..... *28*
*2.1.2 Hydrophilic block addition* ..... *29*
*2.1.3 Statistical copolymers* ..... *31*
*2.1.4 Reverse diblocks: effect of end groups* ..... *31*
2.2 Polymer characterization ..... 34

*2.2.1 Tert-butyl functional homopolymer and diblock copolymers* ..... *38*
*2.2.2 Statistical copolymers* ..... *40*
*2.2.3 Hydroxyl-terminated PPO diblock copolymers* ..... *40*
2.3 Liposome model membranes ..... 42
*2.3.1 Liposome preparation* ..... *42*
*2.3.2 Liposome peroxidation* ..... *42*
2.4 Dynamic Light Scattering ..... 43
2.5 Static light scattering ..... 46
2.6 Langmuir trough and lipid monolayers ..... 47

**Chapter 3 Role of block copolymer architecture in model membrane protection against peroxidation ..... 51**
3.1 Diblock architecture and a model system ..... 51
*3.1.1 Mechanism of liposome damage by peroxidation and shortcomings of DLS* ..... *52*
*3.1.2 Scattered intensity as a measure of liposome population* ..... *53*
*3.1.3 Other scattering techniques* ..... *58*
3.2 Experimental design ..... 59
*3.2.1 Polymers considered* ..... *60*
*3.2.2 Phospholipids and liposome preparation* ..... *62*
*3.2.3 Liposome peroxidation.* ..... *62*
*3.2.4 Multi-angle DLS and SLS* ..... *64*
*3.2.5 Small angle X-ray scattering* ..... *64*
3.3 Liposome peroxidation and protection results ..... 65
*3.3.1 Polymer incubation with liposomes* ..... *65*
*3.3.2 Polymer incubation effects on liposome peroxidation* ..... *67*
*3.3.3 Protective effects of molecular weight: incubation on equal PEO basis* ..... *71*
*3.3.4 Multi-angle DLS* ..... *75*
*3.3.5 Static light scattering* ..... *79*
*3.3.6 SAXS on hydrated multilamellae phospholipids with polymers* ..... *80*
3.4 Conclusions and future outlook ..... 83
*3.4.1 Liposome peroxidation assay* ..... *84*
*3.4.2 Differing interaction mechanisms by different architectures* ..... *84*
*3.4.3 Future outlook: connections to in vivo or in vitro work* ..... *84*

**Chapter 4 Effect of diblock copolymer end groups on membrane interactions ..... 86**
4.1 Diblock copolymers prepared ..... 87
4.2 Liposome incubation with diblock copolymers ..... 89
4.3 Liposome peroxidation with diblock copolymers of varying end groups ..... 94
*4.3.1 Peroxidation results for t-butyl functionalized PPO-PEO* ..... *94*
*4.3.2 Peroxidation results for hydroxyl-functionalized PPO-PEO* ..... *95*
*4.3.3 Liposome size following peroxidation* ..... *97*
*4.3.4 Peroxidation dependence on PEO block length* ..... *100*
4.4 Preliminary connections to *in vivo* studies ..... 101
*4.4.1 Methods* ..... *102*
*4.4.2 P188, Diblock P188, and PEO-8k lengthening contraction injury* ..... *104*

*4.4.3 Tert-butoxy- functional diblock copolymers* ..... *106*
*4.4.4 Hydroxyl-functional diblock copolymers* ..... *108*
*4.4.5 Composite evaluation and hypothesized role of block length and end-groups in membrane stabilization* ..... *110*
4.5 Conclusions and future directions ..... 113
*4.5.1 Anchoring by hydrophobic end groups promotes membrane stabilization in vivo* ..... *114*
*4.5.2 Hydrophobic block length determines association with membranes, with end group exception* ..... *115*
*4.5.3 Uses for liposome model membranes beyond in vivo screening* ..... *116*

**Chapter 5 Block copolymer interactions with model membrane monolayers ..... 117**
5.1 Surface activity in surfactant monolayers ..... 117
*5.1.1 Phase behavior of DPPC* ..... *117*
*5.1.2 Surface activity of P188 and Diblock P188* ..... *120*
5.2 Polymer interactions with synthetic phospholipid monolayers ..... 122
*5.2.1 Monolayer adsorption by poloxamers* ..... *122*
*5.2.2 Area controlled isotherm (adsorption and squeeze out)* ..... *123*
*5.2.3 Fluorescence microscopy of lipid and polymer monolayers* ..... *127*
5.3 Naturally derived lipid monolayers ..... 134
*5.3.1 Light SR and heavy SR purification* ..... *134*
*5.3.2 Area-controlled isotherms of SR monolayers* ..... *134*
*5.3.3 Polymer adsorption and squeeze-out from SR monolayers* ..... *135*
*5.3.4 Fluorescence microscopy with SR model membranes* ..... *137*
*5.3.5 Considerations and conclusions from SR model membranes* ..... *141*
5.4 Summary and future work ..... 141
*5.4.1 Synthetic DPPC monolayers* ..... *141*
*5.4.2 Isolated sarcolemma monolayers* ..... *142*
*5.4.3 Future directions* ..... *142*

**Chapter 6 Collaborative support activities ..... 144**
6.1 Fluorescent tagging of Poloxamer 188 for imaging ..... 144
*6.1.1 Fluorescence tagging by 5-DTAF* ..... *145*
*6.1.2 Azide-functional P188 for click reaction with AlexaFluor 647* ..... *149*
*6.1.3 Rhodamine B tagged Poloxamer 188* ..... *156*
6.2 Blood viscosity ..... 160
*6.2.1 Concentration and shear rate dependence of P188 and PEO solution viscosity* ..... *162*
*6.2.2 Polymer effects on post-ischemic blood viscosity* ..... *165*
*6.2.3 Polymer effects on non-ischemic blood viscosity* ..... *167*
*6.2.4 In vivo implications and future directions* ..... *169*

**Chapter 7 Summary and Future Outlook ..... 170**
7.1 Consideration of a diblock architecture ..... 170
*7.1.1 Confirmation of membrane protection by a diblock architecture* ..... *171*
*7.1.2 Future prospects for a diblock architecture* ..... *171*

7.2 Molecular design and chemical synthesis to study membrane interactions ..... 172
*7.2.1 Synthesis of new diblock copolymer membrane stabilizers ..... 172*
*7.2.2 Significance of end-group functionalities on hydrophobic block ..... 173*
*7.2.3 Future synthetic directions ..... 173*
7.3 Adaptation of a model membrane and membrane stress ..... 174
*7.3.1 New interpretation to dynamic light scattering results ..... 174*
*7.3.2 Connections to in vivo work ..... 175*
*7.3.3 Model membrane recommendations ..... 175*
7.4 Monolayered studies ..... 176
*7.4.1 Naturally derived membrane monolayers ..... 176*
*7.4.2 Further monolayered studies ..... 176*
7.5 Collaborative support and final comments ..... 176

**Bibliography ..... 178**

**Appendix A: Liposome peroxidation protocol ..... 200**

# List of Tables

Table 1.1: Reported CMCs for P188 at various temperatures and detection methods. ..... 9
Table 2.1: Homopolymers and diblock copolymers prepared from a tert-butyl initiator in this work..... 39
Table 2.2: Statistical copolymers prepared from propylene oxide (P), butylene oxide (B), and ethylene oxide (E). ..... 40
Table 2.3: Summary of diblock copolymers with hydroxyl-terminated PPO blocks synthesized. ..... 41
Table 3.1: Polymer summary. ..... 61
Table 3.2: Average liposome $R_h$ and dispersities following polymer incubation at times ($t_I$) of 4 and 24 hours. ..... 66
Table 3.3: Summary of liposome distribution characteristics following peroxidation in presence of polymers. ..... 68
Table 3.4: Comparison of $R_h$ derived from linear fitting of multi-angle DLS results and the 90° result. ..... 77
Table 3.5: SLS following liposome incubation for 1 hour with polymers gave $R_g$. ..... 80
Table 3.6: Peak and spacing obtained from SAXS profiles. Integer ratio of $q_2/q_1$ confirms lamellar structure. ..... 82
Table 4.1: Summary of polymers considered in this chapter. ..... 88
Table 4.2: Liposome size and distribution widths for liposomes incubated with diblock copolymers. ..... 93
Table 4.3: Liposome size distribution characteristics following peroxidation reactions.. 99

# List of Figures

Figure 1.1: Schematic representation of possible two-component block copolymers..... 2
Figure 1.2: Representative plot showing how surface tension measurements can be used to determine CMC..... 5
Figure 1.3: Absorption profiles for DPH dye solubilization technique used to determine CMC of poloxamer P334. ..... 5
Figure 1.4: Chemical structure of poloxamers. ..... 7
Figure 1.5: Connectivity of sarcolemma to actin and extracellular matrix of cardiac myocyte. ..... 12
Figure 1.6: DLS particle size distributions reported by Wang, et al.[89] ..... 18
Figure 1.7: Peroxidation of liposomes incubated with Poloxamer 335 (P335), from Wang, et al.[89] ..... 19
Figure 2.1: $^{1}$H NMR spectra obtained for t-poly(propylene oxide) with proton assignments. ..... 35
Figure 2.2: $^{1}$H NMR spectrum for representative poly(1,2-butylene oxide) with proton assignments. ..... 36
Figure 2.3: Diblock copolymer poly(propylene oxide)-poly(ethylene oxide) and accompanying proton assignments. ..... 37
Figure 2.4: Overlays of $^{1}$H NMR spectra for mE5.3 and OH-P1.9-E5.3 show appearance of PPO backbone peaks around 3.5 ppm and methyl protons at $\delta$ = 1.2 ppm. ..... 37
Figure 2.5: SEC traces for parent poly(propylene oxide), t-P0.9 and diblock copolymers grown from it, t-P0.9-E2.1 and t-P0.9-E8.0. ..... 38
Figure 2.6: SEC traces for mono-methoxy functionalized poly(ethylene oxide), mE2.0, and two diblock copolymers synthesized from the parent block, OH-P0.3-E2.0 and OH-P0.9-E2.0. ..... 41
Figure 2.7: Langmuir trough showing a phospholipid monolayer, Wilhelmy plate, and movable barriers used to control surface area. ..... 48
Figure 2.8: Wilhelmy plate dimensions include width ($w_p$), thickness (negligible, $t_p$) and contact angle, $\theta$. ..... 49
Figure 3.1: Sample autocorrelation function (a) and particle size distribution (b) obtained for liposomes. ..... 55
Figure 3.2: Normalization of average scattered intensity. ..... 56
Figure 3.3: Schematic depicting possible population differences between neat liposomes and polymer-protected liposomes following reaction (hypothetical case). ..... 58
Figure 3.4: Control polymer-liposome incubation experiments at 4 and 24 hour incubation times. ..... 66
Figure 3.5: Average scattered intensities for polymer-incubated liposomes. ..... 67
Figure 3.6: Representative liposome size distributions following peroxidation reactions in the presence of polymers. ..... 68

Figure 3.7: Average scattered intensities following peroxidation in the presence of polymers. 70
Figure 3.8: Schematic illustrating equal molar and equal mass concentrations for P188 and Diblock P188. 72
Figure 3.9: Average scattered intensities for equal PEO content. 74
Figure 3.10: Multi-angle DLS carried out on liposome sample from 60° to 120°. 75
Figure 3.11: Cumulant fitting of multi-angle DLS performed from 60° to 120° gave average decay time, Γ. 76
Figure 3.12: Multi-angle DLS plot for Diblock P188 following liposome peroxidation. 78
Figure 3.13: Scattered intensity (left) and $R_h$ (right) at 90° scattering angle for Diblock P188, obtained 0-2.25 hours after peroxidation. 79
Figure 3.14: SAXS profiles taken on ternary dispersions of water, lipids, and polymers at 37 °C. 81
Figure 3.15: Multilamellar lipid arrangement showing the "flattened" configuration of non-penetrating triblock architectures (*d*-spacing reduced) and the anchored "perpendicular" arrangement (*d*-spacing increased) of the diblock architecture. 83
Figure 4.1: Chemical structures of diblock copolymers of PPO and PEO prepared with different functional groups on the hydrophobic PPO block. Polymer structures are given in the order of synthesis (from left to right). 88
Figure 4.2: Representative liposome size distributions following incubation with (a) tert-butyl-PPO-PEO and (b) hydroxyl-PPO-PEO diblock copolymers. 90
Figure 4.3: Scattered intensity comparison for liposmes incubated with diblock copolymers. 91
Figure 4.4: Scattered intensity results for peroxidation of liposomes in the presence of 5:1 polymer:lipid tert-butoxy- functionalized PPO-PEO diblock copolymers. 94
Figure 4.5: Scattered intensity results from liposome peroxidation experiments with OH-PPO-PEO diblock copolymers. 96
Figure 4.6: Autocorrelation functions for OH-P0.5-E5.3, reactions following 0 h incubation. 99
Figure 4.7: Scattered intensity comparison of liposome peroxidation protection by PEO homopolymers of varying $M_n$ after 0 and 4 hours of pretreatment. 101
Figure 4.8: Lengthening contraction injury protocol stages. 103
Figure 4.9: Lengthening contraction injury force curves for Diblock P188, P188, and PEO-8k. 105
Figure 4.10: Impact of delivery route on P188 stabilization in lengthening contraction injury protocol. 106
Figure 4.11: Lengthening contraction injury force curves for tert-butyl functionalized diblock copolymers (1,000 mg/kg IP). 107
Figure 4.12: Lengthening contraction injury force curves for hydroxyl functionalized diblock copolymers (1,000 mg/kg IP). 109

Figure 4.13: Average isometric force post-injury, normalized to pre-injury isometric force. ..... 110
Figure 4.14: Lengthening contraction injury comparison of identical diblock copolymers ($N_{PO}$ = 16, $N_{EO} \approx 48$) featuring differing end-groups (tert-butyl and hydroxyl). ..... 112
Figure 5.1: Chemical structure of DPPC. ..... 119
Figure 5.2: Area controlled isotherm of DPPC at 25 °C, showing phases and phase coexistence regions. ..... 119
Figure 5.3: Compression isotherms for Diblock P188 and P188, spread at large area per monomer and compressed successively. ..... 121
Figure 5.4: P188 and Diblock P188 insertion into DPPC monolayer. ..... 124
Figure 5.5: P188 and Diblock P188 isotherms following DPPC monolayer adsorption. 126
Figure 5.6: Isotherms showing compression and expansion monolayers of DPPC and (a) Diblock P188 or (b) P188. ..... 127
Figure 5.7: Texas Red DHPE, used to image phospholipid monolayers under a fluorescence microscope. ..... 128
Figure 5.8: Fluorescence microscope configuration with Langmuir trough and lipid monolayer. ..... 128
Figure 5.9: Fluorescence micorgraphs of DPPC monolayers containing 0.5 wt.-% TR-DHPE. ..... 129
Figure 5.10: Monolayers of DPPC and P188 were imaged using a monolayer -isolating ferrule. ..... 130
Figure 5.11: Fluorescence micrographs taken in time on a DPPC monolayer with P188. ..... 131
Figure 5.12: Fluorescence microscopy images taken of a DPPC monolayer before (a) and after Diblock P188 addition (b-f). ..... 133
Figure 5.13: Isothermal compression and expansion of (a) light SR and (b) heavy SR monolayers at 25 °C. ..... 135
Figure 5.14: P188 adsorption to light SR monolayer. ..... 136
Figure 5.15: Polymer adsorption to heavy SR monolayer. ..... 136
Figure 5.16: Compression-expansion isotherms for heavy SR and heavy SR with P188 adsorbed. ..... 137
Figure 5.17: Fluorescence micrographs captured during compression of Light SR monolayer. ..... 139
Figure 5.18: Fluorescence micrographs of Light SR incorporated with Poloxamer 188. ..... 140
Figure 5.19: Monolayer of Light SR with P188 adsorbing shows intermediate phase domains, or rafts around 16 mN/m. ..... 140
Figure 6.1: Chemical structure of 5-(4,6-dichlorotriazinyl)aminofluorescein, 5-DTAF 145
Figure 6.2: Absorbance calibration curve constructed for P188 complexed with cobalt thiocyanate. ..... 148

Figure 6.3: $^{1}$H NMR spectra for P188, tosyl-functionalized P188 (t-P188), and azide-functionalized P188 (a-P188). ..... 153
Figure 6.4: $^{13}$C NMR of azide functionalization steps. ..... 153
Figure 6.5: FTIR spectra for P188, t-P188, and a-P188. ..... 155
Figure 6.6: Calibration curve and tagged polymer absorbance at 556 nm. ..... 157
Figure 6.7: Fluorescence activity of RhB-P188 was reduced following several weeks of storing in ambient light. ..... 158
Figure 6.8: Fluorescence microscope images on HeLa cells incubated with 100 nM RhB-P188. ..... 159
Figure 6.9: RhB-P188 incubated with living HeLa cells for 2 hours. ..... 160
Figure 6.10: Shear-rate dependent viscosities measured for aqueous solutions of PEO-8k and P188 at 25 and 37 °C at varying concentrations. ..... 163
Figure 6.11 Concentration dependence of viscosity shows good agreement between PEO-8k and P188 ..... 164
Figure 6.12: Shear rate sweeps of blood viscosity for post-ischemic and non-ischemic blood. ..... 166
Figure 6.13: Viscosity as a function of shear rate for post-ischemic blood with 3.85 mg/mL polymer. ..... 167
Figure 6.14: Shear-rate dependence of mean blood viscosity for non-ischemic blood. . 168
Figure 6.15: Polymer concentration dependence of mean blood viscosity. ..... 168

# Chapter 1

# Introduction

Oftentimes in the development of medicines or therapeutics, approaches taken by the physical and medicinal sciences are vastly disparate. On one side, license to create and characterize new compounds targeting molecular responses, encouraged by scientific inquiry, and on the other, regimented progress, motivated by the necessarily arduous clinical approval process, drawing intensive focus on new applications and delivery methods for previously or likely-to-be approved compounds. Functional differences aside, the intersection of the two broader fields is lined with opportunities to advance the science and practice of promoting human health. It is at this intersection, decades after the development of a class of polymer molecules for commercial use as solid, nonionic detergents that therapeutic cell membrane stabilization by block copolymer surfactants exists. The work described herein is one thread in a complex tapestry of research efforts seeking to understand the underlying mechanism of therapeutic cell membrane interactions by block copolymers.

## 1.1 Block copolymer definition and structure

Poloxamer 188 (P188), a central molecule of this work, belongs to a series of block copolymer surfactants generally classified as poloxamers (synonymous: Pluronic, Synperonic).[1–3] At the most basic level, block polymers are comprised of two or more chemically distinct polymer chains (or blocks) covalently bonded together. Block polymers comprised of two distinct components are termed block copolymers and can be arranged

in a variety of architectures, from the simplest diblock (e.g. A-B) and symmetric triblock (e.g. A-B-A, B-A-B) cases, to asymmetric (e.g. A-B-A'), multi-block (A-B-A-B-A), or star-type copolymers. Several of these architectures are depicted schematically in Figure 1.1.

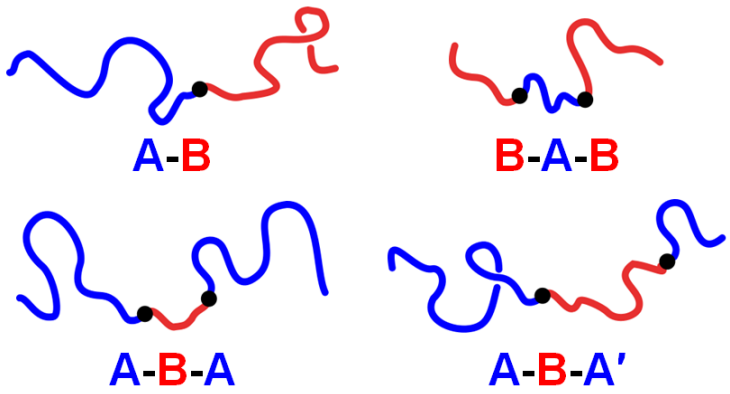


**Figure 1.1:** Schematic representation of possible two-component block copolymers. Within each of these architectures, composition and block lengths can be tuned to dictate self-assembly behavior and accessible morphologies.

As Figure 1.1 suggests, even for block copolymers (i.e. A and B), a practically inexhaustible set of distinct molecules can be prepared by changing the degree of polymerization, *N*, for each block, relative compositions of A and B, and arrangement of blocks. Fortunately, within reasonable limits, the behavior of these molecules follows predictable patterns dictated by inherent thermodynamic properties. Depending on the chemical constituents and molecular properties chosen, block copolymers can be designed to fulfill specific criteria for a host of applications, commercial or specialty, and the structure-function relationship of different combinations of blocks and molecular properties is the subject of considerable study.

The poloxamer family of molecules from which this work stems provides an excellent case study in the relationship of structure and function across varied molecular weights and relative compositions.[4–6] As will be explored in further detail throughout, changes to either block length or composition can have dramatic effects on possible applications and interactions with surrounding matter, as can architecture, functional groups, or even physical state at time of use.

## 1.2 Block copolymer self assembly

### *1.2.1 Assembly in the bulk*

Inherent thermodynamic incompatibilities between block chemistries, quantified by the Flory-Huggins interaction parameter, $\chi$, give rise to phase separation between the distinct blocks.[7–9] This phase separation occurs on short length scales (i.e. microphase separation) because blocks are covalently bonded together, effectively confining maximum domain size to the dimension of stretched chains. Self-assembly by the blocks yields predictable morphologies determined only by the degree of polymerization, composition, and interaction parameter, which has a temperature dependence.[9] These morphologies, which can achieve long-range order, may be extrinsically tuned through synthesis (e.g. block architecture and degree of polymerization) to achieve specialty materials, however the majority of commercial block copolymers are selected for their desirable material properties in the bulk.[10] Commercial applications of block copolymers encompass countless markets and materials, thanks to their structural, surface, or solvent-selective properties.[7,10]

### *1.2.2 Assembly in selective solvents: micellization*

Besides self-assembly by block copolymers in the melt, certain morphologies can be accessed by block copolymers dispersed into a solvent selective to only one of the blocks. These polymeric dispersions self-assemble to minimize contact between solvent and the poorly soluble blocks, and four general forms are possible, namely: spherical micelles, worm-like micelles, bilayered vesicles (also called polymersomes), and networks.[11–16] Just as in the melt, morphologies in solution are tunable through extrinsic properties, which can be controlled by synthetic techniques such as living anionic polymerization.[9] Variations of the four main morphologies may be achieved by incorporating additional blocks (e.g. ABC terpolymers) or altering connectivity between blocks (e.g. star block copolymers).[17,18]

The propensity of a block copolymer solution to micellize is firstly dependent solubility differences between blocks, followed by polymer concentration and temperature. Block copolymer micellization is analogous to surfactant assembly, such as that exhibited by soaps, detergents, and lipid systems,[17,18] and the poloxamers were indeed first developed to serve as powder-form nonionic detergents for commercial use.[1] Of particular interest in

all surfactant systems is a parameter known as the critical micelle concentration, or CMC, and to a lesser extent, the critical micellization temperature, CMT. The CMC is defined as the isothermal surfactant concentration at which micelles begin to form, and above which, results in formation of more aggregates.[18] Similarly, the CMT is the temperature at which micellization occurs for a fixed surfactant concentration.[19] For example, as dispersant concentration is increased above the CMC, thermodynamic equilibrium between unimeric polymers and micelles is maintained.[15,17,18] If molecule size is increased (specifically the poorly soluble part), the free energy of a single dissolved molecule rises, and consequently, the CMC is reduced. The size dependence of CMC is the reason macromolecular surfactants such as block copolymers have such low CMCs, as compared to familiar small molecule surfactants.[18,20–22]

In practice, the CMC is determined by a break in a curve of some signal (e.g. surface tension, scattering, fluorescence, viscosity, etc.) with concentration.[17,19,22,23] For surfactant molecules, surface tension measurements are often effective: the CMC is defined as the concentration at which surface tension (measured by a Wilhelmy plate at the interface) first approaches a constant value. The CMC corresponds to saturation by the surfactant at the interface; additional solute must micellize to minimize free energy of the system. For block copolymer surfactants such as poloxamers, however, CMC is sometimes more subtly marked by a slope change, since polymer rearrangement at the interface will continue to promote surface tension reductions upon further addition. A literature example of surface tension measurements used to determine CMCs for diblock copolymers of polyethylene oxide (PEO) and polypropylene oxide (PPO) is shown by Figure 1.2.[23] As is clear from the data, CMC decreased with increasing hydrophobic PPO block length.

A second method to determine CMC that is widely used is that of dye solubilization. The method typically involves some kind of insoluble fluorescent probe that fluoresces when solubilized by surfactants in micelles. A spectrophotometer is used to measure absorption or emission; depending on the probe and method selected, the resulting curve is characterized by a slope change at CMC. Figure 1.3 shows a CMC study by Alexandridis, et al., performed using solubilization of fluorescent dye 1,6-Diphenyl-1,3,5-hexatriene

(DPH) over temperatures ranging from 15 to 45 °C for poloxamer 334 ($M_n$ = 5.9 kg/mol, $w_{PEO}$ = 0.4).[21,22]

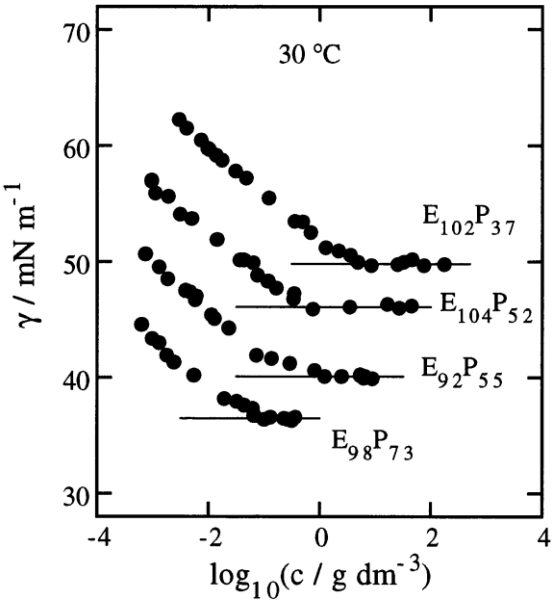


**Figure 1.2:** Representative plot showing how surface tension measurements can be used to determine CMC. Data shown are for diblock copolymers of PEO (E) and PPO (P) at 30 °C, where nomenclature indicates number of repeat units for each block; i.e. molecular weights range from 6.6 to 8.6 kg/mol. Figure reproduced from Altinok, et al.[23]

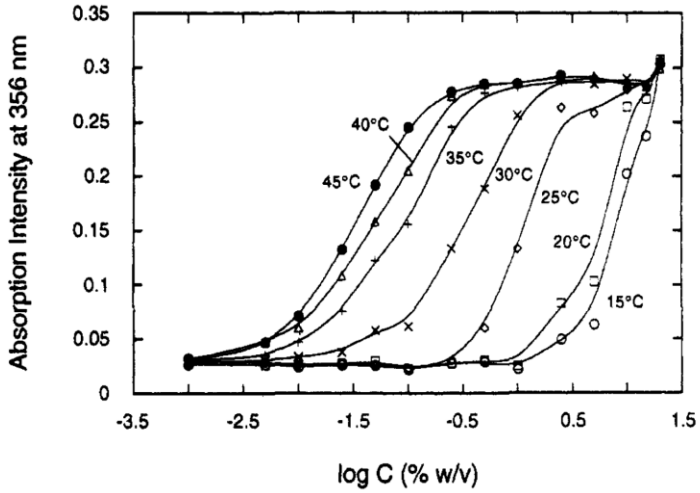


**Figure 1.3:** Absorption profiles for DPH dye solubilization technique used to determine CMC of poloxamer P334. Data are reproduced from Alexandridis, et al.,[21] and show reduced CMCs at higher temperatures.

Here it is seen that the CMC of poloxamer 334 (and all poloxamers) is reduced with rising temperature. This trend can be attributed to dehydration of the PEO blocks and the loss of structuring by water around PEO at elevated temperature (larger negative contribution by entropy term to free energy of micellization).[24] Homopolymers of PEO and PPO exhibit reduced solubility in water at elevated temperatures, a signature behavior of materials with a lower critical solution temperature (LCST).[4] Upon further heating, micelles of poloxamers will form lyotropic liquid crystalline 'gels,' and at even higher temperatures, the solution will macrophase separate forming a turbid solution (i.e. cloud point).[4] The effect of LCST on micellization is more pronounced for the PPO block, and temperature effects on poloxamer micellization are strongly dependent on the PPO content (degree of polymerization, $N_{PO}$).[25] Both surface tension and dye solubilization methods are often used to determine CMCs of a number of surfactants, including block copolymer surfactants such as poloxamers, in addition to other methods previously mentioned.

Although micellization itself is a well-known and naturally-occurring self-assembly process, the formation of micelles by block copolymers is significantly more complex than small molecule species. Standard experimental techniques to determine the CMC are further complicated by polydispersity effects and variable sensitivity at low concentrations across characterization methods.[22]

## 1.3 Poloxamers

Amphiphilicity, the property of P188 that gives rise to micellization in aqueous systems, is of particular medical interest in this work. Like cell membranes in the body, poloxamers exhibit mixed affinity for water; from the Greek roots: "*amphi-*" meaning "both" and "*philia*" meaning "love." Amphiphilicity is particularly relevant to medical applications, which contain numerous polar and nonpolar compounds, and indeed, the efficacy of poloxamers in membrane stabilization is most typically attributed to like-affinities by each block with surrounding components. The path from poloxamer inception to its use as a prevalent medical additive or therapeutic was not direct, however. A brief history of poloxamers is presented to portray just how astounding the leap from industrial surfactant to modern medical marvel was.

*1.3.1 Industrial origins and chemical make-up*

Notably, poloxamers were the first commercially produced block copolymers.[26] In the late 1940s, increasing demand for inexpensive, flake-form alternatives to anionic surfactants for detergent applications led researchers to condense bases onto hydrophilic poly(ethylene oxide).[1] Flake forms of these surfactants lacked effective detergency in the flake-form, due to an imbalance in the hydrophilic poly(ethylene oxide) portion, and properly balanced surface activities led to undesirable liquid or paste forms, which were industrially impractical to produce and implement. Wyandotte Chemical Corporation went on to solve this problem by designing block copolymer surfactants of hydrophilic poly(ethylene oxide) and hydrophobic poly(propylene oxide), now known as poloxamers, or by their trade name, Pluronic (BASF).[1–3]

Poloxamers today are widely available, and found in countless industrial and consumer products. They feature mild, non-ionic amphiphilicity at a range of compositions and molecular weights ranging from 10-80 wt.-% poly(ethylene oxide) and 1 to 15 kg/mol, respectively. As shown by the chemical structure in Figure 1.4, the central poly(propylene oxide) (PPO) block of the poloxamer formula differs in repeat unit from the hydrophilic poly(ethylene oxide) (PEO) tail blocks by a pendant methyl group. Although this difference results in amphiphilicity that is weak compared to the phosopholipid molecules of biological membranes, the body of evidence supporting amphiphilic attraction of poloxamers to biological membranes is vast.[27–34] Poloxamers are categorically symmetric A-B-A triblock copolymers (refer to Figure 1.1), synthesized from the central poly(propylene oxide) block outward to achieve equal length poly(ethylene oxide) tails.

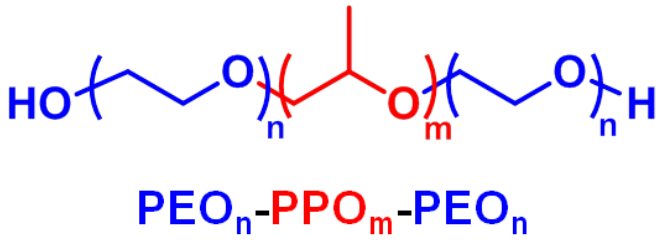


**Figure 1.4:** Chemical structure of poloxamers. Symmetric A-B-A architecture corresponding to hydrophilic poly(ethylene oxide) tails (PEO) and a hydrophobic poly(propylene oxide) central block.

*1.3.2 Poloxamer micellization behavior*

In light of the low concentrations (≤ 150 μM) of poloxamers required to achieve membrane stabilization;[29] it is believed that unimeric interactions with phospholipid bilayers facilitate membrane stabilization.[35] Micellization or aggregation by poloxamers *in vivo* cannot be fully dismissed, however, because the ionic, multi-component nature of physiological systems undoubtedly play a role in poloxamer aggregation. The thermodynamically favorable interactions with more strongly amphiphilic phospholipid membrane components could drive similar analogous aggregation or micellization at the membrane, but no clear evidence of such behavior is available. Current detection methods for micellization in physiological systems are geared towards biodistribution of dye-loaded micelles (i.e. targeted drug delivery),[36] and cannot effectively track the *in situ* development or disassociation of polymeric aggregates *in vivo*. Until some strategy is developed, only pre-delivery micellization characteristics can be investigated, and post-delivery behavior is speculative.

Within the confines of this work, micellization by P188 is not a targeted state, in fact, care is taken to work below reported CMCs. Regardless, micellization by poloxamers has been investigated by a number of groups, and reported CMCs vary over three orders of magnitude for Poloxamer 188.[22,37–39] A summary of literature values of CMC for P188 is tabulated in Table 1.1. At physiological temperature (~37 °C), values range from about 500 μM to about 13 mM. It is important to note the possibility of delivered micelles to animals in *in vivo* experiments; the implications of physiological effects on poloxamer aggregation and dissociation are largely unknown.

**Table 1.1:** Reported CMCs for P188 at various temperatures and detection methods.

| Reported CMC | CMC (mM) | T (°C) | Method | Reference |
|---|---|---|---|---|
| 0.015 g/dL | 0.002 | 20 | Surface tension | Prasad, et al.[40] |
| 10 g/dL | ~12 | 20 | Fluorescent ORB | Nakashima, et al.[41] |
| 1.4 mM | 1.4 | 25 | Methyl yellow dye solubilization | Lopes and Woh[42] |
| 1.25E-4 M | 0.125 | 30 | Surface tension | Maskarinec, et al. 2002[43] |
| 12.5 mg/mL | 1.49 | 36.3 | Scattered light intensity | Zhou and Chu[22] |
| 0.48 mM | 0.5 | 37 | Pyrene dye solubilization, pH 7.4 | Batrakova, et al.[37] |
| 10 wt.-% | ~13 | 37 | DPH dye solubilization | Kabanov, et al.[38] |
| 4-5 wt.-% | ~5 | 37 | Surface tension | Kabanov, et al.[38] |
| 8.333 mM | 8.3 | 40 | DPH dye solubilization | Alexandridis, et al.[21] |
| 3.571 mM | 3.6 | 45 | DPH dye solubilization | Alexandridis, et al.[21] |

*1.3.3 Medical uses of poloxamers*

The amphiphilicity of poloxamers makes possible a wealth of industrial uses and has been attributed to be the chief property driving therapeutic efficacy in a variety of medical applications, beginning with hemodynamic modifiers for cardiopulmonary bypass,[44–46] vaso-occlusive crisis in sickle cell disease,[47–49] or ischemic reperfusion injury,[31,50–52] and extending to the cell membrane stabilization phenomena explored here.[28,29,53,54] Although the surfactancy of poloxamers is relatively weak in comparison to phospholipids,[49] the solubility difference between PEO and PPO is sufficient to micellize (i.e. drug delivery and gel formation),[21,55] lyse membranes (i.e. detergency),[56] or favorably interact with various hydrophobic surfaces in the body (e.g. red blood cells or damaged cell membranes). The particular function poloxamers serve *in vivo* is dictated by molecular properties of the selected formulation (i.e. molecular weight and composition), and to some extent, the dosing and delivery methods employed.[57]

The earliest reports of P188 in clinical research involved use as rheological modifiers in both blood[44,58] and artificial blood.[59–62] In 1989, a perfluorocarbon based artificial blood containing P188 as an emulsifier, Flusol-DA, was the first synthetic oxygen carrier approved by the U.S. Food and Drug Administration for limited use in coronary artery balloon angioplasty surgery,[63] following clinical trials on anemic patients who were predominately Jehovah's Witnesses and did not accept blood transfusions on religious grounds.[61,64] The efficacy of artificial blood in carrying oxygen was mixed, and although Flusol-DA was safe to administer, it was eventually pulled from the market in 1994.[63–65]

Despite the withdrawal of Flusol-DA, the clinical trials performed helped to secure P188's status as a low-toxicity emulsifier,[66] and tangential studies exhibited usefulness in improving hemorheology,[48,49] as well as non-thrombolytic behavior.[67] P188 has been employed in clinical research as a therapeutic agent in sickle cell anemia,[47–49,68] ischemic reperfusion injury,[31,50,51,69] thermal or radiation burn treatment,[28,30,70] myocardial infarction (heart attack),[46,69] and cardiomyopathy (heart failure) as a result of Duchenne Muscular Dystrophy.[29,71–73] These conditions, though resulting from vastly different pathologies, are related by the apparent capacity of a block copolymer surfactant to mitigate symptoms. More specifically, each of these conditions features some vulnerability of involved cell

membranes, which is likely the common link between P188-mitigated maladies and diseases. Despite continued interest in the field and the ongoing research to explain the essential mechanisms at work, a fundamental understanding of poloxamer interactions at the cellular level has not yet been reached.

## 1.4 Physiological background: muscle and membranes

All human cells are encapsulated by a heterogeneous membrane comprised of an amphiphilic phospholipid bilayer, various proteins, and cholesterol. Dozens of lipid species are found in cell membranes, and the exact composition of the membrane is highly dependent on the organism and cell type.[74,75] Regardless of the cell function, the primary function of the cell membrane is to serve as a transport barrier to preserve homeostasis within the cell. Directed transport of ions or other nutrients into cells and waste out of cells is carried out by function-specific proteins that bridge the membrane.[76] While the same is true for the cells making up muscle tissue, the structure and function of muscle cells, such as skeletal or cardiac muscles is quite different from other cells in the body. The following is a general overview of cardiac muscle cells, which were determined to benefit from P188 protection at the sarcolemma, the membrane of particular interest in this work.

### *1.4.1 Hierarchical structure of muscle*

Striated muscle, such as that of the heart or skeletal system, consists of a highly organized hierarchy of modular components.[77] Many of the same organelles found in other cells are present, but these are arranged around an extensive protein scaffold that is attached to the cell membrane.[76] This scaffold, which is arranged as a liquid-crystal, gives rise to the forces causing muscles to contract. Forces are typically generated axially along the myocytes, which are connected to other myocytes by proteins to form long fibers. Each myocyte unit is roughly cylindrical with diameters of 10-20 μm and lengths ranging from 50-100 μm, and within the makeup of each myocyte are myofibrils, fibrous structures made up of subunit sarcomeres.[76,77] Sarcomeres contain the contractile proteins responsible for muscle contraction, and they are subdivided in the myofibril by *Z*-lines or disks, which appear as bands in optical micrographs.

*1.4.2 Sarcolemma*

Surrounding the sarcomere-myofibril-myocyte-muscle fiber arrangement is a plasma membrane called the sarcolemma. The sarcolemma is first and foremost a lipid bilayer, serving as a protective barrier against uncontrolled diffusion by charged molecules.[76] Also contained in the membrane, however are cholesterol and a variety of proteins that regulate ion transport, bind myocytes to the extracellular matrix, and transduce contractions within the cell to the overall muscle.[77,78] One of the proteins of interest to this work is dystrophin, shown in Figure 1.5 linking between the cytoskeleton (actin) and the sarcolemma, which is then coupled to the extracellular matrix by the dystrophin-associated glycoprotein complex (DGC).[73] Dystrophin serves as a kind of force dampener or mechanical reinforcement of the sarcolemma, mitigating stresses of muscle activation on the fragile sarcolemma.[79]

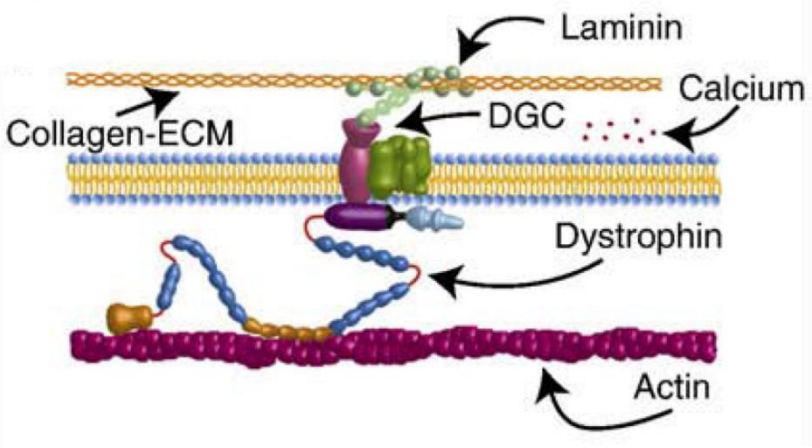


**Figure 1.5:** Connectivity of sarcolemma to actin and extracellular matrix of cardiac myocyte. Figure reproduced from Townsend, et al.[73]

*1.4.3 Duchenne muscular dystrophy pathogenesis and associated cell membrane damage*

By genetic mutation, some patients are unable to express for the dystrophin protein or related protein. Categorically, this class of genetic diseases is referred to as muscular dystrophy, within which several forms of varying symptoms and severity exist. Research has linked the absence of dystrophin to sarcolemma fragility and permeability to $Ca^{2+}$, which is critical to the activation of muscles.[79,80] Permeability of the sarcolemma in dystrophic muscle is believed to arise from mechanical damage to the membrane imposed

by contractile forces that would typically be mitigated by dystrophin, and the consequent $Ca^{2+}$ imbalance can leads to necrosis and progressive muscle wasting and weakness.[29,81]

DMD is diagnosed once in every 3,500 live male births each year and is most easily recognizable by its effect on skeletal muscles.[72,82] Patients are often diagnosed around age five, first presenting with progressive muscle weakness and over-sized calf muscles. Complications of DMD beyond muscle weakness and loss of ambulation typically involve curvature of the spine (scoliosis), respiratory difficulty, and cardiomyopathy.[82,83] Tragically, the disease shortens patient life expectancy to around age 30.[84]

Existing treatments developed to slow the progression of muscle degeneration appear to have little benefit on cardiac muscle, despite both muscles belonging to striated structure class. Muscle strength is typically treated by administering corticosteroids, such as Prednisone. The resultant retention or improvement of muscle strength allows patients to walk and participate in normal daily activities for years longer than patients not receiving steroids. A direct consequence of prolonged ambulation in DMD patients receiving corticosteroids, however, is increased stress on the heart.[29,72,73] Cardiac health is known to progressively decline in DMD, but symptoms of cardiomyopathy do not typically appear until the condition is more advanced.[82] Making matters worse, the progressive decline of skeletal and respiratory muscle may mask early cardiac symptoms of fatigue and difficulty breathing, giving physicians less of a chance to diagnose and treat the cardiomyopathy.[72,82] As current treatment strategies evolve, life expectancy for DMD patients is lengthening, and as a result, it is expected that cardiomyopathy will contribute more strongly to cause of death.[82]

### *1.4.4 Membrane sealing by Poloxamer 188*

In the first study to apply membrane stabilizer Poloxamer 188 to cardiomyopathy of DMD, single, isolated *mdx* myocytes (cardiac muscle cells from a mouse model of DMD), achieved fully restored compliance and calcium levels compared to the control by acute P188 administration.[29] Furthermore, *in vivo* cardiac stress tests (dobutamine infusion) on *mdx* mice given P188 showed significant improvement over the control case in terms of heart function (pressure-volume loops).[29] Chronic dosages of P188 were later shown in a golden retriever muscular dystrophy model (GRMD) to be effective at reducing myocardial

fibrosis associated with cardiomyopathy. Although P188 showed dissimilar effects to *mdx* with respect to acute *in vivo* hemodynamics, its function to prevent fibrosis is believed to slow the progression of myopathy.[54] The use of P188 to treat cardiomyopathy of DMD could have further implications on cardiac disease related to aging or trauma, not to mention other muscle diseases and injuries.

Membrane stabilizers have recently been applied to skeletal muscles within the *mdx* disease model as well.[57,85] Though early experiments reported a deleterious effect of P188 on *mdx* skeletal muscle, recent results have shown that route of delivery is a key factor in determining the membrane stabilizing capacity of P188 and a larger poloxamer, P338, of the same relative PEO:PPO composition (80:20 by weight).[57] These results are especially encouraging, because it was previously believed that P188 was only an effective treatment for cardiomyopathy. Due to the physiological differences of cardiac and skeletal muscles, it is believed that the mechanism of interaction by polymer membrane stabilizers with each would be different, and physiological and biophysical methods are being applied concurrently to study this mechanism.[57]

## 1.5 Biophysical investigations of membrane stabilization

Given the number of existing and potential medical applications for membrane stabilization by Poloxamer 188, a concerted effort to determine the underlying mechanism of membrane interaction by block polymer surfactants has been underway for decades. Biophysical studies dating back to the early 2000s have revealed the importance of the hydrophobic PPO block in determining the nature of polymer-membrane interactions, as well as the delicate balance of molecular weight and composition dictating the various poloxamer formulations' propensities to enhance or disrupt cell membrane integrity.[35,43,86–90] Despite significant advances in the field, the precise mechanism of membrane stabilization remains unresolved.

### *1.5.1 Monolayer model membranes*

Some of the earliest models of poloxamer interactions with model membranes were performed by Lee and coworkers on phospholipid monolayers.[39,43,86,91] As will be discussed in greater detail in Chapter 5, monolayer studies revealed the importance of the

hydrophobic block in determining membrane interactions. Using a Langmuir trough, Lee et al., demonstrated that poloxamer adsorption to the lipid monolayer is localized to regions of reduced packing density (i.e. damage),[43] and that the hydrophobic blocks are critically important to membrane interaction, more so than hydrophilic PEO groups.[86] Grazing incidence x-ray diffraction on P188 and lipid monolayers showed that for condensed lipid phases, poloxamers are excluded completely from the membrane.[87,92] These results corresponded to isothermal compression experiments, and form the basis of a theorized polymer ejection on membrane healing.[92] In situ monolayer work with synthetic phospholipid membranes led to the later exploration of supported monolayers by AFM, which demonstrated the nanoscale perturbations to DPPC morphology induced by P188. Again, above a certain lipid packing density, morphologies of "combined" P188 and lipid monolayers reverted to those of the neat lipid.[93]

*1.5.2 Bilayered model membranes: liposomes*

Liposomes, or more specifically, large unilamellar vesicles (c.a. 50-200 nm diameter), are prepared from multilamellar suspensions of natural or synthetic lipids by extrusion through a membrane of a specified pore size.[94] As a bilayered model membrane, liposomes are a close biophysical parallel to cell membranes, with curvature and barrier properties, and as such, they have been used extensively in the literature to study a variety of biochemical and biophysical phenomena, including polymer interactions with membranes.[27,88,89,95–97] Lipid homogeneity, the absence of native proteins, and their overall size and structure necessitate concurrent work with native cells and tissues, and furthermore, these features highlight the importance of choosing a relevant damage model that is relatable to physiological processes.

Ease of preparation and relative stability of liposomes make them an ideal system on which to screen molecular property contributions to block copolymer interactions with membranes. The binary stability or instability of simple lipid-based liposomes, however, makes inducing damage far more difficult to control than for *in vitro* models. Whereas a cardiac myocyte is a tubular shape 50-100 μm long and 10-20 μm in diameter,[77,98] liposomes are spherical enclosures about three orders of magnitude smaller. Relatively speaking, the membrane of a cardiac myocyte is a flat lamellar sheet, supported by the

cytoskeleton (comprised of myosin, actin, and other cellular proteins including dystrophin).[99] Damage to the membrane, such as the formation of pores, can therefore be localized, and native healing mechanisms, such as "patching" by underlying vesicle fusion, can be activated by cell signaling, initiated by flux of $Ca^{2+}$ or other cations through the damage site.[100–102] Besides the inherent difficulties in imposing a mechanical stress on nanoscale liposomes and measuring the ensuing response, the comparatively tight radius of curvature and corresponding high membrane tension dictate that acute damage to membranes will lead to irreparable instabilities.

Recently, poloxamer interactions with bilayered phospholipid membranes in the form liposomes, have been described by a two-step mechanism: adsorption and insertion, wherein the dynamics between steps are determined by the hydrophobic-hydrophilic balance of the molecule.[33,88,89,97] The profound impact of this balance on membrane integrity has been demonstrated across a series of poloxamers, but most relevant to this work were the differences exhibited by P181 and P188, poloxamers with identical hydrophobic PPO block lengths (PPO degree of polymerization, $N_{PPO}$ = 30) and vastly different hydrophilic PEO contents: 10 and 80 wt.-% PEO, respectively. The more strongly hydrophobic P181 showed evidence of rapid insertion into phospholipid membranes, loosening lipid packing and even rupturing lipid vesicles (liposomes).[33,89,97] In contrast, P188 showed evidence of adsorption at the membrane surface on short timescales (c.a. 4 hours), maintaining membrane integrity.[33,89] The insertion step was eventually exhibited by P188 after incubation times exceeding 24 hours, suggesting that while the mechanism is similar between the two, kinetics of adsorption depend predominantly on hydrophilic block length.[33]

Further evidence of poloxamer absorption and insertion was presented by liposomal studies by Lee and coworkers that investigated interactions by varying poloxamer species with liposomes by a liposome peroxidation technique,[89] isothermal titration calorimetry (ITC),[88,89] and $^{1}$H Overhauser dynamic nuclear polarization NMR spectroscopy (ODNP).[97] While the ITC and ODNP experiments focused on the thermodynamics and kinetics of polymer interactions with lipid membranes, the peroxidation experiment showed promise

as a type of controlled model stress that could potentially be related to the stabilizing effects of particular poloxamers on cell membranes.

*1.5.3 Liposome peroxidation as a model stress*

Lipid peroxidation is a naturally occurring mode of damage common to both cell membrane and liposomal structures.[103–108] Physiologically, membrane damage by reactive oxygen species (ROS) may arise from effects of elevated $Ca^{2+}$ levels (self-perpetuating), such as in ischemia-reperfusion injury,[81,101,109] acute irradiation, as in ionizing radiation injury,[110,111] or even aging,[74,112] among other peripheral causes. Oxidative damage to lipid-based membranes can be initiated by free radicals in a controlled fashion, as is performed in liposome peroxidation. The tight radius of curvature that confers elevated membrane tension relative to *in vivo* cell membranes also serves to facilitate exposure of unsaturated acyl tails to free radicals in solution.[113] One peroxidation reagent favored for its solubility in water and steady rate of decomposition into free radicals under specific heat and light conditions is 2,2-azobis(2-amidinopropane) dihydrochloride (AAPH).[104,107,108,114] Following initiation of AAPH to form two free radical nitrogen species, polyunsaturated fatty acid (PUFA) tails can be peroxidized according to the mechanism in Scheme 1.1.

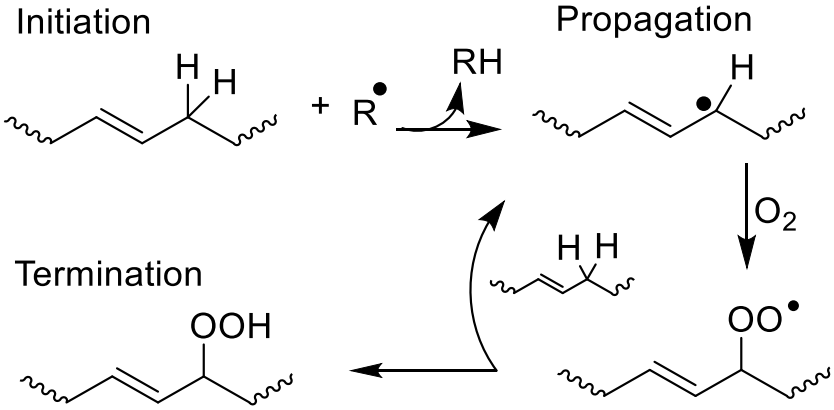


**Scheme 1.1:** Mechanism of lipid peroxidation on unsaturated lipid tails. Adapted from Heuvingh, et al.[115]

*1.5.4 Block copolymer protection against liposome peroxidation*

In the liposome peroxidation experiments by Wang, et al., block copolymer surfactants of varying size and composition were added to liposome dispersions prior to reaction with the free radical generator (AAPH), and protection by polymers was assessed by dynamic

light scattering; more specifically, particle size distributions obtained by DLS following liposome reactions.[89] The analysis involved drawing conclusions from shifts in average $R_h$ (peak position) and height of the particle size distribution. Liposome protection by PEO-8k and P188 are shown in Figure 1.6, adapted from Wang, et al.[89] The PEO-8k case was performed at a higher molar ratio of polymer to liposome than P188, and it was protective at both 0 and 4 hour incubation times. Conversely for P188, the authors interpreted the particle size distribution at 0 h incubation time to demonstrate peroxidation and protection at the 4 h incubation time.[89] (Note that such a particle size distribution as was obtained for P188 with 0 h incubation after oxidation shows signs of poor fitting of likely poor DLS data, and no mention of reproducibility of the result was made.)

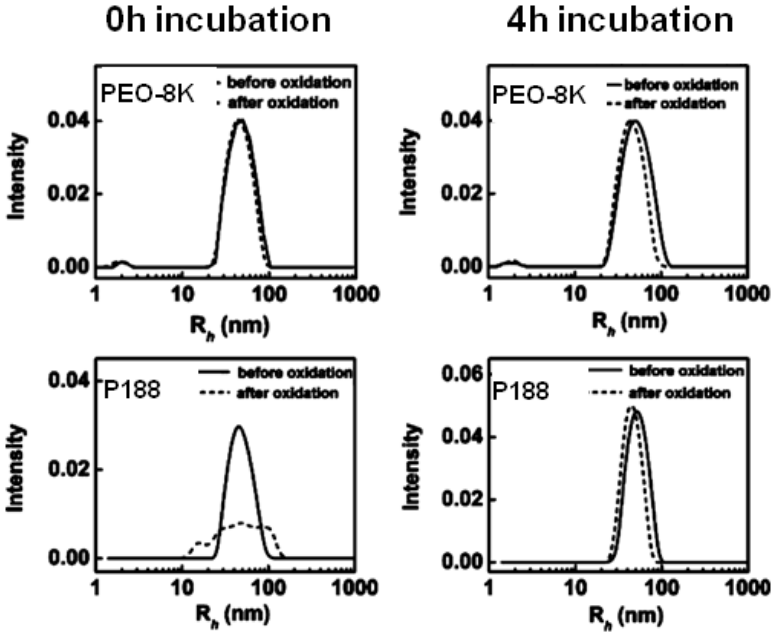


**Figure 1.6:** DLS particle size distributions reported by Wang, et al.[89] PEO-8k (top row), which was administered in a 25:1 polymer:lipid ratio was protective at both 0 and 4 hour incubation or pretreatment. P188 (bottom row) was not protective at 0 h incubation, whereas 4 h incubation is protective.

Wang, et al. also reported non-protective cases, namely DLS results following peroxidation reactions of liposomes incubated with more hydrophobic block copolymers.[89] Particle size distributions obtained before and after oxidation (again at 0 and 4 hours of liposome pretreatment with polymer) for the hydrophobic block copolymers are well represented by the plots for Poloxamer 335 (P335, $M_n$ = 6,500 g/mol, $w_{EO}$ = 0.5) in Figure

1.7. Following the reaction, particle size distributions became quite broad, with shorter peaks centered at smaller $R_h$ than observed in the pre-oxidation cases. For Poloxamer 181 (P181, $M_n$ = 1,750 g/mol, $w_{EO}$ = 0.1), a flattened distribution is reported for 0 h incubation, much like P188 in the hydrophilic polymer class (data not shown).

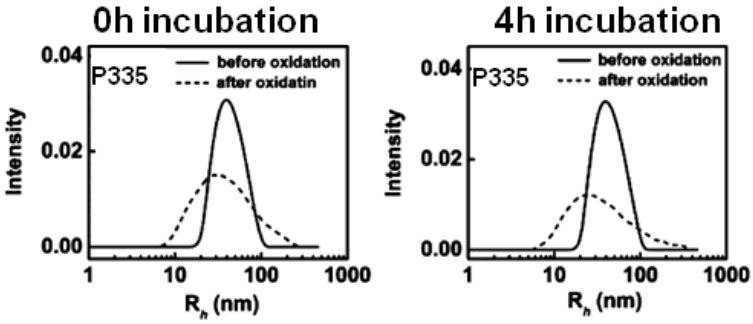


**Figure 1.7:** Peroxidation of liposomes incubated with Poloxamer 335 (P335), from Wang, et al.[89]

Wang and coworkers tied their findings into their hypothesized two-step interaction mode, namely, adsorption and insertion. The more hydrophilic polymers (P188, PEO-8k, and a branched poloxamer species, Poloxamine 1107) were reported to adsorb only within experimental timeframes, and with only minor discrepancy (i.e. P188 at 0 h incubation), protected liposomes against lipid peroxidation. The more hydrophobic poloxamers were quicker to insert into the membrane, which resulted in poor protection against peroxidation. Results obtained from liposome peroxidation experiments appeared to correspond well to the types of membrane interactions predicted from physiological and other biophysical experiments, and liposome peroxidation was identified as a possible screening technique for future polymer chemistries considered. Chapter 3 develops a more quantitative method for analyzing DLS measurements following peroxidation, and Chapter 4 considers a variety of polymers in the technique.

*1.5.5 Development of a model polymer system*

In addition to inherent size and concentration limitations at membranes, the constrained chemical landscape available to researchers investigating block copolymer interactions with biological membranes has slowed overall progress. The triblock archetype of membrane sealing compounds is a convention adopted out of commercial availability, but as a model compound for systematic study, it is not the clearest choice.

The second hydrophilic block adds a level of complication in studying interactions, because changes to hydrophilic block length are either twice as powerful in terms of overall composition (e.g. a study of hydrophilic block length effect), or half-strength as compared to hydrophobic block length changes made to maintain composition (e.g. fixed compositions). Additionally, the second hydrophilic block adds steric hindrance and impedes hydrophobic interaction by the central PPO block. From a synthetic perspective, a simpler model compound in the form of a diblock architecture of PEO-PPO is preferable, and offers access to an infinite library of minute changes to composition and block length.

Based on an expansive literature regarding the solution-phase behavior of block copolymers, diblock and triblock architectures are expected to behave similarly in the dilute to semi-dilute regime. Unfavorable solvent interactions are minimized by the formation of micelles, and the same types of micellar structures (e.g. spherical, wormlike, vesicles) may be formed for both. While the triblock A-B-A architecture of poloxamers would be able to form bridged networks at high micellar concentrations of non-polar solvents, their configuration in aqueous solutions would match that of diblock architectures. Differences between the two architectures would most likely arise at equilibrium conditions, in terms of micellar exchange.[116,117]

The notion that polymers dynamically associate and dissociate from micellar structures has been studied extensively by time-resolved small angle neutron scattering.[117–120] Recent studies employing time-resolved small angle neutron scattering (SANS) have confirmed independent chain exchange by block copolymers and a strong molecular weight dependence on micellar exchange dynamics.[117–120] Follow-up work investigating the architectural dependence of micellar chain exchange found that architectural arrangement of triblocks dictates exchange dynamics: compared to analogous diblock copolymers of type A-B, an A-B-A architecture was found to exchange more rapidly, whereas a reverse B-A-B triblock architecture was much slower.[116] Although it is expected that interactions responsible for membrane sealing are unlikely to follow an equilibrium process, micelle exchange dynamics suggest that amphiphilic interaction dynamics are architecture dependent.

One of the early hypothesized modes of membrane interactions leading to stabilization was that of membrane spanning by the triblock poloxamer.[90,121] For block copolymers of sufficient length (including Poloxamer 188), the hydrophobic block could hypothetically to span the thickness of the hydrophobic region of the cell membrane, c.a. 4-6 nm, with pendant hydrophilic PEO blocks on either side of the membrane. By virtue of its two blocks, a diblock architecture is naturally limited to association at one side of the membrane, though diffusion across the membrane to the interior of the cell would not be excluded. Through use of small angle x-ray scattering (SAXS) and lamellar phospholipid systems, Firestone, et al., showed that the spanning hypothesis was in fact incorrect.[90] Furthermore, they later showed that arrangement of diblock copolymers of PEO and PPO adopt a more brush-like configuration at lamellar interfaces, as compared to triblocks. The net effect of these differences is a measurable increase in *d*-spacing for the diblock copolymers.[122]

Whereas monolayer studies showed strong membrane interaction dependence on hydrophobic block length, the bilayered studies highlighted the importance of the hydrophilic block in reducing membrane penetration, which has been linked to membrane lysing.[33,56] To date, investigations focused on either the hydrophobic or hydrophilic block length are complicated by the presence of the second hydrophilic block on commercially available poloxamers, which further complicates the role relative hydrophobi/hydrophilic composition is thought to play. To this end, a simpler model system is preferential, and a diblock architecture, if efficacious, offers a clear synthetic route to methodical parameter adjustment.

Adoption of a diblock architecture PEO-PPO block copolymer surfactant as a model system bridges an apparent gap in the membrane sealing literature, which offers only two recent studies on the subject.[122,123] Given the strong influence of the hydrophobic block on membrane interactions in both model systems and *in vivo*, it is reasonable to expect that a diblock architecture, with a free hydrophobic end, will lend additional insight into how the hydrophobic PPO block contributes to the net membrane-stabilizing effect exhibited by P188. The hypothesized effect of the exposed hydrophobic block on membrane interaction

is to drive membrane attraction, and whether this is beneficial or detrimental to membrane integrity will be explored in Chapters 3 and 4.

## 1.6 Objectives of this work

Despite significant advances to the field of block copolymer surfactant membrane sealing, a definitive mechanism of interaction has not yet been determined. The objective of this thesis is primarily to establish methods by which to systematically investigate the mechanism of membrane stabilization biophysically, and lay the groundwork for direct connections to physiological observations. As will be shown, this objective was met by exercising synthetic techniques to build a new library of pertinent block copolymers and adapting existing model membrane methods to obtain more information about the systems. Collaborative efforts with members of the physiological and medical community were also initiated and will be discussed. A brief overview of each chapter as it applies to the overarching objective follows.

### *1.6.1 Diblock copolymer synthesis*

Synthetic routes to prepare amphiphilic block copolymers of PEO and PPO by living anionic polymerization have been published,[23,124–128] but for the purposes of membrane stabilization, no synthetic strategies have been pursued. This work will rely on these synthetic methods to supplement established living anionic polymerization methods.[129] Special attention will be paid to the hydrophobic block end group functionalities, which will be shown to be important in directing membrane interactions. Synthesis and polymers prepared will be discussed in Chapter 2.

### *1.6.2 Model membranes*

Cell membranes, whether damaged or intact, are an inherently complex system of study. Membrane composition, which is largely heterogeneous and cell function dependent, plays a significant role in directing interactions between a cell and its local environment. For these reasons, it is both necessary and impossible to employ the native cell membrane in studies examining polymer surfactant interactions at the membrane interface. Two strategies, synthetic and naturally derived lipid membranes have been pursued herein. Each membrane type delivers specific advantages and disadvantages,

which will be discussed throughout the work. Physical models or arrangements of membrane components in this work fall into monolayer, unilamellar vesicle, and multilamellar dispersion classes.

Model membranes composed of synthetic phospholipids (either pure or mixed composition), are widely used in the literature to achieve reproducible, well-controlled systems. Additional features such as curvature, charge, and membrane fluidity, can be addressed by careful selection of physical model and membrane components. As modeling cell membranes is a field of study unto itself, a cursory discussion of membrane selection will be made in Chapters 3, 4, and 5.

Naturally derived membrane materials, isolated from *ex vivo* mammalian cells, are presented in the monolayer membrane work as a means to include crucial cellular proteins in membrane interaction studies. Although the work presented here did not offer strong conclusive evidence regarding polymer-membrane interactions, information regarding polymer effects on membrane phase behavior was obtained from combined Fluorescence microscopy-Langmuir trough experiments and by atomic force microscopy on supported monolayers.

*1.6.3 Model membrane stress*

Unlike cell membranes, which can remain intact even after considerable damage, due to heterogeneity and cytoskeleton support,[76] and are capable of signaling native self-healing pathways, single component model membranes are challenging to stress without inducing catastrophic structural failure. Difficulties for vesicle model membranes (i.e. liposomes) arise especially in the homogeneity of membranes and the high membrane tension coming as a result of the small radius of curvature.

One model membrane stress widely employed in biochemistry is that of lipid peroxidation.[105,108,130] By careful selection of phospholipids containing reactive unsaturation in the fatty acid tails, a controlled reaction can be carried out with the help of a free radical. Though the modes of membrane damage induced by lipid peroxidation are argued in the literature, the ability to control damage to the membrane chemically is a significant step forward. Chapter 3 will feature improvements on an existing liposome peroxidation technique , and Chapter 4 will further investigate the role of polymers in

mitigating damage by peroxidation, using dynamic light scattering (DLS) to assess the capacity for beneficial membrane interactions by block copolymers.

*1.6.4 Miscellaneous activities and collaborations*

As is the nature in all collaborative work, a number of side projects were undertaken to support the work of others. Though these were not stand-alone projects, an overview of two support activities, fluorescence tagging and blood viscosity studies, will be presented in Chapter 6, in the spirit of disclosing paths worth pursuing further and already pursued.

# Chapter 2

# Methods and materials

Several of the general techniques and underlying theory are collected here and described in detail. Direct applications of these techniques will be encountered in later chapters, as well as modifications or adaptations to fit a particular need. Polymers synthesis is described, and polymers prepared are tabulated here for reference. Additionally, liposome preparation and peroxidation methods are described, along with a basic overview of analytical techniques used to describe them (dynamic light scattering and static light scattering). Finally, a discussion of lipid monolayers and a theoretical background to the Langmuir trough is presented.

## 2.1 Polymer synthesis

Diblock copolymers of poly(propylene oxide) and poly(ethylene oxide) were prepared by sequential living anionic polymerizations of propylene oxide and ethylene oxide, respectively, according to established air-free and oxyalkane handling methods.[129,131] Initiation and propagation of propylene oxide occurs at the less substituted carbon in the epoxide ring, as demonstrated in Scheme 2.1, with potassium tert-butoxide as the initiator. The acidic methyl group on the monomer and the living polymer are capable of undergoing monomer or chain transfer reactions, as shown in Scheme 2.2, the effect of which is to terminate the living chain and simultaneously generate a new living chain without changing propagation kinetics.[124,132,133]

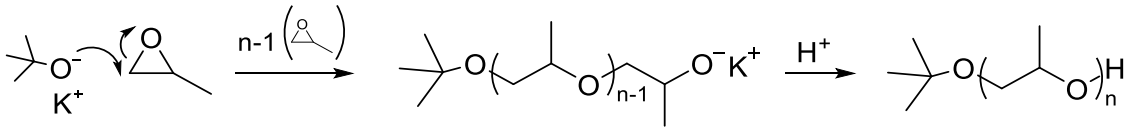

**Scheme 2.1:** Initiation, propagation, and termination of poly(propylene oxide) by living anionic polymerization.

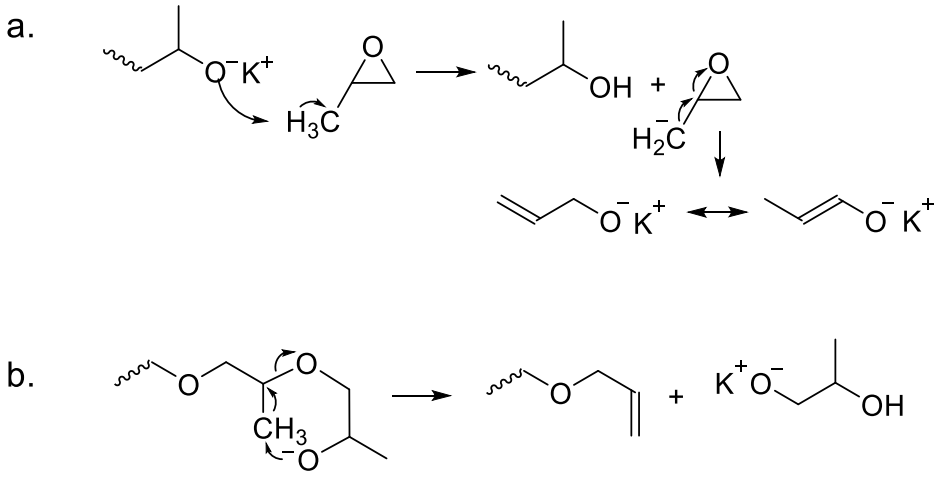

**Scheme 2.2:** Mechanism of chain transfer to monomer (a) and penultimate repeat unit (b).Chain transfer offers two side reactions propylene oxide can undergo that lead to broad molecular weight distribution and lower achievable molecular weights.

Without counteractive measures, the resultant poly(propylene oxide) is characterized by a broad distribution of low molecular weights. Ding, et al.[124–126] and others[132,134] have reported the successful use of 18-crown-6 ether, shown in Scheme 2.3, to favor the propagation step of poly(propylene oxide) by complexing with the potassium counter ion, leading to narrow dispersities at higher molecular weights. Complexation of the counter ion with the "crown" center of the crown ether forms ligand-separated ion pair aggregates that favor propagation kinetics.[124,135] Moreover, the catalytic effect of crown ether allows for reaction reduced temperatures, which is another strategy employed to discourage side reactions of propylene oxide.[132]

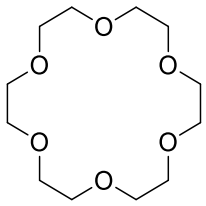

**Scheme 2.3:** 18-Crown-6 ether complexes with potassium counter ions and forms ion pair aggregates which favor propagation kinetics of living anionic polymerization.

A similar synthetic strategy was employed for an ethyl-substituted epoxide, 1,2-epoxybutane to form poly(1,2-butylene oxide) hydrophobic starting blocks. Poly(1,2-butylene oxide), or PBO, is significantly more hydrophobic than the similar poly(propylene oxide), so diblocks of PBO-PEO were prepared to study the effect of changing the hydrophobicity of the block copolymer chemically rather than compositionally. Chain transfer reactions to monomer or penultimate unit are similarly an issue for PBO, and 18-crown-6 ether is reported to improve dispersity and achievable degree of polymerization.[132]

Addition of a second, hydrophilic block, was carried out by reinitiating the mono-hydroxyl terminated hydrophobic starting block with potassium naphthalenide. De-protonated chains were then extended by living anionic polymerization of ethylene oxide, which ring-opens to form narrow dispersity diblock copolymers of controlled molecular weights. An example polymerization of ethylene oxide from a starting PPO block is shown by Scheme 2.4.

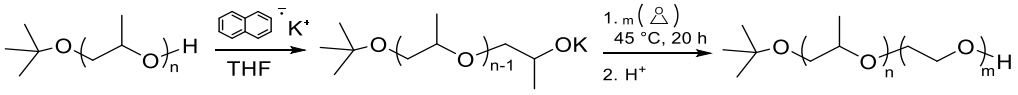


**Scheme 2.4:** Reinitiation of hydroxyl-terminated poly(propylene oxide), followed by living anionic polymerization of ethylene oxide and termination by acidic methanol to form a hydroxyl-terminated PPO-PEO diblock copolymer.

Diblock copolymer surfactants of PPO-PEO or PBO-PEO were prepared by living anionic polymerization in two steps, starting with the hydrophobic poly(propylene oxide) or poly(1,2-butylene oxide) block. Following an intermediate purification and characterization step, poly(ethylene oxide) was grown from starting blocks. Living anionic polymerization techniques require air and water free environments and handling that are described in greater detail elsewhere.[129,131]

*2.1.1 Hydrophobic block synthesis*

To begin, propylene oxide (≥99%, Sigma, atmospheric boiling point, 34 °C[136]) and 1,2-epoxybutane (1,2-butylene oxide, ≥99%, Sigma, atmospheric boiling point, 63 °C[137]) were purified for living anionic polymerization according to standard techniques. First, monomer was degassed by two freeze-pump-thaw cycles before distilling onto dried n-butyllithium.[138] Thawed monomer was stirred at 0 °C over n-butyllithium for 30 minutes before distilling onto fresh n-butyllithium for a second stirring step. Purified monomer was transferred to flame-dried burettes by vacuum distillation, and massed. Ready burettes were held on ice until needed, and two final freeze-pump-thaw cycles were performed on burettes just before connecting to the reactor by flexible stainless steel tubing (Swagelok).

Prior to hydrophobic block synthesis, as-received 18-crown-6 ether (Sigma) was freeze-dried from a 10 vol.-% solution in benzene and massed. An amount corresponding to a 2:1 molar ratio of crown ether to initiator was added to a waiting solvent flask in an argon environment, which was then evacuated and filled with the necessary volume of alumina column-dried tetrahydrofuran to achieve a monomer solution concentration of approximately 10 wt.-% in the reactor. The headspace of the solvent flask was charged with argon at 3 psig.

For synthesis, a 1 L glass reactor with threaded ports was equipped with a glass covered magnetic stir bar, thermocouple port, the sealed flask containing 18-crown-6 ether in tetrahydrofuran, the sealed monomer burette, a glass plug, and a manifold outfitted with

a Teflon-coated silicone septum (SGE) and connected by flexible stainless steel tubing to both a Schlenk line and a pressure gauge with a pressure relief valve set at 10-15 psi (Swagelok) by Ultra Torr vacuum fittings (Swagelok). Teflon ferrules and nylon bushings (ACE Glass) were used to secure each glass connection. The setup was cycled between vacuum and 3 psi argon, with flame heating on reactor walls during evacuation to remove adsorbed water. After the final argon fill, the solvent flask was opened, and 18-crown-6 ether and tetrahydrofuran were emptied into the reactor.

To start the reaction, a known volume of 1.0 M potassium tert-butoxide in tetrahydrofuran was added by syringe to the reactor, through the rubber septum in the manifold, and the mixture was stirred on an ice for 30 minutes to slow and counter the exothermic reaction. Next, monomer was added by burette. The reaction mixture was stirred for 48 hours and allowed to warm up to ambient temperature from ice bath temperatures following initiation. The reaction was terminated by excess acidic methanol (1:10 37 w/w% hydrochloric acid:methanol), degassed by bubbling with argon for thirty minutes. Potassium and crown ether complexes were removed by iterative filtration, solvent removal, and dissolution in fresh tetrahydrofuran until a clear solution was obtained. The final solvent removal step was finished overnight with stirring, and the resultant (clear liquid) mono-hydroxyl terminated poly(propylene oxide) or poly(1,2-butylene oxide) was characterized by SEC and $^{1}$H NMR.

*2.1.2 Hydrophilic block addition*

Following molecular characterization of the starting hydrophobic blocks, poly(ethylene oxide) blocks were grown by reinitiating from the terminal hydroxyl group using potassium naphthalenide.[131] Potassium naphthalenide was prepared in tetrahydrofuran dried over two successive columns of activated alumina. For the reaction, potassium (freshly cut under cyclohexane) was added under argon purge to a dried, tared flask equipped with a glass-covered stirbar. The flask was sealed and dynamic vacuum was applied to remove residual solvent. After massing under static vacuum, tetrahydrofuran was added, followed by with a 10% molar excess of naphthalene (relative to potassium mass) under positive argon pressure. The solution turned a vibrant green almost

immediately on addition of naphthalene and was stirred for a minimum of 12 hours before reinitiation.

Ethylene oxide monomer (≥99.5%, Sigma, atmospheric boiling point, 10.7 °C[139]) was purified as for propylene oxide and 1,2-epoxybutane, with additional care to maintain temperatures below the atmospheric boiling temperature to prevent closed glassware from rupturing. Briefly, ethylene oxide monomer was transferred by vacuum distillation into a flame-dried and vacuum evacuated flask. Frozen monomer was thawed on an ice water bath and degassed by two freeze-pump-thaw cycles. Vacuum distillation onto dried n-butyllithium, followed by stirring on an ice bath was carried out twice, and purified monomer was stored on a salt-ice-water bath until needed.

For poly(ethylene oxide) synthesis, a glass air-lock was added to the reactor assembly to isolate the contents from air prior to gaseous monomer addition by stainless steel flexible tubing. To begin, mono-hydroxyl terminated poly(propylene oxide) or poly(1,2-butylene oxide) was added to a tared reactor with a glass covered stirbar and stirred under dynamic vacuum overnight. The final mass was recorded before addition of a volume of dry tetrahydrofuran under positive argon pressure sufficient to achieve approximately 10 wt.-% polymer and monomer in solvent. Tetrahydrofuran was added under argon to the hydrophobic starting block and stirred to dissolve while heating to 45 °C with a water bath. Argon pressure was relieved to 3 psi upon equilibration at 45 °C.

During reactor heating, a burette containing ethylene oxide monomer was degassed once more by freeze-pump-thaw, before being attached by flexible stainless steel tubing to the airlock. Air space in the tubing was cycled between 3 psi argon and vacuum six times. After thermal equilibration of the polymer and solvent solution at 45 °C, potassium naphthalenide was slowly titrated through the septum by plastic syringe until a transparent green color persisted for more than 30 minutes. The syringe was left in the septum for the duration of reinitiation to minimize the possibility of introducing air. Following 30 minutes of stirring at the final titration, the potassium naphthalenide syringe was removed, and dynamic vacuum to the flex-tubing on the burette was closed off (static vacuum). Next, the stopcock separating reactor from airlock was opened to equilibrate argon pressure in the tubing, and finally, the stopcock to the thawed ethylene oxide monomer on ice/water bath

was opened slowly. Reactor pressure was monitored during slow addition of ethylene oxide, and pressure increases of about 4 psi (maximum gauge pressure 7 psi) were allowed before cooling the monomer back down in the ice bath. Total addition time varied by amount of monomer added, but batches of 10-20 g of ethylene oxide typically took in excess of 30 minutes.

Following completion of monomer addition, the empty burette was left open to the reactor for overnight reaction. The completed reaction was terminated 20 hours later using an excess of acidic methanol solution, degassed by bubbling with argon for 30 minutes. The reactor was vented following one hour of stirring, and diblock copolymer was recovered by solvent removal. Dried polymer was dissolved in chloroform and filtered through paper to remove potassium salts, and dried. For sufficiently large diblock copolymers ($\geq$ 3,000 g/mol), dialysis was performed to remove trace naphthalene: polymer was dissolved to 10 wt.-% in chloroform and dialyzed against chloroform in 2,000 MWCO benzoylated cellulose dialysis tape (Sigma), with three or more total solvent changes made at hourly intervals. Dialyzed diblock copolymers were dried with stirring before freeze-drying from benzene.

*2.1.3 Statistical copolymers*

In addition to diblock copolymers, statistical copolymers comprised of ethylene oxide and propylene oxide or propylene oxide and 1,2-epoxybutane repeat units were prepared. Reactions were initiated by potassium tert-butoxide in tetrahydrofuran with 2:1 crown ether:initator. Ethylene oxide containing copolymers were prepared at 40 °C, whereas 1,2-epoxybutane containing polymers were carried out starting at 0 °C and allowed to warm to 25 °C. Reactions proceeded for 40 hours before termination by excess acidic methanol. Final polymers were purified by successive dissolution in THF and filtration through paper, and finally freeze-drying from benzene. SEC was used to quantify dispersity, and molecular weight and final composition were checked by $^{1}$H NMR.

*2.1.4 Reverse diblocks: effect of end groups*

To study the relative impact of the terminal functional groups on the hydrophobic PPO block on membrane association and stabilization, diblock copolymers (OH-PPO-PEO) were prepared from a mono-functional PEO by reinitiation of the terminal hydroxyl group

by potassium naphthalenide, as shown in Scheme 2.5, followed by PPO addition and termination by a hydroxyl group on PPO. Two mono-methoxy poly(ethylene oxide) polymers (mPEO) were purchased from Sigma Aldrich and characterized by SEC and $^{1}$H NMR to check dispersity and verify labeled molecular weights. Polymers were freeze-dried from benzene to remove trace water. Purification of propylene oxide was carried out in the usual manner. Reinitiation of the terminal hydroxyl group on mPEO was performed using potassium naphthalenide in tetrahydrofuran at 40 °C. Following addition of propylene oxide, the reaction was stirred and allowed to proceed for about 20 hours before termination by acidic methanol.

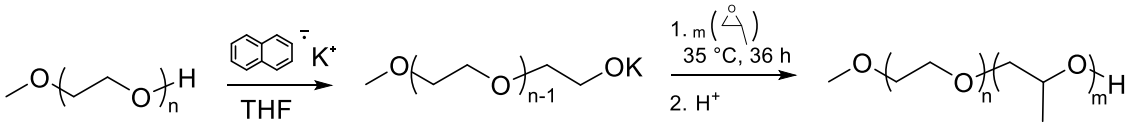


**Scheme 2.5:** Reinitiation of hydroxyl-terminated poly(ethylene oxide), followed by living anionic polymerization of propylene oxide and termination by acidic methanol.

In a second synthetic attempt, crown ether was added along with the solvent in an effort to increase conversion. Tetrahydrofuran was collected on freeze-dried crown ether in a 2:1 molar ratio and added to freeze-dried mPEO under positive argon pressure with stirring. Potassium naphthalenide was again used to initiate chains, and the reaction temperature was reduced to 30 °C to slow immediate initiation. Following a thirty minute reinitiation time, the temperature was increased to 35 °C, where it was maintained for the remainder of the reaction. Reaction time was extended to about 45 hours, and to minimize risk of contamination by air, a kinetic study was not performed. Living chains were again terminated by acidic methanol.

Both batches of synthesized OH-PPO-PEO diblock copolymers were filtered through paper in tetrahydrofuran to remove salt precipitates and crown ether, if applicable. Tetrahydrofuran was removed by rotary evaporation, and dissolution, filtration, and evaporation steps were repeated once more. Dried polymers were dissolved in dichloromethane and washed against distilled water in multiple water changes with mild agitation, as PEO-PPO diblock copolymers readily partition into the aqueous phase. Following the final water wash, the organic phase was dried by rotary evaporation. The

polymer films were dissolved in benzene and freeze-dried in a vacuum oven for several days to remove traces of solvent and naphthalene.

Final purification was performed by dialysis against chloroform to remove all remaining salts, crown ether (if applicable), and naphthalene. Polymers were dissolved in chloroform at a concentration of about 0.2 g/mL and placed in 2,000 MWCO benzoylated cellulosic dialysis tubing (Sigma). Samples were dialyzed in about 400 mL of chloroform with gentle stirring and four solvent changes over 24 hours. Dialyzed polymers were dried by rotary evaporation and freeze-dried from benzene. Yields were lower for low molecular weight polymers near the tubing molecular weight cutoff, due to diffusion through the membrane. To improve yield, biological grade cellulose ester tubing (100-500 g/mol MWCO) could be used, however aqueous dialysate must be substituted for chloroform, as cellulose ester is incompatible with organic solvents. Polymers could be dried by lyophilization to remove water.

A brief note regarding the two synthetic schemes employed here. Reinitiation of hydroxyl-terminated polymers by potassium naphthalenide for anionic ring-opening polymerization is the preferred technique for reinitiation of hydroxyl-terminated polymers for the ring opening polymerization of ethylene oxide. Part of the reason for this is the absence of byproducts besides naphthalene and dihydronaphthalene.[131] The polymerization carried out in the absence of crown ether was intended to determine whether naphthalene could sufficiently complex with potassium to add propylene oxide units. Although a kinetic study was not performed, PO conversions were calculated to be about 65% and 45%, for the 2,000 g/mol and 5,300 g/mol mPEO starting blocks, respectively. Despite poor conversions, dispersities remained narrow. Because crown ether has been reported to increase kinetics of propylene oxide addition,[124] a subsequent reaction was carried out with crown ether at an extended reaction time, which brought PO conversions to 91% and 87% of expected degrees of polymerization for 2,000 g/mol and 5,300 g/mol mPEO starting blocks, respectively.

## 2.2 Polymer characterization

Starting block molecular weights and dispersities were determined by $^1$H NMR and SEC, respectively. To determine molecular weights, end group analysis and peak integration was performed on the $^1$H NMR spectrum of a 10 mg/mL solution of polymer in deuterated chloroform ($CDCl_3$, Cambridge Isotope Laboratories). Spectra were obtained on a 500 MHz Varian Inova or a Bruker AV-500 NMR. An acquisition time of 5 s and a delay time of 20 s were chosen to ensure chain relaxation between pulses, for a minimum of 16 scans in $^1$H NMR. Sample $^1$H NMR spectra for poly(propylene oxide) and poly(1,2-butylene oxide) are given in Figure 2.1 and Figure 2.2, along with proton assignments.

Molecular weights for parent PPO blocks were calculated from end group analysis of $^1$H NMR spectra, using peak integrations for the *t*-butyl end group ($\delta \approx 1.19$, s) and the methyl protons at ($\delta = 1.13$-$1.15$, t).

Similarly, molecular weights and compositions for diblock copolymer species were determined by $^1$H NMR. The *t*-butyl end groups provided strong signal ($\delta \approx 1.19$ ppm) from which to base compositional calculations. A representative $^1$H NMR from obtained for diblock poly(propylene oxide)-*b*-poly(ethylene oxide) sample t-P0.9-E2.1 (sample details listed in Table 2.1) is shown with proton assignments in Figure 2.3.

Overlays of $^1$H NMR spectra obtained for a parent block of mono-methoxy polyethylene oxide (mE5.3) and a daughter diblock OH-PPO-PEO (OH-P1.9-E5.3) are shown in Figure 2.4. The peak at $\delta = 3.35$ ppm corresponds to the methoxy end group on the parent block. After growth of the PPO block, two broad peaks appear around $\delta = 3.5$ ppm, obscuring the methoxy proton peak. Molecular weights of OH-PPO-PEO diblock copolymers were calculated from the molecular weight of the parent block and the methyl peaks at $\delta = 1.2$ ppm.

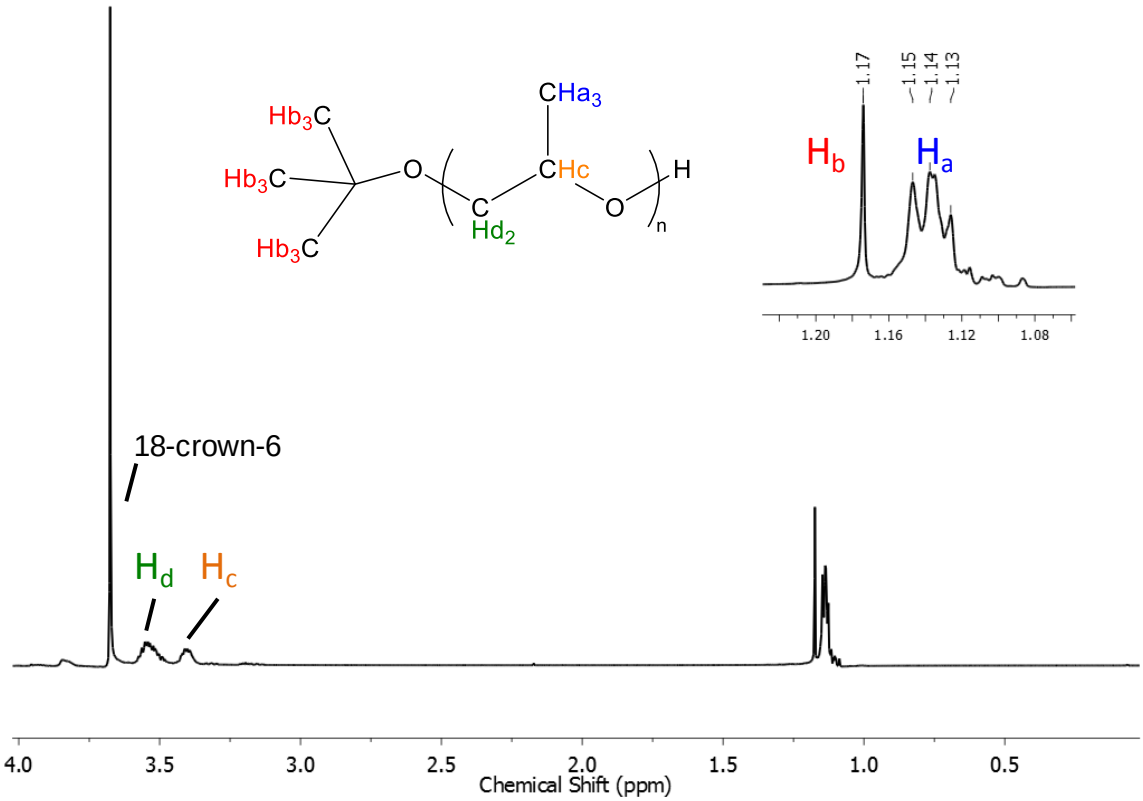


**Figure 2.1:** $^{1}$H NMR spectra obtained for t-poly(propylene oxide) with proton assignments. Peak at $\delta$ = 3.7 ppm corresponds to 18-crown-6 ether residue. Presence of 18-crown-6 in starting block did not alter reactivity of ethylene oxide, but lead to slight discrepancies in expected compositions. Furthermore, residual 18-crown6 ether was removed by dialysis of diblock copolymers.

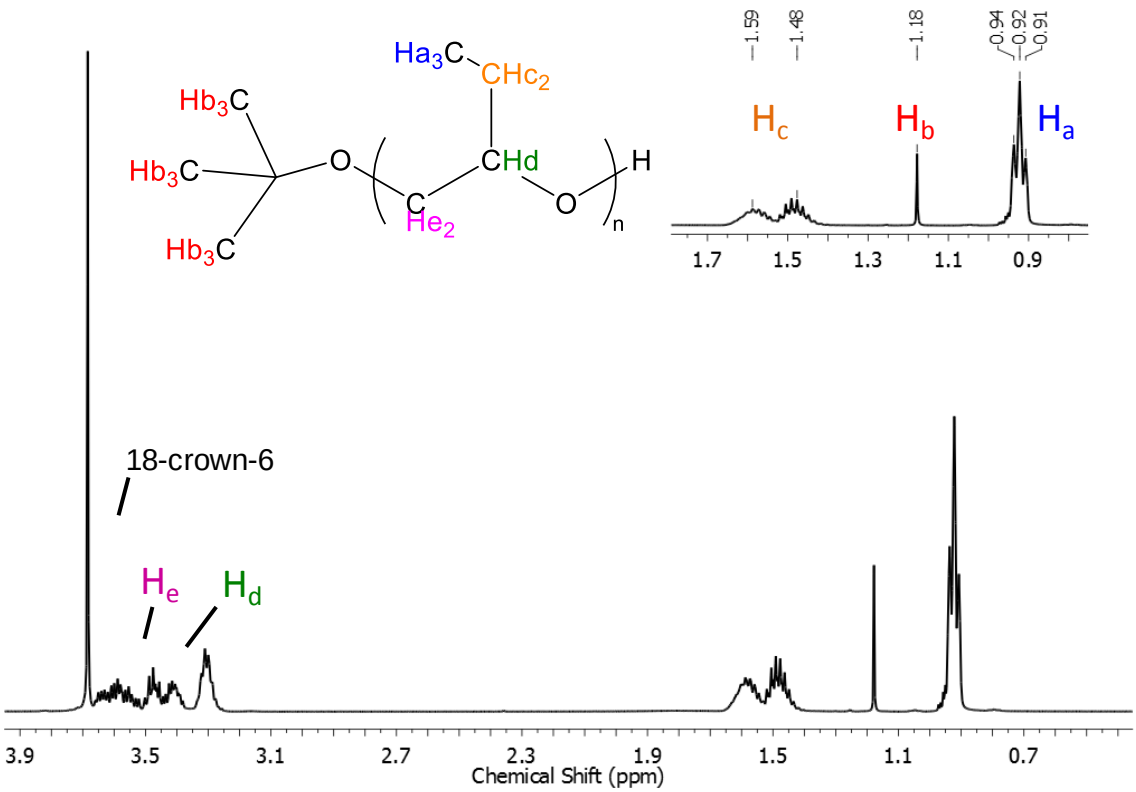


**Figure 2.2:** $^{1}$H NMR spectrum for representative poly(1,2-butylene oxide) with proton assignments. 18-crown-6 ether is again present in the spectrum but is removed by dialysis after growth of second hydrophobic block.

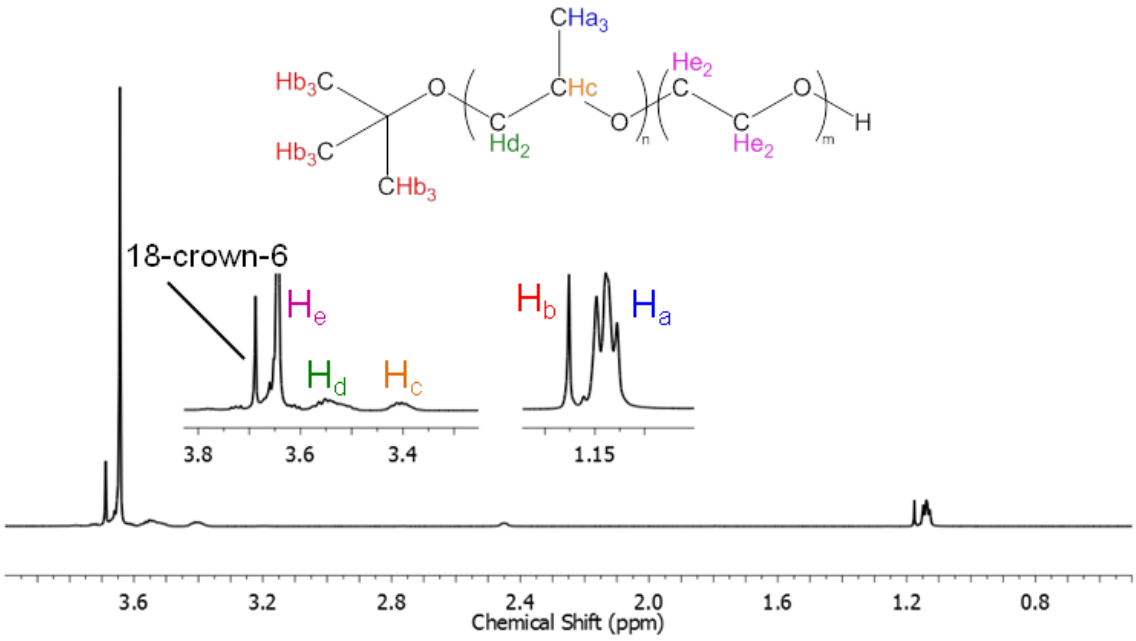


**Figure 2.3:** Diblock copolymer poly(propylene oxide)-poly(ethylene oxide) and accompanying proton assignments**.**

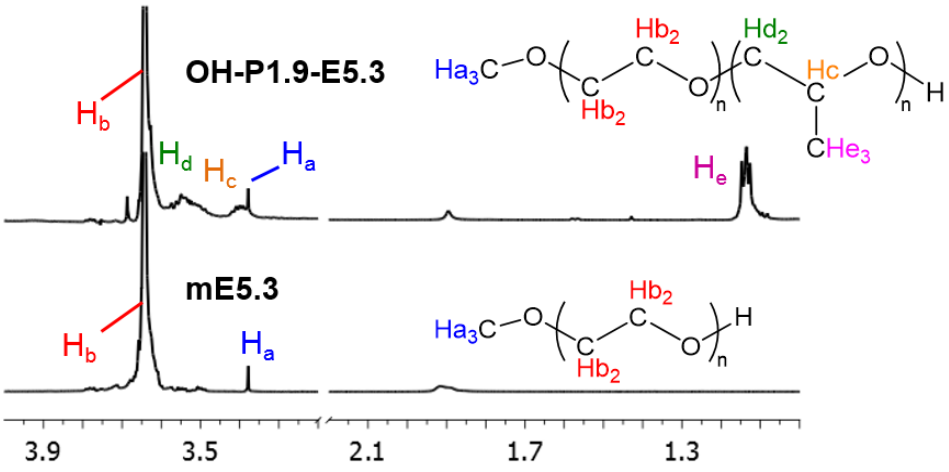


**Figure 2.4:** Overlays of $^{1}$H NMR spectra for mE5.3 and OH-P1.9-E5.3 show appearance of PPO backbone peaks around 3.5 ppm and methyl protons at δ = 1.2 ppm. The break corresponds to a flat baseline. Small peaks around δ = 1.9 ppm correspond to residual tetrahydrofuran.[140]

*2.2.1 Tert-butyl functional homopolymer and diblock copolymers*

Homopolymer and diblock copolymer molecular weight distributions and dispersities were determined by size exclusion chromatography (SEC) with tetrohydrofuran as the effluent and polystyrene standards. Representative SEC plots are provided for a series of t-PPO polymers in Figure 2.5: t-P0.9, t-P0.9-E2.1, and t-P0.9-E8.0. Data were normalized to account for concentration variation and arbitrarily shifted along the *y*-axis. Larger molecular weights correspond to lower elution volumes.

Molecular characteristics for all tert-butyl- functional homopolymers of PBO and PPO, as well as corresponding diblock copolymers are summarized in Table 2.1. Sample nomenclature is as follows: "B," "P," and "E," signify repeat units 1,2-butylene oxide, propylene oxide, and ethylene oxide, respectively. Numerals following each block designation indicate molecular weight of that block in units of kg/mol. Polymers showed narrow dispersities and diblock copolymer compositions ranged from about 60 to 90% by weight PEO for PPO diblocks and 40-60% for PBO diblocks.

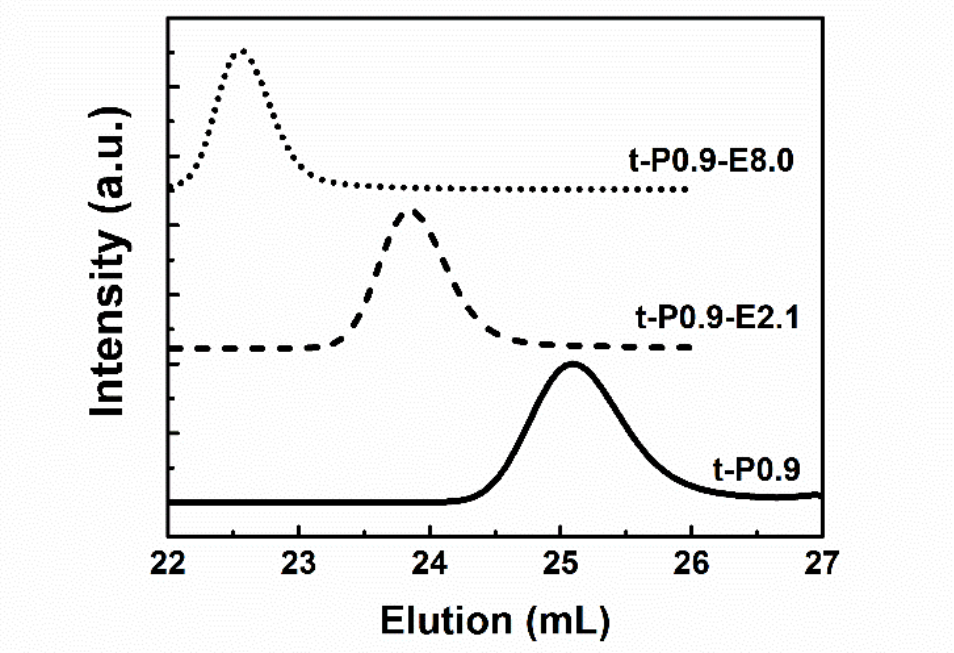


**Figure 2.5:** SEC traces for parent poly(propylene oxide), t-P0.9 and diblock copolymers grown from it, t-P0.9-E2.1 and t-P0.9-E8.0.

**Table 2.1:** Homopolymers and diblock copolymers prepared from a tert-butyl initiator in this work.

| **Polymer** | $M_n$[a] (kg-mol$^{-1}$) | $N_{PO}/N_{BO}$ | $N_{EO}$ | $Đ$[b] | $w_{PEO}$[a] |
|---|---|---|---|---|---|
| Poly(propylene oxide) | | | | | |
| P0.9 | 0.9 | 16 | - | 1.08 | - |
| P0.9-E2.1 | 3.0 | 16 | 48 | 1.05 | 0.70 |
| P0.9-E8.0 | 8.9 | 16 | 182 | 1.04 | 0.90 |
| P1.2 | 1.2 | 21 | - | 1.08 | - |
| P1.2-E1.9 | 3.1 | 21 | 43 | 1.04 | 0.61 |
| P2.9 | 2.9 | 49 | - | 1.12 | - |
| P2.9-E3.8 | 6.7 | 49 | 87 | 1.09 | 0.57 |
| Poly(1,2-butylene oxide) | | | | | |
| B2.3 | 2.3 | 32 | - | 1.06 | - |
| B2.3-E1.3 | 3.6 | 32 | 30 | 1.07 | 0.36 |
| B2.3-E3.5 | 5.8 | 32 | 80 | 1.04 | 0.60 |
| B3.0 | 3.0 | 42 | - | 1.05 | - |
| B3.0-E4.2 | 7.2 | 42 | 96 | 1.03 | 0.58 |
| B4.8 | 4.8 | 67 | - | 1.04 | - |

[a]Determined by end group analysis in $^1$H NMR.

[b]Obtained from SEC.

*2.2.2 Statistical copolymers*

Three statistical copolymers were synthesized to demonstrate the method as a possible route for future studies in tuning hydrophobicity of the hydrophobic block; i.e. reduce hydrophobicity of a component by including a less hydrophobic repeat unit in its chain. Statistical copolymers prepared are summarized in Table 2.2, where nomenclature now reflects the molar composition of the more hydrophobic group, followed by total molecular weight in kg/mol (i.e. EB08-9.4 is 8% butylene oxide repeat units, total molecular weight of 9.4 kg/mol).

**Table 2.2:** Statistical copolymers prepared from propylene oxide (P), butylene oxide (B), and ethylene oxide (E). Molecular weight, dispersity, weight fraction of ethylene oxide, and mole fractions of butylene oxide and propylene oxide are listed as well.

| **Sample Name** | **$M_n$[a] (g/mol)** | **Đ[b]** | **$w_{PEO}$[a]** | **$x_{BO}$[a]** | **$x_{PO}$[a]** |
|---|---|---|---|---|---|
| EP08-9.4 | 9,400 | 1.03 | 0.89 | - | 0.08 |
| EB10-10.4 | 10,400 | 1.03 | 0.84 | 0.10 | - |
| PB50-4.4 | 4,400 | 1.06 | - | 0.50 | 0.50 |

[a]Determined by end group analysis in $^1$H NMR

[b]Obtained from SEC

*2.2.3 Hydroxyl-terminated PPO diblock copolymers*

The block copolymers prepared from mono-methoxy terminated PEO are shown in SEC traces in Figure 2.6. Again, distributions have been normalized to account for concentration variations, and peaks show uniform breadth. Molecular properties of OH-PPO-PEO diblock copolymers obtained by $^1$H NMR and SEC are compiled in Table 2.3 for convenience. Polymers showed narrow dispersities with diblock compositions ranging from about 70 to 90% by weight PEO, well within expected range of solubility and effective membrane stabilization.[89]

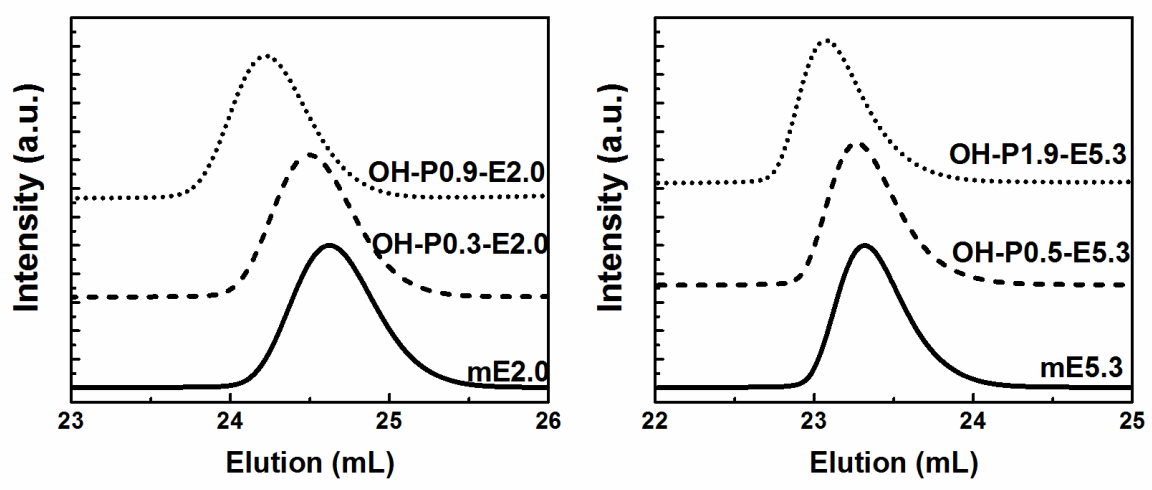


**Figure 2.6:** SEC traces for mono-methoxy functionalized poly(ethylene oxide), mE2.0, and two diblock copolymers synthesized from the parent block, OH-P0.3-E2.0 and OH-P0.9-E2.0.

**Table 2.3:** Summary of diblock copolymers with hydroxyl-terminated PPO blocks synthesized. Repeat units of PPO and PEO are designated by "P" and "E," respectively.

| **Polymer** | | $M_n$[a] **(kg/mol)** | $N_{PO}$ | $N_{EO}$ | $Đ$[b] | $w_{PEO}$[a] |
|---|---|---|---|---|---|---|
| mE2.0* | | 2 | - | 46 | 1.04 | 1 |
| | OH-P0.3-E2.0 | 2.3 | 5 | 46 | 1.05 | 0.87 |
| | OH-P0.9-E2.0 | 2.9 | 16 | 46 | 1.03 | 0.70 |
| mE5.3* | | 5.3 | - | 120 | 1.03 | 1 |
| | OH-P0.5-E5.3 | 5.8 | 9 | 120 | 1.04 | 0.91 |
| | OH-P1.9-E5.3 | 7.2 | 32 | 120 | 1.03 | 0.74 |

*Purchased from Sigma

[a]Determined by end group analysis in $^1$H NMR

[b]Obtained from SEC

Many of the polymers prepared were used for various experiments in the chapters of this thesis, though some were not pursued beyond preliminary studies (e.g. poor aqueous solubility). The full library is presented as a reference for future studies, and each chapter will specifically refer to polymers used within.

## 2.3 Liposome model membranes

### *2.3.1 Liposome preparation*

Liposomes were prepared according to standard methods described in detail elsewhere.[141–143] Briefly, 6:3:1 molar ratio mixtures of POPC:PLPC:PLPG phospholipids in chloroform (10 mg/mL) were prepared and dried into a thin film in a conical vial under a weak stream of compressed air. Films were dried further under vacuum for one hour to ensure all traces of chloroform were removed. Dried phospholipid films were hydrated with ultrapure water with a resistivity of 18.2 MΩ·cm from a Millipore Direct Q-3 water system (EMD Millipore, Billerica, MA). Hydrated phospholipid films (10 mM in lipids) were heated above 37 °C and vortex-mixed to yield a homogeneous opaque suspension of multilamellar vesicles. Suspensions were extruded nineteen times through a 100 nm polycarbonate filter using an Avanti Mini-Extruder, also heated above 37 °C.[141–143] Large unilamellar vesicles (LUVs) produced were stored at 4 °C for up to 1 week, and were characterized by dynamic light scattering (DLS) to determine hydrodynamic radius, $R_h$, and distribution width, (dispersity, $\mu_2/\Gamma^2$).

### *2.3.2 Liposome peroxidation*

Model membranes were subjected to oxidative stress by way of a peroxidation reaction well-documented in the literature.[104,107,108,114,144] The azo compound, 2,2'-azobis(2-amidinopropane) dihydrochloride, a water-soluble free radical generator with well-known kinetics of disassociation has been favored for reproducibility and steady free radical generation within experimental time frames.[108,145] Initiation at 37 °C and 254 nm light conditions is first order and follows the reaction shown in Scheme 2.6.

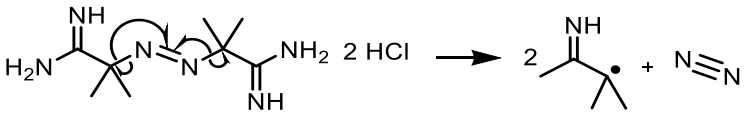

**Scheme 2.6:** AAPH initiation generates two free radicals.[108]

Peroxidation reactions were carried out at phospholipid and AAPH concentrations of 25 μM and 15 mM, respectively. To investigate the role of lipid-polymer interactions in protection against liposome peroxidation, aqueous solutions of polymers were prepared in stock concentrations, filtered to remove dust, and added to liposome-containing reaction volumes in a five times molar excess to phospholipid concentration, unless otherwise indicated. Protection against liposome peroxidation by polymers was tested by introducing AAPH after polymer-liposome incubation times of 0, 4, or 24 hours. The 4 and 24 hour incubation times were chosen to look for temporal effects of polymer interactions, such as destructive membrane disruption. Following polymer incubation, liposome peroxidation reactions were carried out in glass vials for 30 minutes at 37 °C and under UV light at $\lambda$ = 254 nm. Immediately following reactions, sample volumes were quenched to 25 °C by five-fold dilution in ultra-pure water, and scattering was performed to assess liposome population characteristics.

## 2.4 Dynamic Light Scattering

Characterization of liposome size distributions was performed at dilute concentrations by dynamic light scattering (DLS) on a Brookhaven BI-200SM DLS (Brookhaven Instruments Corporation, Holtsville, NY) at a 90° scattering angle, using a 633 nm HeNe laser operating at 20 mW. Prior to experiments, decahydronaphthalene (decalin) in the sample cell was pumped through a filter for 10 minutes to remove dust, and additional solvent was added if needed. Decalin is used for refractive index ($n_D$) matching with glass sample holders, which for this work were 20 mL glass scintillation vials. Interior surfaces of the vials were cleaned prior to scattering with filtered acetone and agitation and allowed to dry. Immediately before measurements, the outside surfaces of the vials were cleaned with methanol and a lint-free wipe and allowed to dry.

Prepared liposomes (stock concentration, 10 mM phospholipid in ultrapure water) were diluted to a final concentration of 5 μM in a 10 mL scattering volume. Scattering

experiments were performed for 10 minutes, from 1 μs to 1 s delay times. Autocorrelation functions obtained from DLS were fit by the method of cumulants to determine liposome size and distribution characteristics.[146–148]

For a system of small, non-interacting particles exhibiting Brownian behavior, scattered light intensity fluctuations can be correlated in time by the photodetector of the DLS. From signal correlations, sample-specific information about particle diffusion and characteristic sizes may be derived.[148] The intensity correlation function obtained from the DLS, $g^{(2)}(\tau)$ for scattered intensity, *I*, at time *t* and delay times of $\tau$ is given by Equation 2.1:

$$g^{(2)}(\tau) = \langle I(t) I(t+\tau) \rangle \tag{0.1}$$

This correlation function can be related to the field correlation function, $g^{(1)}(\tau)$, by way of the Siegert relation, which is explained in detail elsewhere.[146,147,149] Except in cases of few scatterers or non-ergodic systems, the Siegert relationship generally holds, and is given by Equation 2.2:

$$g^{(2)}(\tau) = I_0{}^2 \left(1 + \gamma g^{(1)}(\tau)^2\right) \tag{0.2}$$

where $I_0{}^2$ is the square of the average intensity detected and $\gamma \approx 1$. For a dilute, monodisperse sample of rigid, globular scatterers, the first order autocorrelation function is given by the exponential decay in Equation 2.3:

$$g^{(1)}(\tau) = \exp(-\Gamma \tau) \tag{0.3}$$

where $\Gamma$ is the decay rate, defined by Equation 2.4:

$$\Gamma = Dq^2 \tag{0.4}$$

and *D* and *q* are the translational diffusion coefficient and magnitude of the scattering vector, respectively. For reference, *q* is defined in Equation 2.5, with *n* being the refractive index of the solvent, $\lambda_0$ the wavelength of the incident light, and $\theta$ the scattering angle.

$$q = \frac{4\pi n}{\lambda_0} \sin\left(\frac{\theta}{2}\right) \tag{0.5}$$

In a sample of polydisperse particles, a continuous, normalized distribution of decay rates is used to describe the field correlation function. The distribution is given by Equation 2.6:

$$g^{(1)}(\tau) = \int_0^\infty G(\Gamma)\exp(-\Gamma\tau)\,\mathrm{d}\Gamma \tag{0.6}$$

where

$$\int_0^\infty G(\Gamma)\mathrm{d}\Gamma = 1. \tag{0.7}$$

By executing series expansions and simplifications, the distribution in Equation 0.6 can be expressed in its cumulant form, shown in Equation 2.8.

$$g^{(1)}(\tau) = A\exp(-\Gamma\tau)\left(1 + \frac{\mu_2}{2!}\tau - \frac{\mu_3}{3!}\tau^2 + \cdots\right) + B \tag{0.8}$$

Here $\mu_i$ are the $i^{th}$ moments of the distribution, and $A$ and $B$ are fitting parameters. Combining the Seigert relation (Equation 0.2) and Equation 0.8, experimentally obtained intensity field correlations were fit for $A$, $B$, $\Gamma$, and $\mu_2$, using a nonlinear least squares fitting algorithm (Levenberg-Marquardt) in MATLAB. The third moment of the distribution, $\mu_3$, was only considered when fitting of the second moment was insufficient (arbitrary cutoff, sum of squares $\geq 0.2$). The functional form is shown in Equation 2.9.

$$g^{(1)}(\tau)^2 = A\exp(-2\Gamma\tau)\left(1 + \frac{\mu_2}{2!}\tau - \frac{\mu_3}{3!}\tau^2 + \cdots\right)^2 + B \tag{0.9}$$

From the cumulant fitting, $\Gamma$ and $\mu_2$ were used to determine particle size distribution characteristics. The translational diffusion coefficient $D$ was determined from the definition of $\Gamma$ in Equation 4 and experimental parameters. It was then substituted into the Stokes-Einstein equation (Equation 2.10) to determine the hydrodynamic radius, $R_h$, of an assumed spherical geometry. The Stokes-Einstein equation is given by:

$$D = \frac{k_B T}{6\pi\eta R_h} \tag{0.10}$$

where $k_B$ is the Boltzmann constant, $T$ is absolute temperature, and $\eta$ is solution viscosity. Further analysis of DLS data is treated in Chapters 3 and 4, specifically with regard to scattered light intensity and multi-angle DLS measurements.

## 2.5 Static light scattering

Static light scattering (SLS) is often employed in determination of the weight average molecular weight, $M_w$, and radius of gyration, $R_g$, for polymers in solution.[150] A brief treatment of the theory of light scattering is presented here, and the interested reader is directed to Hiemenz and Lodge for a rigorous derivations from basic principles.[150] The most basic form of light scattering from a dilute polymer solution (valid for $qR_g \rightarrow 0$) is given by the Equation 2.11

$$R_\theta = KcM\left\{1 - 2BcM\cdots\right\} \tag{0.11}$$

where $c$ is concentration, $B$ is the second virial coefficient, $M$ is molecular weight, and $R_\theta$ and $K$ are defined by Equations 2.12 and 2.13, respectively. The Rayleigh ratio, $R_\theta$ is the normalized scattered intensity per unit volume:

$$R_\theta \equiv \frac{I_{ex} r^2}{I_o} \tag{0.12}$$

where $I_{ex}$ is the excess scattering, or scattering due to concentration fluctuations, $r$ is a distance, and $I_o$ is the incident scattered intensity. Units of $R_\theta$ are inverse length. The variable $K$ in Equation 0.11 is a collection of optical terms:

$$K \equiv \frac{4\pi^2 n^2 \left(\partial n / \partial c\right)^2}{\lambda_0^4 N_{av}} \tag{0.13}$$

where $n$ is refractive index, $\lambda_0$ is wavelength of incident light, and $N_{av}$ is Avagadro's number. The variable $\partial n/\partial c$ is the refractive index increment, which is sample specific and may be experimentally determined by a differential refractometer.

To account for the finite size of a polymer, a form factor is added. The form factor, $P(\theta)$, is the ratio of actual ($I_{ex}$, excess scattering) to theoretical (Rayleigh) excess scattered intensity, quantifying the net reduction in scattered intensity caused by phase differences between light scattered from different monomers along the polymer chain. For sufficiently small $qR_g \leq 1$ (Guinier regime), the form factor is given by Equation 2.14:

$$P(q) = 1 - \left(\frac{q^2}{3}\right) R_g^2 + \cdots \tag{0.14}$$

where higher order terms are negligible. A plot of $1/I_{ex}$ versus $q^2$ should be linear, with slope $R_g^2/3$. Another common alternative is the Guinier plot, which is $\ln(I_{ex})$ versus $q^2$, with a slope of $-R_g^2/3$. The resultant $R_g$ determined is shape-independent.[150]

Molecular weight determination by SLS is complicated by the refractive index increment. Combining the polymer scattering equation (Equation 0.11) and the form factor (Equation 0.14) and rearranging gives the Zimm equation, which can be used to experimentally determine molecular weight and $R_g$, by performing scattering at multiple concentrations and scattering angles. The Zimm equation is shown by Equation 2.15:

$$\frac{Kc}{R_\theta} = \frac{1}{M_w}\left(1 + \frac{q^2}{3} R_g^2 + \cdots\right) + 2Bc + \cdots \tag{0.15}$$

The technique is also useful for investigating micellization behavior by block copolymers, as aggregates will have characteristic rise in $M_w$ as compared to unimers; an aggregation number can be determined by taking the ratio of aggregate $M_w$ to unimer $M_w$.[151]

## 2.6 Langmuir trough and lipid monolayers

Phospholipid-based monolayers are typically prepared from a synthetic phospholipid (or purified extracted phospholipid) dissolved in some organic solvent or alcohol and applied directly to the surface of water or buffer contained in a Langmuir trough, illustrated schematically in Figure 2.7. Following solvent evaporation, a monolayer of amphiphilic phospholipids remains at the interface. Arrangement of the lipids on the interface is manipulated by way of movable barriers that can be used to change the available area on which lipids may pack and order.[152] Restrictions on available surface area encourage

phospholipid packing at the interface to become more and more ordered, and ensuing thermodynamic phase transitions lead to an increase in lipid surface activity. These thermodynamic phases serve as a two-dimensional analog to ideal gases in three dimensions. In the limit of an ideal gas, molecules are so far apart they have no interaction with neighboring molecules. Increased packing density induces higher order: liquid, followed by solid. Similarly, lipids are described by gaseous, liquid, and solid-like phases.

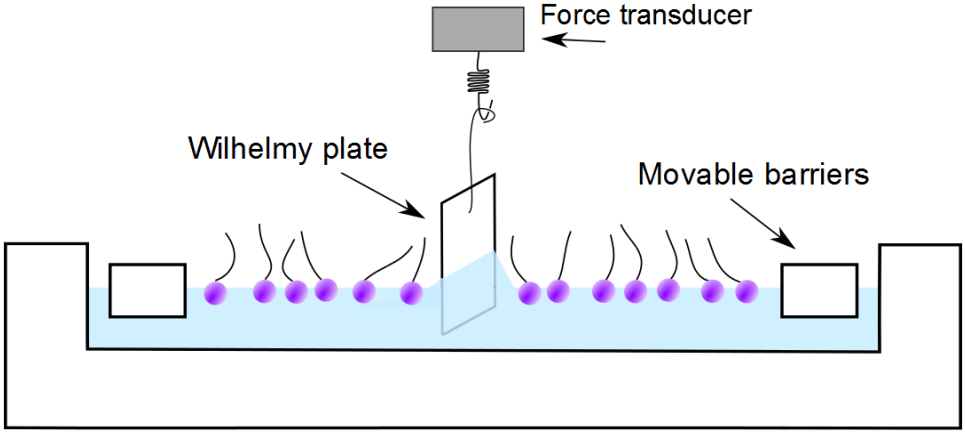


**Figure 2.7:** Langmuir trough showing a phospholipid monolayer, Wilhelmy plate, and movable barriers used to control surface area.

As with other surfactant species, surface activity of lipids serves to reduce the surface tension of the subphase (water). Changes in surface activity are monitored using a Wilhelmy plate suspended from a force transducer. Forces acting on the plate at the interface include gravity, buoyancy of the plate, and surface tension of the subphase acting along the contact angle of wetting. A simple force balance in Equation 2.16 can be used to calculate the surface tension from the measured force acting on the plate:

$$F_{\downarrow} = m_p g + 2\left(t_p + w_p\right)\gamma\cos\theta - \rho_l V_p g \tag{0.16}$$

where $F_{\downarrow}$ is the net downward force, $m_p$ is the mass of the plate, $g$ is the gravitational constant, $t_p$ and $w_p$ are known plate dimensions, $\gamma$ is surface tension, $\theta$ is the contact angle, $\rho_l$ is density of the subphase, and $V_p$ is volume of plate submerged in the subphase. Wetting behavior and dimensions of the Wilhelmy plate are depicted schematically in Figure 2.8.

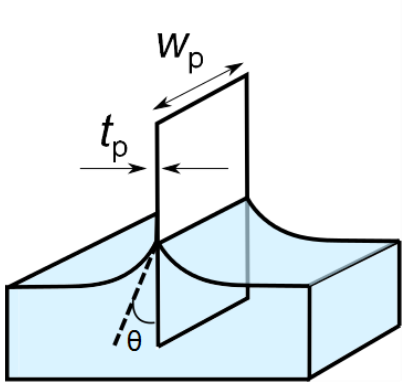


**Figure 2.8:** Wilhelmy plate dimensions include width ($w_p$), thickness (negligible, $t_p$) and contact angle, θ. Surface tension of the subphase wetting the plate is described by the cosine of the contact angle.

In order to determine the surfactant-induced changes to surface tension acting on the plate, a net downward force is calculated between pure subphase and monolayer-containing subphase. Following cancellation of constants (weight and buoyancy) and assumption of negligible plate thickness, $t_p$, and a 90° wetting angle for the paper Wilhelmy plate, the net change in force can be expressed by Equation 2.17:

$$\Delta F_{\downarrow} = 2w_p(\gamma - \gamma_0) \tag{0.17}$$

where width of the plate ($w_p$) is a known input, and $\gamma_0$ is the surface tension of the pure subphase (for water, $\gamma_0 =$ 72.2 mN/m at 25 °C). For Langmuir monolayers, the change in surface tension due to the surfactant is typically expressed as a surface pressure, $\pi$, as shown in Equation 2.18:

$$\pi = \gamma_0 - \gamma. \tag{0.18}$$

Upon combination of Equations 0.17 and 0.18, surface pressure is expressed by Equation 2.19:

$$\pi = -\frac{\Delta F_{\downarrow}}{2w_p} \tag{0.19}$$

where the negative sign yields a positive value of π for a reduction in surface tension.

To setup an isotherm compression experiment, the Teflon-coated trough is first cleaned with mild organic solvents (e.g. isopropanol, acetone) and copious ultrapure water (Millipore, 18.2 MΩ·cm) with vacuum aspiration. A known volume of ultrapure water is

used to fill the trough, and the water level is just high enough to wet the Wilhelmy plate. The plate is tared to $\pi = 0$ mN/m at the bare interface and $\pi = \gamma_0$ just above the interface. Following preparation of the subphase, a small volume of phospholipid dissolved in organic solvent (e.g. dipalmitoyl phosphatidylcholine, DPPC, in chloroform) is deposited by glass syringe on the interface by gently touching drops to the surface. Due to the immiscibility of the carrier solvent with the subphase and the surface tension, phospholipids disperse over the interface instantaneously. Carrier organic solvent is allowed to evaporate for 5-10 minutes before compression.

Following data collection, monolayers are aspirated from the interface and the trough is cleaned with copious ultrapure water, clean, lint-free polypropylene cloths, and mild organic solvent if necessary. At the conclusion of the sessions, fresh ultrapure water is added to the trough and the trough is enclosed by a protective cover to reduce the risk of contamination by airborne dust.

# Chapter 3

# Role of block copolymer architecture in model membrane protection against peroxidation

Systematic investigation of the mechanism of membrane stabilization by block copolymer surfactants presents a number of technical challenges, owing to the complexity of physiological systems and the size scale of involved species. Although a number of models of membrane damage and repair have been previously considered,[29,33,35,89,111] the balance required to choose systems which are both physiologically relevant and carefully controlled often favors one over the other. In this chapter, a common biochemical mode of cell membrane damage, peroxidation, is applied to a bilayered model membrane and analyzed by dynamic light scattering.

## 3.1 Diblock architecture and a model system

Prior to 2005, all of the investigations of therapeutic membrane interactions by block copolymer surfactants were limited to the commercially available poloxamers, triblock copolymers belonging to an established parameter space of molecular weight and relative hydrophobic/hydrophilic ratio. Although earlier work detailed the laboratory preparation of a simpler diblock architecture of PEO-PPO,[124–126] only two relevant diblock architecture studies emerged,[122,123] and membrane stabilization work has continued to focus on the initial P188 compound and related poloxamer formulations. Given both the similarities and differences exhibited by the limited diblock copolymer systems considered relative to poloxamers, it is surprising that more rigorous investigations of the diblock architecture

have not been pursued. This chapter seeks to establish whether a diblock architecture is at all capable of membrane stabilization. Following the lead of Wang, et al. in their identification of the hydrophilic block length as being the kinetic driver of adsorption versus insertion in a model bilayered system,[33,89] a diblock analog to P188, Diblock P188, is chosen for investigation. Here, the two polymers share hydrophilic PEO block lengths ($N_{EO}$ = 75), as well as relative PEO/PPO composition ($w_{PEO}$ = 0.8).

*3.1.1 Mechanism of liposome damage by peroxidation and shortcomings of DLS*

Lipid peroxidation is a naturally-occurring phenomenon associated with aging and various modes of trauma.[51,109,110,112] It is typically associated with membrane damage, the effects of which may induce increased permeability of the cell membrane, which can be fatal to the health of the cell.[81] The consequences of lipid peroxidation on membrane integrity are somewhat ambiguous, since phospholipids are too small to visualize in real-time ($D$ ~ 100 nm), and the majority of work in the field (both *in vitro* and liposome model membranes) involves chemical analysis of peroxidation byproducts,[107,153,154] rather than the structural changes invoked. Despite uncertainties in the precise nature of peroxidation, the hypothetical effect of lipid peoxidation on liposomes can be ascertained from numerous investigations of large and giant unilamellar vesicles.

Upon entering the lipophilic inter-membrane space, free radicals (also, reactive oxygen species) initiate peroxidation at unsaturated reactive sites on the lipid alkyl tails. Due to the close-packing of reactive acyl tails, the peroxyl groups formed facilitate propagation to nearby lipid tails.[107,113,155,156] Resulting from lipid peroxidation are a widely debated variety of structures and rearrangements.[103,107,130] Although the literature elucidating the oxidation products is extensive, most pertinent to this work is the likely conformational changes associated with terminated peroxyl species (i.e. –OOH functional groups). Heuvingh, et al. have hypothesized that migration by the hydrophilic –OOH to the interface imposes elevated lateral tension on the already strained membrane.[115] Also, considering the membrane instabilities associated with elevated lyso-compounds (i.e. cleavage of one of two acyl tails),[103] it is likely that upon sufficient extent of peroxidation, membrane lysis or rupture are reasonably expected modes of failure.[115]

In practice, measurement of ruptured liposomes presents unavoidable difficulty. Dynamic light scattering (DLS) is commonly used to characterize liposomes for a variety of experimental methods, and analysis traditionally yields particle size distributions and their corresponding characteristics. The technique is limited, however, by the total scattered intensity detected, which is a strong function of particle size, i.e. dilute unimers will not contribute to a signal dominated by 100 nm liposomes.[157] Given the hypothesized liposome rupture as a result of peroxidation and the low scattered intensity expected for liposome fragments, particle size distributions alone only indicate that there is or is not enough signal to make a good autocorrelation function and fit. As such, particle size distributions are an extremely limited measure for quantifying the extent of peroxidation experienced by a liposome sample. In their study, Wang, et al. qualitatively assessed polymer protection against lipid peroxidation from DLS obtained particle size distributions.[89] The authors refrained from drawing strong conclusions from the results of liposome peroxidation experiments, but they did base support of their polymer interaction hypothesis on them. Though lipid peroxidation is a well-known biochemical technique, DLS as a measure of liposome peroxidation is a new technique, and some improvement on the methodology can be made.

*3.1.2 Scattered intensity as a measure of liposome population*

Despite the insufficiency of particle size distribution characteristics to quantitatively describe liposome peroxidation, DLS does offer a provocative metric by which to assess polymer protection against lipid peroxidation apart from autocorrelation function fitting. By taking advantage of the underlying scattered intensity measurements – used to construct the correlation function, but not typically reported – ambiguity in the particle size distributions may be circumvented by instead accounting for the population of liposomes. Under several assumptions, the scattered intensity can be used to assess particle population, with the advantage of direct statistical comparison of replicates.

Firstly, and most importantly, it is assumed (and supported by statistical replicates) that if initiated in the unsaturated acyl tail region of the membrane, lipid peroxidation goes to completion in the timeframe of the reaction (30 minutes), to the catastrophic end of the liposome. Implied is that fully peroxidized liposomes are fragmented, irreparable, and no

longer detectable by DLS. This assumption is consistent with control groups in the previous study,[89] and it is further supported by the observed drop in scattered intensity to background levels following complete peroxidation. Next, it is assumed that all remaining liposomes, whether protected fully or partially peroxidized, undergo no measurable changes to apparent liposome sizes. As will be shown, this assumption is supported by insignificant changes to $R_h$ following reactions for numerous replicates at three incubation times, as well as narrow distribution widths ($\mu_2/\Gamma^2$), with few exceptions. Distribution widening could be attributed to the formation of fused particles or micellar structures, however, no systematic widening was observed for any of the systems considered. The assumption of constant particle size is necessitated by the strong dependence of scattered intensity on particle size; for the Rayleigh scattering regime ($qR < 1$), $I \sim R^6$.[150,157,158] Departure from constant particle size would make intensities difficult to compare, and as such, particle size must be evaluated with intensity as an internal check.

To illustrate how scattered intensity can be used to assess liposome population before and after peroxidation, neat liposomes will be considered alongside a negative control: namely, full peroxidation of liposomes by the free radical generator AAPH. First, the autocorrelation function obtained from a sample of freshly prepared liposomes (6:3:1 POPC:PLPC:POPG) at a scattering angle of 90°, as well as corresponding particle size distribution are shown in Figure 3.1. For the sample shown, the second cumulant fit gave $R_h$ = 64.8 nm, and the distribution width, $\mu_2/\Gamma^2$ is 0.12.

When a liposome sample with similar characteristics to Figure 3.1 is subjected to peroxidation reaction conditions, the scattered intensity measured by DLS drops to background levels. As such, no suitable autocorrelation function is obtained, and subsequently, no particle size distribution can be calculated. Raw scattered intensity as a function of time is shown for the liposome sample from Figure 3.1 along with a representative peroxidized liposome sample in Figure 3.2a. Note that scattered intensities are clearly centered around some average value across the duration of the experiment, and for simplicity, data can be averaged in time to obtain a single value of average scattered intensity. For the samples shown, average scattered intensities are 19.9 kcps and 2.1 kcps for liposomes and peroxidized liposomes, respectively.

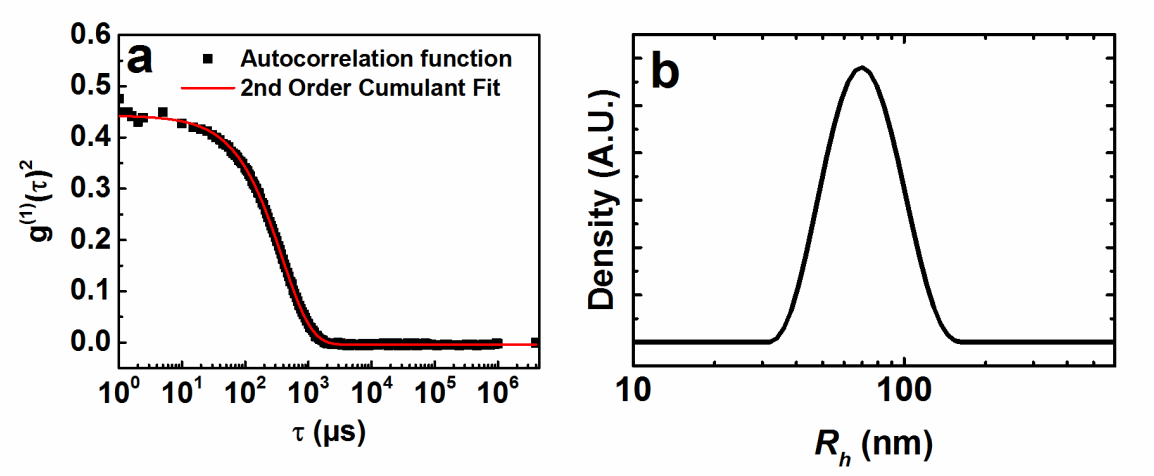


**Figure 3.1:** Sample autocorrelation function (a) and particle size distribution (b) obtained for liposomes. The line in (a) shows fitting by the method of cumulants.

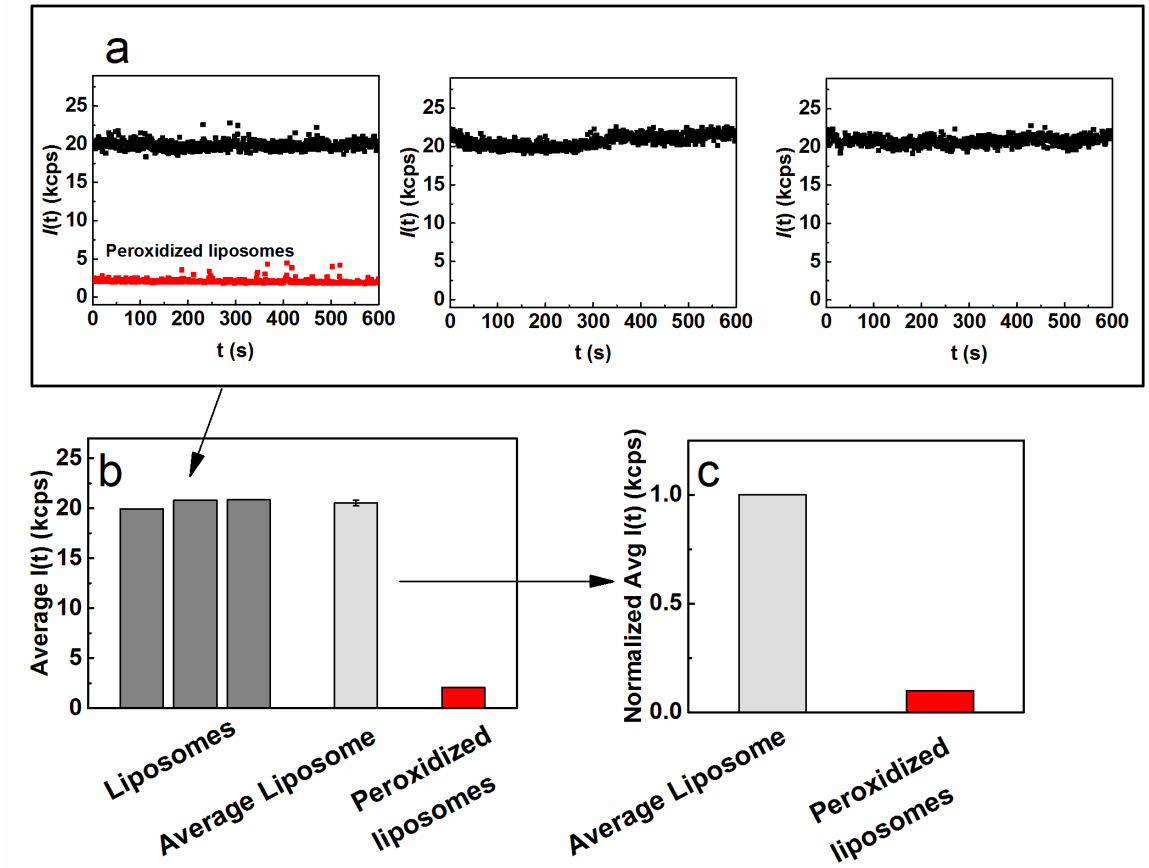


**Figure 3.2:** Normalization of average scattered intensity. Raw scattered intensity in time (a) shown for three liposome samples. Average intensities across the 10 minute experiment are shown by dark gray columns in (b), and the batch average is shown by a light gray color, with error bars representing standard error of the mean. In (c), the batch average and peroxidized liposome case are normalized by the batch average. By normalizing data to the batch, scattered intensities can be compared across varied batches.

For a given batch of liposomes, multiple samples at the same concentration should yield identical scattered intensities, within instrumental error. Batch to batch variations may occur, however, so direct comparison of average scattered intensities is not possible. To account for liposome batch variations, scattered intensities were normalized to a three-sample average intensity measured for neat liposomes, as illustrated in Figure 3.2a. One representative sample of peroxidized liposomes is also shown in Figure 3.2a, in order to illustrate how experimental data can be compared to the liposome control case, in Figure 3.2b and c. The benefit of normalized scattered intensities is the capability it provides to compare results across various batches, providing a more robust, statistical analysis of liposome population and reaction extent. Statistical analysis across a sufficient population of replicates is used to determine whether changes to liposome population are significant.

To further illustrate this point, consider the intermediate peroxidation case. Given the stark contrast between the full and fully peroxidized liposomes, the normalized average scattered intensity is expected to provide information about intermediate cases, i.e. partially peroxidized liposome samples. An example of partial peroxidation is shown schematically in Figure 3.3. Here, a sample of liposomes is fit with a particle size distribution that reflects an average $R_h$ and distribution width, $\mu_2/\Gamma^2$. A second sample of liposomes, this time partially peroxidized (again assuming fragmentation), and with enough scattered intensity to obtain an autocorrelation function, is fit with an identical particle size distribution, complete with indistinguishable distribution characteristics. Particle size distributions for both, while the same, result from two very different scenarios, as reflected by corresponding scattered intensities. The importance of liposome size distributions cannot be excluded, however, because block copolymer and phospholipid aggregates could form upon liposome rupture (more likely for higher molecular weight polymer species approaching critical micelle concentration). In such cases, mid-level scattered intensities with significant changes to $R_h$ or size dispersity would be expected.

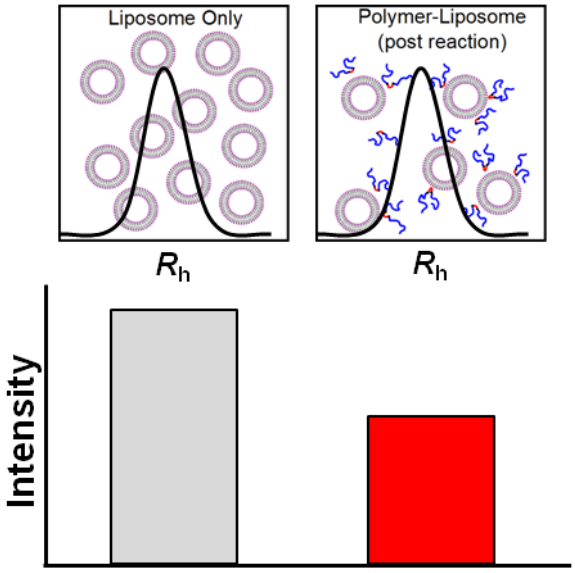


**Figure 3.3:** Schematic depicting possible population differences between neat liposomes and polymer-protected liposomes following reaction (hypothetical case).Due to likelihood of membrane rupture rather than liposome size change after peroxidation, liposome size distributions (overlaid) would be expected to give equal width and Rh for both the unreacted liposomes (left) and a polymer-liposome system following peroxidation. Changes to liposome population may be quantified by scattered intensity (schematically depicted below), which reflects loss of liposomes due to peroxidation.

### *3.1.3 Other scattering techniques*

Dynamic light scattering holds the distinct disadvantage that it is both simple to operate and to misinterpret the output. The myth of simple evaluation of DLS data is perpetuated by casual references in the literature to particle size determination in countless papers and the prevalence of software packages from which parameters may be obtained without further reflection. Various techniques that can be used to verify particle size can be employed, including TEM or SEM techniques, SANS or SAXS, or even scanning probe microscopy. To check the reliability of parameters determined by DLS data, however, multi-angle DLS and static light scattering (SLS) can be used.

Multi-angle DLS involves conducting DLS measurements at a range of angles, rather than one, to obtain better accuracy of parameters, avoiding some loss of detection of specific sizes at specific angles.[159] One obvious disadvantage of multi-angle DLS is the time it takes to make one measurement (10 minutes minimum per angle studied). For time-invariant samples (such as liposome incubation with polymers), extended measurement time should

make no difference. For liposome peroxidation samples, this extended time proved to be too long to obtain reproducible results, as will be shown.

Although SLS is a powerful technique commonly used to determine micellization behavior by polymers in solution by way of $M_w$, the technique is limited in the context of liposome peroxidation and polymer association to application of the Guinier plot to determine $R_g$. This is a consequence of the ambiguity of the refractive index increment, $\partial n/\partial c$, for the heterogeneous mixture resulting from peroxidation. This mixture is expected to contain unimeric polymers, liposomes, polymers interacting with liposomes, and likely some combination of polymer-lipid aggregates and lipid micelles. Though future experiments could perhaps define unreacted liposome-polymer $\partial$n/$\partial$c, as a means to determine polymer aggregation at membranes, for the purposes of this chapter, SLS has been restricted to Guinier plots to determine $R_g$, as described in Section 2.5.

In combination with the DLS experiments at a fixed angle (90°), multi-angle DLS and SLS offer a fuller understanding of the mechanism of interaction by block copolymers with model membranes. The results will show that the diblock architecture does, as expected, interact with membranes differently, and the implications of the result may yield further insight into the mechanism of membrane stabilization in the future.

## 3.2 Experimental design

The design of this study is derived from a recent paper by Wang, et al.[89] focusing on the capacity of beneficial membrane adsorption by block copolymers to protect against liposome peroxidation. The study concluded that hydrophilic poloxamers (≥ 70 wt.-% PEO) readily adsorbed to the membrane and effectively slowed the diffusion of a free radical compound into the reactive intermembrane space, thereby "protecting" against peroxidation.[89]

The peroxidation reaction itself is short-lived and rapidly leads to conformational changes of phospholipids in the membrane.[115] A resultant rise in membrane tension can lead to catastrophic rupture,[106,108,115,160] which is irreparable by block copolymer surfactants, even for larger lipid vesicles (~1 μm) with significantly lower degrees of curvature than the ~0.1 μm liposomes considered here.[33] Because block copolymer

surfactants have been shown to protect against rather than repair membrane tension-induced damage to liposomes (e.g. by osmotic stress),[33] characterizing liposome protection from peroxidation on the basis of size alone provides an incomplete description of the damage incurred. Liposome size distribution characteristics determined by DLS before and after peroxidation are monitored alongside the normalized scattered intensity of liposome samples as a measure of liposome population following peroxidation. Between the limits of a negative control (i.e. background scattering) and scattering due to neat liposomes, the scattered intensity can be used to differentiate between a full population of protected liposomes of characteristic size $R_h$ and a partial population of liposomes of the same characteristic size, i.e. polymer-induced protection of some fraction of the total population of liposomes.

*3.2.1 Polymers considered*

In order to investigate polymer protection against liposome peroxidation, three polymers were compared (structures shown in Scheme 3.1). The first, P188, could be directly compared to previously reported results.[89] The same study featured another polymer, PEO-8k, however the concentration was changed to a 5x excess.[89] The polymer motivating the study was a diblock copolymer (Diblock P188) analogous to half of the P188 molecule ($M_n$ = 4,300 g/mol; $w_{PEO}$ = 0.8).

Poloxamer 188 was generously provided by BASF (Pluronic F68, Wyandotte, MI), and its diblock analog (Diblock P188) was purchased from Polymer Source (P1862-EOPO, Montreal, Quebec). PEO-8k, PEO-4k, and the free radical generator 2,2'-azobis(2-amidinopropane) hydrochloride (AAPH) were purchased from Sigma and used as-received. A summary of polymer properties, as determined by SEC and $^1$H NMR is presented in Table 3.1.

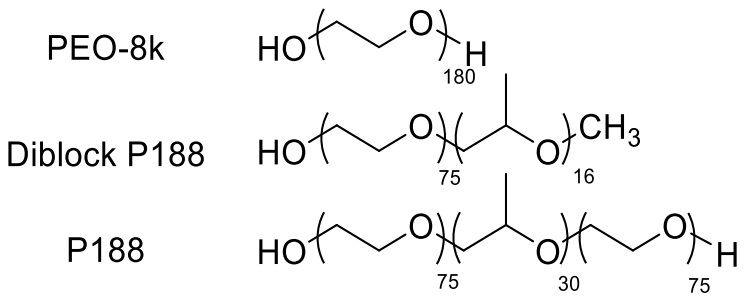


**Scheme 3.1:** Polymer structures for PEO-8k, Diblock P188, and P188.

**Table 3.1:** Polymer summary.

| Sample | $M_n$[a] (g/mol) | $Đ$[b] | $w_{PEO}$[a] | $w_{PEO}$[c] |
|---|---|---|---|---|
| Diblock P188 | 4,200 | 1.07 | 0.81 | 0.84 |
| P188 | 8,400 | 1.06 | 0.80 | 0.83 |
| PEO-4k | 4,000 | 1.03 | - | - |
| PEO-8k | 8,000 | 1.04 | - | - |

[a]Specified by supplier. [b]Determined by SEC. [c]Determined from molar ratios in $^1$H NMR.

*3.2.2 Phospholipids and liposome preparation*

Liposomes were prepared from a mixture of three unsaturated phospholipids, which are all reactive to the peroxidation reaction. These lipids included 1-palmitoyl-2-oleoyl-*sn*-glycero-3-phosphocholine (POPC), 1-palmitoyl-2-oleoyl-*sn*-glycero-3-[phosphor-rac-(1-glycerol)] sodium salt (POPG), and 1-palmitoyl-2-linoeloyl-*sn*-glycero-3-phosphocholine (PLPC), purchased in chloroform from Avanti Polar Lipids (Alabaster, AL) and used without further purification. Ultrapure water with resistivity of 18.2 MΩ·cm was obtained from a Millipore Direct Q-3 water system (EMD Millipore, Billerica, MA).

The precise mixture of lipids selected for this study was based on the experimental details of Wang et al.[89] The majority component (60 mol.-%), POPC, is zwitterionic and features one degree of unsaturation on the alkyl tail. The complementary POPG (10 mol.-%) features identically monounsaturated alkyl tail while differing in the net-negative charge of the polar head group, mimicking the charged content of cell membranes and preventing aggregation by electrostatic repulsion.[161] PLPC, though not strictly necessary in terms of reactivity, adds heterogeneity to the membrane, and the second degree of unsaturation makes PLPC considerably more reactive to peroxidation than the monounsaturated lipids.[154] Chemical structures for each of the phospholipids used are shown by Scheme 3.2.

*3.2.3 Liposome peroxidation.*

Peroxidation reactions were carried out on fresh liposomes at phospholipid concentrations of 25 μM with 15 mM AAPH. For polymer-incubated liposomes, aliquots were prepared with a constant polymer to phospholipid molar ratio of 5:1, unless otherwise specified. Full experimental details are outlined in Chapter 2.3, and a detailed protocol is provided in Appendix A. Prior to peroxidation experiments, DLS was used to determine average hydrodynamic radii, $R_h$, and size distribution width ($\mu_2/\Gamma^2$) for the prepared liposomes. Phospholipid reactivity was checked by performing control peroxidation reactions (negative control: liposomes reacted with AAPH for 30 min at 37 °C, $\lambda$ = 254 nm) at the start of each session. Complete peroxidation was verified by dramatic loss of scattering signal to background scattering levels, or a reduction of about 80%, relative to liposome scattered intensity.

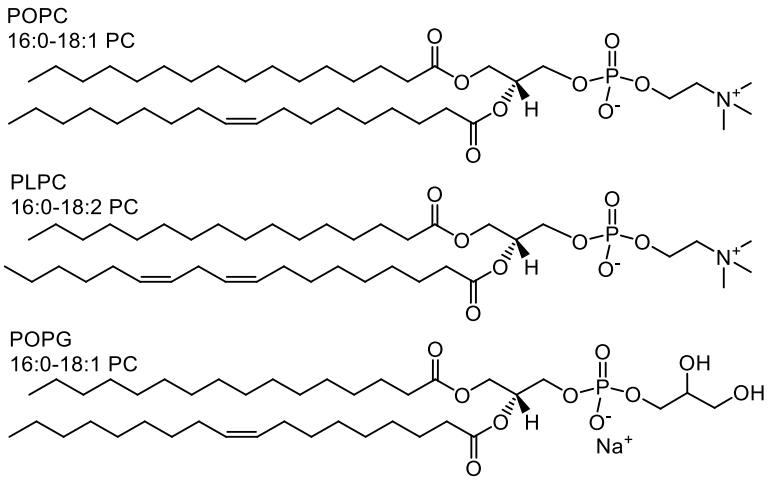


**Scheme 3.2:** Chemical structures of unsaturated phospholipids used to prepare reactive liposomes.

Following DLS measurements on diluted samples, (10 minute sampling time, 90°, HeNe laser at $\lambda$ = 637 nm, 25 °C, delay times from 1 µs to 1 s), autocorrelation functions were fit by the method of cumulants to determine $R_h$ and the distribution width, $\mu_2/\Gamma^2$, and size distributions were fit by the REPES model in the GENDIST software package. Statistical analyses were performed in JMP Pro.

*3.2.4 Multi-angle DLS and SLS*

Multi-angle DLS was performed as per sample preparation explained above, but measurements were taken in 10° intervals from 60° to 120°. Data from each scattering angle were fit by the method of cumulants, and the cumulant-derived decay times were plotted as a function of the scattering vector and fit to the first cumulant to determine the Z-average diffusion coefficient. From this was calculated $R_h$ by the Stokes-Einstein equation.[162]

Static light scattering was performed from scattering angles between 15° and 155° on the same instrument as DLS measurements, equipped with a HeNe laser operating at 637 nm. Data were measured until three replicates with a threshold tolerance were obtained, and results were averaged by the instrument software package. Solvent (water) was background subtracted prior to fitting by Guinier analysis,.

*3.2.5 Small angle X-ray scattering*

To investigate the architectural implications of the diblock versus triblock architecture on lipid hydration, small angle X-ray scattering (SAXS) was performed on multilamellar phospholipid dispersions in Milli-Q water, incorporated with polymers at varying loadings. Samples were prepared from 1,2-ditetradecanoyl-*sn*-glycero-3-phosphocoline (DMPC), a 14 carbon saturated lipid (depicted in Scheme 3.3). DMPC has a transition temperature of 24 °C, and experiments were performed at physiological temperature (37 °C). Scattering volumes were prepared at a total surfactant loading of 20 wt.-%, in correspondence with the literature.[90,122] Polymers were added to dispersions at polymer:lipid ratios of 0.1 (10 mol.-%) and 0.2 (20 mol.0%), respectively, and samples were gently mixed before loading into the sample cell.

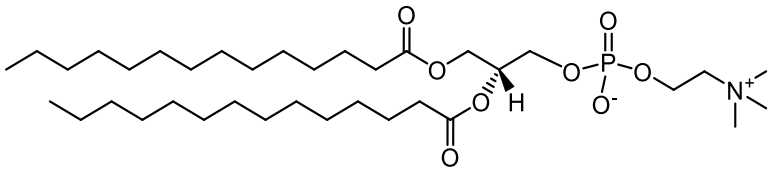

**Scheme 3.3:** Chemical structure of phospholipid 1,2-ditetradecanoyl-*sn*-glycero-3-phosphocoline (DMPC).

Scattering measurements were performed using a SAXSess camera and a lab scale X-ray generator operating at 45 kV and 40 mA, with a Cu $K_\alpha$ slit-collimated radiation source. Temperature control was achieved with a temperature control fixture set to 37 °C. Samples (~20 µL) were loaded into a well-cleaned 1 mm quartz capillary. Data was collected for 15 minutes, and films were processed in a drum scanner and profiles extracted by SAXSquant software.

## 3.3 Liposome peroxidation and protection results

### *3.3.1 Polymer incubation with liposomes*

To determine whether the polymer species themselves would disrupt membrane integrity or impact liposome characteristics (e.g. liposome swelling or compaction), DLS measurements were performed on neat liposomes incubated with each polymer species for 4 and 24 hours. Representative liposome size distributions for these control incubation experiments are shown in Figure 3.4, and calculated liposome sizes and distribution widths are given in Table 3.2. Size distributions show little variation between incubation times or polymers, with respect to distribution widths and peak centers, which corresponds well to cumulant-determined liposome size distribution characteristics. Independent DLS measurements on neat polymer solutions at the experimental concentrations gave no measurable scattered intensity above background levels, excluding the possibility of significant contributions to scattering by polymer micelles or aggregates in solution (data not shown).

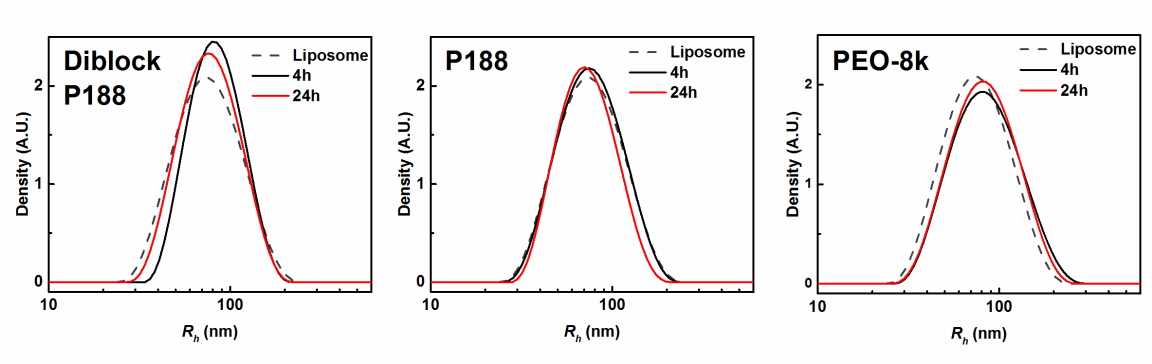


**Figure 3.4:** Control polymer-liposome incubation experiments at 4 and 24 hour incubation times. Representative liposome size distributions are shown after 4 and 24 hours of incubation with Diblock P188, P188, and PEO-8k. Neat liposome size distributions are shown on each plot for reference (- -).

**Table 3.2:** Average liposome $R_h$ and dispersities following polymer incubation at times ($t_I$) of 4 and 24 hours. No significant differences in $R_h$ ($p < 0.05$; one-way ANOVA) were observed following polymer-liposome incubation. Standard error is reported for $N \geq 6$ replicates.

| **Liposomes incubated with:** | **Average $R_h$ (nm)** | **Average dispersity ($\mu_2/\Gamma^2$)** | **Average $R_h$ (nm)** | **Average dispersity ($\mu_2/\Gamma^2$)** |
|---|---|---|---|---|
| Neat liposomes | 68.0 ± 1.0 | 0.20 ± 0.02 | | |
| | *Incubation time:* | | | |
| | 4 h | | 24 h | |
| Diblock P188 | 69.0 ± 2.3 | 0.27 ± 0.05 | 71.1 ± 3.6 | 0.13 ± 0.09 |
| P188 | 71.2 ± 1.7 | 0.17 ± 0.04 | 70.5 ± 1.1 | 0.22 ± 0.04 |
| PEO-8k | 68.5 ± 1.0 | 0.25 ± 0.06 | 74.3 ± 2.1 | 0.12 ± 0.06 |

Scattered intensities of control incubation experiments are shown in Figure 3.5, normalized to neat liposomes. In all incubation control cases, no significant changes were detected liposome average size, distribution width, or scattering intensity relative to neat liposomes (one-way ANOVA, $p < 0.05$), which confirms that polymer interactions with model membranes do not serve to disrupt or swell the membranes on experimental time scales. These results indicate that for Diblock P188, interaction with phospholipid membranes is innocuous to liposome characteristics following 4 or 24 hours of incubation.

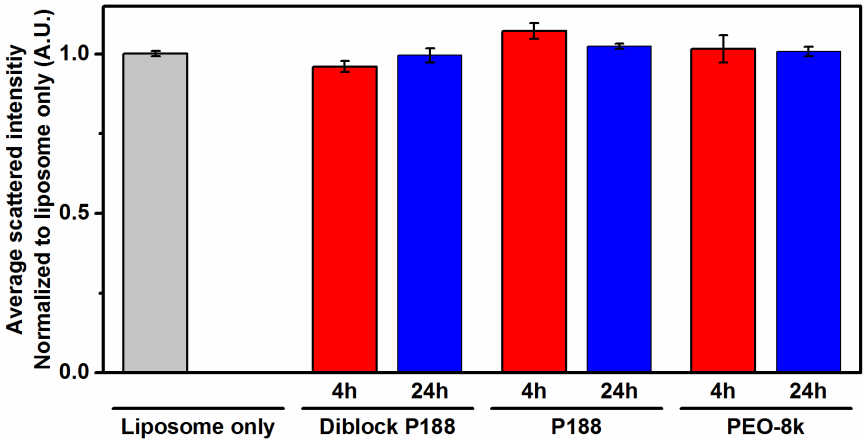


**Figure 3.5:** Average scattered intensities for polymer-incubated liposomes.Intensities are normalized to liposome scattered intensities and are shown with error bars representing standard error of the mean for $N \geq 6$ replicates. The data show no statistical differences between measured scattered intensities for neat liposomes and any length of polymer-liposome incubation scattered intensity.

### *3.3.2 Polymer incubation effects on liposome peroxidation*

Block copolymer protection against liposome peroxidation by AAPH was tested across equimolar concentrations of P188, Diblock P188, and PEO-8k following liposome-polymer incubation times of 0, 4, and 24 hours, respectively. Representative liposome size distributions following incubation and peroxidation conditions after the varying incubation times are shown in Figure 3.6, along with calculated average $R_h$ and dispersities in Table 3.3.

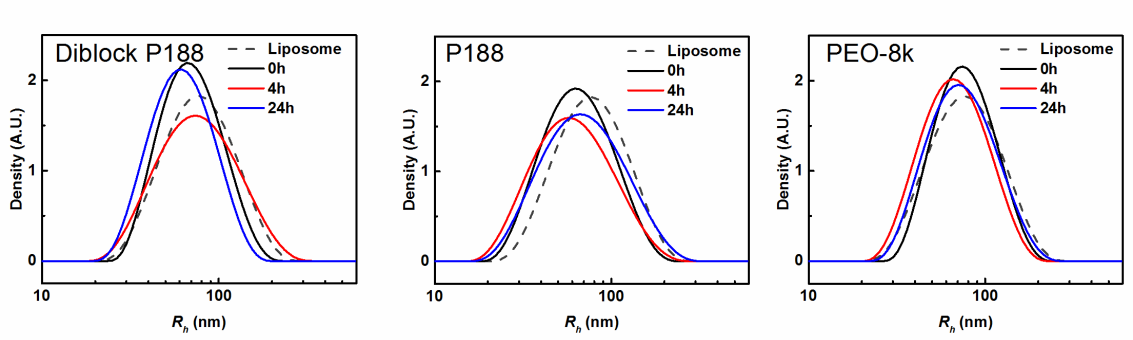


**Figure 3.6:** Representative liposome size distributions following peroxidation reactions in the presence of polymers. Data are shown for 0, 4, and 24 hours of liposome incubation with (from left to right) P188, Diblock P188, and PEO-8k. A representative size distribution for un-reacted liposomes is shown in each for comparison (- -).

**Table 3.3:** Summary of liposome distribution characteristics following peroxidation in presence of polymers. Liposome $R_h$ and dispersities given follow liposome peroxidation conditions (AAPH, 30 minutes, 37 °C, λ = 254 nm), for incubation times ($t_I$) of 0, 4, and 24 hours with P188, Diblock P188, and PEO-8k. Standard error reported for $N \geq 9$ replicates.

| **Sample** | **Average $R_h$ (nm)** | **Average dispersity ($\mu_2/\Gamma^2$)** | **Average $R_h$ (nm)** | **Average dispersity ($\mu_2/\Gamma^2$)** | **Average $R_h$ (nm)** | **Average dispersity ($\mu_2/\Gamma^2$)** |
|---|---|---|---|---|---|---|
| Neat Liposomes | 68.0 ± 1.0 | 0.20 ± 0.02 | | | | |
| | *Incubation time* | | | | | |
| | 0 h | | 4 h | | 24 h | |
| Diblock P188 | 66.9 ± 2.0 | 0.28 ± 0.06 | 60.5 ± 2.3 | 0.42 ± 0.07 | 64.2 ± 3.0 | 0.20 ± 0.07 |
| P188 | 52.7 ± 2.3 | 0.29 ± 0.06 | 49.7 ± 3.3 | 0.39 ± 0.07 | 51.2 ± 2.8 | 0.31 ± 0.09 |
| PEO-8k | 66.1 ± 4.1 | 0.34 ± 0.08 | 63.8 ± 4.0 | 0.32 ± 0.10 | 58.3 ± 5.0 | 0.41 ± 0.16 |

While increasing polymer-liposome incubation time before addition of AAPH led to a small decrease in post-reaction liposome size across each polymer type, a statistically significant ($p < 0.05$; Student's *t*-test) reduction in $R_h$ appeared for P188. Because P188 showed no effect on liposome size in the polymer-liposome incubation experiments (see Table 3.2) and no such result appears for Diblock P188 or PEO-8k, this result was surprising. It is possible that during liposome peroxidation, the rise in membrane tension induced by conformational changes to phospholipids and localized reduction in lipid packing density serves to attract hydrophobic interactions by block copolymers near reaction sites, in the same manner that has been reported in studies of polymer adsorption to monolayers below a threshold lipid packing density.[35,43] Based on the hygroscopic nature of PEO and the equimolar basis of our solutions, (by mass, P188 has twice the total PEO as compared to Diblock P188) the higher PEO concentration of P188 at the AAPH-compromised interface could osmotically drive liposome dehydration and shrinkage.[163] The effects of PEO concentration are considered on a mass-basis later, and differences between the protective interactions by amphiphilic block copolymers and homopolymer PEO species will be discussed.

As previously described, liposome size distribution characteristics alone are insufficient to assess liposome peroxidation protection by block copolymers. By including scattered intensity as a metric of the extent of the liposome population remaining following peroxidation, quantitative comparison of protective strengths of each polymer can be made across incubation times, independent of signal quality, which deteriorates beyond a reasonable distribution fit if peroxidation damage becomes too significant. Scattered intensities were normalized to neat liposome scattered intensities for their respective experimental sessions to account for sample-to-sample variation. Average scattered intensities are compiled in Figure 3.7 for liposome peroxidation experiments across each polymer species and incubation time.

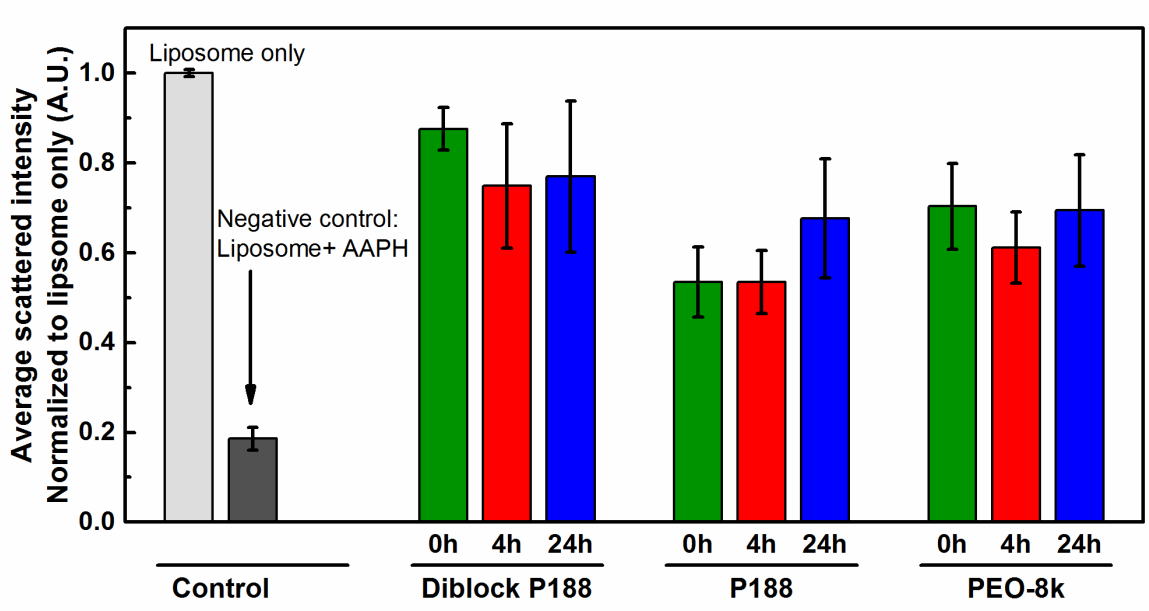


**Figure 3.7:** Average scattered intensities following peroxidation in the presence of polymers. Error bars represent standard error measured across all replicates (N ≥ 9) of P188, Diblock P188, and PEO-8k liposome peroxidation experiments. Liposomes were incubated for 0, 4, or 24 hours with respective polymer solutions prior to peroxidation reaction. A Student's *t*-test was performed between the negative control (shown in black; liposome and AAPH reaction in absence of polymer) and each of the respective data sets, and all reported results are statistically significant, with $p < 0.05$. Average scattered intensities showed that all three polymer species were protective at the 5:1 molar ratio studied.

Each of the polymers in this study showed statistically significant improvement in average scattered intensity over the negative control case for each incubation time (one-way ANOVA, Dunnett's test against negative control, liposomes reacted with AAPH, $p < 0.05$). Diblock P188 showed higher scattered intensities than P188 at the 0 hour incubation time ($p < 0.05$; Tukey-Kramer HSD), but based on the "anchoring" hypothesis[122] and the reduced $R_h$ observed in the P188 case, the higher scattered intensity is likely a combination of population protection and liposome size preservation, as compared to the neat liposome case, rather than strictly better population protection. Because of the difference in measured $R_h$ between Diblock P188 and P188, and the strong dependence of scattered intensity on particle size, no clear advantage by one polymer over the other can be declared. The results do clearly demonstrate Diblock P188 is effective in protecting liposomes from peroxidation. No statistically significant differences in liposome protection were measured across incubation times, contrary to adsorption-insertion expectations.[33,89]

*3.3.3 Protective effects of molecular weight: incubation on equal PEO basis*

Interestingly, PEO-8k showed similar protective effects to the block copolymer species at the same molar concentration, suggesting that total PEO present may play a more vital role in membrane protection than hydrophobicity, a finding not previously reported. To investigate the PEO contribution to membrane protection further, identical length PEO blocks (Diblock P188 and P188) and varied length PEO (PEO-4k and PEO-8k) were considered at equal mass concentrations, rather than equal molar concentrations. In both cases, the larger polymer is roughly twice the overall molecular weight of the smaller, and by way of reminder, both block copolymers have the same relative PEO:PPO compositions. A pictorial guide to the design of these equal mass experiments is shown in Figure 3.8.

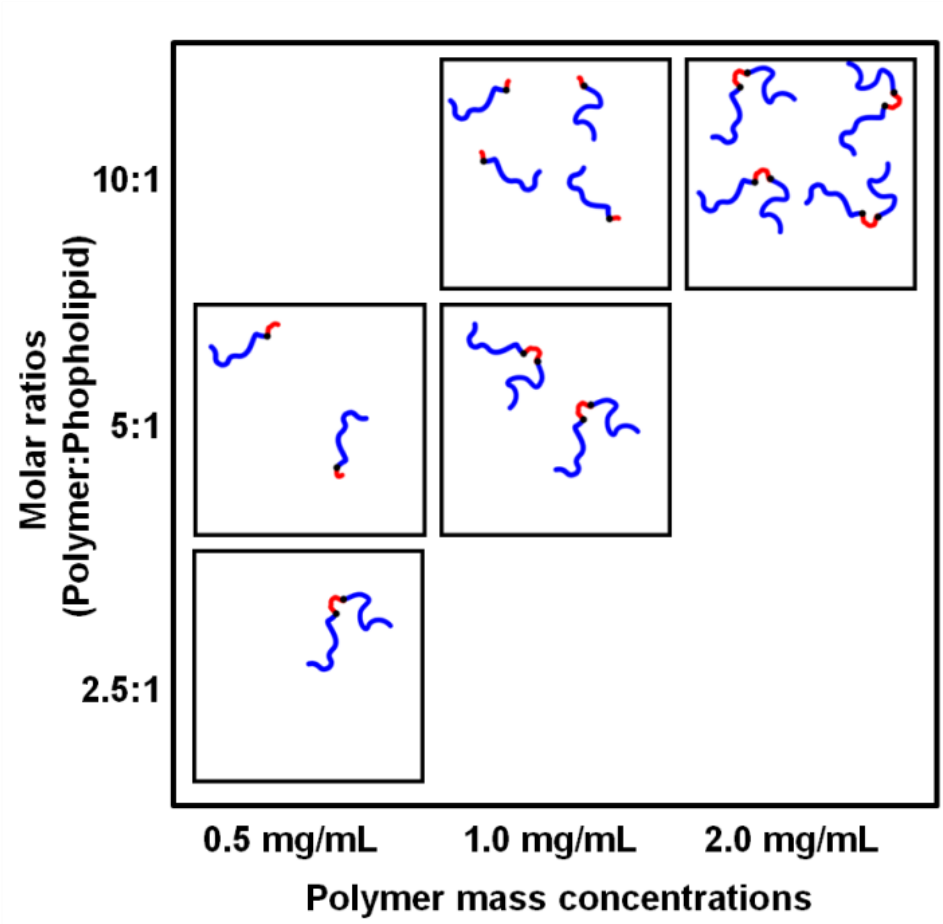


**Figure 3.8:** Schematic illustrating equal molar and equal mass concentrations for P188 and Diblock P188. Liposomes are implicit, and molar ratios of polymer:phospholipid are shown in gray bars below each line. Polymer mass concentrations are given along the top.

Up until this point, peroxidation results were obtained using an equimolar 5:1 molar ratio (125 μM in polymer) of polymer:phospholipid (Figures 3.4-7). The first equal mass comparison maintained the 5:1 molar ratio for Diblock P188, equivalent to about 0.5 mg/mL, and correspondingly, a 2.5:1 molar ratio of P188. Peroxidation conditions were held constant (0 h polymer incubation time, 30 min reaction with AAPH at 37 °C and λ = 254 nm) throughout, and a direct comparison of 0.5 mg/mL polymer loadings are shown by average scattered intensity in Figure 3.9a. The converse scenario involving a 5:1 molar ratio of P188 (1 mg/mL), corresponded to a Diblock P188 molar ratio of 10:1. This case is shown along with the 5:1 Diblock P188 case in Figure 3.9a.

As seen in Figure 3.9a, liposomes incubated with Diblock P188 resulted in higher scattered intensity following peroxidation than P188 at equal PEO content at both the 0.5 mg/mL and 1.0 mg/mL concentrations. This is consistent with the 0 h incubation equimolar concentration results in Figure 3.7, which showed significantly higher scattered intensity for 5:1 Diblock P188 (0.5 mg/mL) versus 5:1 P188 (1.0 mg/mL) ($p < 0.05$, Tukey-Kramer HSD). Diblock P188, with its short, exposed hydrophilic block, is expected to be favorably attracted to the liposome membrane (i.e. anchoring), promoting tight arrangement of PEO tails much like a short-chain micellar structure, helping to slow diffusion of the free radical AAPH into the intermembrane space. The longer P188 molecule, with its constrained hydrophobic block, is not as free to pack at the membrane or penetrate below the hydrophilic lipid headgroups; at reduced molar concentrations it would reasonably exhibit reduced surface coverage. This is supported by previous work which described a "flattened" configuration by the triblock architecture at a phospholipid bilayer,[90,122] in contrast to a more brush-like, anchored configuration exhibited by a diblock architecture with similar block lengths.[122]

The PEO case, shown in Figure 3.9b, exhibited higher scattered intensity with longer PEO chain length as mass concentration of polymer was increased. Without a hydrophobic group to draw molecules to the membrane interface, polymer capacity to protect against peroxidation shows a strong dependence on PEO chain length. The added entropic benefit of coiling by the longer chains should lead to a more densely packed hydration layer of PEO and water outside the liposome membrane, a type of physical barrier barring diffusion

of reactive free radicals into the membrane.[104] In combination with the equimolar PEO block results in Figure 3.7, dramatic mechanistic differences between homopolymer and block copolymer species are confirmed, and furthermore, they reveal that by exposing the hydrophobic block (as in Diblock P188), liposome protection can be achieved at a lower overall mass-loading. This finding has significant pharmacological relevance, and validates the pursuit of a diblock architecture as a model compound for future work.

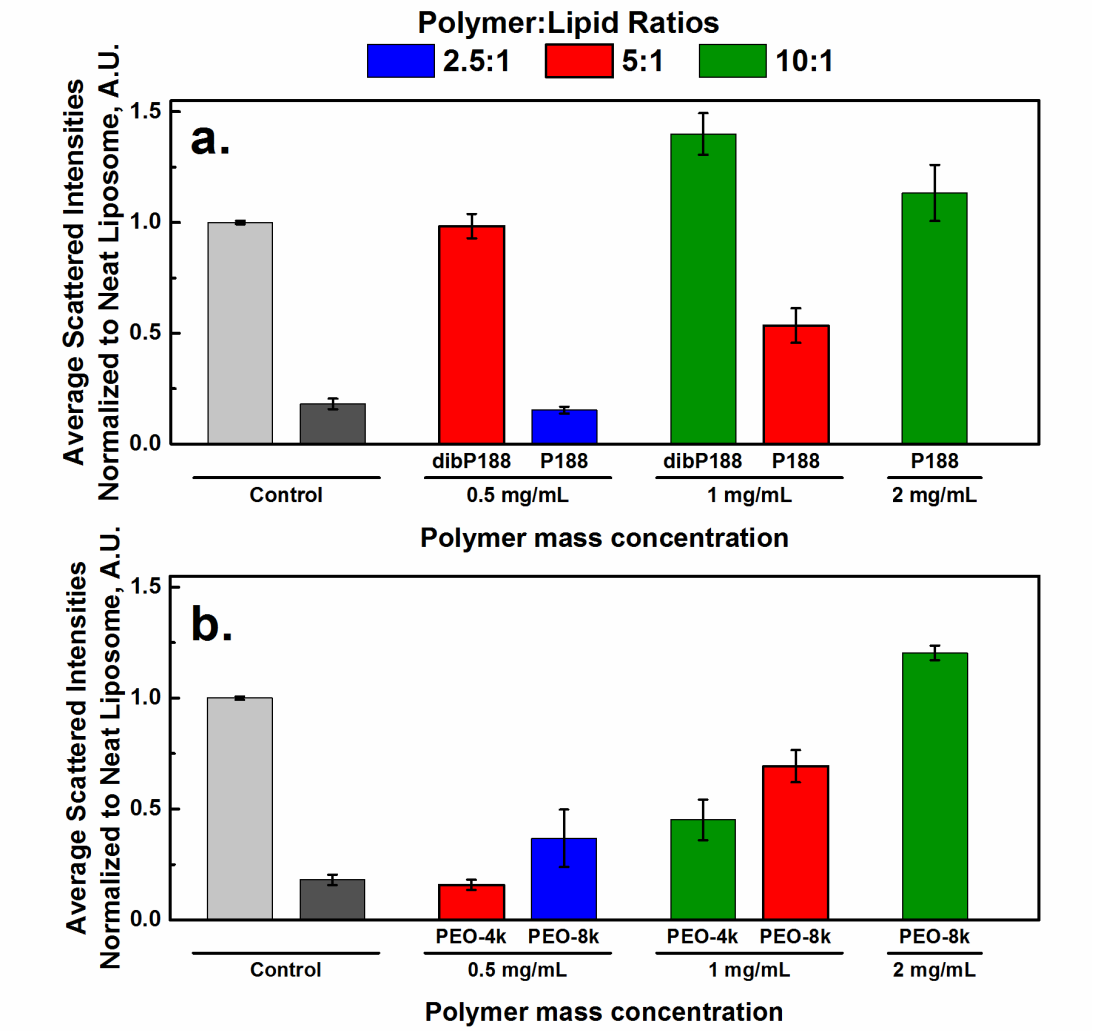


**Figure 3.9:** Average scattered intensities for equal PEO content. Data are normalized to neat liposome case (left) following liposome peroxidation reaction in the presence of (a) PEO-PPO block copolymers, Diblock P188 and P188, and (b) PEO polymers, PEO-4k and PEO-8k, arranged by equal mass concentrations in solution (i.e. equimolar in PEO repeat units). The 5:1 polymer:phospholipid ratio represents the standard molar concentration described previously. Error bars represent standard error measured across all replicates ($N \geq 6$).

*3.3.4 Multi-angle DLS*

To assess the quality of particle size and distribution width results obtained by DLS at a fixed (90°) angle, multi-angle DLS was performed. A sample multi-angle DLS plot was first constructed for neat liposomes, as shown in Figure 3.10. Scattering was performed at 10° intervals from 60° to 120°, and cumulant fitting was used to determine the average decay time, Γ, at each angle. Two linear regressions are shown in Figure 3.10. The zero fit line indicates a linear regression forced through the intercept, in agreement with the theoretical relationship of Γ and $q^2$ (Equation 2.4). The line fit reflects a standard linear regression, which yielded a small intercept (relative to Γ) as a consequence of experimental error. Agreement between both lines is close because the calculated *y*-intercept was small relative to maximum Γ.

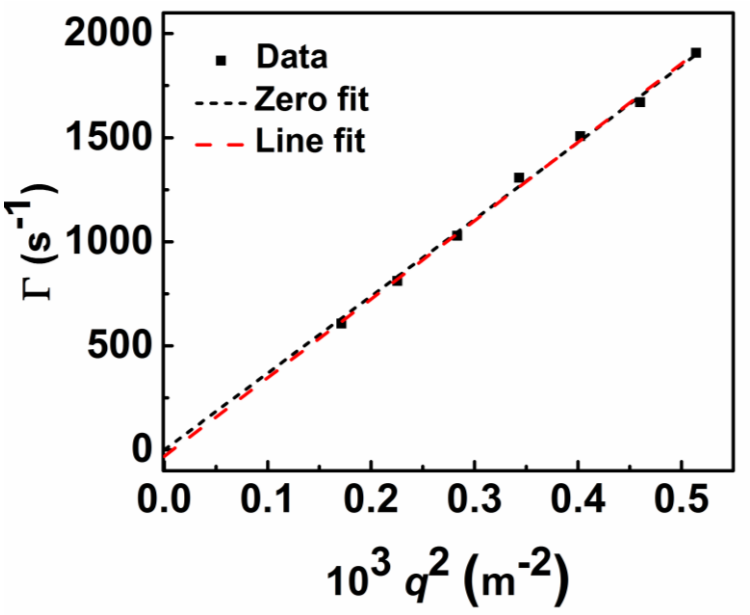


**Figure 3.10:** Multi-angle DLS carried out on liposome sample from 60° to 120°. Short dashed line (zero fit) indicates a linear regression forced through the origin, whereas the long dashed line (line fit) shows the regular linear regression of the data.

Next, polymer incubation was investigated. Because no significant differences between 4 and 24 hour incubation times were detectable by DLS at 90°, results shown in Figure 3.11 were taken after a shorter incubation time (1 hour) Again, the plots show average decay time, Γ, versus $q^2$, along with linear regressions with and without forcing through zero, as indicated by the fitting lines in the plots.

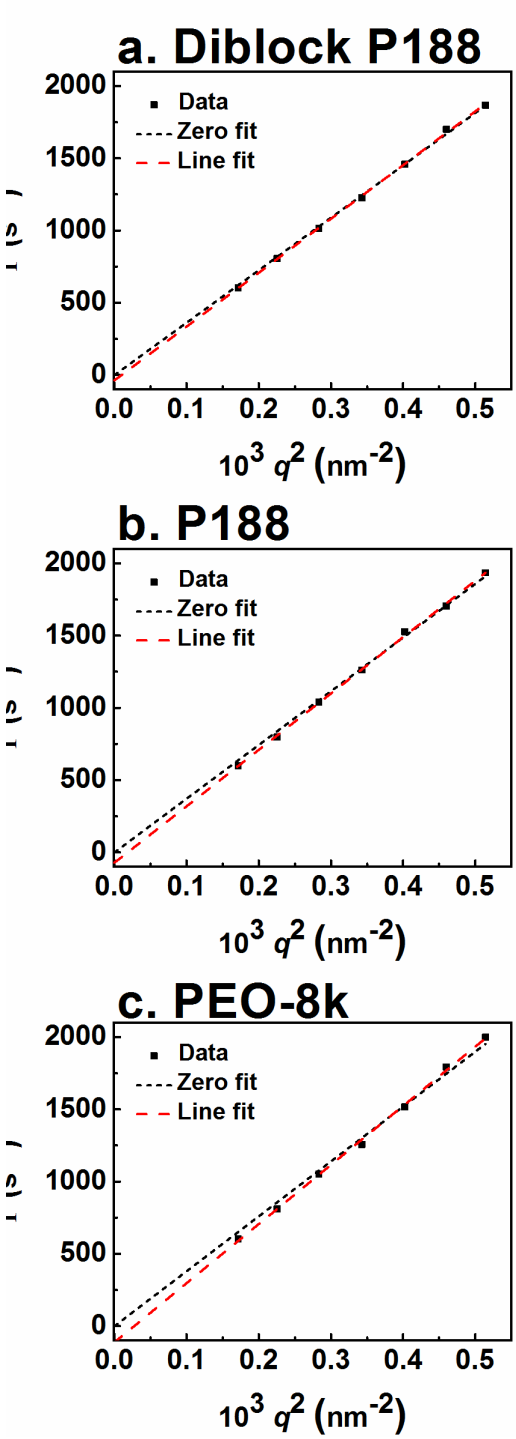


**Figure 3.11:** Cumulant fitting of multi-angle DLS performed from 60° to 120° gave average decay time, Γ. Plotted against q2, the slope gives an apparent diffusion coefficient, D. Short dashes show fit forced through origin, whereas longer dashes show best fit of data. Lines show good agreement.

Each of the linear regressions performed for Figure 3.11 showed small *y*-intercepts, indicating good agreement with theory. Diffusion coefficients calculated from each fit were used to determine $R_h$, according to the Stokes-Einstein equation (Equation 2.10). These are listed in Table 3.4 for each fit, along with the result obtained at 90° for each of the three polymers for comparison. Interestingly, multi-angle DLS obtained $R_h$ showed good agreement with 90° $R_h$ for liposomes and liposomes incubated with Diblock P188, and a drop in $R_h$ calculated from multi-angle DLS for P188 and PEO-8k, as compared to the 90° result. The multi-angle fit, which is expected to be more accurate, raises some concern about the apparent $R_h$ comparisons made at a single scattering angle.

**Table 3.4:** Comparison of $R_h$ derived from linear fitting of multi-angle DLS results and the 90° result. Samples refer to liposomes incubated with polymer (5:1 polymer to phospholipid) for one hour prior to measurement.

| | $R_h$ (nm) | | |
|---|---|---|---|
| **Sample** | **Zero Fit** | **Line Fit** | **90° Result** |
| Liposome Only | 66.4 | 65.0 | 64.3 |
| Diblock P188 | 67.6 | 65.9 | 68.0 |
| P188 | 61.2 | 58.3 | 66.6 |
| PEO-8k | 59.9 | 55.6 | 66.9 |

A single peroxidation sample was measured by multi-angle DLS, Diblock P188. The reaction was performed at the 0 h incubation time condition, and prior to multi-angle DLS, scattering was performed at 90° to obtain a baseline value of scattered intensity (the date-normalized intensity at the 90° scattering angle was initially 0.51, $R_h$ = 50.2 nm, $\mu_2/\Gamma^2$ = 0.31). Multi-angle scattering was performed after a 60 minute delay (e.g. scattering of other replicates at 90°), beginning with 90°, then moving from 60° to 120° at 10° intervals. Finally, after multi-angle scattering was complete, a final measurement was taken at 90°. Results of multi-angle DLS are shown in Figure 3.12. It is evident from the zero and linear fits that data show significant deviation from theoretical expectation, and the *y*-intercept reached a value corresponding to about 15% of the maximum decay rate. Calculated $R_h$ for each of the fits were: zero fit: $R_h$ = 48.3 nm, and linear fit: $R_h$ = 38.3 nm.

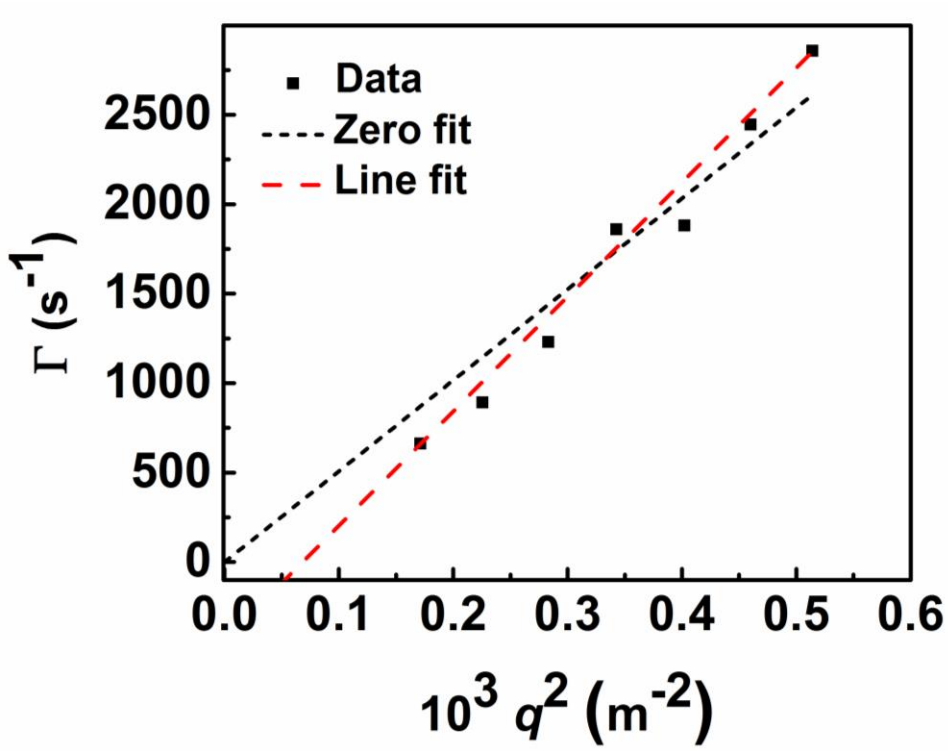


**Figure 3.12:** Multi-angle DLS plot for Diblock P188 following liposome peroxidation. Scattering was performed under 0 h incubation time conditions.

The poor fits by the first cumulant relationship in Figure 3.12 suggests that time between reaction and scattering is an important factor in consistency of results. Scattered intensities and corresponding $R_h$ obtained at times ranging from 0 to 2.25 hours after peroxidation are shown from 90° DLS in Figure 3.13. Initially, scattered intensity of this Diblock P188 sample is 0.51, relative to liposome only. After an hour, the intensity dropped to 0.41, and another small drop occurred after that. Apparent hydrodynamic radii calculated at each time and 90° scattering angle show no trend in time, ranging from 45-52 nm.

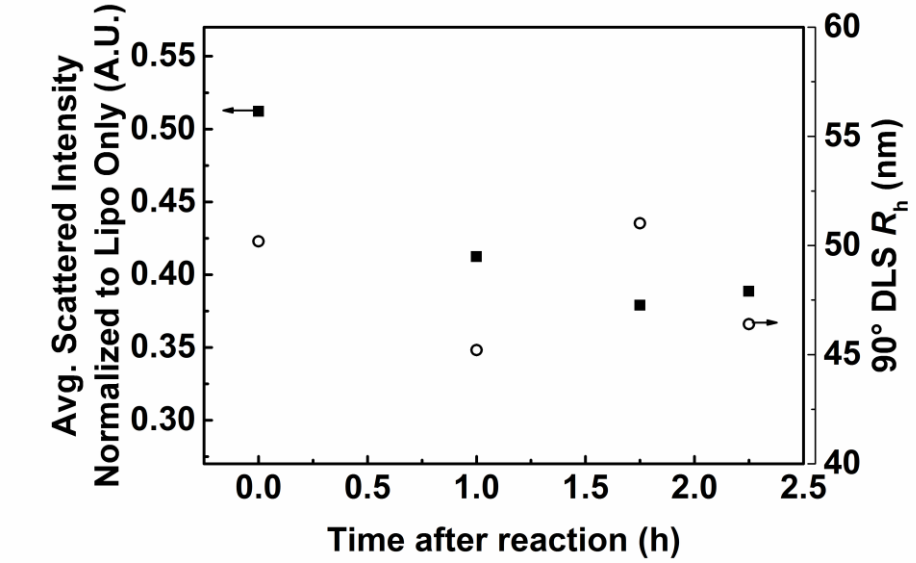


**Figure 3.13:** Scattered intensity (left) and $R_h$ (right) at 90° scattering angle for Diblock P188, obtained 0-2.25 hours after peroxidation. While scattered intensity (■) drops, $R_h$ (○) follows no trend, suggesting no change within experimental error.

*3.3.5 Static light scattering*

Next, static light scattering (SLS) was performed in order to compare apparent $R_h$ from DLS with $R_g$. Guinier analyses were used to determine $R_g$ from the slope of $\ln(I_{ex})$ and $q^2$ for polymers incubated with liposomes for 1 h (data not shown). Calculated $R_g$ are shown along with $R_h$ determined by multi-angle DLS for each case in Table 3.5. The ratio of $R_g/R_h$ is the shape factor. Spherical micelles would give a value of 0.774, whereas other, more extended shapes give higher values.[164,165] Again, the ratio highlights the drop in $R_h$ measured by multi-angle DLS for P188 and PEO-8k. As will be discussed in the upcoming

SAXS measurements, the difference is likely due to the difference in ability of the hydrophilic PEO and the constrained hydrophobic block of P188 to anchor in the bilayer.

**Table 3.5:** SLS following liposome incubation for 1 hour with polymers gave $R_g$. Data are shown along with $R_h$ multi-angle $R_h$ (zero fit). Ratios of $R_g/R_h$ can give structural information.

| | *SLS* | *Zero Fit* | |
|---|---|---|---|
| **Sample** | $R_g$ **(nm)** | $R_h$ **(nm)** | $R_g/R_h$ |
| Liposome Only | 59.6 ± 0.6 | 66.4 | 0.90 |
| Diblock P188 | 59.1 ± 0.6 | 67.6 | 0.87 |
| P188 | 59.1 ± 0.6 | 61.2 | 0.97 |
| PEO-8k | 60.9 ± 1.3 | 59.9 | 1.02 |

*3.3.6 SAXS on hydrated multilamellae phospholipids with polymers*

To further demonstrate the effect of architecture on membrane interactions, multilamellar phospholipid systems incorporated with varying concentrations of P188 and Diblock P188 were analyzed by small angle x-ray scattering (SAXS). Measurements were performed on samples containing 20 wt.-% total surfactant (DMPC and polymer included), with molar ratios of polymer to lipid of 0.1 (10 mol.-%) or 0.2 (20 mol.-%). Results in Figure 3.14 show SAXS scattering profiles taken for DMPC lamellae with 10 and 20 mol-% additions of polymer at 37 °C. The results are in agreement with similar scattering results obtained for multilamellar dispersions of DMPC with poloxamers in the literature.[90,122]

Peak characteristics of the scattering profiles in Figure 3.14 are summarized in Table 3.6. From the primary peak, *d* spacing of the lamellae was determined. Further evidence of the proposed "flattened" configuration by P188 is suggested by the 5-6 Å reduction of lamellar spacing induced by both 10 and 20 mol.-% loadings of P188 in the DMPC lamellae. This spacing effect is further reduced for 10 and 20 mol.-% Diblock P188, with only a 2-3 Å reduction. Reductions in lamellar spacing are consistent with dehydration effects, and comparison of the 10 mol.-% P188 case with the 20 mol.-% Diblock P188 reflects the same equal mass basis comparison as was described in Figure 3.9a, since by mass, Diblock P188 is half that of P188.

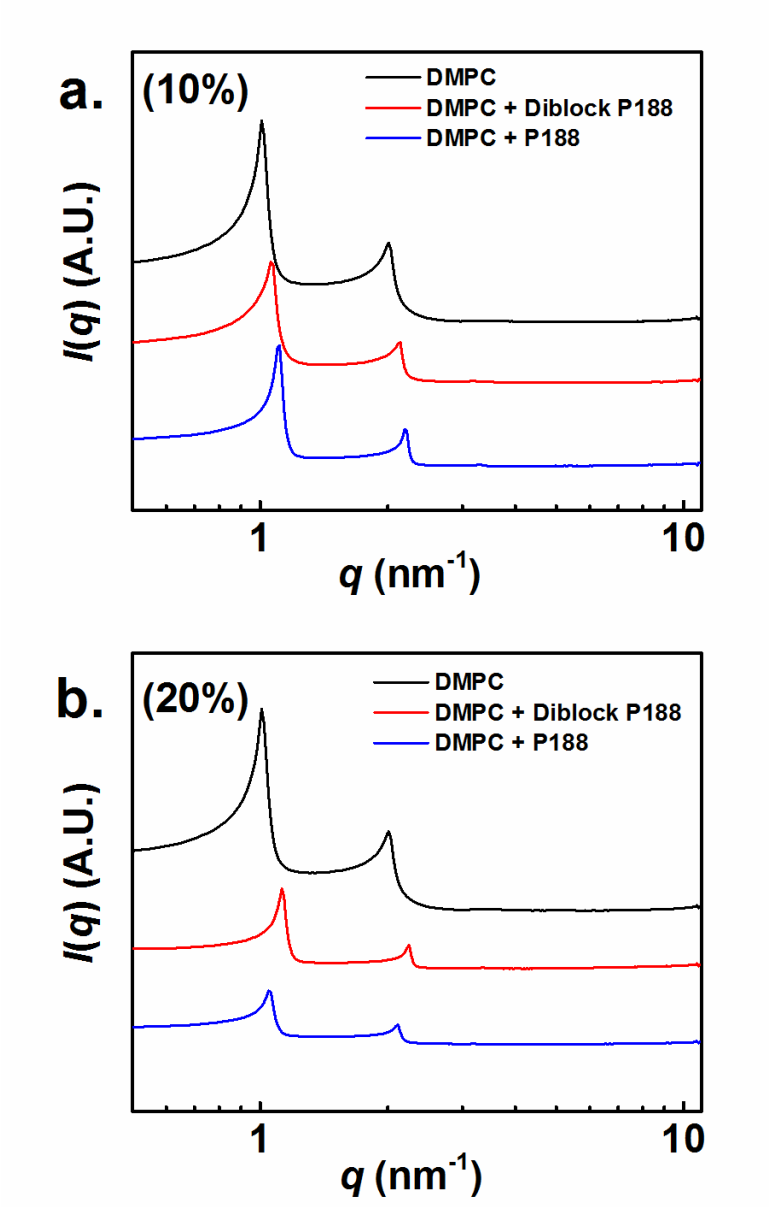


**Figure 3.14:** SAXS profiles taken on ternary dispersions of water, lipids, and polymers at 37 °C. Samples in (a) are 10 mol.-% polymer and (b) are 20 mol.-% polymer, where mole percent is calculated on the basis of total surfactant, totaling 20 wt.-% of the dispersion.

**Table 3.6:** Peak and spacing obtained from SAXS profiles. Integer ratio of $q_2/q_1$ confirms lamellar structure.

| Sample | $q_1$ nm$^{-1}$ | $q_2$ nm$^{-1}$ | $q_2/q_1$ | $d$ (Å) |
|---|---|---|---|---|
| DMPC | 1.01 | 2.01 | 1.99 | 62.4 |
| 10% Diblock P188 | 1.06 | 2.14 | 2.02 | 59.3 |
| 20% Diblock P188 | 1.05 | 2.12 | 2.02 | 60.0 |
| 10% P188 | 1.11 | 2.19 | 1.97 | 56.5 |
| 20% P188 | 1.12 | 2.25 | 1.99 | 55.9 |

The SAXS patterns in Figure 3.14 and *d*-spacing reported in Table 3.6 lend some insight into the different interaction mechanisms between the triblock P188 architecture and the new Diblock P188, in agreement with DLS results following peroxidation and incubation. Earlier SAXS studies on DMPC lamellae with P188 argued for poor incorporation by the middle PPO block into the membrane, leaving it in a flattened configuration at the lamellar interface.[90,122] This is shown schematically in Figure 3.15, which shows hypothesized differences between triblock and diblock copolymer interactions with lamellar phospholipids. The same studies reported a similar drop in *d*-spacing for P188 and DMPC samples.[90,122] Since PEO is hygroscopic, it is reasonable to point to the slight drop in *d*-spacing as a product of bilayer dehydration. The same bilayer compression was observed by DLS following liposome peroxidation with P188, for which $R_{h,app}$ (90°) fell relative to liposomes first incubated with other polymers. Similarly, multi-angle DLS revealed a drop in $R_h$ following 1 hour of incubation of liposomes with P188.

The diblock architecture, which is expected to anchor in the membrane, also reduced *d*-spacing (see Table 3.6), though to a lesser extent than P188. Several longer diblock PEO-PPO copolymers ($N_{EO}$ = 119-287; $N_{PO}$ = 19-60) studied by Firestone, et al. actually increased *d*-spacing over the neat lamellae.[122] Again, the schematic in Figure 3.15 shows the hypothetical arrangement of anchored diblock copolymers, in a "perpendicular" arrangement to the bilayer. Swelling by diblock copolymers was explained as perpendicular arrangement of block copolymers, anchored in the lipid bilayer by the exposed hydrophobic block. Since Diblock P188 is smaller than any of the polymers

investigated in that study ($N_{EO}$ = 75; $N_{PO}$ = 16) and lamellar spacing decreased by less than for the P188 samples (even at equal mass concentrations, 10% P188 and 20% Diblock P188), it is hypothesized that the perpendicular arrangement of Diblock P188 has a reduced effect on *d*-spacing as compared to P188 and longer diblock copolymers because membrane dehydration and polymer swelling of bilayers offset each other. Based on literature results and the data presented here, bilayer swelling and compression by dehydration appears to have a molecular weight dependence, and SAXS studies on additional diblock copolymer formulations (i.e. with longer PEO blocks) would clarify the finding.

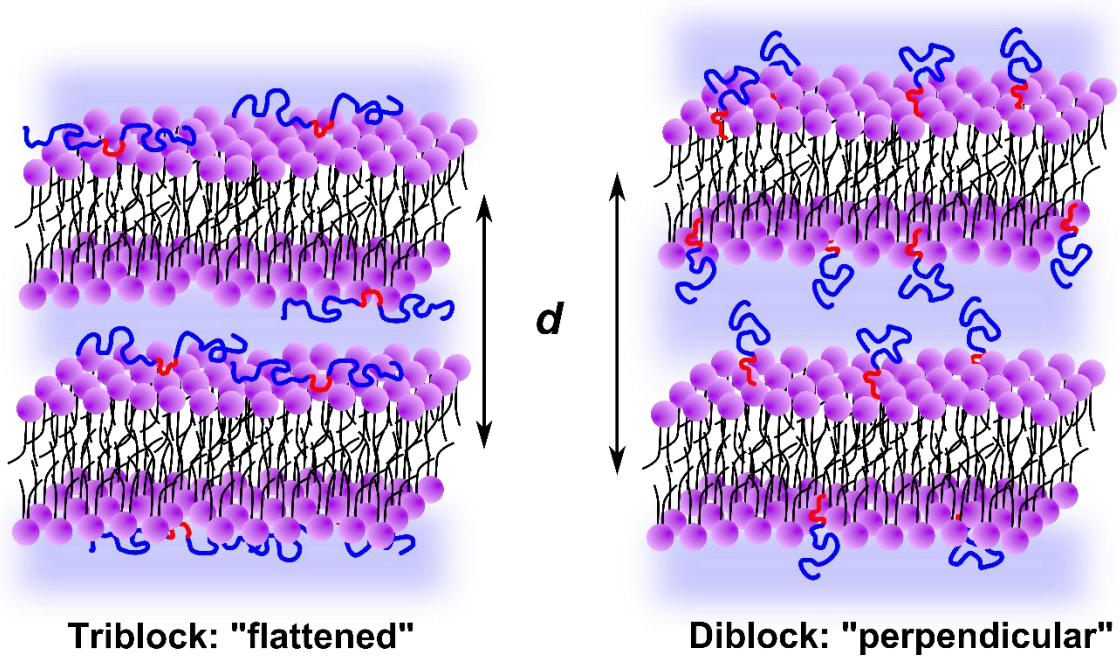


**Figure 3.15:** Multilamellar lipid arrangement showing the "flattened" configuration of non-penetrating triblock architectures (*d*-spacing reduced) and the anchored "perpendicular" arrangement (*d*-spacing increased) of the diblock architecture.

## 3.4 Conclusions and future outlook

In this work, a diblock architecture is, for the first time, considered for use as a block copolymer surfactant membrane stabilizer. In comparing peroxidation protection results between Diblock P188, P188, and PEO-8k, a concentration-dependent protective capacity against liposome peroxidation was found for all three polymer architectures. Similar, if not improved protective ability was demonstrated by Diblock P188, as compared to P188, at a

lower mass concentration. Besides the potential pharmacological benefits of Diblock P188, these results show that further insight into the membrane stabilization mechanism is accessible by pursuit of chemically similar alternatives to the standard poloxamers employed, (i.e. synthesis incorporating new chemical constituents or architectures).

*3.4.1 Liposome peroxidation assay*

Results affirmed and extended previous liposome protection work.[89] Furthermore, the analysis of scattered light intensity as a metric of protection capacity by polymers offers insight into extent of peroxidation damage that cannot be achieved by liposome size distribution characteristics alone. The approach opens the way to efficiently screen additional block copolymer chemistries for related applications. Future work employing a diblock architecture as a model compound should aim to explore the role of block lengths in membrane stabilization and to establish a connection between physiological and biophysical results.

*3.4.2 Differing interaction mechanisms by different architectures*

Fixed angle and multi-angle DLS, as well as SLS and SAXS were used to investigate the differences in interaction by the triblock architecture of P188 and its diblock copolymer analog, Diblock P188. Hydrodynamic radii and lamellar swelling characteristics showed agreement, in that P188 had a mild compressive effect on membranes, which were explained by poor incorporation into the membrane and bilayer dehydration by PEO chains coating the membrane in a flattened configuration. The hypothesized perpendicular arrangement of Diblock P188 at the bilayer had much less of an effect on membrane dimensions, even at equal mass loading as compared to P188. This "net-zero" swelling, was hypothesized to result from balancing effects of polymer swelling (by hydrophobic group anchoring) and dehydration (by coiled PEO at the interface). Further inquiry to confirm or reject this hypothesis should consider diblock architectures featuring systematic investigation of hydrophilic and hydrophobic block lengths.

*3.4.3 Future outlook: connections to in vivo or in vitro work*

Finally, the liposome peroxidation technique emerges as a low-cost screening measure to identify molecular characteristics that favor membrane interaction. In particular, it is expected to streamline concurrent efforts to determine the physiological mechanism of

membrane stabilization and protection in a Duchenne Muscular Dystrophy disease model.[29,166] Work to determine the existence of a link between these biophysical results and physiological experiments is ongoing. The following chapter explores two new systems of diblock copolymers and puts them alongside an *in vivo* membrane damage protocol in order to assess correlation strength of liposome peroxidation to the animal model.

# Chapter 4

# Effect of diblock copolymer end groups on membrane interactions

Previously, a liposome peroxidation assay was used to screen for favorable membrane-polymer interactions in a model membrane. The connection of liposome peroxidation to *in vivo* membrane damage was made hypothetically. Naturally occurring lipid peroxidation by reactive oxygen species is known to cause cell membrane damage,[51,109] and conformational changes to lipids undergoing peroxidation have also been hypothesized to invoke permeability in the membrane.[115] Permeabilized cell membranes promote the uncontrolled flux of critical ions across the membrane, to the detriment of cell viability.[72,81] A connection between the two model systems is sought in this chapter, as commonalities would facilitate membrane stabilizer development through rapid assessment of protective capability of block copolymer candidates in an inexpensive synthetic membrane.

To probe the possible links between model membranes and *in vivo* membrane damage, a strategic collection of block copolymers has been prepared, following the discovery of effective membrane protection by a diblock copolymer architecture in Chapter 3. There, using the liposome peroxidation technique, Diblock P188 was found to confer excellent protection against liposome peroxidation at a reduced mass concentration relative to P188, the classical membrane stabilizer comprised of three blocks and exactly twice the molecular weight of Diblock P188. The finding motivates continued work with diblock architectures as model systems by which to study membrane interactions by amphiphilic

block copolymers. The diblock architecture is simpler to prepare, and with its exposed hydrophobic block, it offers a promising alternative to a long-held paradigm of medical treatment by triblock architectures that is explained more by commercial abundance than specific merits.[31,43,48,53]

## 4.1 Diblock copolymers prepared

Bearing in mind that molecular weight and relative hydrophobic/hydrophilic composition play a role in directing membrane interactions,[86,89] a series of diblocks were synthesized with two different end group functionalities on the hydrophobic PPO block. In the first synthesis, PPO was grown from a tert-butoxide initiator, terminated, and reinitiated to grow PEO, which was terminated with a hydroxyl group. The resulting diblock copolymers are named t-PPO-PEO, to reflect the tert-butoxide group on the hydrophobic species (e.g. t-P0.9-E2.1, $M_{PPO}$ = 900 g/mol, $M_{PEO}$ = 2,100 g/mol). A second group of diblocks were prepared from commercially available α-methoxy-ω-hydroxyl poly(ethylene oxide). Potassium naphthalenide was used to reinitiate the hydroxyl functional group on purchased methoxy-PEOs, and blocks of PPO were grown and terminated by a hydroxyl group. These polymers follow the nomenclature OH-PPO-PEO (e.g. OH-P0.3-E2.3, $M_{PPO}$ = 300 g/mol, $M_{PEO}$ = 2,300 g/mol), indicating the hydroxyl functionality on the PPO block. Note that while the PEO block has a methoxy functional group rather than the hydroxyl group found on the t-PPO-PEO species, it is not expected to make an impact on membrane interactions, due to the length and hydrophilicity of the PEO block and low hydrophobicity of the methoxy, relative to PEO. Further synthetic detail can be found in Chapter 2. Representative structures of both t-PPO-PEO and OH-PPO-PEO diblock copolymers are shown, in order of synthesis in Figure 4.1.

A summary of block copolymers considered in this chapter is presented in Table 4.1. Molecular weight and compositions were determined by $^1$H NMR (500 MHz, in $CDCl_3$) and dispersities were determined by SEC with tetrahydrofuran as the eluent.

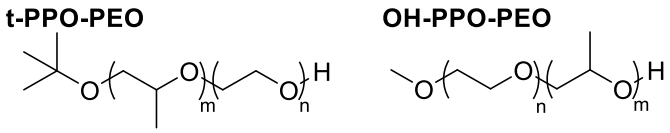


**Figure 4.1:** Chemical structures of diblock copolymers of PPO and PEO prepared with different functional groups on the hydrophobic PPO block. Polymer structures are given in the order of synthesis (from left to right).

**Table 4.1:** Summary of polymers considered in this chapter. Polymers are grouped by functional groups on hydrophobic PPO blocks, and then by like PEO compositions of about 70 and 90 wt.-%, respectively.

| Sample | $M_n$ (g/mol) | $N_{PO}$ | $N_{EO}$ | $w_{PEO}$ | $x_{EO}$ | Đ[a] |
|---|---|---|---|---|---|---|
| t-P0.9-E2.1 | 3,000 | 16 | 48 | 0.69 | 0.75 | 1.05 |
| t-P0.9-E8.0 | 8,900 | 16 | 182 | 0.90 | 0.92 | 1.04 |
| OH-P0.9-E2.0 | 2,900 | 16 | 46 | 0.70 | 0.74 | 1.03 |
| OH-P1.9-E5.3 | 7,200 | 32 | 120 | 0.74 | 0.79 | 1.03 |
| OH-P0.3-E2.0 | 2,300 | 5 | 46 | 0.87 | 0.90 | 1.05 |
| OH-P0.5-E5.3 | 5,800 | 9 | 120 | 0.91 | 0.93 | 1.04 |

[a]Sample names designate α-functional group: “t” is tert-butoxy “OH” is hydroxyl

[b]Dispersities determined by SEC.

## 4.2 Liposome incubation with diblock copolymers

As was the case in the previous investigation of polymer protection against liposome peroxidation, diblock copolymer incubation experiments were performed first to check for changes to liposome characteristics induced by exposure to polymers alone. Besides establishing whether polymers were innocuous to liposomes, incubation experiments also sought to determine whether liposome size or size distributions were affected by polymers of varying size, composition, and terminal functional group on the hydrophobic block. One could reasonably expect dehydration of liposomes by sufficient PEO at the surface (smaller $R_h$), particle fusion by interaction between adsorbed polymers, or possibly even a rise in $R_h$ due to an adsorbed layer of polymer at the surface. Two incubation times, four and twenty-four hours, were considered, in line with insertion expectations from previously reported works[33,89] as well as to maintain consistency with experiments described earlier in Chapter 3.

Incubation samples were prepared in a 5:1 polymer to phospholipid molar ratio in 2 mL aliquots, which were held at 25 °C for four or twenty-four hours. Following incubation times, samples were transferred to clean vials and diluted 5x for scattering by DLS (10 minutes, 1 μs to 1 s delay times, 90 °, 637 nm HeNe laser, 20 mW power, 25 °C). Autocorrelation functions obtained were fit by the method of cumulants to determine particle size distribution characteristics, and distributions were obtained by REPES fitting in the GENDIST software package. Liposome size distributions obtained for t-PPO-PEO and OH-PPO-PEO diblock copolymers are shown in Figure 4.2.

As is shown by Figure 4.2, liposome size distributions showed minimal variation between incubation times or polymer samples, relative to liposome only distributions. Raw scattered intensities collected from incubated samples were averaged and normalized to the liposome only scattered intensity for each of the replicates. Normalized average intensities were analyzed in JMP Pro 11 statistical software to determine the mean, standard error, and statistical difference by Tukey-Kramer HSD. Scattered intensities obtained from DLS measurements are reported in Figure 4.3. Unless otherwise noted in Figure 4.3, $N \geq 3$ for each polymer-liposome combination and incubation time. Error bars report standard error of the mean, and statistical difference from the liposome only case is indicated accordingly.

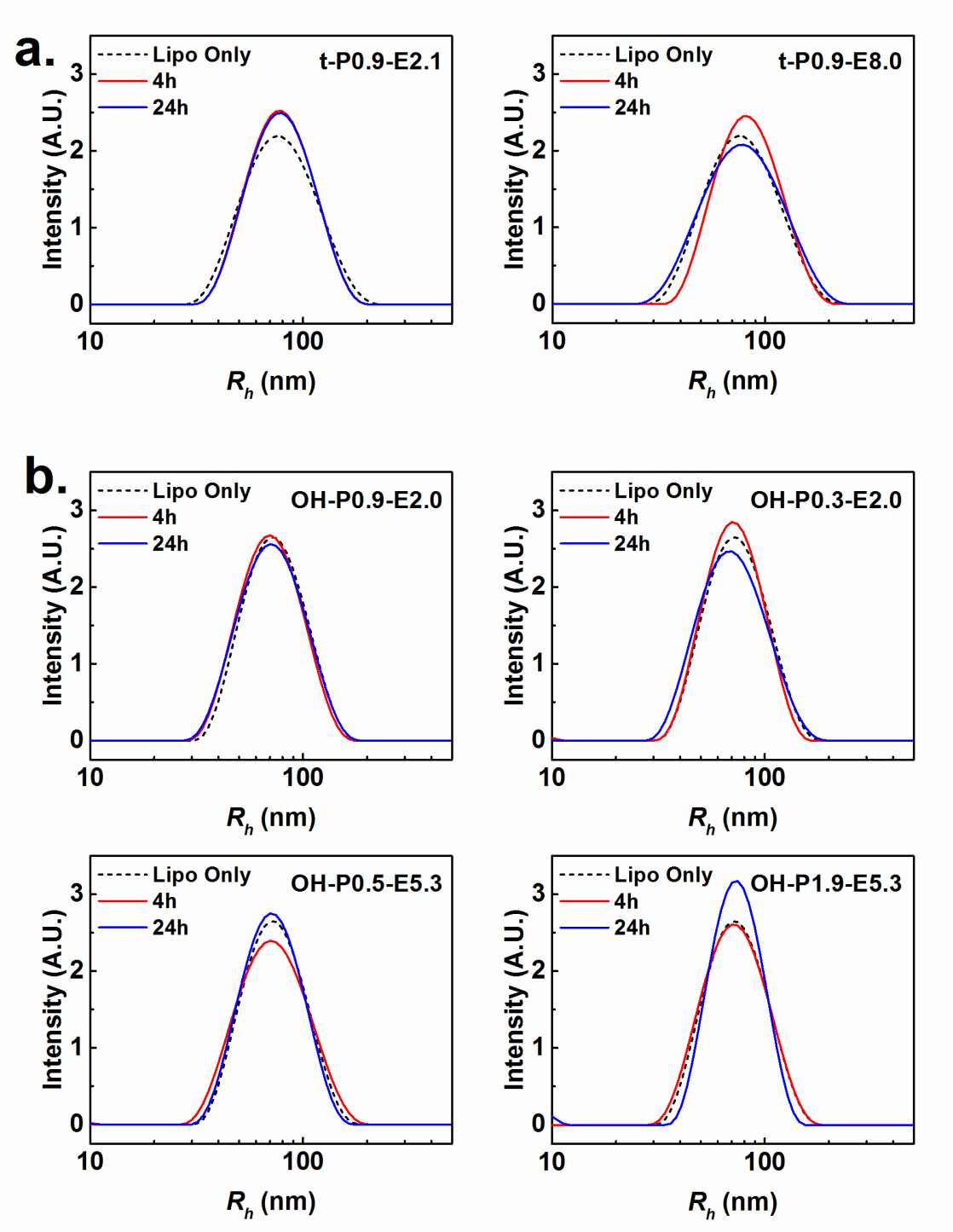


**Figure 4.2:** Representative liposome size distributions following incubation with (a) tert-butyl-PPO-PEO and (b) hydroxyl-PPO-PEO diblock copolymers. Liposome only curves are shown for reference by dashed lines.

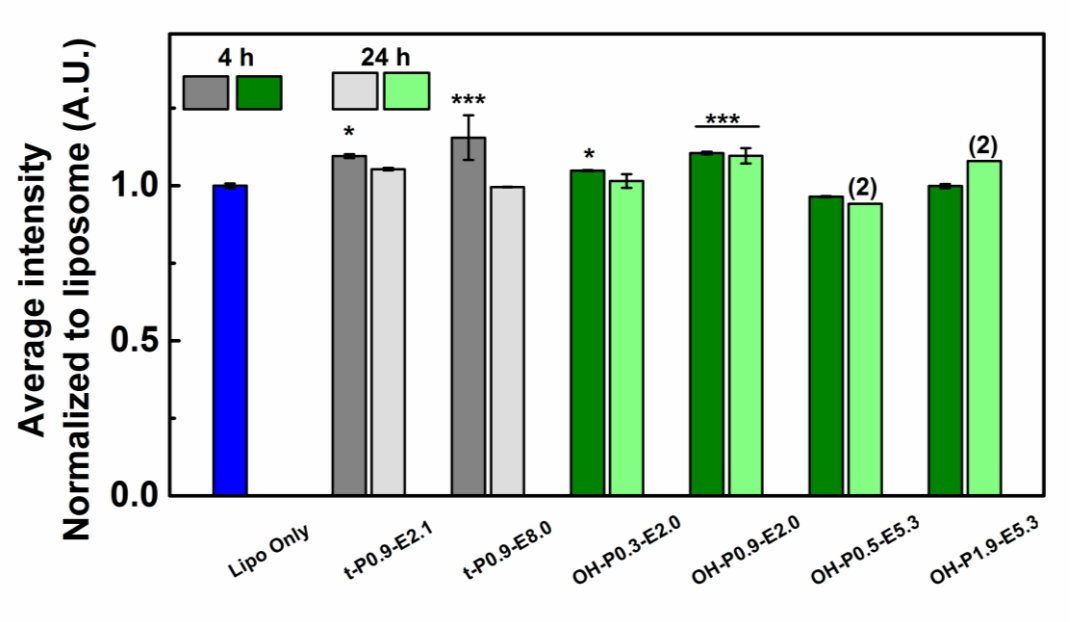


**Figure 4.3:** Scattered intensity comparison for liposmes incubated with diblock copolymers. Dark shading is four hour incubation, lighter is 24 hour incubation, and nomenclature indicates functional group on hydrophobic PPO block. Error bars correspond to standard error of the mean, with $N \geq 3$. Exceptions are shown in parentheses. Statistically different averages from liposome only case are indicated, (Tukey-Kramer HSD, $*p < 0.05$, $***p < 0.0001$).

Normalized scattered intensities in Figure 4.3 are not as tightly clustered around 1.0 as the earlier results for P188, Diblock P188, and PEO-8k, but all are within 10% of the average liposome only scattered intensity. Significant differences (Tukey-Kramer HSD) require closer inspection in liposome size calculations from cumulant fitting, which can be found in Table 4.2. Note that independent liposome controls are reported ($N$ = 9 for each) for diblocks with each of the two functional groups ("OH and "t"). Liposomes treated with "t" diblocks were prepared at a higher temperature ($T$ = 50 °C, as compared to $T$ = 40 °C), which resulted in systematically larger liposomes. The lower preparation temperature was later determined to yield better batch reproducibility, especially with respect to lipid reactivity to peroxidation.[167]

As is clear from the data in Table 4.2, liposome characteristics were not changed by four or twenty-four hour incubation with either tert-butoxy- or hydroxyl- functionalized diblock copolymers synthesized. Results were confirmed by Tukey-Kramer HSD statistical comparison, $p < 0.05$, with the same $N$ as for Figure 4.3. The only change incurred in any incubation experiment in Table 4.2 was a rise in distribution width for both 4 and 24 hour incubation experiments with t-P0.9-E8.0. The origin of this apparent distribution widening appears from the autocorrelation functions (data not shown) to be due to dust (elevated signal at long relaxation times, $\tau$). Because both 4 and 24 hour incubation times for t-P0.9-E8.0 had few replicates ($N$ = 3), the average values were highly sensitive to discrepancies. Further incubation experiments would be necessary to confirm that dust, and not some physical phenomenon, was the cause of the widening observed.

**Table 4.2:** Liposome size and distribution widths for liposomes incubated with diblock copolymers. No statistically significant differences in average $R_h$ were measured for either hydroxy- or tert-butoxy- functionalized diblocks.

| **Liposomes incubated with:** | **Average $R_h$ (nm)** | **Average dispersity ($\mu_2/\Gamma^2$)** | **Average $R_h$ (nm)** | **Average dispersity ($\mu_2/\Gamma^2$)** |
|---|---|---|---|---|
| Neat liposomes | 69.5 ± 1.7 | 0.13 ± 0.04 | | |
| | *Incubation time:* | | | |
| | 4 h | | 24 h | |
| t-P0.9-E2.1 | 73.1 ± 1.5 | 0.10 ± 0.05 | 73.0 ± 2.3 | 0.13 ± 0.03 |
| t-P0.9-E8.0 | 69.2± 1.4 | 0.28 ± 0.05 | 70.2 ± 2.6 | 0.24 ± 0.07 |
| Neat liposomes | 68.0 ± 1.0 | 0.20 ± 0.02 | | |
| | *Incubation time:* | | | |
| | 4 h | | 24 h | |
| OH-P0.3-E2.0 | 66.1 ± 0.2 | 0.14 ± 0.01 | 66.2 ± 0.9 | 0.13 ± 0.01 |
| OH-P0.9-E2.0 | 66.4 ± 0.4 | 0.12 ± 0.01 | 65.7 ± 0.2 | 0.13 ± 0.01 |
| OH-P0.5-E5.3 | 65.6 ± 0.2 | 0.15 ± 0.01 | 64.9 ± 1.2 | 0.17 ± 0.02 |
| OH-P1.9-E5.3 | 65.0 ± 0.4 | 0.16 ± 0.01 | 65.5 ± 0.2 | 0.16 ± 0.01 |

## 4.3 Liposome peroxidation with diblock copolymers of varying end groups

Having established that diblock copolymers imposed no detrimental or significant change to liposome characteristics by incubation experiments, the capability of diblock copolymers to protect liposomes against peroxidation was investigated. For each of the following test conditions, polymers were added to liposomes at a 5:1 molar ratio of polymer:phospholipid 0, 4, or 24 hours before adding the free radical generator, AAPH.[89] Reaction volumes were briefly mixed and reacted for 30 minutes at 37 °C under UV light, $\lambda$ = 254 nm. At the conclusion of reactions, sample volumes were diluted five-fold by ultrapure water and immediately measured by DLS.

### *4.3.1 Peroxidation results for t-butyl functionalized PPO-PEO*

Normalized scattered intensity results for peroxidation experiments performed on liposomes in the presence of tert-butoxy- functional PPO-PEO diblock copolymers are shown in Figure 4.4. Liposome scattered intensity and the negative control (liposomes reacted with AAPH in the absence of polymer) are shown for reference. Results shown are for $N \geq 6$, with error bars reporting standard error of the mean.

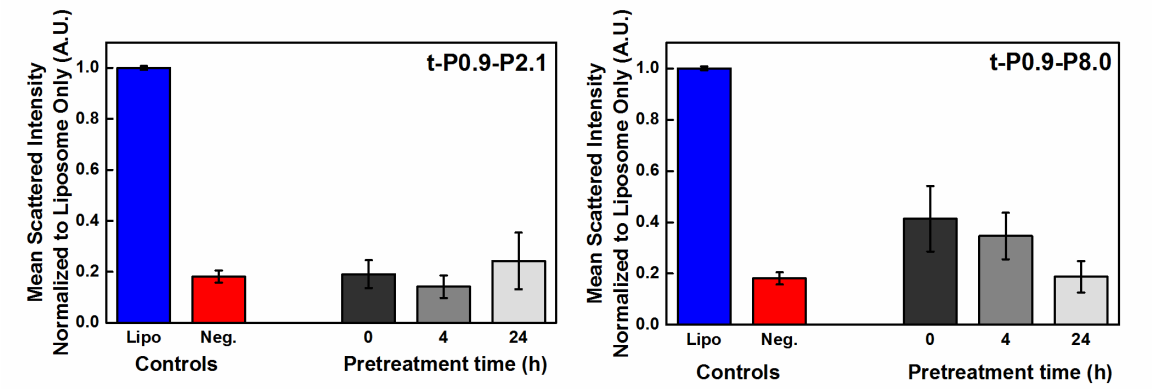


**Figure 4.4:** Scattered intensity results for peroxidation of liposomes in the presence of 5:1 polymer:lipid tert-butoxy- functionalized PPO-PEO diblock copolymers. Data are normalized to liposomes (Lipo), and negative control shows scattered intensity of liposomes reacted with AAPH in the absence of block copolymers. Error bars show standard error of the mean for $N \geq 6$.

The two tert-butoxy- functional PPO-PEO diblock copolymers shown in Figure 4.4 have hydrophobic block lengths equal to Diblock P188 ($N_{PPO}$ = 16). As shown in Chapter 3, the protective capacity of Diblock P188 against peroxidation was quite high, with normalized intensities reaching 70-80% of the liposome only control case. The two tert-

butoxy-functional diblock copolymers shown above differ in PEO composition from Diblock P188 by ±10 wt.-%, i.e. t-P0.9-E2.1 is 70 wt.-% PEO, and t-P0.9-E8.0 is 90 wt.-% PEO. They also differ in PPO functional group; Diblock P188, which was commercially prepared, features a methoxy-functional group on the PPO block, which would be less hydrophobic in comparison to the tert-butoxy groups on t-PPO-PEO polymers.

The low scattered intensities exhibited by both compositional variations on Diblock P188 suggest one of two scenarios. First, neglecting end-groups, it could be naively reasoned that the 80 wt.-% PEO composition is a "sweet spot" for membrane protection by a PPO block of this length. However, strong protection by the PEO-8k sample in Chapter 3 (65-70% scattered intensity relative to liposome only case), with an identical PEO block length relative to t-P0.9-E8.0 and no hydrophobic block, negates this theory. The alternative scenario is that the more hydrophobic tert-butoxy- end groups detrimentally interact with lipid membranes undergoing early stages of peroxidation. Along this line of reasoning, it is possible that early peroxidization events and conformational changes in the membrane are exacerbated by the migration of nearby diblock copolymers deep into the membrane (i.e. "anchoring"); in this case, the presence of the bulkier tert-butoxy end group could further raise membrane tension and hasten liposome rupture. Combined with the non-detrimental effect of liposome incubation by t-PPO-PEO, the second explanation is better aligned with reported results of non-association by poloxamers with non-permeabilized membranes and adsorption to membranes of reduced lipid density.[39,43]

*4.3.2 Peroxidation results for hydroxyl-functionalized PPO-PEO*

Because the effective removal of the second hydrophilic poloxamer block (i.e. diblock architecture), exhibited higher protection at equal PEO mass concentrations of Diblock P188 and P188, it is reasonable to expect that subtle changes to the end groups of the free hydrophobic block would be significantly impactful as well. To investigate the significance of diblock copolymer end groups on membrane interactions, the diblocks containing hydroxyl-terminated PPO were prepared. Peroxidation experiments performed on liposomes incubated with hydroxyl-PPO-PEO diblock copolymers are summarized by scattered intensity results in Figure 4.5.

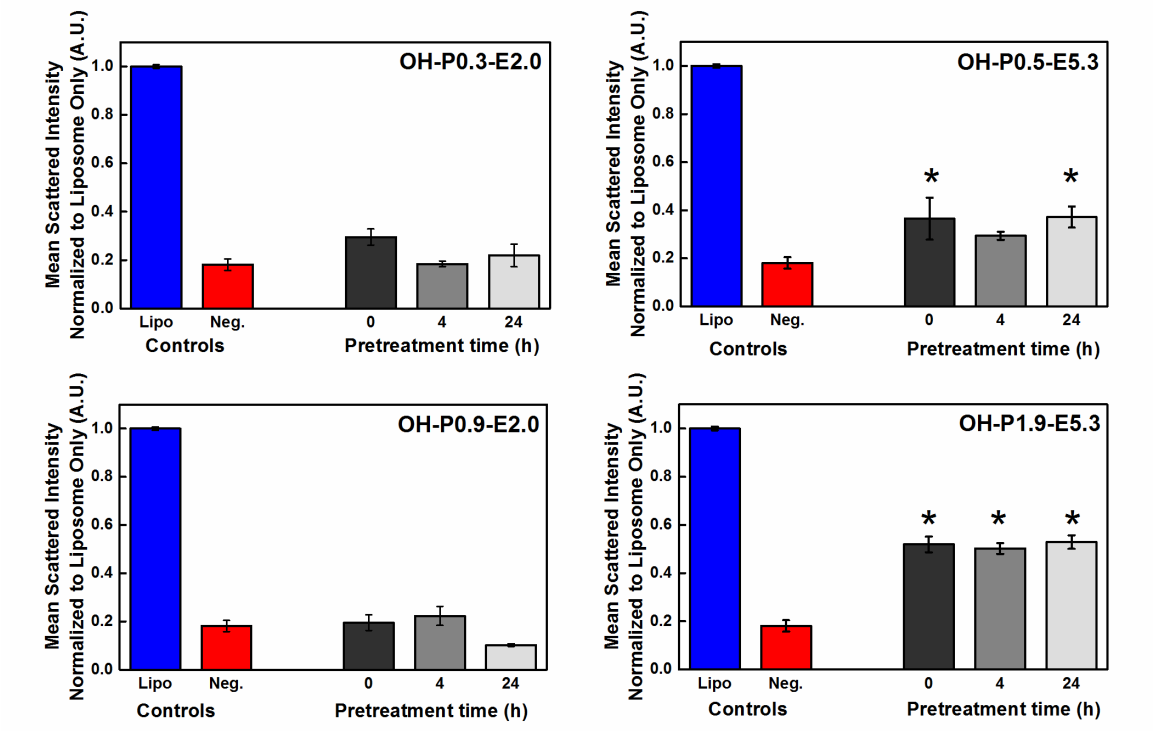


**Figure 4.5:** Scattered intensity results from liposome peroxidation experiments with OH-PPO-PEO diblock copolymers. Negative control represents intensities following reaction of liposomes with AAPH in the absence of polymers. For polymer pretreated samples, $N = 5$, and error bars show standard error of the mean. (*$p < 0.05$, Tukey-Kramer HSD against negative control).

Statistical analysis on average scattered intensities in Figure 4.5 ($N = 5$, Tukey-Kramer HSD, $p < 0.05$) showed that diblocks prepared from the 2,000 g/mol methoxy-PEO precursor showed insignificant difference from the negative control (liposomes reacted with AAPH, in the absence of polymer). On the contrary, significant improvement was exhibited by the diblocks prepared from the longer 5,300 g/mol methoxy-PEO precursor. Here, the longer PPO block (OH-P1.9-E5.3) showed about 50% of the scattered intensity of the untreated liposome control, and even the difference in scattered intensity exhibited by the smaller OH-P0.5-E5.3 was statistically significant at 0 and 24 hours of polymer pretreatment. Although the four hour pretreatment with OH-P0.5-E5.3 did not yield statistical significance against the negative control ($p = 0.53$, Dunnett's method), it was not statistically different than pretreatment at 0 or 24 hours. Further experimentation is expected to elucidate statistical questions raised by the OH-P0.5-E5.3 sample.

*4.3.3 Liposome size following peroxidation*

As was discussed in Chapter 3, DLS offers helpful insight into diminishing populations of relatively unchanged particles, such as liposomes protected against peroxidation by P188 or Diblock P188. In general, scattered intensities obtained from protective cases corresponded to small or negligible changes to size distribution characteristics returned from fitting routines performed on autocorrelation functions. Challenges remain, however, and are demonstrated in the end-group functionalized diblock copolymers featured here.

To start, the non-protective cases (scattered intensities insignificantly different than the negative control case, or background) yielded too little signal to fit autocorrelation functions. This was not initially a cause for concern in the t-PPO-PEO diblocks; after all, the scattered intensity metric is a strong indicator of a total loss of a population of liposomes. The partially protected cases of OH-PPO-PEO diblocks, however, presented a very different story. Autocorrelation functions obtained following reactions of liposomes incubated with OH-P0.5-E5.3 are shown for four protective replicates (of five total) in Figure 4.6, along with a liposome autocorrelation function for reference and a table of characteristic $R_h$ and $\mu_2/\Gamma^2$. Here, decays of autocorrelation functions for the liposomes incubated with OH-P0.5-E5.3 and then reacted with AAPH occur at shorter decay times,

indicating smaller particle sizes, and plateau heights were diminished, as compared to the liposome only case. The general form of autocorrelation functions is clearly monomodal, with noise at short decay times, but distribution widths for samples reacted in the presence of OH-P0.5-E5.3 are significantly higher than what is considered acceptable (in general $\mu_2/\Gamma^2 \leq 0.2$).[147]

Together with the scattered intensity plots for OH-P0.5-E5.3 in Figure 4.5, autocorrelation functions and corresponding particle sizes bring some clarity to the minimal protective effect observed across all incubation times. As previously mentioned, scattered intensity of DLS is volume-weighted,[159] and in the range of Rayleigh scattering (~ λ/10, or ~60 nm), intensity scales with $R^6$.[150,157] As such, the fundamental assumption underlying the population counting strategy of scattered intensity, that is, the assumption of constant particle size, breaks down for this system of diblock copolymers, and direct comparisons of scattered intensity between populations of neat liposomes and post-reaction liposomes cannot be made. The break-down is observed in all time points of the two protective diblock copolymers, OH-P0.5-E5.3 and OH-P1.9-E5.3, compiled in Table 4.3.

Aside from deviating from the assumption of constant particle size, negating a quantitative assessment of liposome population before and after reaction, the drastic reduction in apparent particle sizes and distribution widths raises mechanistic questions for the hydroxyl-terminated diblock copolymers. The significant rise in distribution width, together with the dramatically smaller particle size, suggest heterogeneity in phospholipid assemblies. Possible components could include liposomes, fused liposomes, and polymer-phospholipid aggregates, all further complicated by likely liposome dehydration by polymers at the elevated reaction temperature (37 °C). Why these particular polymers facilitated such significant changes when P188, Diblock P188, and PEO-8k remained so consistently similar to neat liposomes is unknown. At the very least, the study could be repeated to determine if the effect was liposome-related, but further investigation of diblock copolymer interactions with model membranes by more powerful methods (i.e. SANS[168,169] or $^1$H NMR[97]) would help to determine the cause of the anomalous results.

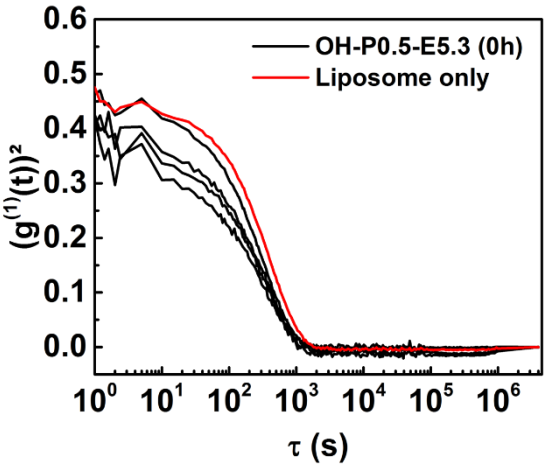


| Sample | $R_h$ (nm) | $\mu_2/\Gamma^2$ |
|---|---|---|
| Liposome only | 64.8 | 0.13 |
| OH-P0.5-E5.3 | 41.3 | 0.50 |
| | 38.0 | 0.63 |
| | 42.1 | 0.55 |
| | 47.9 | 0.26 |

**Figure 4.6:** Autocorrelation functions for OH-P0.5-E5.3, reactions following 0 h incubation. Representative liposome only curve is shown for reference, and cumulant-fitting determined $R_h$ and distribution width are given in accompanying table.

**Table 4.3:** Liposome size distribution characteristics following peroxidation reactions. Parameters were obtained by cumulant fitting of autocorrelation functions for 0, 4, and 24 h incubation times prior to reaction.

| Sample | $R_h$ (nm) | $\mu_2/\Gamma^2$ | $R_h$ (nm) | $\mu_2/\Gamma^2$ | $R_h$ (nm) | $\mu_2/\Gamma^2$ |
|---|---|---|---|---|---|---|
| Liposome only | 64.8 | 0.13 | | | | |
| OH-P0.5-E5.3 | 0 h | | 4 h | | 24 h | |
| | 41.3 | 0.50 | 26.7 | 1.05 | 39.2 | 0.74 |
| | 38.0 | 0.63 | 33.7 | 0.84 | 21.7 | 1.21 |
| | 42.1 | 0.55 | 39.2 | 0.64 | 45.6 | 0.51 |
| | 47.9 | 0.26 | 21.0 | 1.27 | 49.6 | 0.44 |
| OH-P1.9-E5.3 | 0 h | | 4 h | | 24 h | |
| | 40.6 | 0.37 | 35.0 | 0.55 | 41.9 | 0.40 |
| | 48.0 | 0.37 | 43.0 | 0.39 | 43.3 | 0.37 |
| | 37.3 | 0.48 | 42.7 | 0.35 | 46.3 | 0.33 |
| | 51.3 | 0.31 | 39.3 | 0.44 | 41.9 | 0.42 |
| | 44.6 | 0.31 | 37.7 | 0.46 | | |

*4.3.4 Peroxidation dependence on PEO block length*

Since the diblocks featuring the longer PEO block were the protective cases (non-background scattering) in the peroxidation results above, the methoxy-PEO-OH precursors to the OH-PPO-PEO diblocks were examined to determine what, if any, role PPO plays in liposome protection. Scattered intensity results for pretreatment time (incubation) of 0 and 4 hours are shown, together with di-hydroxy-PEO results (PEO-4k and PEO-8k) in Figure 4.7. The shorter PEO homopolymers, m-PEO-2k and PEO-4k, showed no statistical improvement over the negative control, whereas both m-PEO-5.3k and PEO-8k did. No statistically significant differences between the 5,300 g/mol and 8,000 g/mol PEO samples were discernible ($p < 0.05$, Tukey-Kramer HSD).

Based on these additional PEO homopolymer results, a few conclusions about beneficial interactions by polymers with synthetic bilayered membranes may be drawn. First, for liposome protection against peroxidation, a critical PEO block length emerges at the chosen molar concentration (5:1 polymer:lipid ratio). Difference between protection (5,300 g/mol PEO) and peroxidation (4,000 g/mol PEO), suggest the existence of a narrow molecular weight window at which the protective effect becomes significant. This phenomenon is further complicated by the addition of the hydrophobic PPO block. Diblock P188, with a PEO block at about 3,400 g/mol, would not be expected to protect liposomes against peroxidation based on PEO block length alone, but the additional 900 g/mol PPO block participates in attraction, protection, or both. As shown in Chapter 3, increased PEO concentration relative to liposomes may enable a protective effect by shorter PEO blocks; it is expected the same would apply to 2,000 g/mol PEO.

If overall molecular weight, rather than PEO molecular weight, were the critical parameter, the observed absence of protection by t-P0.9-E2.1 and OH-P0.9-E2.0 would be easily reconciled, but since the t-P0.9-E8.0 diblock also showed no protective effect, the end group on PPO is again raised as a vital contributor to membrane interactions. Here, highly hydrophobic tert-butoxy- functional groups could enhance membrane disruption effects initiated by lipid peroxidation. As lipid conformation changes drive membrane tension up and lipid spacing apart,[104,115] hydrophobic regions of the membrane would be exposed to nearby hydrophobic blocks, and instead of the weak interactions expected for

PPO, the stronger end-group interaction could pin or "anchor" the diblock to the membrane, allowing bulky and hygroscopic PEO to further increase membrane tension, rather than encapsulate or coat it.

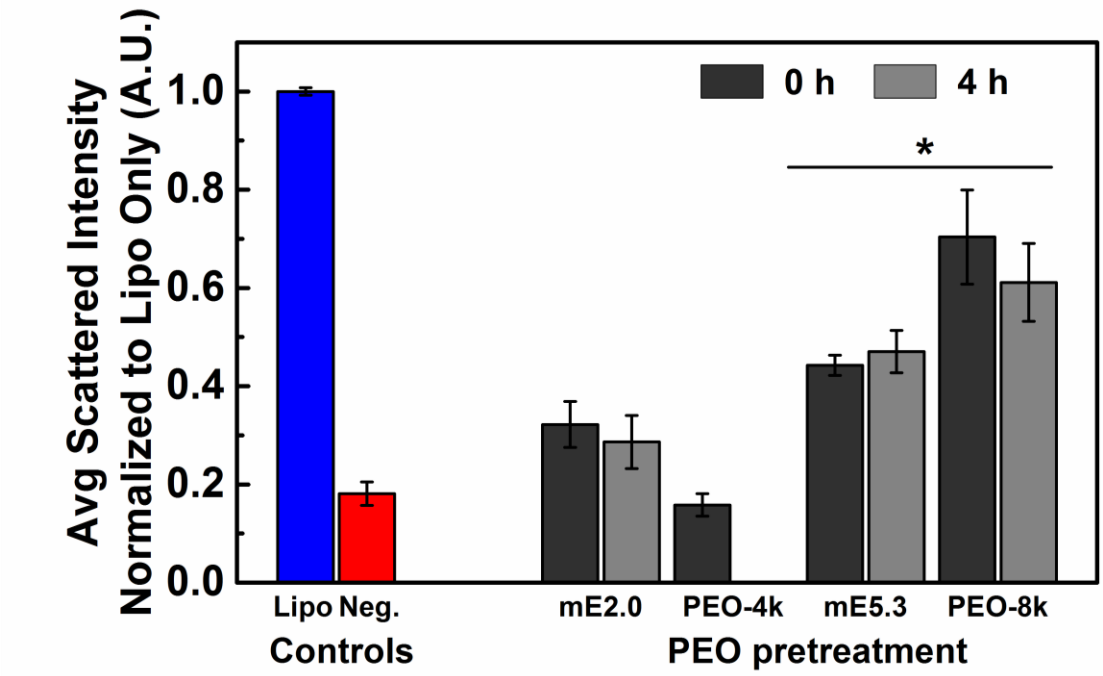


**Figure 4.7:** Scattered intensity comparison of liposome peroxidation protection by PEO homopolymers of varying $M_n$ after 0 and 4 hours of pretreatment. Nomenclature indicates mono-methoxy- functionalized: m-PEO. PEO-4k and PEO-8k are di-hydroxy- functionalized. Error bars show standard error of the mean for $N \geq 5$ replicates.

## 4.4 Preliminary connections to *in vivo* studies

One of the primary goals of liposome peroxidation studies was to develop a facile route to screening block copolymer surfactant chemistries for potential impact on *in vivo* models of membrane instability. The screening assay would offer the benefit of inexpensive, repeatable sampling carried out in a controlled, freely-available system. Because the environment surrounding model membranes or even isolated muscle cells is so different than the tissue of an *in vivo* physiological model, it is important to understand how or if *in vitro* liposome peroxidation experiments are capable of predicting *in vivo* outcomes. It has been shown in parallel work that P188 is capable of preserving skeletal muscle function against a limb-lengthening injury protocol in a mouse model of Duchenne Muscular Dystrophy, the *mdx* mouse, where the hallmark of the disease is a pronounced

muscle cell membrane susceptibility to contraction induced damage.[57] Because P188 also showed a positive protective effect in the liposome peroxidation results in the literature[89] and the previous chapter, confirmation of the technique as a screening assay could be found in careful assessment of other block copolymers, such as those investigated here.

The following *in vivo* experiments were performed by Evelyne Houang in the Department of Integrative Biology and Physiology at the University of Minnesota, under the supervision of Professor Joseph Metzger.

*4.4.1 Methods*

An *in vivo* lengthening contraction injury protocol (Figure 4.8) was performed on anesthetized *mdx* (*C57BL/10*ScSn-DMD*mdx*) or wild type *BL/10* (*C57BL/10*ScSn) mice.[57,170,171] At least 30 minutes prior to the injury protocol, block copolymer solution (150 mg/mL in sterile saline) or an equivalent volume of saline was administered intraperitoneally (IP). The hind paw of each test subject was secured to a foot-plate equipped with a servomotor (Figure 4.8a). Torque acting on the plate due to muscle contraction was measured with the servo motor controlling the angle at which the paw extends from upward to downward. Contractions of the anterior crural muscle compartment were induced by electrical stimulation of the peroneal nerve via percutaneous electrodes. A pre-injury isometric torque was initially measured to obtain baseline muscle contractile properties.

The lengthening injury protocol involved passive flexing of the foot by 19° by the servo motor (i.e. muscle shortening, Figure 4.8b) followed by an isometric contraction (100 ms) and another stimulation (50 ms) as the muscle compartment contracted while the servo motor simultaneously moved the paw 19° past neutral (a total of 38° ankle rotation, Figure 4.8c). Maximum force acting on the plate was recorded for each of 50 successive contractions, with 10 seconds of rest in the neutral foot position (rest, Figure 4.8d) to avoid fatigue. A final isometric force reading was taken following the lengthening protocol.

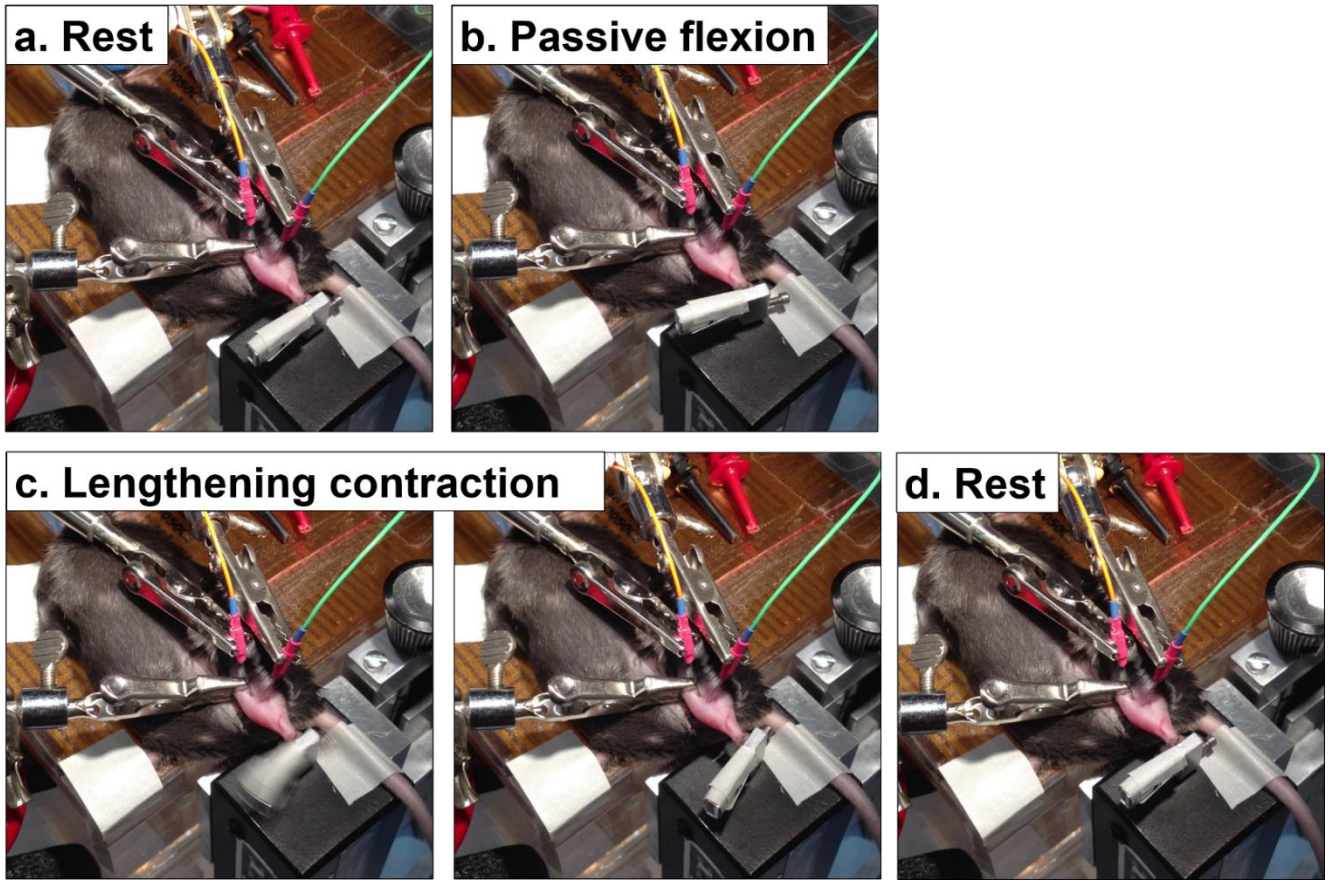


**Figure 4.8:** Lengthening contraction injury protocol stages. Rest (a) shows neutral ankle and placement of electrodes. Passive flexion (b) move foot plate to 19° position. Following peroneal nerve stimulation, lengthening contraction (c) and return to rest (d). Cycle is repeated 50 times, 10 seconds apart.

*4.4.2 P188, Diblock P188, and PEO-8k lengthening contraction injury*

Lengthening contraction injury protocols were first performed for the base polymers motivating the work, P188 and both Diblock P188 and PEO-8k. Shown in Figure 4.9 are average force curves for control (*C57BL/10* Saline and *mdx* Saline) mice and *mdx* mice treated with respective polymers by intraperitoneal (IP) injection 30 minutes prior to experiments. Dosages of polymers are held at a fixed 1,000 mg/kg for all experiments. Data are normalized to peak force for comparison. Plots which zoom in on the initial 15 lengthening contractions are also shown, highlighting the most significant differences between polymer-treated *mdx* subjects and the *mdx* control animals treated with saline.

Data in Figure 4.9 show several key features. First, the lengthening injury protocol shows a drop in force over the duration of the experiment for both the wildtype (*C57BL/10*) and *mdx* mouse. The key difference between the two is the sharp drop-off by force over the first 15 contractions. It is important to note that healthy, wild-type muscle will easily recover from the induced injury in the protocol (e.g. similar to muscle soreness following jogging), whereas force recovery by *mdx* or DMD skeletal muscle is far reduced.[171] From the data in Figure 4.9, only Diblock P188 shows a slight trend of improvement over the *mdx* case, although it is not statistically significant. Parallel work has shown that if P188 is instead delivered subcutaneously (i.e. under the skin in a fatty deposit at the scruff of the neck), it shows marked improvement over the *mdx* negative control.[57] A comparison of delivery methods is made in Figure 4.10, where a lower dose (460 mg/kg) of P188 was delivered subcutaneously (SubQ) and intraperitoneally (IP). Controls were untreated, rather than treated by saline, but no delivery-dependent saline effect on control results were observed (data not shown).

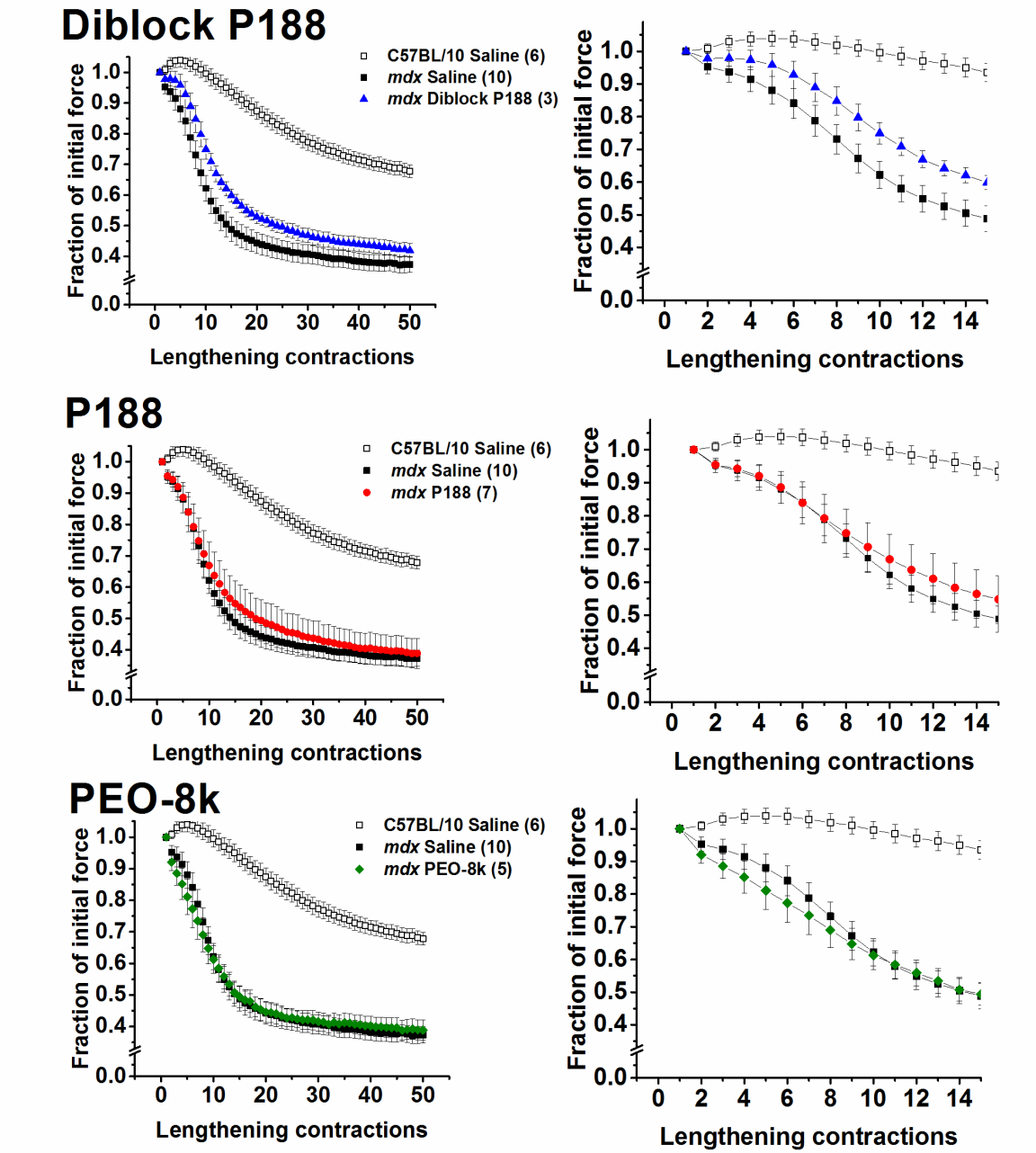


**Figure 4.9:** Lengthening contraction injury force curves for Diblock P188, P188, and PEO-8k. Data in the right column are zoomed in on the initial 15 contractions. Error bars show standard error of the mean, and number of replicates is indicated in parentheses. Data collected by Evelyne Houang.

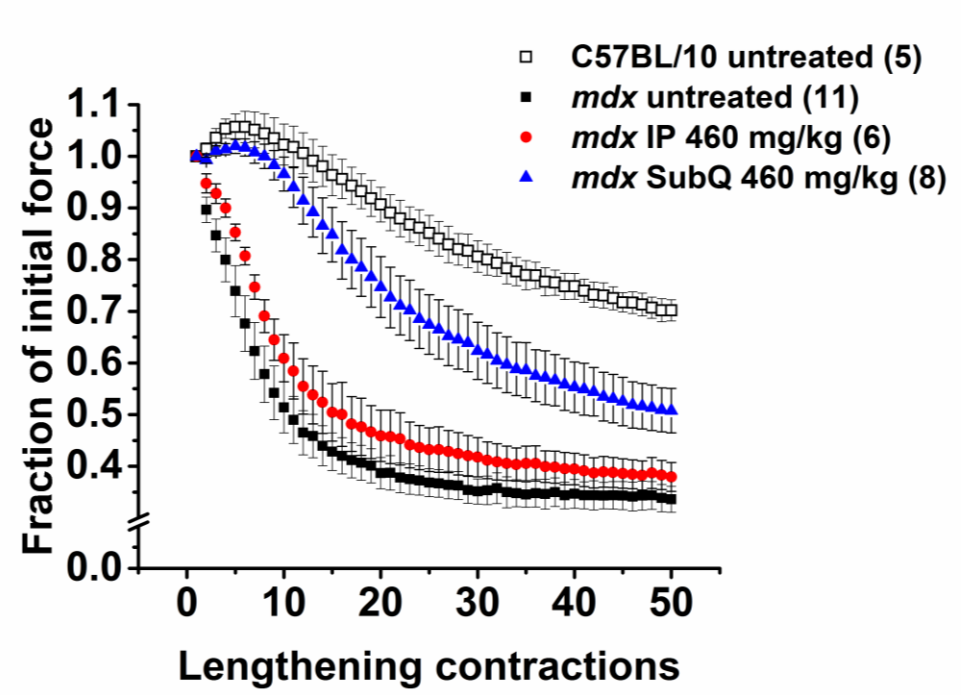


**Figure 4.10:** Impact of delivery route on P188 stabilization in lengthening contraction injury protocol. Data collected by Evelyne Houang and reported in Houang, et al.[57]

As is clear from Figure 4.10, both pharmacokinetics (i.e. distribution of a drug in the body) and pharmacodynamics (i.e. the physiological effects of the drug on the body) significantly impact protection against injury in *mdx* mice. Diblock copolymer experiments described below were performed in parallel to P188 experiments, using IP delivery, and as will be shown, they gave very different results. Keeping in mind the delivery dependence of P188, diblock copolymer results may shed some light on the reasons for the drastic differences shown in Figure 4.10. Results of the delivery route study affirm the complexity of the membrane stabilization mechanism and open the way for future investigations.

*4.4.3 Tert-butoxy- functional diblock copolymers*

Next, tert-butoxy functional diblock copolymers were investigated. As compared to the methoxy-terminus on PPO in Diblock P188, the tert-butoxy group on PPO in these diblocks is considerably more hydrophobic. Liposome peroxidation experiments previously discussed showed no significant protection by either t-P0.9-E2.1 (70 wt.-% PEO) or t-P0.9-E8.0 (90 wt.-%), but strong protection against peroxidation was demonstrated by Diblock P188, of equal hydrophobic block length and at 80 wt.-% PEO,

compositionally intermediate to both t-PPO-PEO species. For lengthening contraction injury experiments of tert-butoxy functionalized diblock copolymers, IP delivery of 1,000 mg/kg was again administered 30 minutes prior to experiments. Figure 4.11 shows normalized force as a function of contraction number for the entire duration of the experiment, along with magnified plots for the initial 15 contractions.

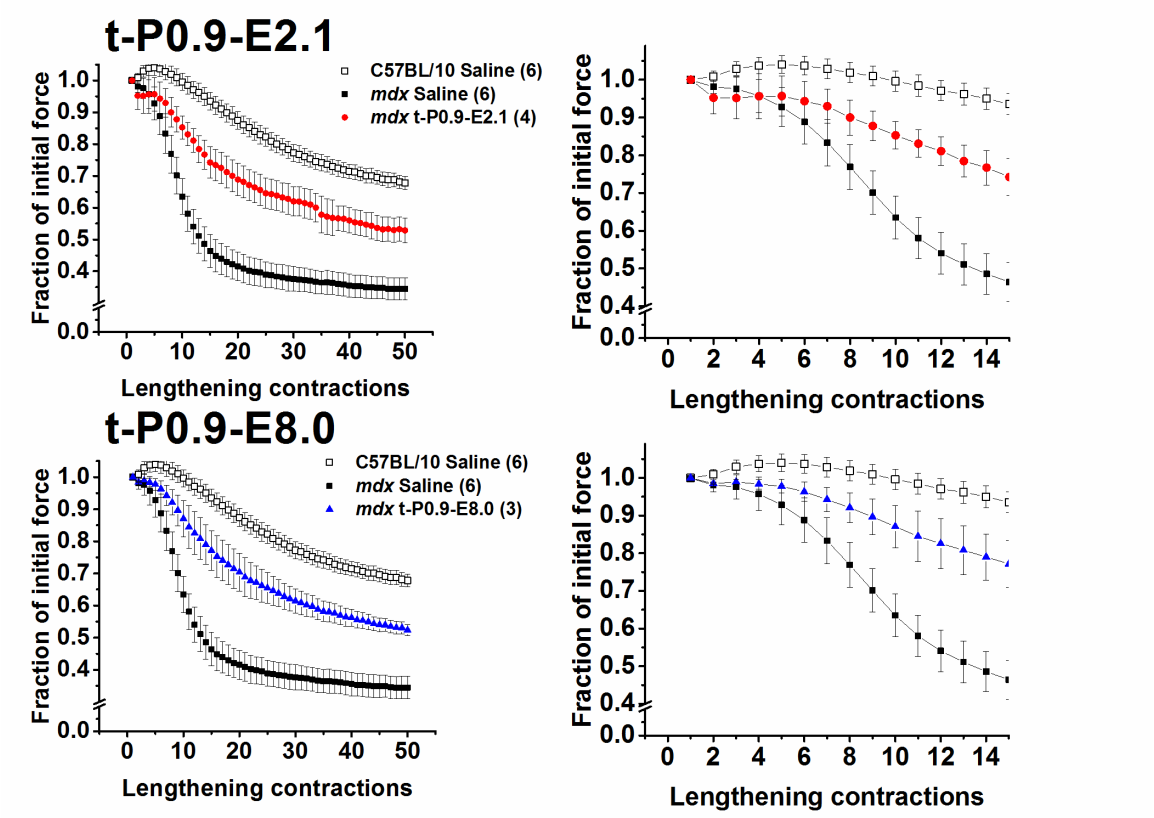


**Figure 4.11:** Lengthening contraction injury force curves for tert-butyl functionalized diblock copolymers (1,000 mg/kg IP). Left shows full experiment, and right shows first 15 contractions. Error bars show standard error of the mean, and number of replicates is listed in parentheses. Data collected by Evelyne Houang.

In stark contrast to Figure 4.9, tert-butoxy functional diblock copolymers exhibited marked improvement in skeletal muscle protection against lengthening contraction injury in Figure 4.11. It is important to note that compositionally, t-P0.9-E2.1 and t-P0.9-E8.0 bracket Diblock P188 (70 and 90%, respectively for t-PPO-PEO, and 80% for Diblock P188), and all three share a common PPO block length ($N_{PO}$ = 16). The results make clear the importance of the hydrophobic block interaction and the sensitivity of membrane interaction to the functionality of the hydrophobic block, but they also indicate that the

PEO block length is not as critical a factor to in vivo membrane stabilization as was observed in peroxidation experiments. A more detailed discussion regarding the significance of the end groups will follow the hydroxyl- functional diblock copolymers.

*4.4.4 Hydroxyl-functional diblock copolymers*

After investigating diblock copolymers with a more strongly hydrophobic end group, the hydroxyl-functionalized diblock copolymers were considered. Recall that liposome peroxidation results showed better protection by hydroxyl-functionalized diblocks of a sufficiently long PEO block length, namely OH-P0.5-E5.3 and OH-P1.9-E5.3, but the shorter PEO block lengths were not protective. Having isolated an end-functional group that does not inherently bar liposome protection against peroxidation, namely the hydroxyl end group, the role of molecular characteristics on membrane interactions could be directly compared

Results of the lengthening injury protocol for the final group of diblock copolymers are shown in Figure 4.12 (no data for OH-P0.3-E5.3). Notably, one polymer, OH-P0.5-E5.3 shows a statistically significant protective effect (two-way ANOVA against *mdx* control, $p < 0.05$), whereas neither of the other two polymers did. This result highlights the importance of the hydrophobic block length as a key contributor to membrane stabilization, alongside end group functionality.

Recall that previously, two t-PPO-PEO diblock copolymers imparted better protection against muscle injury than Diblock P188, with a methoxy-terminated PPO block of the same length ($N_{PO} = 16$). The result was attributed to the strong hydrophobic character of the tert-butoxy end group, as compared to the methoxy group on Diblock P188. Here, however, a diblock copolymer (OH-P0.5-E5.3) with a hydroxyl-functional group on PPO has conferred protection to membrane-impaired muscle undergoing the lengthening contraction injury; i.e. a strongly hydrophobic end group is not required to induce beneficial membrane interaction and stabilization. This finding draws close attention to the key distinction between OH-P0.5-E5.3 and the other two hydroxyl-functional PPO-PEO diblock copolymers tested *in vivo*, namely, hydrophobic block length.

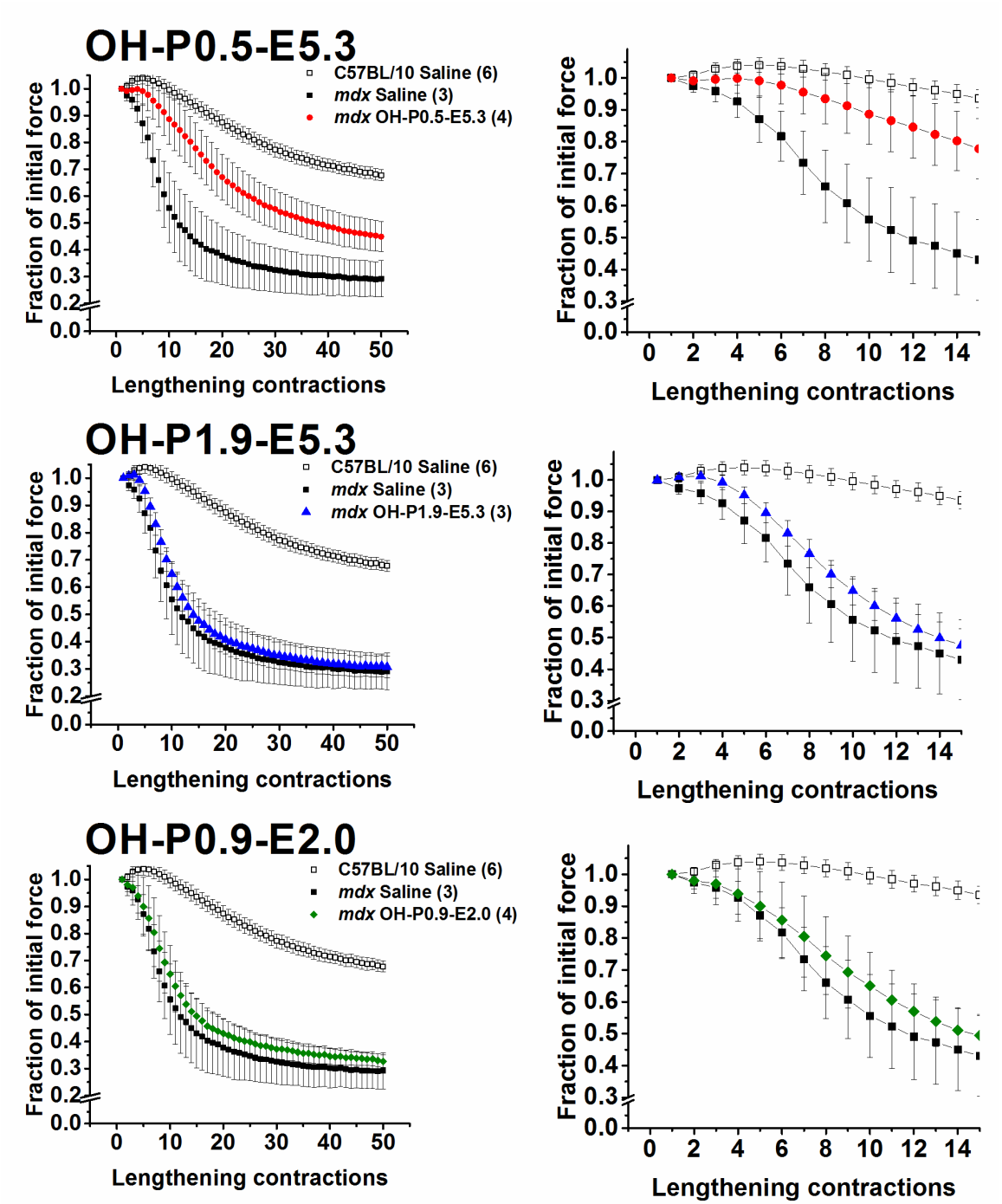


**Figure 4.12:** Lengthening contraction injury force curves for hydroxyl functionalized diblock copolymers (1,000 mg/kg IP). Left shows full experiment, and right shows first 15 contractions. Error bars show standard error of the mean, and number of replicates is listed in parentheses. Data collected by Evelyne Houang.

*4.4.5 Composite evaluation and hypothesized role of block length and end-groups in membrane stabilization*

To summarize the *in vivo* study described above, a plot showing the extent of injury induced by the 50 lengthening contractions protocol is shown. Figure 4.13 features averages of isometric force post-injury protocol normalized to pre-injury isometric force. Note that the wild-type *C57BL/10* test group show about a 40% drop in muscle function over the course of the injury. Protective polymers, as indicated by statistical significance, conferred nearly matched retention of pre-injury isometric force as compared to the wild-type test group.

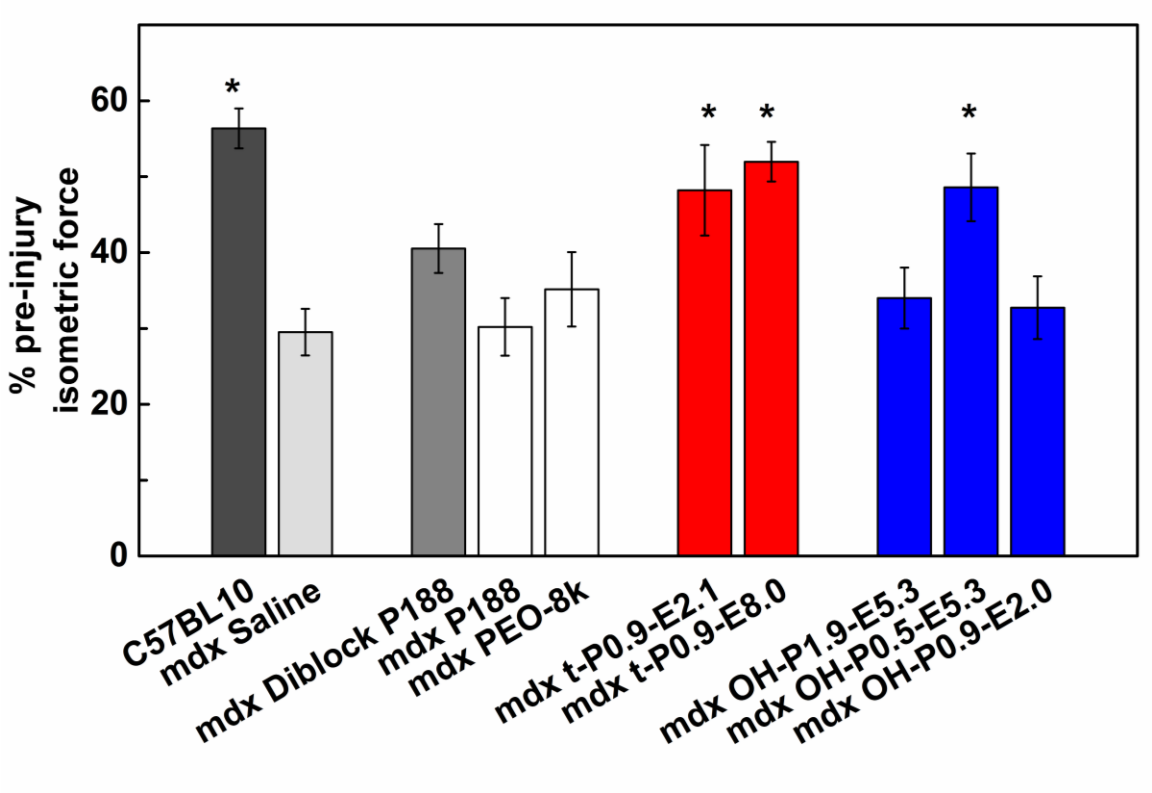


**Figure 4.13:** Average isometric force post-injury, normalized to pre-injury isometric force. Error bars show standard error of the mean. Statistical significance (two-way ANOVA against *mdx* Saline, $p < 0.05$) is indicated by (*). Data collected by Evelyne Houang.

Based on data showing membrane stabilization *in vivo* by diblock copolymers with specific molecular characteristics, a hypothesis can be formed linking PPO block length and end group functionalities. PPO is mildy hydrophobic, especially as compared to the hydrophobicity of the alkyl-tails of the phospholipid bilayer. For this reason, it is

hypothesized that PPO is most likely to arrange in the interfacial region between polar lipid heads and nonpolar alkyl tails, rather than deep into the hydrophobic inner membrane. This hypothesis is supported by electron density mapping of poloxamers interacting with lipid bilayers, which reflected increased electron density just below the glycerols, corresponding to PPO blocks of P188.[172] Beyond some critical degree of polymerization (e.g. $9 \leq N_{PO,crit} < 16$), physical size constraints would block the ability of the PPO to arrange at this interface, and the PPO would either be rejected from the membrane or would penetrate further, disrupting the lipids with bulky PEO, as was hypothesized to inflict harm to liposomes by hydrophobic poloxamers in the original liposome peroxidation study.[89] Data reflected this in the comparison between OH-P0.5-E5.3 and OH-P1.9-E5.3: longer PPO blocks conferred no membrane stabilization *in vivo*.

Experimental results also suggest that the end groups on PPO can counter the block length constraints at the polar-nonpolar interface in the membrane. Membrane stabilization, which would be considered a favorable interaction by a longer hydrophobic block with the cell membrane, can be invoked by attaching a more strongly hydrophobic end group (e.g. tert-butoxy-) to hydrophobic PPO. This is clearly illustrated by *in vivo* comparison of two identical diblocks: t-P0.9-E2.1 and OH-P0.9-E2.0; the former proved to be a membrane stabilizer *in vivo*, whereas the latter showed no benefit (see Figure 4.14). Here, it is believed that the strongly hydrophobic tert-butoxy end group on t-P0.9-E2.1 serves as a compatibilizer with the polar region of the intermembrane space, anchoring the PPO block to the membrane. In this respect, the nonpolar end group can be thought of as a third block ($N = 1$) on the block copolymer.

In both the functionalized diblock copolymers and short PPO diblock copolymers, anchoring by PPO would trap PEO at the membrane surface. PEO, which will not penetrate into the membrane, swells with water and can protect the membrane against detrimental ion flux while natural cell membrane healing mechanisms are activated.[34,100,173]

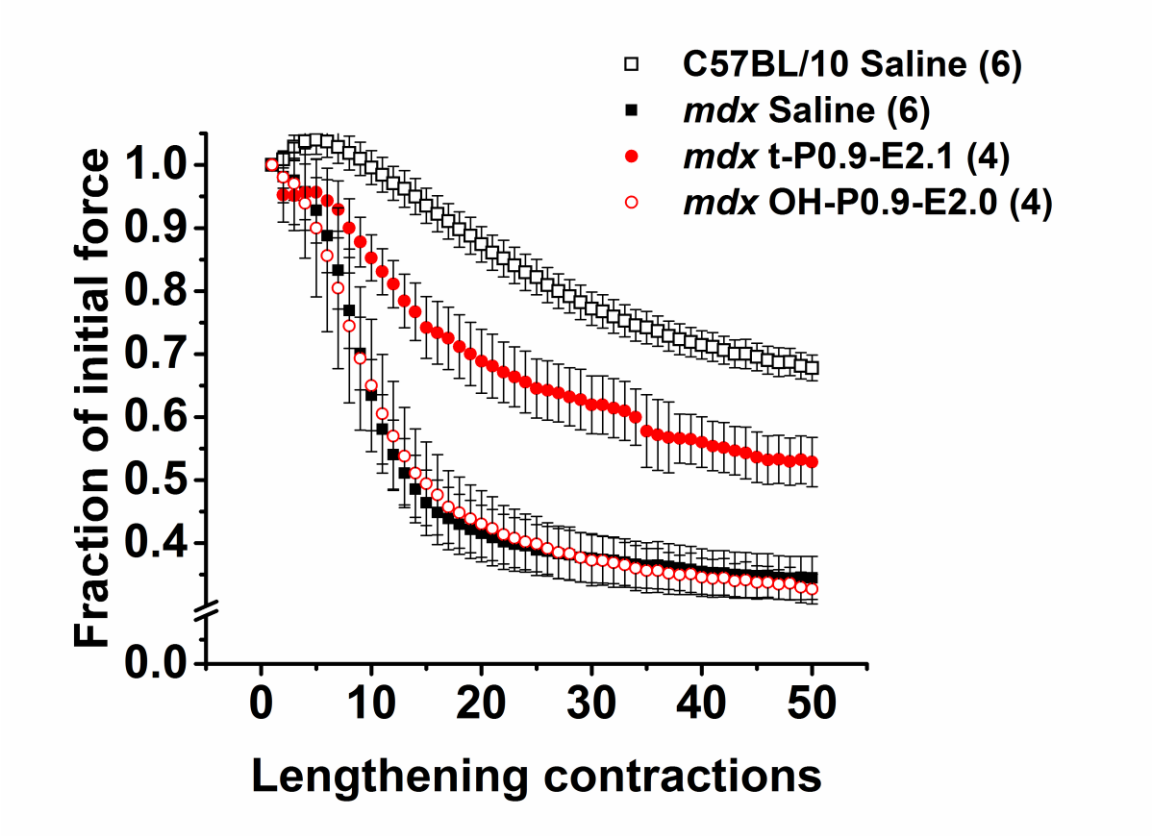


**Figure 4.14:** Lengthening contraction injury comparison of identical diblock copolymers ($N_{PO}$ = 16, $N_{EO}$ ≈ 48) featuring differing end-groups (tert-butyl and hydroxyl). Data show statistically significant protection by t-P0.9-E2.1 as compared to *mdx* Saline (two-way ANOVA, $p < 0.05$).

Comparing experimental data to hypothetical interaction, several supporting points can be made. First, the 500 g/mol PPO block in OH-P0.5-E5.3 has a degree of polymerization of about 9. Here, below the hypothesized critical block length, energetics of incorporation are favorable. The PEO block length is sufficient to protect or stabilize the membrane at a low polymer loading, due to the anchoring at the membrane. Though OH-P0.3-E2.0 was not tested, by this hypothesis, it would be expected to confer protection against lengthening-contraction injury.

The next group of diblock copolymers consisted of PPO block lengths of 16 repeat units. The methoxy-functional group on Diblock P188 showed a slight trend of improvement as compared to the control *mdx* case, but no statistically significant protection was conferred. Tert-butoxy functional groups, however, conferred substantial protection. This suggests that the hydrophobic strength of the methoxy group on Diblock P188 is insufficient to compensate for unfavorable mixing by the longer PPO chain length with alkyl lipids. This end-group attraction and anchoring is further confirmed by direct comparison of the tert-butoxy- and hydroxyl- functionalized diblock copolymers of equivalent PPO block length and composition, t-P0.9-E2.1 and OH-P0.9-E2.0, compared in Figure 4.14.

Finally, given the dramatic differences observed in ability to confer protection against lengthening contraction injury between P188 delivery routes (IP and SubQ), and the interplay of hydrophobic block length and end groups in determining efficacy of membrane interaction, it is unclear what effect a change in delivery method would have on the results obtained so far. Further work in membrane stabilizer delivery routes is ongoing, and careful consideration of PPO block length must be made alongside end group functionality.

## 4.5 Conclusions and future directions

Previously, a diblock architecture of P188 showed protective capacity that exceeded the triblock P188 architecture in protective capacity against liposome peroxidation on an equal mass basis. It was hypothesized that exposure of the hydrophobic block enhanced interaction by the block copolymer with the hydrophobic interior of the lipid bilayer. The

ensuing "anchoring" effect led to protection at lower mass concentrations, which is pharmacologically advantageous.

In this chapter, the interaction by diblock copolymers with membranes was considered at the level of end-group functionality, and a connection between an *in vitro* model membrane stress and an *in vivo* membrane damage protocol was sought. Two classes of block copolymers were synthesized, tert-butoxy- and hydroxyl- functional PPO blocks. Polymers were assessed by DLS in the liposome peroxidation assay discussed in Chapter 3, as well as by an *in vivo* method of muscle injury. Although experiments did not indicate a direct correlation exists between liposome and *in vivo* systems, several key conclusions can be drawn from the combination of the two techniques.

*4.5.1 Anchoring by hydrophobic end groups promotes membrane stabilization in vivo*

Hydrophobically terminated diblock copolymers (t-P0.9-E2.1 and t-P0.9-E8.0) conferred protection in an *in vivo* lengthening contraction injury model. This result came in direct contrast with Diblock P188, end-functionalized with a methoxy group, which conferred little to no improvement over the control. Results by liposome peroixidation reflected an anticorrelation: tert-butyoxy functional diblock copolymers exhibited no protective capacity against peroxidation, whereas Diblock P188 was strongly protective, as indicated by DLS scattered intensity and liposome size distribution characteristics. Furthermore, the complete lack of protection by t-P0.9-E8.0 was in direct contrast with the 8,000 g/mol PEO (PEO-8k) tested in Chapter 3. This result was concluded to mean that the strongly hydrophobic tert-butoxy terminus is involved in liposome disruption during peroxidation, despite it being inert to liposomes during incubation times up to 24 hours. Results were consistent with the findings of Wang et al.,[89] who reported that polymers that could insert or "anchor" in the membrane were not protective against peroxidation, whereas polymers that instead remain adsorbed at the surface of the membrane would. Diblock P188, with its methoxy-PPO, was not hydrophobic enough to disrupt liposomes during peroxidation and was similarly not hydrophobic enough to "anchor" for membrane stabilization *in vivo*.

The anti-correlation of peroxidation and *in vivo* results support the hypothesis that end groups are significantly important to membrane interaction, while simultaneously

confirming that interaction mechanisms are vastly different between the two models. This is not surprising, given the vast differences between nanoscale vesicles of phospholipids and the microscale, cytoskeleton-supported sarcolemma of muscle cells. Further work to develop a more realistic biophysical model of membrane damage is needed and might be found in supported bilayers[174,175] or bicelles,[176–179] rather than liposomes.

*4.5.2 Hydrophobic block length determines association with membranes, with end group exception*

Next, a series of hydroxyl terminated diblock copolymers was considered. Here, results were mixed in both the liposome and *in vivo* experiments. Protection against peroxidation was allowed by diblock copolymers with sufficiently long PEO block lengths. Results indicated a strong preference for longer PEO blocks in protecting membranes from peroxidation, which was supported by protection (although to a lesser extent) by a homopolymer of the same molecular weight (5,300 g/mol). Liposome protection was not shown by either of the two short PEO diblock copolymers or the PEO homopolymer they were prepared from. *In vivo* experiments using the same polymers showed an intriguing PPO block length effect on conferring protection. The shortest PPO block, 500 g/mol, showed excellent protection against muscle injury, whereas the diblock copolymers with longer PPO blocks (900 and 1,900 g/mol) were not protective. It was also observed that the hydroxyl-functionalized equivalent to t-P0.9-E2.1 showed no membrane stabilization effect whatsoever.

From the combination of the two diblock copolymer class results, it was hypothesized that hydrophobic block length above some critical value ($9 \leq N_{PO,crit} < 16$) hinders the ability of the hydrophobic block to arrange in the interior of the membrane. The disassociation by longer PPO blocks with the strongly hydrophobic inner membrane space could be overcome by attaching a third "block," with $N = 1$, that is, a hydrophobic end group, to compatibilize the PPO block with the strongly hydrophobic alkyl tails. The balance needed between PPO block length and hydrophobic end group to achieve the hypothesized "anchoring" conferring protection remains an open question. Further investigation of the parameter space could be conducted by preparing longer t-PPO blocks, or even amphiphilic diblock copolymers with a stronger hydrophobic constituent (e.g.

polybutylene oxide). If the latter route is taken, the hydrophobic block length would have to be short enough relative to PEO to remain water-soluble.

*4.5.3 Uses for liposome model membranes beyond in vivo screening*

The liposome offers the advantages of a bilayered model membrane without the heterogeneity of native cell membranes. Despite the absence of direct connections to *in vivo* results in this chapter, the liposome peroxidation assay can distinguish between varying block copolymer characteristics, and in that sense, should complement and inform biophysical experiments performed on a grander scale, such as pre-screening polymers for use in liposome-based small angle neutron scattering and related techniques.[168,169,180–182] Alternative paths to consider would include performing the peroxidation reaction on giant unilamellar vesicles (GUVs), which can be viewed under an optical microscope, perhaps even with fluorescently tagged polymers or dye solutions within in the vesicles. GUVs would also correspond better to *in vitro* experiments being carried out on isolated myofibers,[57,183] and hypo-osmotic swelling experiments could be used to invoke membrane damage by mechanical stress.[33,115]

# Chapter 5
# Block copolymer interactions with model membrane monolayers

## 5.1 Surface activity in surfactant monolayers

Phospholipid monolayers have been used extensively to understand structure-function relationships between cell membrane components, including lipids,[184] proteins,[185,186] cholesterol,[187–189] and more recently, poloxamers.[39,43,86] It is widely accepted that monolayers can be used to model the outer leaflet of cell membranes, although key features of the monolayered model are arguably non-cell-like: namely, dimension, composition, and its flat configuration. Despite these limitations, monolayered models are favorable for their ease of use in thermodynamic, rheological, imaging, and scattering experiments.[190] Additionally, a variety of naturally derived and synthetic phospholipids are available in high purity, which makes monolayer compositions far simpler to control and manipulate than function-specific cell membranes.

### *5.1.1 Phase behavior of DPPC*

The synthetic phospholipid chosen for this work, 1,2-dipalmitoyl-sn-glycero-3-phosphocholine, (i.e. dipalmitoyl phosphatidylcholine or DPPC), features fully saturated 16 C tails and a zwitterionic headgroup, shown in Figure 5.1. Investigations of DPPC phase behavior in a monolayer are experimentally facile because the DPPC transition temperature (41 °C) is above ambient and physiological temperatures, and the saturation lends chemical stability to films spread in an air atmosphere. Comprehensive studies on the phase behavior

of DPPC have been previously performed and serve to justify it as a well-understood model system.[184,191]

A sample isothermal plot of surface pressure as a function of mean molecular area is shown for synthetic dipalmitoylphosphatidylcholine (DPPC) on water in Figure 5.2. Data were collected in monolayer compression mode, but expansion would be expected to follow the same path (little hysteresis). Mean molecular area is simply the trough area normalized to the concentration of insoluble phospholipids applied to the interface. As shown by Figure 5.2, phospholipids impart the greatest changes to surface tension at the lowest area per molecule (i.e. high surface pressure). These observed changes to surfactant behavior arise from increased phospholipid ordering at reduced surface areas, i.e. phase transitions.[191] The concept of ordering and phase transitions of phospholipids is analogous to an ideal gas in two dimensions.[19] For an ideal gas, energetic interactions of neighboring gas molecules are negligible (i.e. no pressure exerted on the bounds of the system) until the volume is reduced isothermally. Upon further isothermal compression, an ideal gas will begin to semi-order into a liquid, and then a solid. Similarly, phospholipid molecules at a large area per molecule on the interface exert no surface pressure, and isothermal reduction of the available space between molecules leads to increased surface pressure, due to ordering and phase transitions.

Phospholipid phase transitions may be discerned by slope changes in Figure 5.2. At low values of molecular area, the liquid condensed phase becomes relatively incompressible, yielding large changes to surface pressure following only small changes to available area.[192] While the position along the *x*-axis of the observed transitions can change at different rates of compression or temperature conditions, the general form of the isotherm is maintained and reversible. On compression beyond collapse (around 70 mN/m), lipids fold down into the subphase and are not recoverable on the interface, due to energetically favorable micellization events in the subphase. Following monolayer collapse, isotherms will exhibit transitions which are shifted toward smaller mean molecular area, reflecting the reduction in the amount of material at the interface.

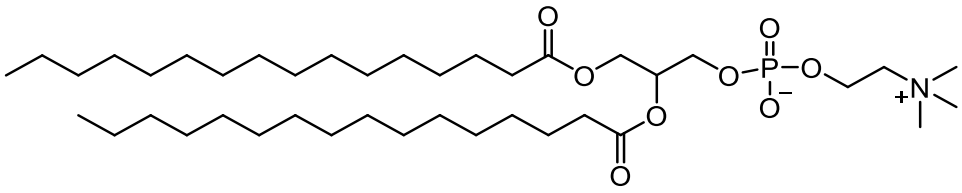

**Figure 5.1:** Chemical structure of DPPC.

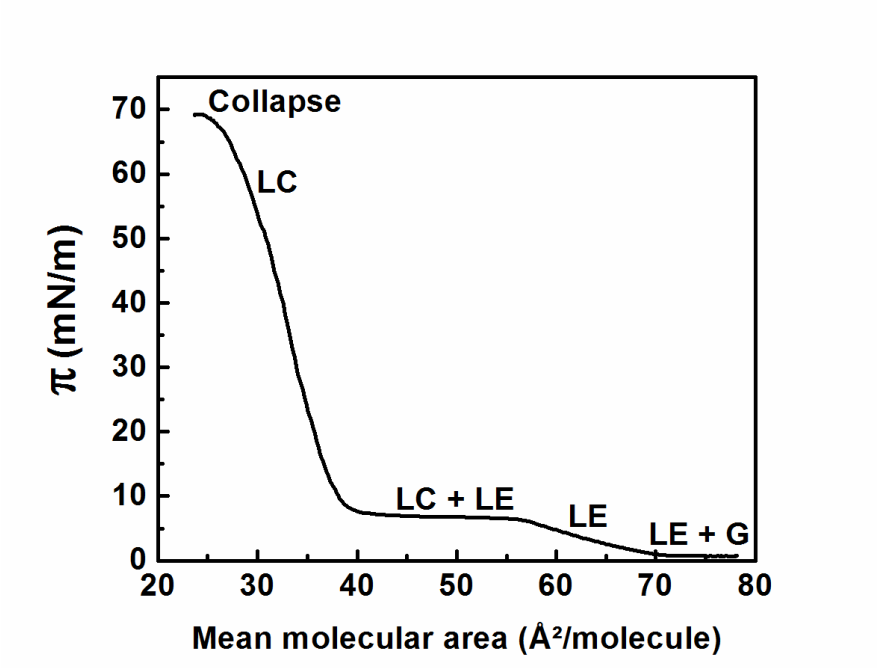


**Figure 5.2:** Area controlled isotherm of DPPC at 25 °C, showing phases and phase coexistence regions. Moving in order from low molecular area to high area: LC (liquid condensed), LE (liquid expanded), and G (gaseous) phases.

*5.1.2 Surface activity of P188 and Diblock P188*

Before considering block copolymer surfactant effects on monolayer model membranes, the surface activity of P188 and Diblock P188 were characterized at the air-water interface of a Langmuir trough.[193–198] Unlike phospholipids, which form an insoluble Langmuir monolayer when spread on the aqueous subphase, the PEO-PPO block copolymer surfactants considered here are soluble. The result is an equilibrium relationship between surface concentration, surface tension, and composition of the subphase; soluble surfactants like P188 are said to form a Gibbs monolayer, referring to the thermodynamic Gibbs adsorption law.[18,199]

Because the rate of desorption from a low concentration film of soluble P188 molecules on the interface into the subphase is comparatively slower than the experimental timescale of compression isotherms, the film may be treated like an insoluble Langmuir monolayer.[195] On compression from large area per monomer, surface pressure rises to a first plateau, termed a monomer saturation point and hypothesized to correspond to polymer chains oriented parallel to the interface.[195] Despite this "ordering," no evidence of Bragg scattering has been reported for P188 films compressed to 29 mN/m, either by small angle x-ray reflection or grazing incidence x-ray diffraction.[92]

Compression isotherms for Diblock P188 and P188 are given in Figure 5.3. Beyond the first plateau (monomer saturation), surface pressure continues to rise for P188, which has been attributed to a transition from a flat to a brush-like arrangement of PEO tails.[195] This is not seen for Diblock P188 at the concentration spread on the interface, but in line with other PEO-based block copolymers, surface pressure would be expected to similarly increase as PEO chains transition to a brush-like configuration.[196,197] Hysteresis emerges in successive compressions to low areas per monomer, which agrees well with the short time scale insoluble Langmuir monolayer hypothesis.[195]

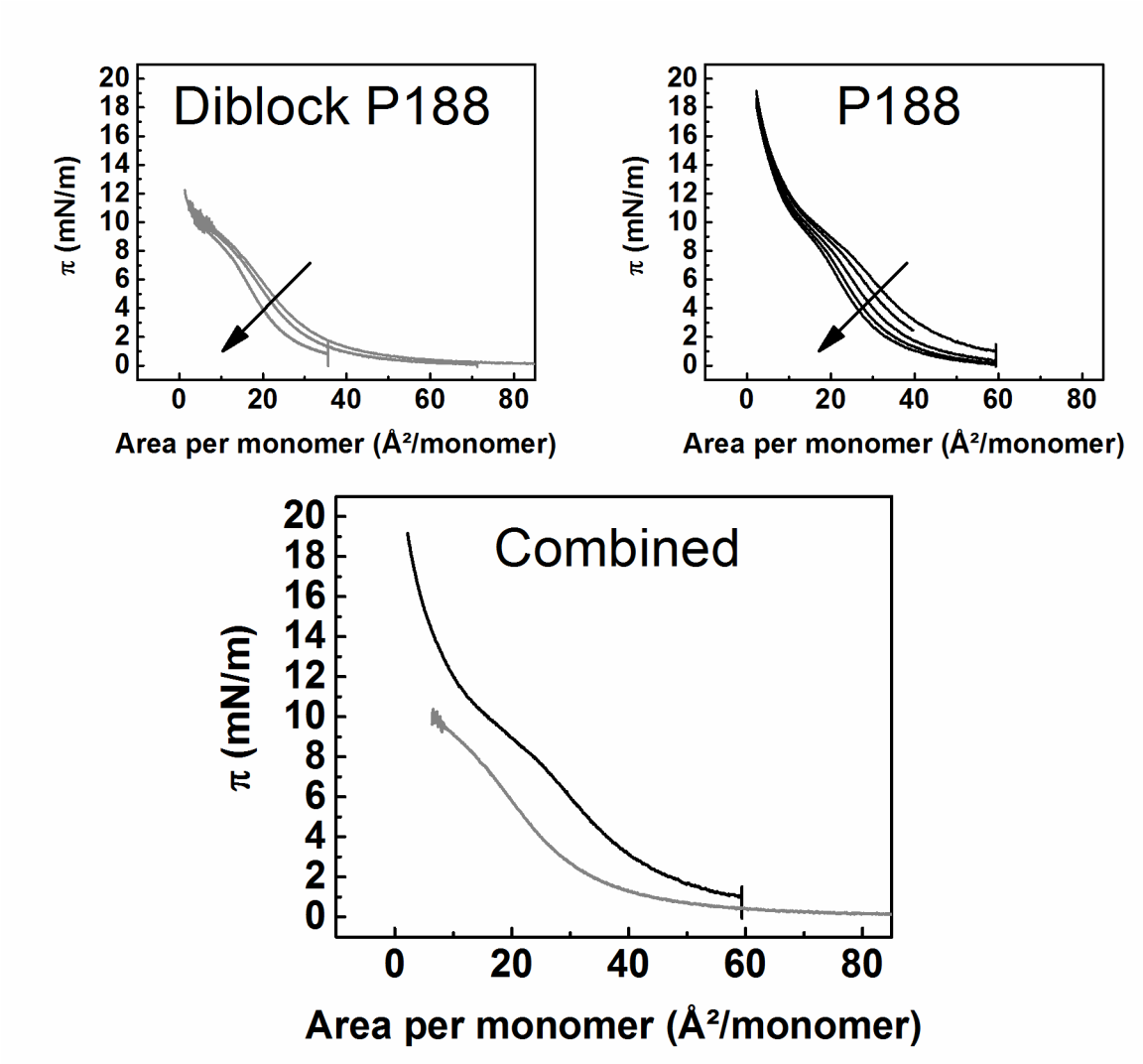


**Figure 5.3:** Compression isotherms for Diblock P188 and P188, spread at large area per monomer and compressed successively. Arrows indicate successive compressions; hysteresis is attributable to a pseudo-Langmuir like collapse at low area per monolayer, due to short times between compressions. The combined plot (right) shows transition plateaus for Diblock P188 and P188 occur at similar surface pressures, but approximately 2x separated area per monomer, reflecting identical PEO block lengths and an overall doubled concentration of PEO blocks in P188.

Understanding the behavior of P188 and Diblock P188 at the interface is useful for reference, and with a more sophisticated Langmuir trough setup, more detailed information regarding the film rheology[200,201] and ordering effects in lipid films[87,92,123] may be obtained. Here, the key information gained from simple experiments was the expected surface activity of the two polymers (from equilibrium adsorption pressure and maximum compression behavior) and a cursory observation of the kinetics of the Langmuir film-like hysteresis on compression. As a result of isotherms in Figure 5.3, recovery times between successive compressions were lengthened.

## 5.2 Polymer interactions with synthetic phospholipid monolayers

Perturbations to phospholipid monolayer phase behavior may be invoked by the presence of heterogeneities. For example, incorporation of cholesterol, a small, rigid sterol present in cell membranes at about 30-50 wt.-% composition, serves to dramatically alter membrane fluidity and phase behavior;[27,187,194] changes that can be measured by area-controlled surface pressure isotherms and observed by fluorescence microscopy on the interface. Besides multi-component monolayers, heterogeneities may be introduced from the subphase, requiring surface active components to disperse and adsorb at the interface. On a clean interface, subphase additions and subsequent adsorption lead to a defined "surface excess," corresponding to the theoretical saturation concentration at the interface. Saturation on a Langmuir trough is detectable by plateau in the surface pressure in time, which builds from 0 mN/m following subphase addition.

### *5.2.1 Monolayer adsorption by poloxamers*

Because poloxamers are non-reactive and non-ionic surfactants, there is great interest in understanding the ultimate fate of injected poloxamers after being administered to a patient. To study this, Maskarinec and coworkers adopted an area-controlled monolayer experiment, in which a phospholipid film incorporated with an equilibrium concentration of adsorbed Poloxamer 188 was compressed isothermally.[43,86] The lipid monolayers, which served to model the outer leaflet of the cell membrane, exhibited changed phase behavior as compared to neat lipids, as a result of P188 additions. Using area and pressure controlled isotherms, it was determined that P188 adsorption to the membrane was drawn to areas of

reduced packing density, i.e. LE phases. Moreover, above a critical surface pressure, corresponding to tight lipid packing, block copolymer adsorption to the interface could not occur, and on compression, lipid films containing P188 or other hydrophilic poloxamers would eject or "squeeze-out" polymer near these critical surface pressures.[43,86,87,202]

The squeeze-out phenomenon and limited interfacial adsorption of P188 above critical surface pressures is hypothesized to correspond to the seemingly inert effect of P188 on healthy tissue. It is hypothesized that block copolymer surfactants adsorb to regions of reduced packing density (i.e. damaged cell membranes), and on lipid rearrangement and healing by natural processes, the polymers are pushed back out and cleared by the kidneys.[43] In a patient, polymer squeeze-out upon membrane restoration would be highly favorable for acute injury, but for chronic, incurable disease, the same phenomenon would dictate ongoing therapy throughout the life of the patient.

Adsorption by poloxamers to the interface from the subphase has been reported as a means to understand the impact of bulky polymer groups on lipid packing, phase behavior, and surface pressure.[35,43,86] Following a representative isothermal compression-expansion cycle on the monolayer, poloxamers are introduced to the subphase under the movable barrier of the Langmuir trough. The poloxamers, which are surface-active, begin to adsorb to the monolayer, and surface pressure is monitored in time at a fixed surface area, until some equilibrium value is reached. The equilibrium surface pressure achieved by polymer adsorbed to a fully expanded monolayer of DPPC ($\pi_{DPPC}$ = 0 mN/m) depends on the molecular properties of the polymer species, but $\pi_{eq}$ of about 20-25 mN/m has been reported for Poloxamer 188.[43,87] Adsorption time to reach equilibrium is typically thirty minutes or less and is determined by leveling off of the surface pressure. Grazing incidence x-ray diffraction (GIXD) has indicated that P188 works into spaces between lipids at the interface, pushing or "corralling" lipid regions toward order.[87]

*5.2.2 Area controlled isotherm (adsorption and squeeze out)*

Using an area-controlled technique, block copolymer adsorption and squeeze-out was compared between P188 and a diblock analog (Diblock P188, $M_n$ = 4,300 g/mol, 80 wt.-% PEO). Polymer solutions were prepared at stock concentrations of 10 mM and small volumes (50 µL) were added to the subphase beneath an equilibrated DPPC monolayer at

large areas per molecule ($\pi = 0$ mN/m; 2 µL of 10 mg/mL). Upon polymer addition, surface pressure rose rapidly, corresponding to polymer adsorption to the interface. Surface pressure was monitored in time until equilibration was reached, indicated by a plateau (about 30 minutes). P188 and Diblock P188 insertion into a DPPC monolayer are shown in Figure 5.4, at equimolar concentrations. To test whether surface pressure corresponded to maximum surface coverage by Diblock P188, the molar concentration was doubled (100 µL of a 10 mM solution). Similarity of the two Diblock P188 curves in Figure 5.4 confirms that the maximum surface concentration is exceeded, and the subphase acts like a reservoir of polymer.

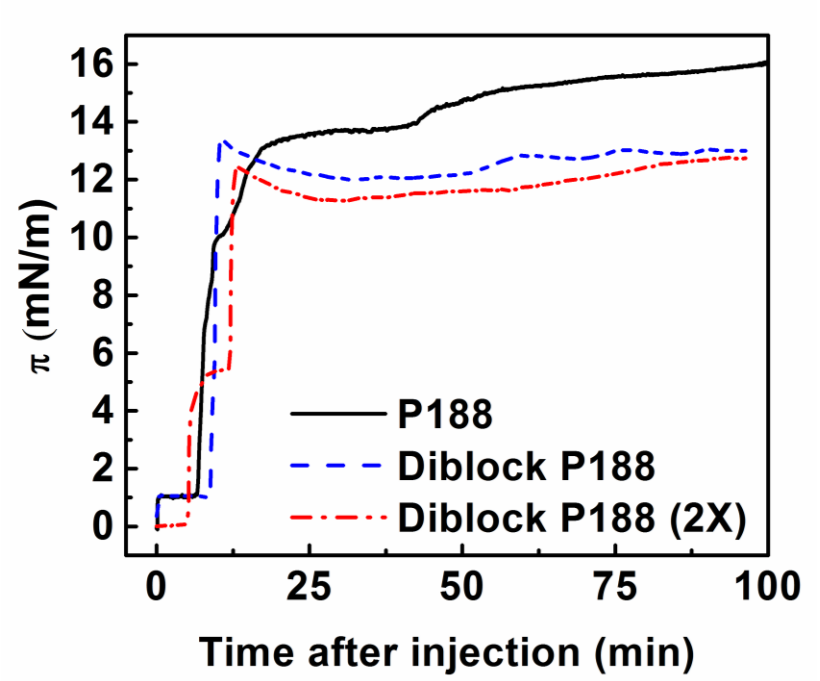


**Figure 5.4:** P188 and Diblock P188 insertion into DPPC monolayer. P188 (—) shows a surface pressure rises to about 16 mN/m after 100 minutes, whereas smaller Diblock P188 (- - ) corresponds to surface pressure rise of about 13 mN/m. The Diblock P188 (2X) curve (- · ) reflects doubling the molar concentration of Diblock P188 in efforts to have equivalent PEO and PPO contents. No change to equilibrium adsorption suggests that surface excess has been reached at the lower molar concentration.

Two features in the polymer adsorption curves in Figure 5.4: P188 and Diblock P188 insertion into DPPC monolayer.Figure 5.4 are noteworthy. First, a striking difference in the shape of the adsorption curves exists between the two polymer architectures. This is likely due to the different configurations of the hydrophobic PPO block; Diblock P188,

showing a sharp peak in the adsorption profile, would be expected to adsorb quickly, due to both the exposed hydrophobic block and singular PEO block. The adsorption by P188, in contrast, shows more gradual adsorption, perhaps due to kinetic limitations on surface arrangement by the constrained PPO block and higher total PEO content per molecule. Second, differences in the equilibrium adsorption surface pressures between P188 and Diblock P188 can be attributed to differences in the degree of polymerization, *N*. Diblock P188, with its shorter PPO block and half as much PEO per molecule as compared to P188, exerts less lateral pressure on lipids. This trend is consistent with a comparison of poloxamers of varying molecular weights; higher surface pressures were attained for adsorption to DPPC monolayers by larger molecules.[86]

Following adsorption and equilibration at maximum area per DPPC molecule, monolayers containing P188 and Diblock P188 were compressed isothermally. The isotherms, shown in Figure 5.5, are characterized by a slight increase in surface pressure as mean molecular area is decreased, until the critical "squeeze-out" pressure is achieved (P188 at $\pi$ = 26 mN/m and Diblock P188 at $\pi$ = 19 mN/m), and the isotherm assumes the form of the neat DPPC LC phase in a steep climb towards collapse (c.a. 70 mN/m at 25 °C)

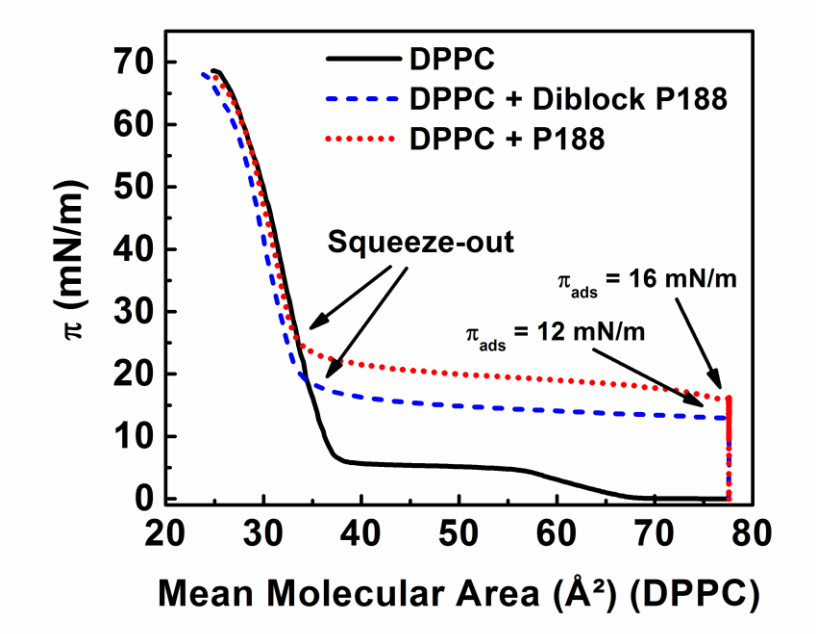


**Figure 5.5:** P188 and Diblock P188 isotherms following DPPC monolayer adsorption. Squeeze-out occurs at π = 26 mN/m for P188 and about 19 mN/m for Diblock P188.

After rejection from the DPPC monolayer at high surface pressures, polymer adsorption was fully reversible. Upon expansion at a slow rate, surface pressure followed a similar curve to the compression, at only slightly reduced surface pressures, which were then restored in time at the maximum molecular area (see Figure 5.6). In general, varying the rate of area expansion following compression will slightly change path of the isotherm (hysteresis), but for polymer re-adsorption, the pressure was quickly restored.

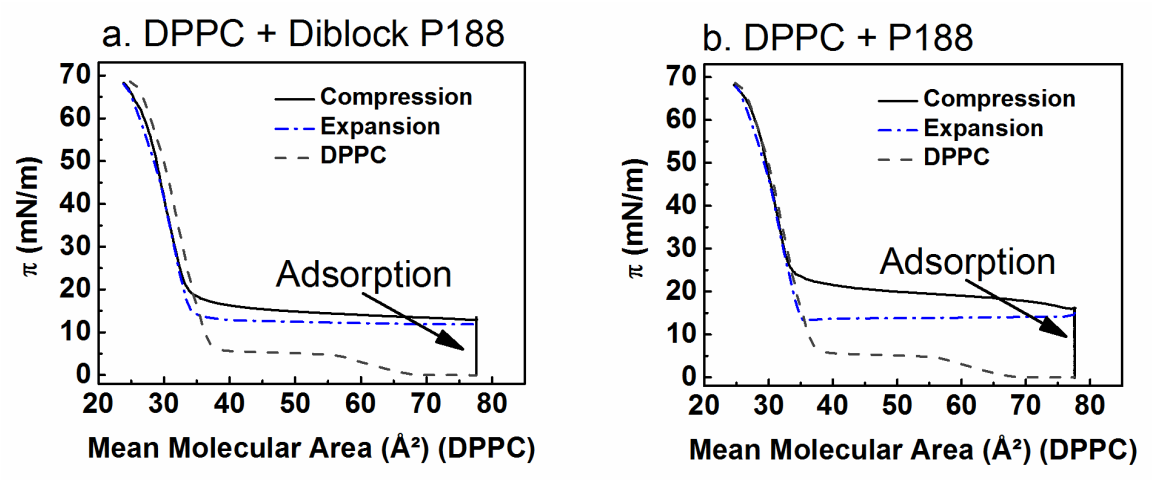


**Figure 5.6:** Isotherms showing compression and expansion monolayers of DPPC and (a) Diblock P188 or (b) P188. Expansion traces showed slight hysteresis, along with fast recovery to adsorption surface pressure.

### *5.2.3 Fluorescence microscopy of lipid and polymer monolayers*

Apart from slightly reduced adsorption and squeeze-out surface pressures, area-controlled experiments for Diblock P188 with DPPC monolayers were qualitatively similar to experimental and literature results obtained for P188.[43,86] To further supplement results, epifluorescence microscopy, henceforth referred to as fluorescence microscopy, was used to visualize changes to monolayer phase behavior induced by block copolymer adsorption.[203] In fluorescence microscopy of a monolayer, a small amount (~0.5 wt.-%) of a fluorescently tagged lipid probe (Texas Red 1,2-Dihexadecanoyl-*sn*-Glycero-3-Phosphoethanolamine Triethylammonium Salt; TR DHPE, Invitrogen) is added to the DPPC solution in chloroform. Texas Red DHPE, shown in Figure 5.7, with a bulky fluorescent Texas Red molecule on the polar headgroup, preferentially assembles into disordered phases. Under fluorescence conditions ($\lambda_{excitation}$ = 595 nm; $\lambda_{emission}$ = 615 nm), disordered phases in the monolayer appear bright, and condensed phases appear dark.

A schematic depiction of reflected light fluorescence microscopy on a monolayer is illustrated in Figure 5.8. The xenon arc lamp is a high intensity light source; a fluorescent probe-specific emission filter is used to direct only the desired radiation (e.g. TR, $\lambda_{excitation}$ = 595 nm) onto the fluorophore. Light absorbed by the fluorophore excites electrons to a higher energy level, and upon relaxation, light is emitted at a longer wavelength (e.g. TR,

$\lambda_{emission}$ = 615 nm). A dichroic mirror and excitation filter are used to filter out reflected emission light before it reaches the camera.

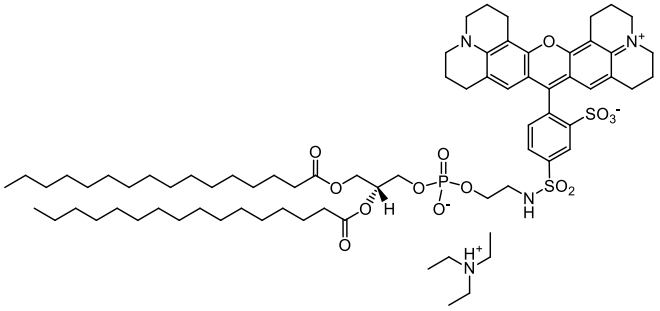

**Figure 5.7:** Texas Red DHPE, used to image phospholipid monolayers under a fluorescence microscope. The bulky Texas Red on the polar head group preferentially migrates to regions of lipid disorder on the monolayer.

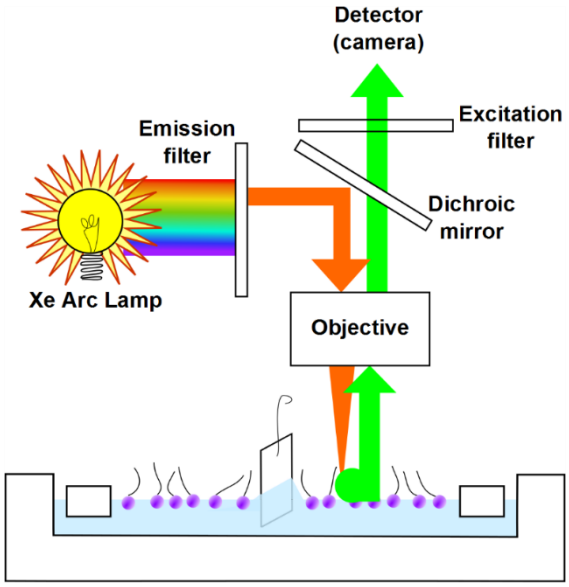


**Figure 5.8:** Fluorescence microscope configuration with Langmuir trough and lipid monolayer.

Synthetic phospholipid monolayers, such as those of DPPC, have been imaged using combined fluorescence microscopy and Langmuir troughs throughout the literature.[43,203–208] As the monolayer is compressed through phases of the isotherm (shown in Figure 5.2), microscopic features evolve through nucleation and growth. Fluorescence microscopy is most effective within the LE phase and its coexistence with G and LC; at the strictly G phase, there is little to no contrast to image and in the LC phase, the fluorophores are excluded from the monolayer due to steric constraints. Evolution of DPPC morphologies is shown in Figure 5.9, depicting the transition from larger to smaller area per molecule.

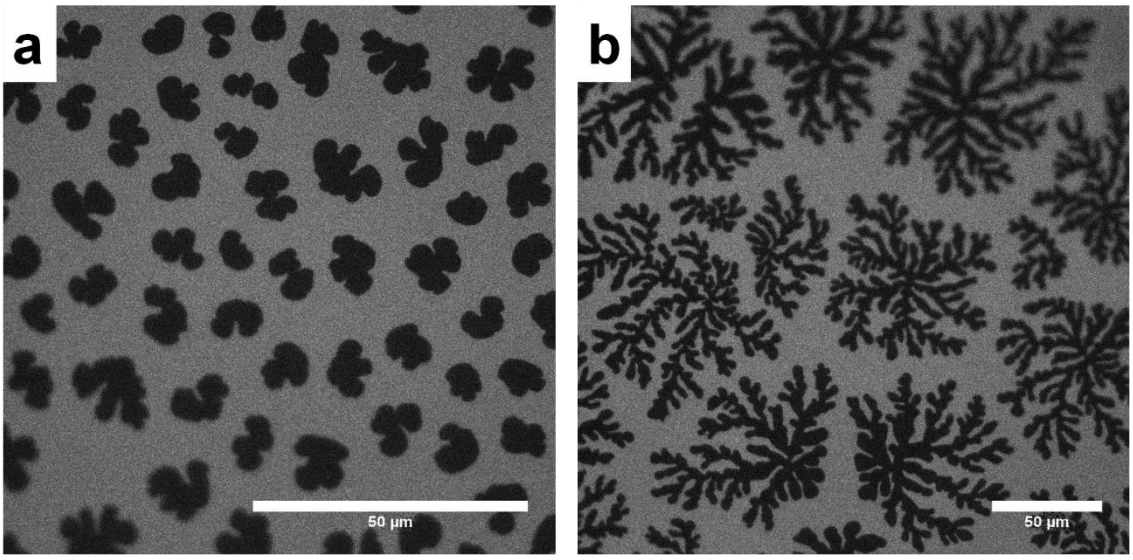


**Figure 5.9:** Fluorescence micorgraphs of DPPC monolayers containing 0.5 wt.-% TR-DHPE. Scale bars are 50 µm. Morphological differences from (a) to (b) arise from compression within the LE/LC phase coexistence.

Fluorescence microscopy techniques have been combined with Langmuir monolayers to visualize the influence of P188 on synthetic phospholipid monolayers in several prior investigations.[35,39,43,86] From these studies, P188 adsorption to the monolayer was shown to reduce ordering of lipid domains, increasing the prevalence of the LE phase.[43] For head-group tagged lipids, the poloxamer squeeze out event (lift-off on the compression isotherm corresponding to the LC phase) cannot be imaged by fluorescence microscopy, therefore fluorescence microscopy was performed on monolayers within LE/LC phase coexistence (c.a. 5-15 mN/m). Spread monolayers of DPPC were first cycled through compression and expansion to obtain the neat lipid isotherm, before then adding polymer to the subphase at

some expanded surface area corresponding to maximum area per molecule or a slightly elevated surface pressure capable of being imaged (c.a. 5 mN/m).

Fluorescence micrographs were taken on a DPPC monolayer with P188 added to the subphase. In an effort to reduce monolayer drift, a ferrule arrangement (shown in Figure 5.10) was used to isolate a small region of monolayer with a shallow depth. The technique was developed for use in confocal microscopy of monolayers, for which exposure time is on the order of 1 s.[209] Due to the shallow depth of subphase, polymer adsorption is not expected to occur in the field of view within the same experimental timeframe as elsewhere in the monolayer. To facilitate polymer distribution, monolayer "mixing" was performed, a single compression-expansion cycle following polymer addition. Micrographs in Figure 5.11 follow monolayer mixing: to a monolayer at a low surface pressure (about 0 mN/m), P188 was added to the subphase, equilibrated for about 11 minutes, and then compressed and expanded in one cycle to "mix" the subphase. Figure 5.11a shows the monolayer just prior to mixing, with a phase morphology resembling that of neat DPPC. Figure 5.11b follows compression and expansion, and the images in Figure 5.11c-f were obtained in the time following expansion.

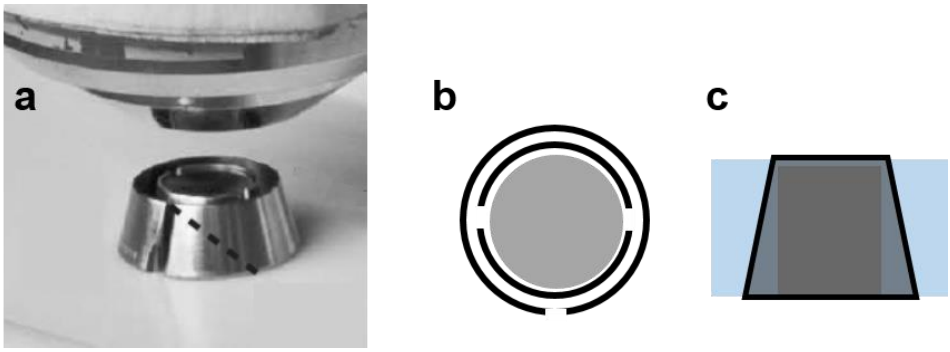


**Figure 5.10:** Monolayers of DPPC and P188 were imaged using a monolayer -isolating ferrule.[209] View in (a) shows objective with two concentric ferrules and a stainless steel post. Ferrules serve to cut the monolayer, isolating a shallow region of subphase that does not drift on short timescales. Figure in (b) shows the concentric ferrules from the objective vantage point, with openings that allow the monolayer to flow during compression. Side view in (c) shows how ferrules cut through monolayer, isolating a small region.

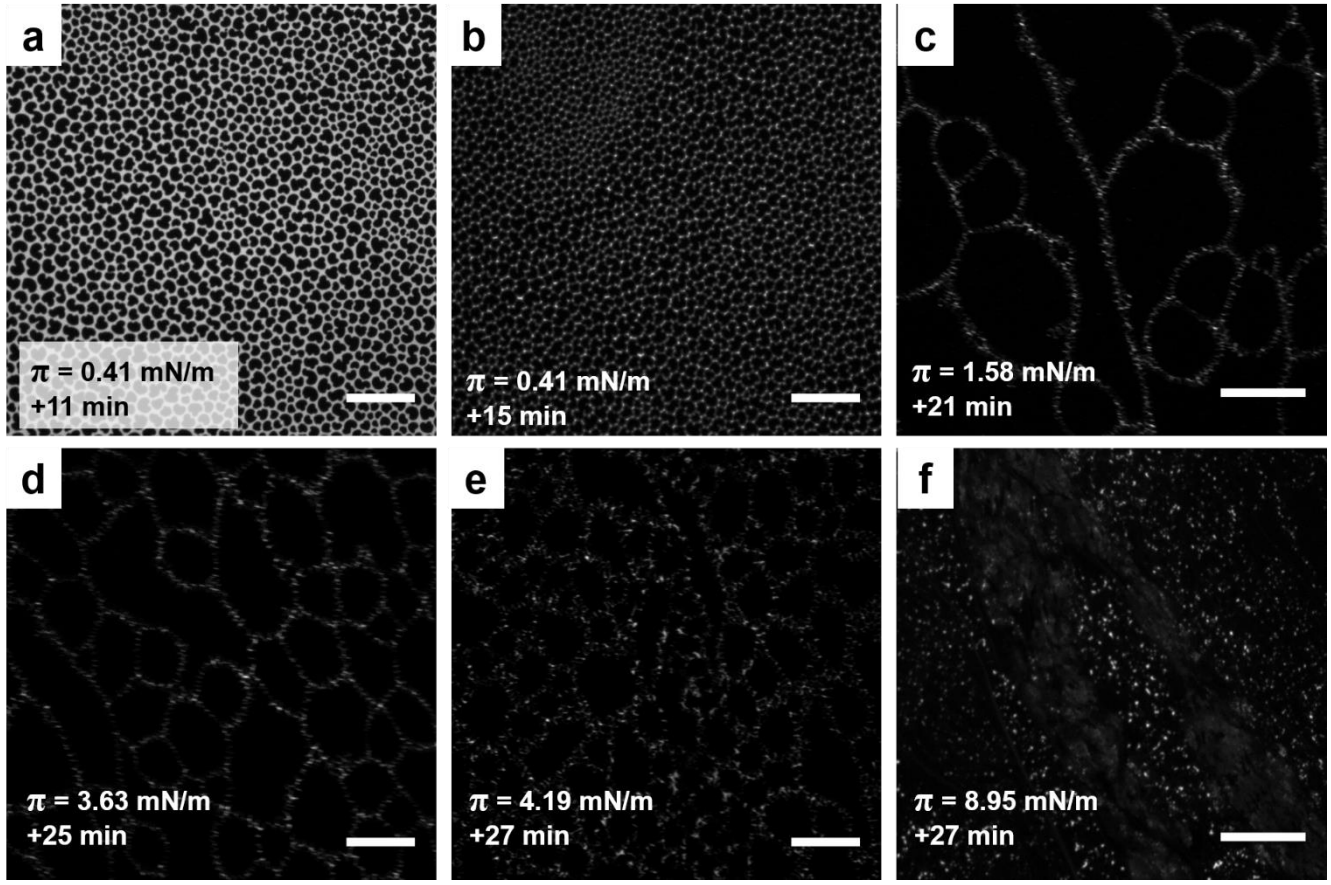


**Figure 5.11:** Fluorescence micrographs taken in time on a DPPC monolayer with P188. Images were taken with the help of a monolayer cutting post, which prevented adsorption of P188 to the imaged monolayer without mixing by monolayer compression and expansion. The image in (a) is a pre-mixed monolayer, (b) is just after mixing, and (c-f) are at maximal spreading area.

Micrographs of DPPC containing P188 show deviations from expected DPPC morphologies, with an initial shift to a condensed phase, followed by equilibration leading towards the final heterogeneous morphology shown in Figure 5.11f. Intermediate shades of gray and black indicate varying degrees of fluidity in the monolayer, and the micrograph is in relative agreement with literature reported P188-DPPC morphologies.[43]

Fluorescence micrographs of DPPC with Diblock P188 were taken without the aid of the monolayer-isolating ferrules and are shown in Figure 5.12. Diblock P188 was added at a film surface pressure of 3.2 mN/m (Figure 5.5a, DPPC before addition) and Figures Figure 5.12b-f were taken throughout the 12 minutes following addition, unevenly spaced in time. No significant changes to surface pressure were noted during the initial adsorption time from which images were captured, but considerable heterogeneities can be observed from one image to the next. Figure 5.12b and c are reminiscent of characteristic DPPC morphologies, with some extension and extortion consistent with prior P188 work.[43] Though some extent of morphological change in time is to be expected, micrographs better represent spatial variations in the film, due to rapid movement of the fluid-like packing of the LE phase. Following the bulk adsorption event depicted in Figure 5.4, contrast was lost, and no further images were taken.

Fluorescence microscopy performed on DPPC monolayers with P188 and Diblock P188 showed mixed results with similarities and differences between the two polymer systems. Both polymers showed disruptions to classical DPPC phase behavior at low to middle surface pressures (around 3-9 mN/m), and monolayers were highly heterogeneous following polymer adsorption. Limitations to the technique, namely loss of contrast by condensed phases, impeded investigation of polymer squeeze out by optical microscopy.. Classical DPPC phase behavior, characterized by chiral morphologies, was distorted by the respective adsorption of both the triblock and diblock copolymer architectures to the interface.

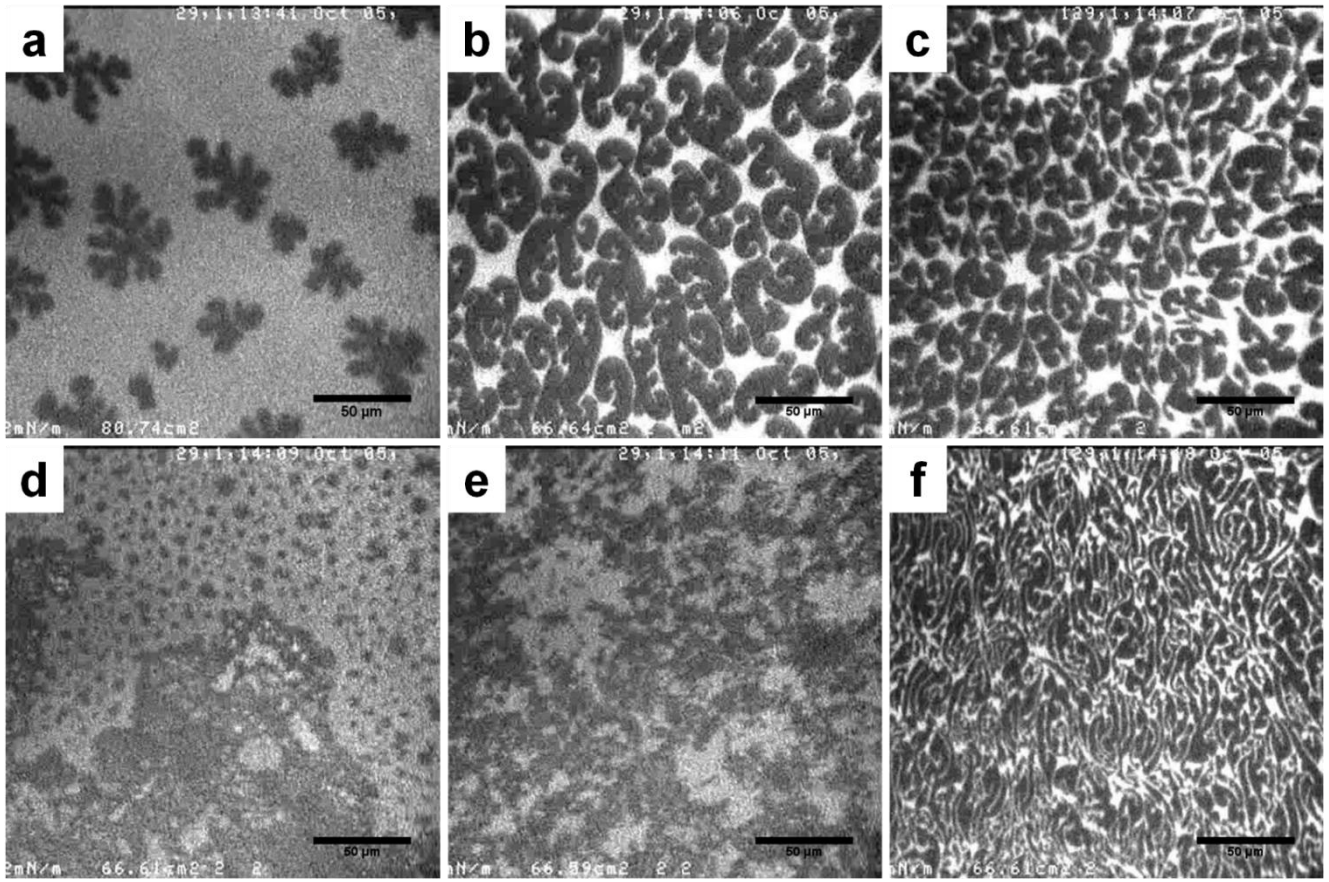


**Figure 5.12:** Fluorescence microscopy images taken of a DPPC monolayer before (a) and after Diblock P188 addition (b-f). Scale bars are 50 µm, and 0.5 wt.-% TR-DHPE has been added for contrast, where dark phases are condensed phases. Surface pressure rise (widespread adsorption) has not yet occurred, but heterogeneities in DPPC phases, characterized by elongated domains (**b**, zero minutes) and (**c**, one minute), intermediate phases (**d**, three minutes) and (**e**, five minutes) and finely defined LC (**f**, twelve minutes) evolved over the course of about 12 minutes post-addition.

## 5.3 Naturally derived lipid monolayers

In an effort to understand the block copolymer interaction with *in vivo* membranes, sarcolemmal membranes isolated from *ex vivo* fast-twitch skeletal muscle cells of New Zealand white rabbits were used in monolayer experiments.[210,211] Native sarcolemmal membrane material is advantageous because the heterogeneous mixture of proteins, lipids, and cholesterol better matches *in vivo* models than would a synthetic, single-component phospholipid membrane.[74] Membrane components were obtained as fractions from a muscle cell digestion and isolation technique and stored frozen before use.[210] Samples of crude SR were thawed and fractionated into heavy, intermediate, and light sarcoplasmal reticulum (SR) by sucrose gradients.[211]

### *5.3.1 Light SR and heavy SR purification*

Briefly, thawed crude SR samples were deposited on freshly prepared sucrose gradients comprised of 50, 40, 35, and 25% (w/v) sucrose in 20 mM MOPS, buffered to pH 7.0. Gradients were prepared in centrifuge tubes and maintained at 4 °C throughout preparation and separation. Sealed centrifuge tubes were placed in a SW 32 Ti Rotor (i.e. swinging bucket) attachment, and centrifuged at 22,000 rpm (83,000 g) and 4 °C for 12 hours. Lipids and proteins between the 25% and 35% layers of gradients were removed by pipette and washed with 20 mM MOPS (pH 7.0). Light SR was pelleted by centrifugation at 35,000 rpm in a Ti-45 rotor for 90 minutes at 4 °C. Pellets were constituted in about 1 mL of MOPS buffer and stored at -80 °C until needed. Additionally, the more abundant "heavy SR" layer was kept and pelleted. Heavy SR samples were diluted with MOPS by a factor of 1.5, for ease of dispersal at the interface.

### *5.3.2 Area-controlled isotherms of SR monolayers*

Monolayers of light SR or heavy SR were prepared by depositing 5-15 µL of the corresponding SR suspension on a 20 mM MOPS buffer. Due to the multi-component nature of the natural membrane materials, additions were characterized by surface-excess behavior, or Gibbs monolayers, as was already seen in the poloxamer isotherms (see Figure 5.3). Compression of these membranes gave a steady rise in surface pressure with area, and distinct phase transitions were obscured by the heterogeneous composition. Maximum surface pressures between 30 and 35 mN/m were achieved on full compression; however,

unlike DPPC (insoluble), holding the trough barriers at the area corresponding to the maximum surface pressure for extended times resulted in dropping surface pressure (not shown). Since the drop of surface pressure could be attributed to membrane components desorbing back into the subphase, isotherms for SR monolayers were performed in continuous compression-expansion cycles to maintain a relatively constant membrane content. Cyclic isotherms exhibited hysteresis, which was less pronounced for the higher purity light SR samples. Isotherms shown for SR monolayers are reported as a function of trough area, since an average molecular area is not easily quantified. Sample compression-expansion isothermal cycles are shown in Figure 5.13 for light SR (a) and heavy SR (b), respectively.

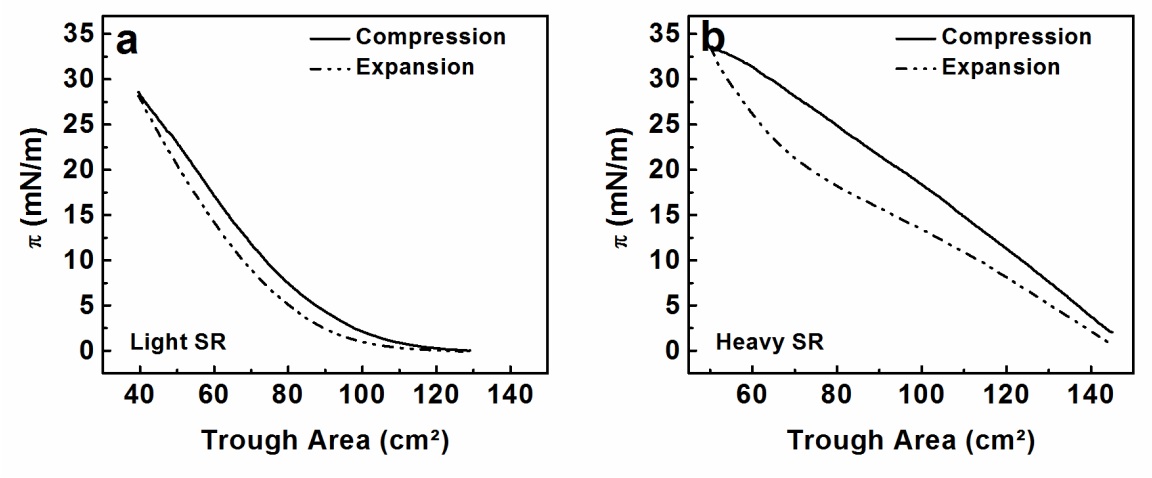


**Figure 5.13:** Isothermal compression and expansion of (a) light SR and (b) heavy SR monolayers at 25 °C. Both SR types are comprised of naturally derived sarcolemmal membrane components obtained from the fast-twitch skeletal muscle of New Zealand white rabbits.

*5.3.3 Polymer adsorption and squeeze-out from SR monolayers*

Addition of P188 to the subphase below a light SR monolayer (compressed above nominal surface pressure to 12 mN/m for imaging) resulted in adsorption similar to that which was observed for DPPC monolayers, as shown by Figure 5.14. Equilibration to a final surface pressure of about 16 mN/m occurred within one hour, as determined by the eventual plateau of surface pressure in time. The origin of the pressure spike and slow surface pressure decay at low adsorption times is unknown, but since surface pressure again climbs (as did P188 in Figure 5.4), it may be an artifact of polymer addition.

Diblock P188 and P188 adsorption to heavy SR are shown in Figure 5.15. Similar to adsorption to synthetic monolayers of DPPC, equilibrium adsorption pressures were about 12 and 16 mN/m, respectively, for Diblock P188 and P188. The similarities between equilibrium surface pressures regardless of monolayer compositions (DPPC, light SR, or heavy SR) confirm that polymer surface activity itself drives adsorption, rather than specific interactions. Unlike adsorption profiles for DPPC in Figure 5.4, both polymers show a gradual rise of surface pressure. Rounding of the Diblock P188 adsorption profile is likely due to PPO interactions with soluble membrane components in the subphase.

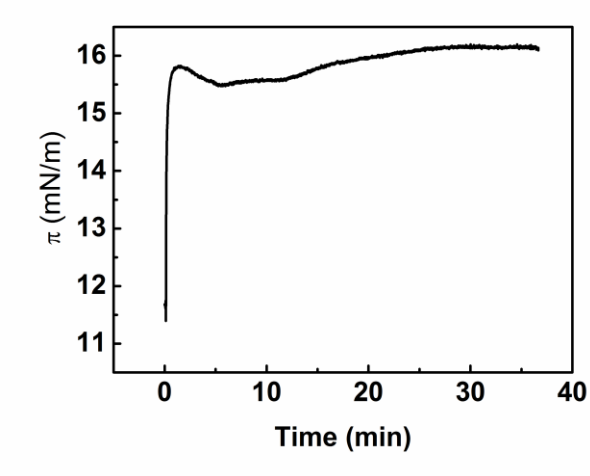


**Figure 5.14:** P188 adsorption to light SR monolayer. The monolayer was first compressed to ~11.5 mN/m for the purposes of monitoring adsorption by fluorescence microscopy.

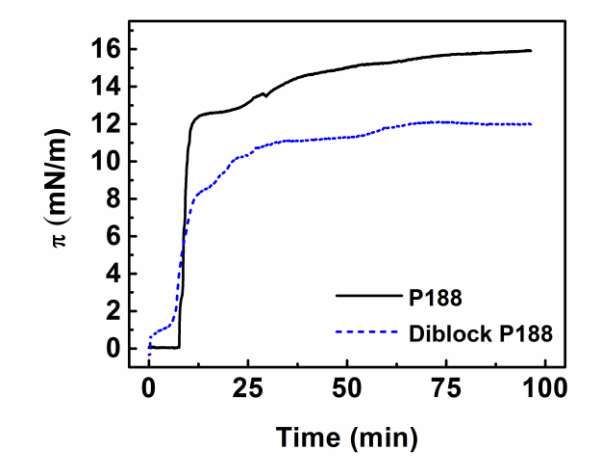


**Figure 5.15:** Polymer adsorption to heavy SR monolayer.

Compression isotherms performed on SR monolayers containing adsorbed P188 or Diblock P188 showed a very different result from the neat DPPC monolayers (see Figure 5.16). Although no sharp phase transitions can be seen in SR compression-expansion isotherms, the same "squeeze-out" event exhibited by Diblock P188 and P188 in DPPC (Figure 5.5) appears in compression isotherms of heavy SR monolayers with adsorbed polymers. For Diblock P188, a definitive squeeze-out pressure is not observed (Figure 5.16), though it likely occurs after a small reduction in trough area. The squeeze-out observed for P188 from heavy SR (Figure 5.16b) is far more pronounced, observable at a pressure of about 20 mN/m, which suggests P188 desorption into the subphase is more favorable at normal or "healthy" lipid packing of the membrane. This finding is consistent with results of DPPC compression isotherms, and agrees with the hypothesis that surface active block copolymers serve to temporarily associate with damaged membranes until healthy packing densities are restored.[35]

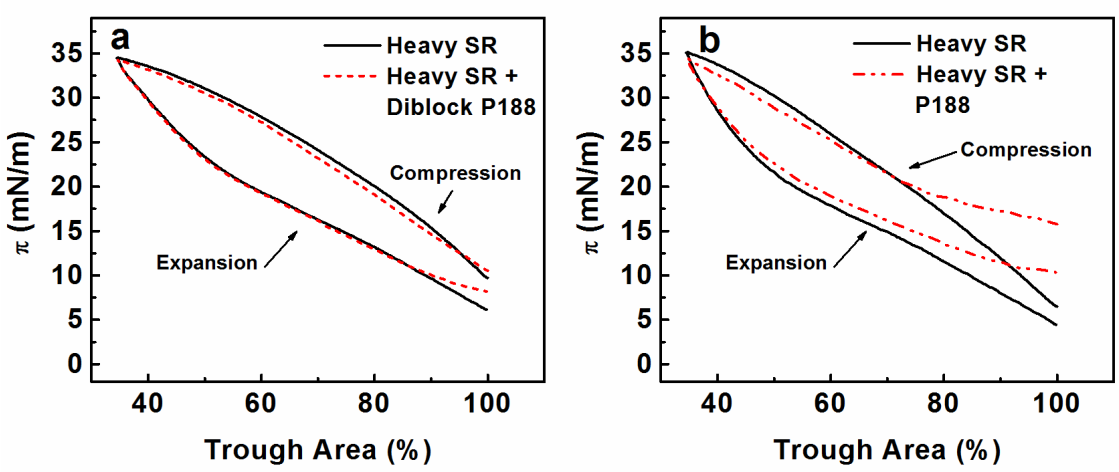


**Figure 5.16:** Compression-expansion isotherms for heavy SR and heavy SR with P188 adsorbed. Isotherms were performed on 20 mM MOPS subphases at 37 °C.

*5.3.4 Fluorescence microscopy with SR model membranes*

Just as for synthetic DPPC monolayers, naturally-derived SR monolayers were imaged using fluorescence microscopy. Again, TR-DHPE was used as a fluorophore, with bright regions corresponding to fluid-like phases and dark regions corresponding to crystalline or ordered lipid arrangements. Whereas neat DPPC monolayers showed only binary phase contrast, the multi-component Light SR monolayers have a more pronounced grayscale, as

shown in fluorescence micrographs captured throughout compression from 0.9 mN/m to 29.3 mN/m in Figure 5.17. While heterogeneities in the monolayer are clearly visible, small condensed phase regions (dark spots) in the membrane remain present and of fixed size (10-20 μm) throughout the full compression. As the highest surface pressure (29.3 mN/m) is approached, condensed phase regions become more tightly packed, and line tension (non-circular domains) begins to distort domain morphologies.

Unlike DPPC, which is insoluble in the water subphase and forms widespread condensed phases at high surface pressures that cannot be imaged by fluorescence microscopy, Light SR may be imaged at much higher surface pressures. The reason for this lies in heterogeneous composition of the sarcolemmal membrane. With components including cholesterol, proteins, and numerous lipid species, isotherms and corresponding micrographs represent conglomerate phase behavior. As such, no clear phase transitions were noticed, and presumably bulky, unlikely to order components in the membrane helped to maintain the fluidity necessary for imaging even at elevated surface pressures.

After establishing expected morphology for the Light SR monolayer, polymer additions were made and analyzed by fluorescence. In the following experiment, Light SR was compressed to the minimum trough area (40 $cm^2$) and a surface pressure of 11 mN/m, at which time 10 μL of 12 mM P188 was added under the monolayer. Epifluorescence micrographs of the Light SR monolayer incorporated with 1 wt-% TR-DHPE are given by Figure 5.18. Images are shown chronologically, 15 minutes (Figure 5.18a and b) and 40 minutes (Figure Figure 5.18c) after P188 addition, at which times surface pressures are at 14 mN/m and 18.3 mN/m, respectively. Most notably, following the addition of P188, large "rafts" of an intermediate gray phase appear, surrounded by a lighter fluid-like phase and containing small condensed regions reminiscent of neat Light SR. Here P188 seems to impose some ordering within the fluid-like phase, but after sufficient time, the effect is more evenly distributed, and at the elevated P188-adsorbed surface pressure, the matrix phase is much more smoothly distributed. The formation of rough-edged raft-like domains appeared in an independent P188 adsorption experiment; micrographs from 16 mN/m are shown in Figure 5.19. On further compression, rafts were no longer observed (data not shown).

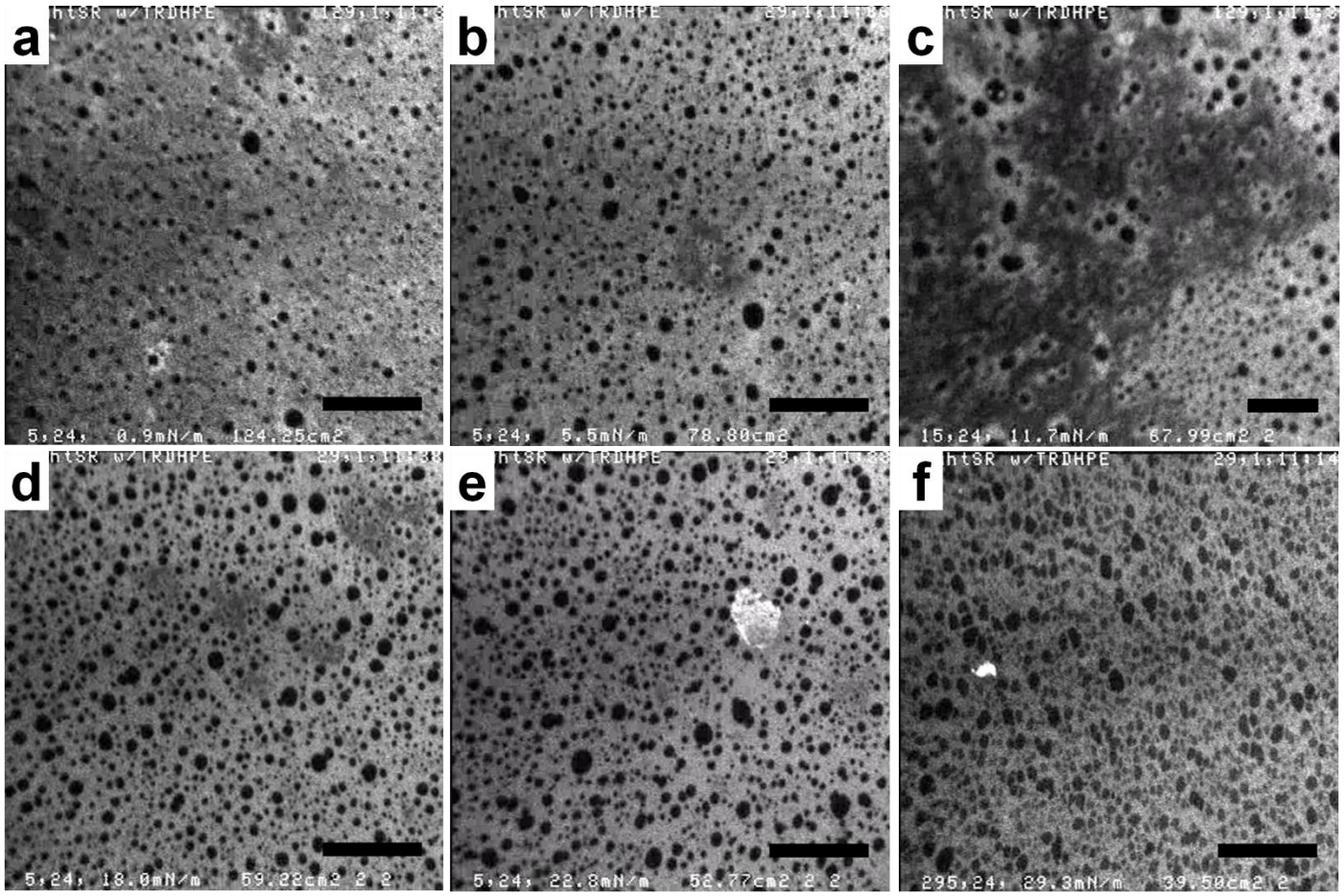


**Figure 5.17:** Fluorescence micrographs captured during compression of Light SR monolayer. Scale bars are 50 µm. Monolayer surface pressures are as follows: (a) 0.9 mN/m; (b) 5.5 mN/m; (c) 11.7 mN/m; (d) 18.0 mN/m; (e) 22.8 mN/m; (f) 29.3 mN/m.

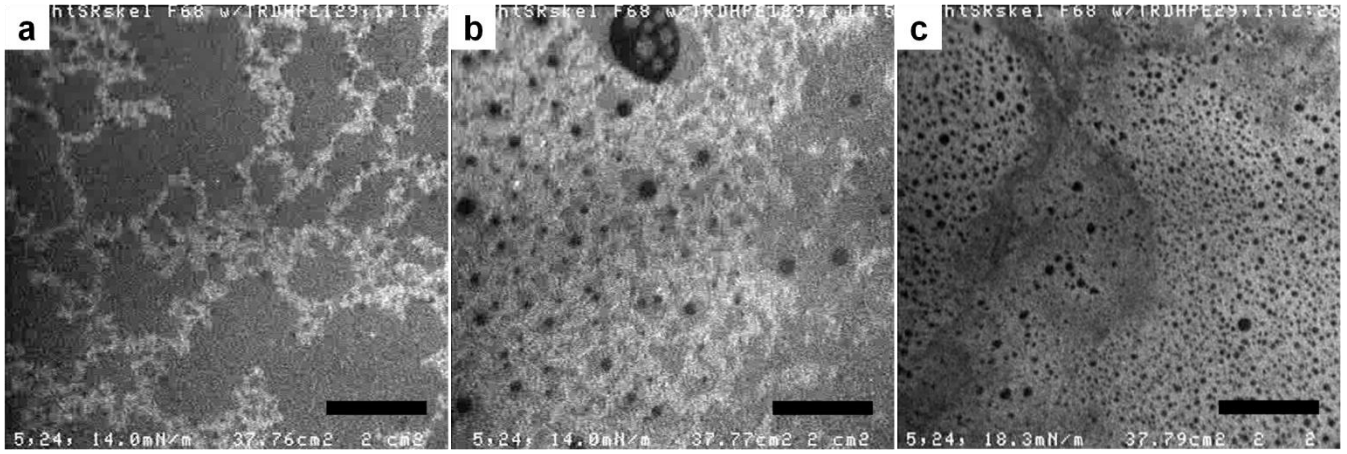


**Figure 5.18:** Fluorescence micrographs of Light SR incorporated with Poloxamer 188. Scale bars are 50 µm. Images in (a) and (b) were taken 15 minutes after P188 addition (at a surface pressure of 11 mN/m), and surface pressure is about 14 mN/m. Image in (c) was taken 40 minutes after addition, and surface pressure has raised to about 18 mN/m.

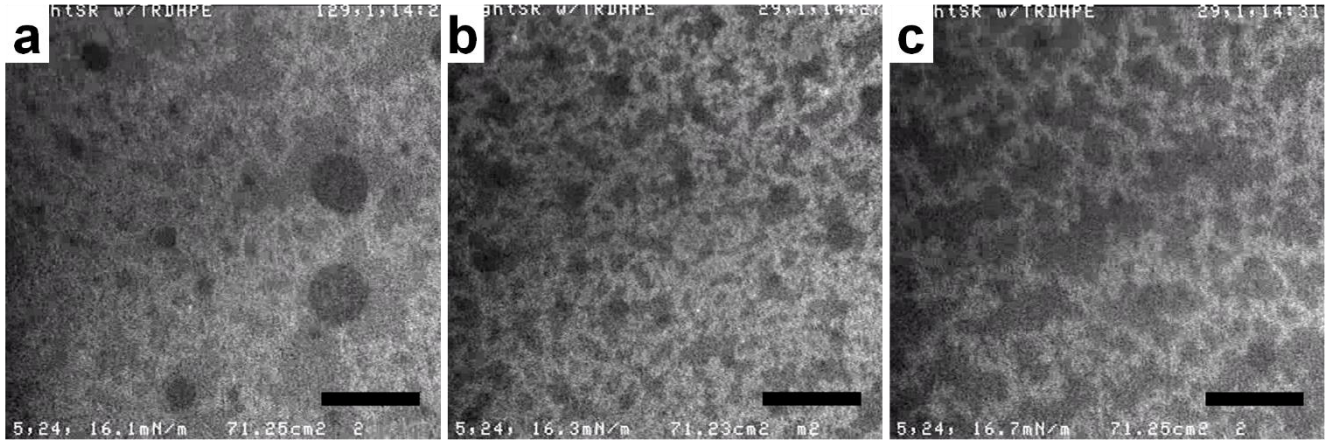


**Figure 5.19:** Monolayer of Light SR with P188 adsorbing shows intermediate phase domains, or rafts around 16 mN/m.

*5.3.5 Considerations and conclusions from SR model membranes*

Isolated sarcolemmal membranes from rabbit skeletal muscle were employed in monolayer investigations of block copolymer membrane stabilizers with native membrane components. Langmuir trough isothermal compression experiments on neat sarcolemma monolayers showed lower overall compressibility than synthetic monolayers, likely due to solubility of membrane components and the heterogeneity of cell membranes. This also corresponded to lower adsorption pressures achieved by P188 and Diblock P188 (~16 and 12 mN/m, respectively) than were achieved in synthetic DPPC monolayers. Differences reflect the importance of choosing a system which closely resembles the electronic and molecular environment of a native cell membrane. Despite the compositional differences between sarcolemma and synthetic phospholipid monolayers, P188 and Diblock P188 exhibited similar adsorption behavior to the interface in both monolayer types.

Although the use of the muscle-native sarcolemmal membrane components in monolayered studies addresses the compositional concerns of the homologous monolayer experiments, natural lipids, with varying degrees of unsaturation and levels of charge, are sensitive to degradation by oxidation under ambient conditions. Protein denaturation and oxidation of majority component cholesterol, when exposed to air, would also be of concern. While polymer adsorption to a sarcolemmal-based monolayer is valuable from a fluorescence microscopy standpoint, the system cannot be preserved in a manner to maintain sample correlation to the native membrane or even consistency between runs.

## 5.4 Summary and future work

In this chapter, synthetic and naturally derived membranes were studied in a monolayer film system on a Langmuir trough. Monolayered model membranes were used to simulate reductions in lipid packing experienced by damaged cell membranes, and adsorption behavior by block copolymer membrane stabilizers and subsequent impacts on phase behavior were studied.

*5.4.1 Synthetic DPPC monolayers*

For synthetic model membranes comprised of DPPC, the triblock architecture of P188 adsorbed to a higher equilibrium surface pressure than an analogous diblock architecture

(Diblock P188) corresponding to half of the triblock length and equivalent PEO/PPO relative composition. This effect was attributed to hydrophobic PPO molecular weight dependence on surface activity and lateral surface pressure in a phospholipid monolayer. Fluorescence microscopy performed on DPPC monolayers incorporated with both P188 and Diblock P188 indicated that polymer adsorption imposes film heterogeneity and departure from the expected chiral morphologies of DPPC. Similar types of morphological changes were induced by both architectures, though direct implications for damaged cell membranes are not immediately clear.

*5.4.2 Isolated sarcolemma monolayers*

A naturally derived membrane model was obtained and purified from rabbit skeletal muscle, and isothermal compressions of the multi-component monolayer showed no phase transitions, as a consequence of the many varieties of lipid, sterol, and proteins present in natural membranes.[74] Naturally derived membranes were partially soluble, which added a degree of complication to polymer adsorption experiments. Similar to synthetic monolayers, adsorption to sarcolemmal membrane monolayers showed higher equilibrium surface pressure for P188 than the smaller Diblock P188. Fluorescence microscopy on naturally derived monolayers indicated a similar ordering effect by both polymer species, in the form of rough-edged "rafts" of intermediate compression around 14-16 mN/m, in coexistence with fluid-like and compressed phases. Heterogeneity exhibited by membrane monolayers in fluorescence microscopy was similar before and after polymer addition.

*5.4.3 Future directions*

In addition to area-controlled isotherms and simultaneous fluorescence microscopy, monolayered models may be applied in various other techniques. Confocal microscopy in conjunction with the Langmuir trough has been used to quantitatively track the adsorption of fluorescently tagged chitosan to lung surfactant monolayers.[207] This was accomplished by taking *z*-stacks spaced 0.5 μm apart through the interface and computing axial fluorescence profiles for the chitosan fluorescent channel. The method could fairly simply be adapted to instead consider fluorescently tagged poloxamer-type membrane stabilizers, though experimental design of polymer injection under the subphase is complicated by methods to stabilize the monolayer for the ~1 s raster scans required.

Supported monolayers or even bilayers have been studied by atomic force microscopy techniques.[209,212,213] Supported monolayers can be prepared by Langmuir-Schaefer deposition,[214] inverted Langmuir-Schaeffer deposition,[93,209] or Langmuir-Blodgett techniques.[215] By selecting pertinent surface pressures for film deposition, lipid phase behavior and phase perturbations induced by block copolymer adsorption can be imaged by tapping-mode AFM at nanometer resolution. Images yield information about lateral arrangement of phospholipids, and height profiles can be used to find holes, lipid-phase changes, or polymer deposits. Additionally, force profiles can be obtained at varying locations on the monolayer to obtain information about mechanical properties of the film, which are related to phase and composition.[216] Bilayered phospholipid membranes require environmental AFM, which involves tapping mode under water. Preliminary AFM measurements on supported monolayers were taken using DPPC monolayers with adsorbed Diblock P188 and P188 at varying surface pressures, but environmental AFM is expected to provide more useful information with respect to polymer-induced changes to lipid packing, stiffness, and phase behavior

# Chapter 6

# Collaborative support activities

Beyond the primary objectives of this thesis, a handful of collaborative endeavors were pursued in support of the physiological investigation of therapeutic interactions by block copolymers with membranes. This chapter outlines two such projects, fluorescent tagging of P188 and polymer solution viscosity, as it relates to bolus administration in a large animal model.

## 6.1 Fluorescent tagging of Poloxamer 188 for imaging

One of the most formidable difficulties surrounding investigations of membrane interactions by Poloxamer 188 and related block copolymer surfactants is that of experimental observation of the interaction at molecular resolution. The polymers, which are relatively small ($R_g \approx 3$ nm for P188, assuming equal statistical segment lengths of PEO and PPO, $b = 6.0$ Å[150]) and dilute in therapeutic doses, offer little in the way of imaging contrast from the organic components of the membrane lipids. Standard optical microscopy cannot achieve the needed resolution to directly image polymer interactions, and even cryo-TEM methods are inaccessible, due to similar electron densities between membranes and the water-soluble alkoxide based polymers and no functionalities reactive to common TEM staining techniques. This is to say nothing of the suppression of the native environment imposed by the c.a. 100 nm film thickness of vitrified aqueous solution on the TEM grid, which might have additional consequences on polymer association behavior.[217]

Dihydroxyl-terminated poloxamers contain sufficient reactivity to chemically attach a variety of tagging molecules. Fluorescent dyes,[218–221] radioactive tags,[220–225] and antibody-binding molecules (i.e. biotin)[226,227] are commonly used to track species of interest in biological applications, with a growing number of studies incorporating them into PEO-based polymer systems, including poloxamers. Applying the same chemistries to hydroxyl groups on poloxamers or diblock copolymers, tagged molecules can be imaged or quantified in localized regions or tissue or at the membrane. The following is a summary of three tagging strategies pursued for fluorescence and confocal microscopy, along with commentary for each on ease of execution, purification, and analysis, as well as inherent disadvantages.

*6.1.1 Fluorescence tagging by 5-DTAF*

In a paper seeking to probe poloxamer adsorption in a biologically non-invasive way, Ahmed and coworkers devised a synthetic scheme to conjugate a fluorescein derivative, 5-(4,6-dichlorotriazinyl) aminofluorescein (5-DTAF) to hydroxyl-terminated poloxamers.[218] The triazinyl group reacts by nucleophilic aromatic substitution with alcohols in aqueous solutions under basic conditions at room temperature, following a two-step addition and elimination mechanism. The structure of 5-DTAF is shown in Figure 6.1.

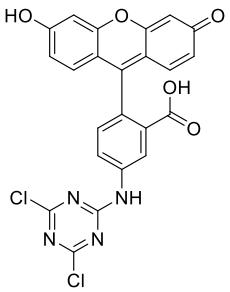


**Figure 6.1:** Chemical structure of 5-(4,6-dichlorotriazinyl)aminofluorescein, 5-DTAF

For fluorescence tagging of P188 by 5-DTAF, the following synthetic and purification steps were performed. The reaction mixture was prepared in a 2:1 molar ratio of 5-DTAF:P188. Stock solutions (50 mg/mL) of 5-DTAF were prepared in dimethylsulfoxide (DMSO), and a stock solution of P188 was prepared (6 w/v% in 0.1 M sodium bicarbonate ($NaHCO_3$) and buffered to pH = 9.3. 1 mL reaction volumes were combined and reacted

in the dark overnight. The reaction mechanism is shown by Scheme 6.1, which depict the polymer addition (with resonance) and chlorine elimination from the triazine ring.

Reactions were purified the next day on a PD-10 disposable desalting column (GE Healthcare, Pittsburgh, PA) filled with Sephadex G-25 medium, to remove Cl salts and excess dye. Columns were prepared by three full volume washes (3.5 mL) with 0.05 M sodium chloride, followed by the reaction volume (supplemented by 0.05 M NaCl to reach a 3.5 mL addition) and two full volume washes of 0.05 M sodium chloride. Following addition of the 5-DTAF and P188 solution to the column, the first 3 mL collected off of the column were discarded, and about 6 mL of eluted solution were retained. Volumes were split into two Amicon Ultra-15 centrifugation filter tubes with 3,000 g/mol molecular weight cutoff (Millipore, Billerica, MA) and centrifuged at 7,000 gs for a total of 90 minutes to remove residual free dye and to concentrate polymer. Final sample volumes were about 450-500 µL of tagged P188.

Once purified, polymer concentration was assessed by a cobalt thiocyanate complexation procedure outlined in Ahmed, et al.[218] Identical complexation steps were performed on neat P188 standards at varying known concentrations and the unknown concentration of 5-DTAF-P188. Cobalt thiocyanate was prepared from the reaction of 3 g of cobalt nitrate with excess ammonium thiocyanate in 100 mL of water, to achieve a 0.16 M solution. To a 1.5 mL centrifugation tube was added 50 µL of the cobalt thiocyanate solution, 100 µL aliquot of the aqueous polymer solution, and 200 µL of ethyl acetate. The solution was vortexed and then centrifuged at 11,600 gs for 30 minutes, or until a pellet (complexed polymer and cobalt thiocyanate) formed. On pellet formation, the blue supernatant was carefully removed by micropipette and replaced by 400 µL of ethyl acetate. Careful washing of the pellet was performed by several cycles of alternately pulling up and pushing out ethyl acetate into the tube, before the sample was again centrifuged. Wash steps were repeated until the supernatant remained clear after centrifugation, or about five times. Finally, the pellet was dissolved in 10 mL acetone, and 0.5 mL volumes were prepared at 10x dilution for absorbance readings.

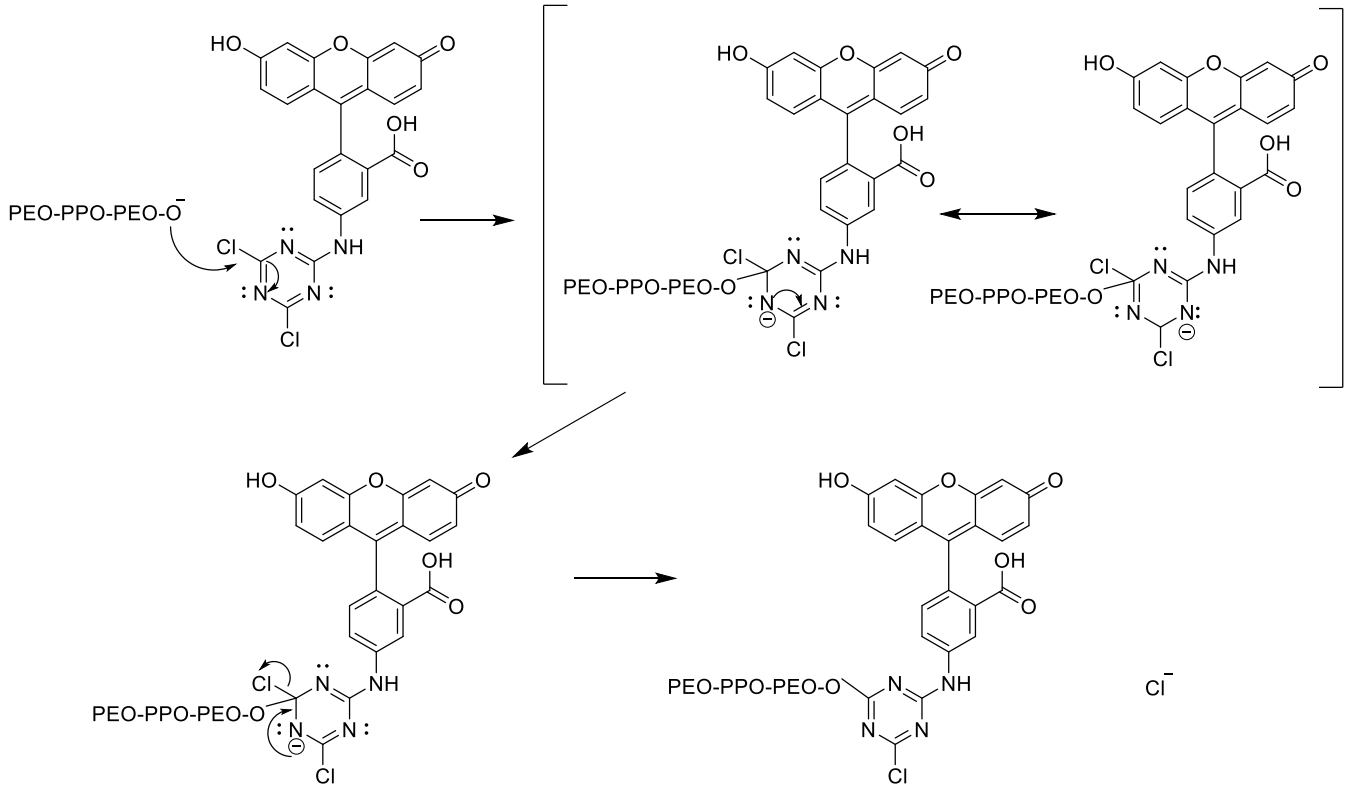


**Scheme 6.1:** Synthetic route to 5-DTAF labeled poloxamer. Scheme adapted from Ahmed, et al.[218]

Calibration curves for P188 concentration and 5-DTAF concentrations were prepared to assess sample concentration and tagging efficiency. A cobalt thiocyanate calibration curve for P188 concentration was prepared from stock concentrations ranging from 0.5 mM to 7.1 mM. A single cell spectrophotometer was used to scan the absorbance wavelengths, and a maximum value was found at 332 nm. The calibration curve is shown in Figure 6.2. When similarly complexed with cobalt thiocyanate, independent batches of 5-DTAF labeled P188 gave absorbance readings corresponding to P188 concentrations of 8.8 and 9.2 mM, respectively. Labeling efficiency was determined from a 5-DTAF calibration curve and known P188 concentrations. The 5-DTAF standards were prepared by diluting 50 mg/mL 5-DTAF in DMSO with HEPES buffer (pH = 8.0), and the calibration curve was prepared by measuring absorbance at 492 nm at each of the concentrations (Figure 6.2). Two independent samples of 5-DTAF tagged P188 gave final concentrations of 0.16 mM and 0.26 mM, corresponding to labelling efficiencies of 0.9-1.6% of available hydroxyl groups. Based on low tagging efficiencies and tedious product recovery, 5-DTAF labeling was abandoned for methods for which larger quantities of tagged poloxamer could be obtained readily. Efforts to image 5-DTAF labeled P188 in confocal microscopy on a phospholipid monolayer yielded very low signal at the level of noise, due to poor labeling efficiency.

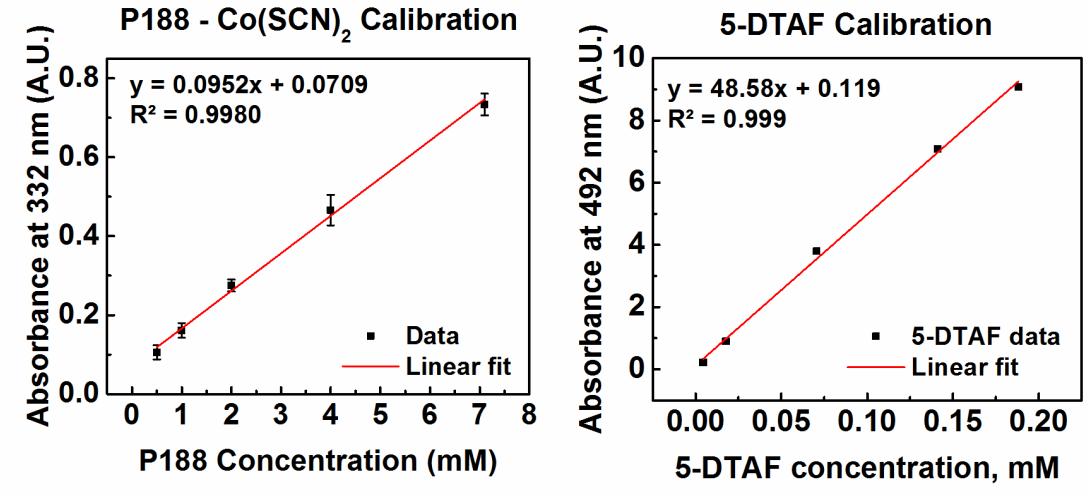


**Figure 6.2:** Absorbance calibration curve constructed for P188 complexed with cobalt thiocyanate. Error bars indicate standard error of the mean for $N = 3$.

*6.1.2 Azide-functional P188 for click reaction with AlexaFluor 647*

In the optical investigation of block copolymer localization in tissue and at cell membranes, the balance between selecting an effective molecular probe and maintaining a native environment is difficult to achieve. Radioactive labeling strategies such as tritium ($^{3}H$) or $^{14}C$, or iodine-based tags would likely impose no changes to membrane interactions, but low detection levels (especially low-energy tritium),[224] short half-lives, and the special handling required make them less favorable for initial localization experiments. Fluorescent dyes such as 5-DTAF, Rhodamine B, and Alexa Fluor, which are conversely stable for longer times, all contain conjugated aromatic rings, with molecular weights ranging from about 500 g/mol (5-DTAF and Rhodamine B) to upwards of 1,500 g/mol (Alexa Fluor). Relative to the poloxamers or even smaller diblock species, these hydrophobic entities would be of significant consequence, and it could be reasonably expected that they would alter membrane interactions from those exhibited the neat block copolymers. To address the concern of specific membrane-dye interactions, a click-reactive azide functionality was considered.[228]

Since its inception, copper-free click chemistry has emerged as a useful way to label and image proteins and other molecules of interest *in vivo*.[228,229] The reaction proceeds by strain in an eight-membered ring, dibenzocyclooctyne, as depicted generically in Scheme 6.2. A variety of click-functionalized fluorescent tags are available for purchase, and they can be used to detect azide functionalities with significant sensitivity.

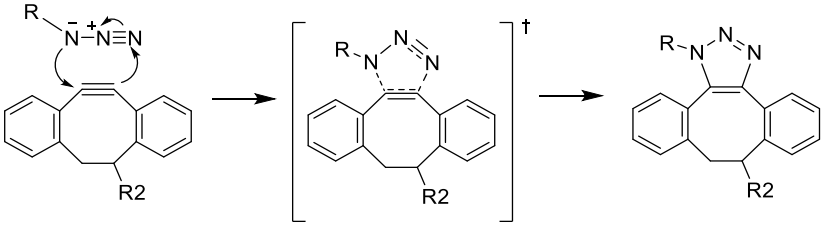


**Scheme 6.2:** Click reaction of an azide-functionalized moiety (R) with the DIBO-functionalized dye (R2).

The promise of click-reactive poloxamer tagging lies in the notion that azide-functionalized poloxamers would be administered *in vivo*, and polymers within isolated *ex vivo* tissue samples could then be reacted *in situ* with click-functional dye to locate poloxamer accumulation sites. The advantages of this strategy are numerous. Compared to

direct tagging by a fluorescent probe, azide-functionalization is both inexpensive and simple to perform on a large (tens of grams quantity) experimental scale. Furthermore, postponement of fluorescent tagging until tissue and organ harvest would reduce the waste associated with systemic delivery of a fluorescently labeled moeity, limiting tag to only samples of interest, while diminishing the likelihood of photo-bleaching by prolonged exposure to environmental conditions. Finally, azide groups, while potentially reactive, are unlikely to perturb the mechanism of membrane interaction in the way a bulky aromatic group would. One potential drawback to *ex vivo* tagging of P188 and other membrane stabilizers is that interactions, believed to be nonspecific with membranes, might not be strong enough to sustain histological preparatory steps and washing of the free dye away. This is a question that only *ex vivo* imaging can truly answer. Azide functionalization of Poloxamer 188 was performed in two steps: tosylation[230] and azide substitution, which are shown in Scheme 6.3.

For tosylation, hygroscopically adsorbed water was removed from a known quantity of P188 by azeotropic distillation from toluene, which was carried out at 60 °C until approximately half of the toluene volume was removed. To the P188 and toluene solution was added a 10x excess of triethylamine and a 5x molar excess of p-toluene-sulfonylchloride. The reactor was sealed under positive argon pressure and stirred at room temperature overnight. To purify tosylated P188, 10 mL of methanol were added to the toluene solution to form an azeotrope, and solvent was removed by rotary evaporation. The polymer residue was redissolved in dichloromethane, precipitated from cold diethyl ether, filtered and dried in a 40 °C vacuum oven outfitted with a dry ice and isopropanol cold trap. Dried tosylated P188 was analyzed by $^{1}H$ and $^{13}C$ NMR (500 MHz) in dimethylsulfoxide-d6 and $CDCl_3$, respectively. Tosylation was verified by the appearance of aromatic protons in $^{1}H$ NMR, as well as the methyl protons from the tosyl group. It should be noted that the tosyl functional groups on P188 would be less reactive and less susceptible to decomposition than azide functional groups, so bulk synthesis of functionalized P188 should halt after tosylation, from which small, necessary batches of azide-functionalized P188 can be prepared.

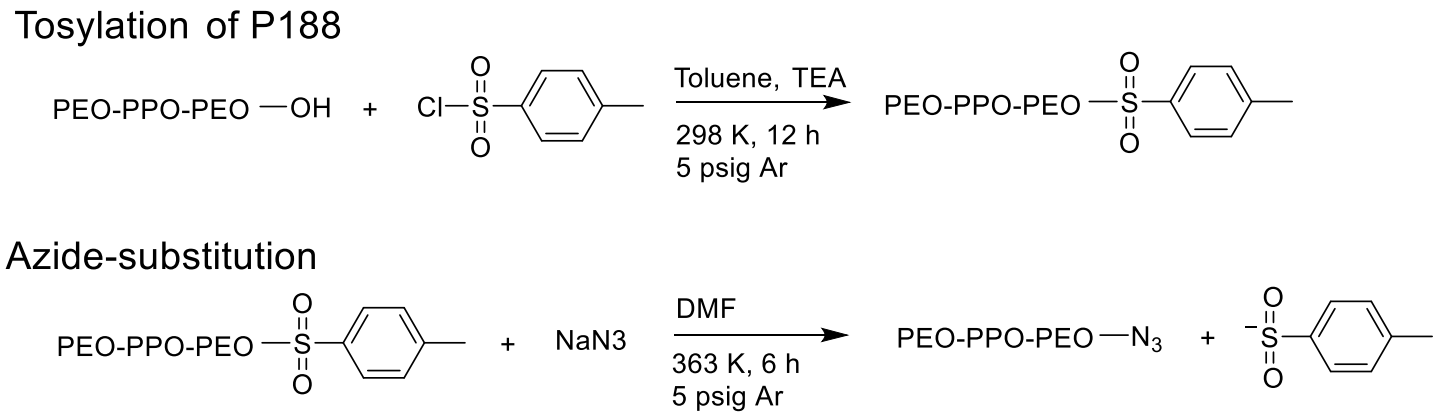


**Scheme 6.3:** Two step functionalization of P188 for click-reactive dyes. Reactions are shown generically at one functional end of the difunctional P188 molecule. First, hydroxyl-terminated P188 is tosylated. In the second step, tosylated P188 is reacted with sodium azide**.**

For azide substitution, 4 Å molecular sieves (Sigma) were first regenerated by heating under vacuum to 250 °C for 3 hours and cooling under vacuum overnight. To dried molecular sieves was added dimethyl formamide (DMF), before sealing the flask with a rubber septum and purging the headspace with argon. DMF was dried over molecular sieves overnight before use. A known quantity of tosylated P188 (~10 g) and a 10x molar excess of sodium azide were added to a three-neck flask, and about 200 mL of dried DMF were transferred by cannula to the reactor. Special care was taken to handle sodium azide, which reacts with water to form acutely toxic hydrazoic acid and with several types of metal to form explosives. Only plastic or glass utensils were used to transfer or store it. The reaction solution was sealed under argon and heated to 90 °C with stirring to react for 6 hours and cooled overnight.[231]

Following the substitution reaction, azide-functionalized P188 was recovered and purified. Solvent (DMF) was removed by rotary evaporation with heating to 70 °C. The dried residue was dissolved into dichloromethane and washed twice with a brine solution and twice with water. Sodium sulfate was added to the organic phase to remove traces of water, and filtered out.[232] Azide-functionalized P188 was precipitated from dichloromethane into cold diethyl ether, and filtered precipitate was freeze-dried from benzene.

Product characterization was performed by NMR and FTIR techniques. First, $^{1}$H NMR (DMSO-d6, 500 MHz) was used to show the appearance and disappearance of tosyl groups after respective reaction steps. Relevant chemical shifts for the tosyl groups, indicated in Figure 6.3 were aromatic peaks around 7.3 and 7.5 ppm, as well as peaks at 4.11 and 2.41 ppm. Strong magnification of signal in Figure 6.3 indicates faint aromatic peaks in the a-P188 trace, suggesting incomplete leaving by tosyl groups, but a quantitative efficiency was indeterminable because signal was too low to integrate.

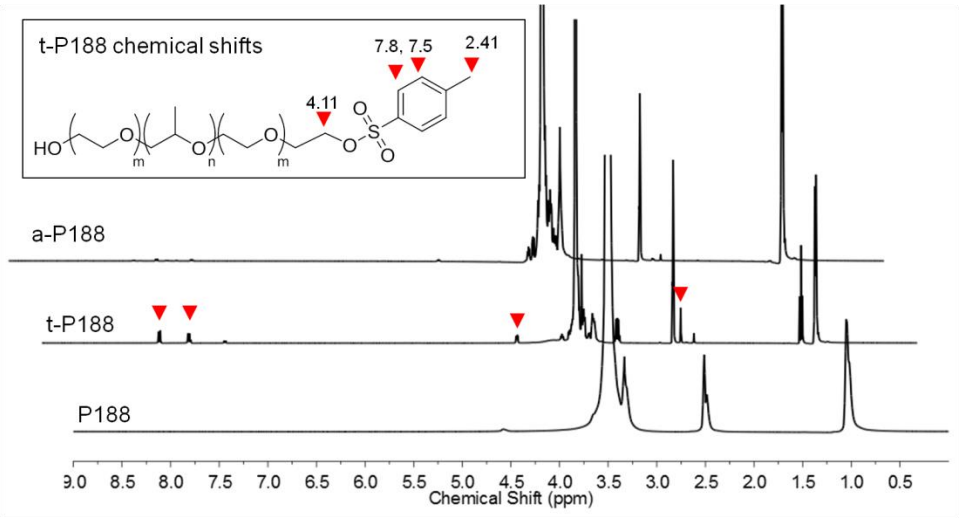


**Figure 6.3:** $^{1}$H NMR spectra for P188, tosyl-functionalized P188 (t-P188), and azide-functionalized P188 (a-P188). Samples were dissolved in DMSO-d6, and spectra were collected at 500 MHz. Arrows on t-P188 structure indicate relevant peaks on t-P188 specturm. Additional methyl protons at $\delta$ = 1.11 ppm are attributed to residual triethylamine.

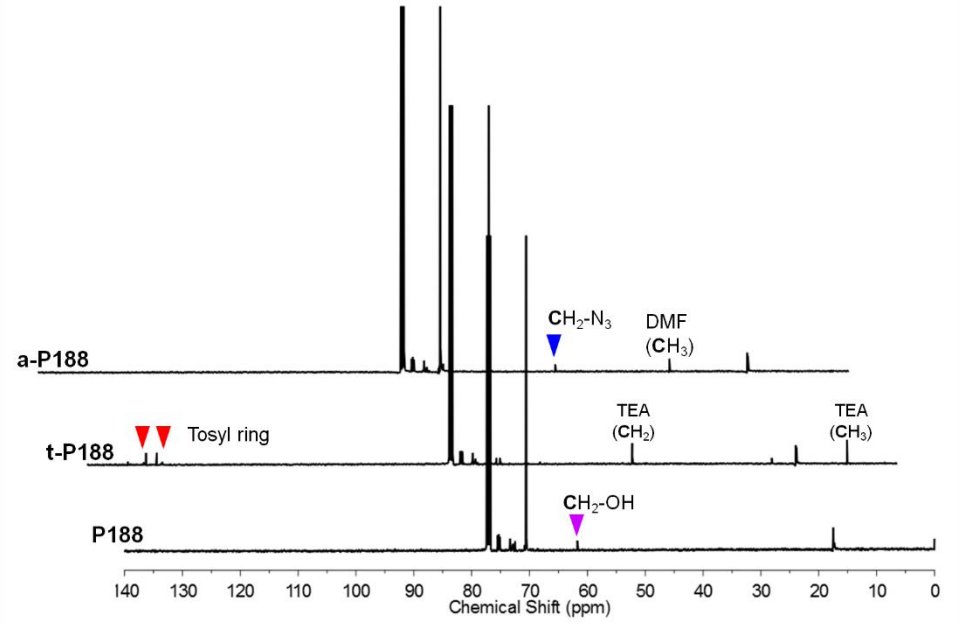


**Figure 6.4:** $^{13}$C NMR of azide functionalization steps. Identifying peaks are labeled, along with residual solvent peaks from triethylamine (TEA, t-P188 trace) and dimethylformamide (DMF, a-P188 trace).[140,232]

Next, $^{13}C$ NMR was used to confirm successful azide substitution, because chemical shifts by protons adjacent to azide groups ($\delta$ = 3.5 ppm) are obscured by the strong PEO/PPO alkyl proton signal between 3.4 and 3.6 ppm. Spectra obtained by $^{13}C$ NMR ($CDCL_3$, 500 MHz), are shown in Figure 6.4, with pertinent identifying peaks labeled. Again, tosyl-group peaks disappear following azide substitution ($\delta$ = 128 ppm, 130 ppm), and a peak corresponding to azide-adjacent carbon appears at $\delta$ = 50.66 ppm.

Finally, azide substitution was independently confirmed by FTIR. Spectra (32 scans) for P188, tosylated P188 and azide-functionalized P188 are shown in Figure 6.5, with relevant stretching frequencies for tosyl and azide groups indicated at about 600 $cm^{-1}$ and about 2,100 $cm^{-1}$, respectively.[232] The small peaks just down-shifted from azide (about 1,900 $cm^{-1}$) are due to known noise from the FTIR spectrometer.

Reaction of azide-functionalized P188 with the copper-free click reagent, Alexa Fluor 647 DIBO alkyne ($\lambda_{excitation}$ = 647 nm, $\lambda_{emission}$ = 668 nm; Invitrogen, Carlsbad, CA) can be performed at room temperature under physiological conditions. Dry label was used as received and stored in a -20 °C freezer until needed, and it was dissolved in DMSO to form a stock solution. Pre-labeled P188 was prepared by reacting a 1.5x excess of Alexa Fluor DIBO alkyne with azide-functionalized P188 in phosphate buffered saline (PBS). The reaction volume was stored at room temperature in the dark for one day before dialysis against PBS for one day. Preliminary confocal microscopy on isolated rat cardiac myocytes was inconclusive, and conditions were not optimized. The bulky structure of Alexa Fluor dyes is anticipated to interfere with P188-membrane interactions, which is another case of non-native interactions. Preferably, azide-functionalized P188 or other membrane stabilizer would be administered *in vivo*, and fixed histological samples would be reacted with DIBO alkyne click dyes in explanted tissue rather than isolated cells. Further work with azide-substituted P188 is recommended.

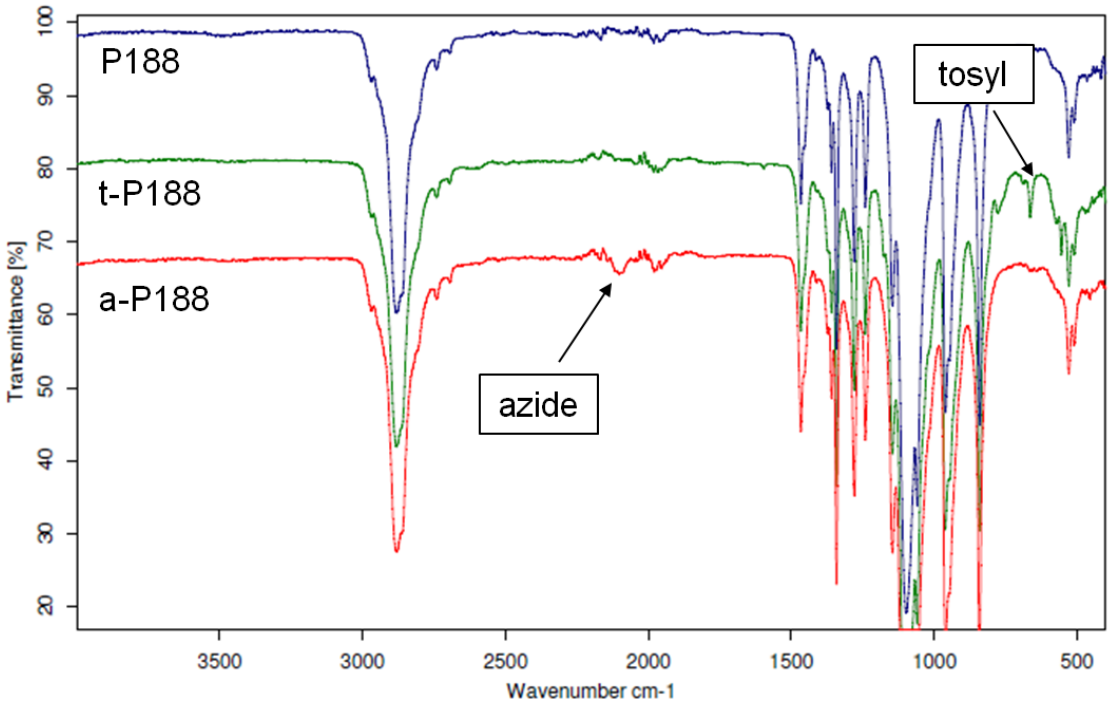


**Figure 6.5:** FTIR spectra for P188, t-P188, and a-P188.

Vibrational stretching by tosyl and azide functional groups are indicated at 600 and 2,100 cm-1, respectively.

*6.1.3 Rhodamine B tagged Poloxamer 188*

A final fluorescent tagging method was pursued as a proof of concept, using a Rhodamine B-based label. Rhodamine B derivatives are easily synthesized from Rhodamine B base, which is inexpensive and prevalent in physiological labeling contexts. For these reasons, it would be favorable for bulk preparation for large animal studies, which require c.a. 25 g of total polymer per animal. *In situ* or *ex vivo* imaging of RhB-functionalized P188 is planned. Tagging was performed in two steps by Wenjia Zhang according to the reaction in Scheme 6.4, which involves transforming Rhodamine B base (Sigma) to Rhodamine B acid chloride,[233] before reacting with terminal hydroxyl groups on P188, to yield Rhodamine B functionalized P188, RhB-P188. Labeled P188 was dried by rotary evaportation and free dye molecules were removed by iterative dialysis against chloroform in benzoylated cellulose dialysis tubing (2,000 MWCO, Sigma). Dialyzed RhB-P188 in chloroform was dried by rotary evaporation before finally freeze-drying from benzene.

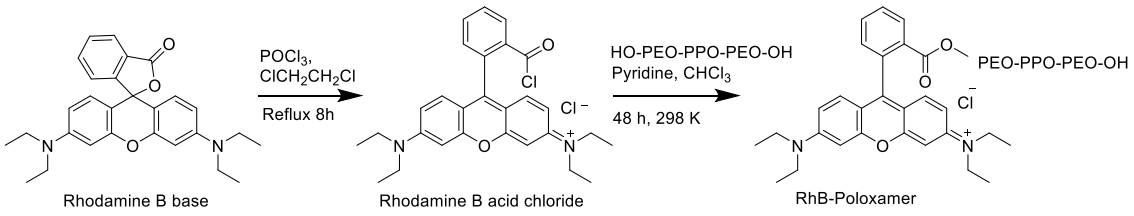


**Scheme 6.4:** Synthetic route of Rhodamine B tagged P188 from Rhodamine B base.

Tagging efficiency was estimated by a calibration curve for Rhodamine B base maximum absorption at (556 nm) for concentrations ranging from about 5 to 20 µM. A RhB-P188 sample of known concentration in water was compared to the calibration curve in Figure 6.6 to determine the equivalent concentration of Rhodamine B; a ratio of dye and polymer concentration yielded an estimated tagging efficiency of 1.6 dye molecules per difunctional P188.

As for the pre-labeled Alexa Fluor-P188 in the previous section, preliminary imaging experiments with RhB-P188 were performed on a cellular system using a fluorescence microscope. Stock solutions of Rhodamine B base, RhB-P188, and P188 were prepared in cell culture media to achieve 100 nM final concentrations. Fluorescent activity of RhB-P188, which had been unwittingly exposed to ambient light for several weeks, was assessed

by absorbance at 540 nm. Absorbance measured for a 50 nM solution of RhB-P188 (concentration calculated on the basis of the tagging efficiency, 1.6 RhB groups per molecule) corresponded to absorbance by about 17 nM Rhodamine B base, as shown in Figure 6.7. In order to prevent future unwanted photobleaching, care should be taken to reduce Rhodamine B labeled P188 from exposure to light.

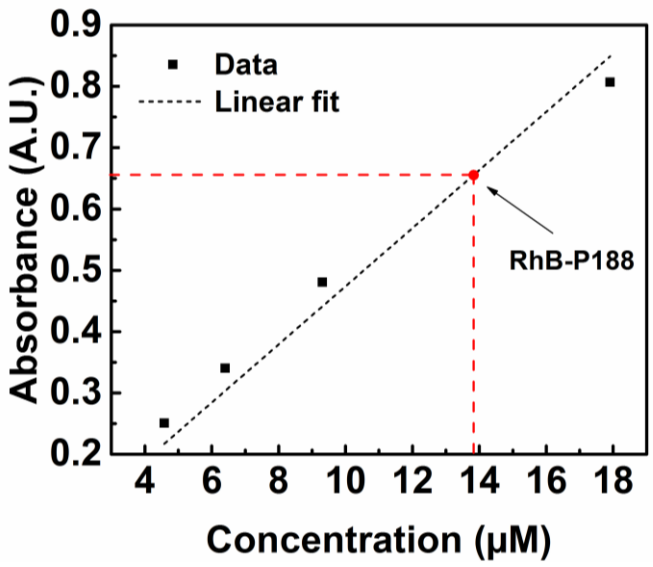


**Figure 6.6:** Calibration curve and tagged polymer absorbance at 556 nm.

The model system selected for imaging were human epithelial cells, HeLa, derived from human cervical cancer cells and widely used in various forms of medical research.[234] Living HeLa cells were cultured by Yogesh Dhande in Dulbecco modified Eagle medium (DMEM) with phosphate buffered saline (PBS). Cells were incubated with 100 nM P188, Rhodamine B base, or RhB-P188 at 37 °C for one to two hours (as indicated). Prior to imaging, cells were washed twice with DMEM and PBS medium. An RFP filter cube (540/593 nm) was used to image Rhodamine B containing samples. Figure 6.8 shows bright field and RFP filter channels, along with overlaid images taken at 20x magnification for P188 and Rhodamine B base controls, as well as 1 and 2 hour incubations of RhB-P188. As shown in Figure 6.8, no fluorescent signal was detected on the RFP channel for control P188, and bright field images indicate uniform cell health across all samples.

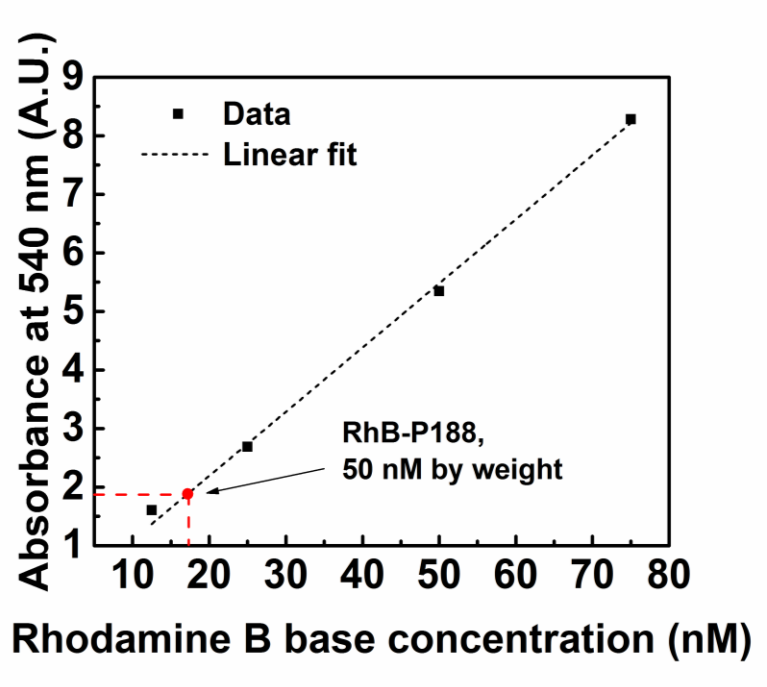


**Figure 6.7:** Fluorescence activity of RhB-P188 was reduced following several weeks of storing in ambient light.

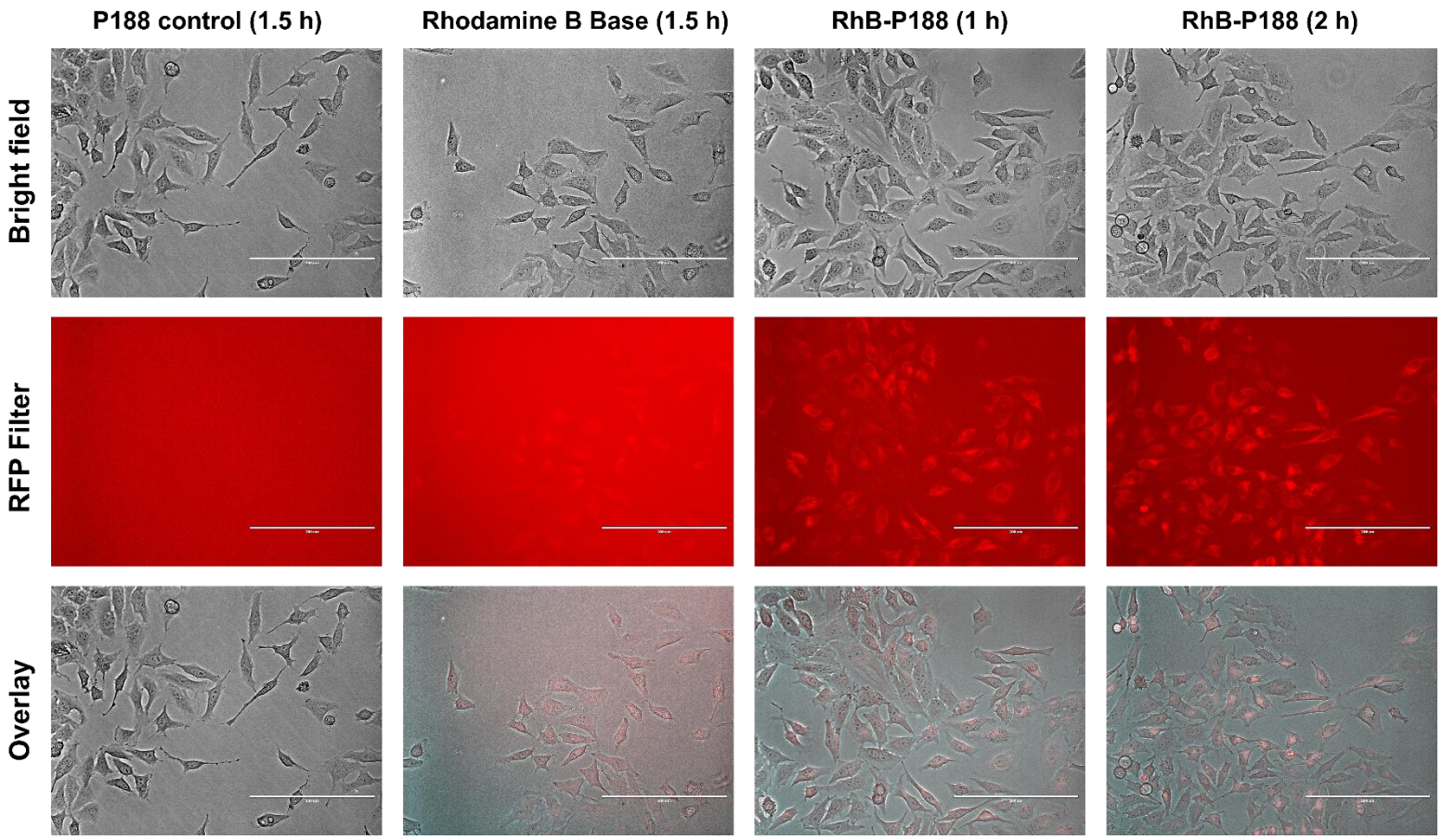


**Figure 6.8:** Fluorescence microscope images on HeLa cells incubated with 100 nM RhB-P188. Scale bars are 200 µm. P188 shows no signal in RFP, and some signal by free Rhodamine B base controls showed no signal in RFP filter. RhB-P188 shows high intensity in the RFP channel and overlays, consistent with RhB. Contrast has been enhanced for ease of viewing.

Higher magnification (40x) images of RhB-P188 incubated HeLa cells are shown in Figure 6.9. The RFP channel indicates localized concentrations of tagged P188 at cells, but fluorescence microscopy cannot provide any information regarding location within or around the three-dimensional cell and cell membrane structure. For this, confocal microscopy could be used to generate z-stacks through the depth of the cell, from which intensity profiles may be extracted to locate highest fluorescent tag density.[207]

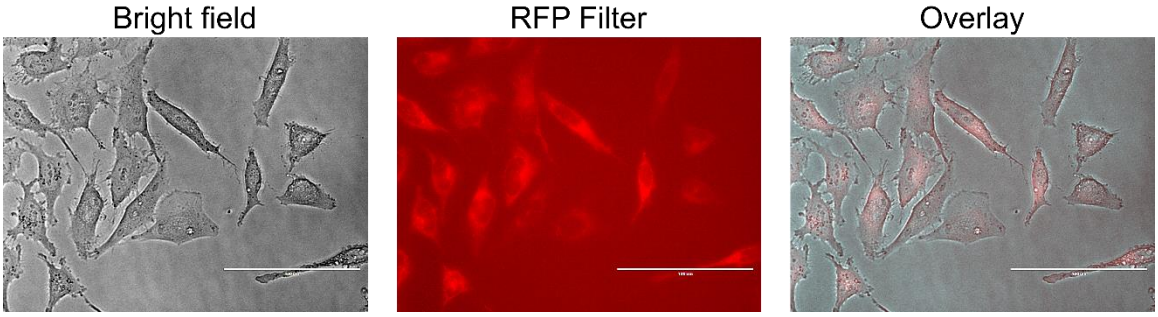


**Figure 6.9:** RhB-P188 incubated with living HeLa cells for 2 hours. Images are taken at 40x magnification; scale bars are 100 µm.

Although the HeLa cell model does not directly translate to the muscle cells or animal tissue of interest in membrane stabilization protocols, the RhB-P188 incubation study serves as a proof of concept for imaging in culture. Results suggest that interactions by tagged polymers with membranes are strong enough to withstand washing steps, and signal by even very low concentration RhB-P188 is sufficient to discern tagged polymer localization at cells. Optimization of imaging conditions (i.e. better preservation techniques for RhB-P188, higher tagged loading, or even labels at preferred excitation/emission wavelengths) would lead to a powerful, never-before seen method of studying P188 interactions with cell membranes.

## 6.2 Blood viscosity

Prior literature has identified P188 as a useful treatment method for the treatment of ischemia reperfusion injury, either at the circulatory level[31,46] or localized reperfusion injuries caused by a variety of maladies.[50–52,235] Ischemia, referring to the cessation of blood flow (and therefore oxygen delivery) to tissue, was once believed to cause the irreparable damage to the heart following cardiac arrest.[236] In fact, it was later determined that the return of oxygenated blood to hypoxic cells is the greater source of damage, and

considerable work has been done to understand the mechanism and treatments of ischemia reperfusion injury. [236]

An ongoing effort by Yannopoulos and cowokers to understand the effects and treatments of ischemic reperfusion injury following cardiac arrest has recently incorporated the P188 molecule into a bundled post-conditioning therapy to mitigate ischemic reperfusion injury following cardiac rest in a porcine model.[69] The study involved bolus injections of P188 (250 mg/kg) in the second minute of resuscitation following 17 minutes of cardiac arrest. If resuscitation was successful following compressions and defibrillation, P188 was administered intravenously for four hours (460 mg/kg delivered).[69] Significant improvements in hemodynamics, 48 hour survival, and neurologic function were reported for the bundled post-conditioning treatment. Results suggest that P188 plays a role, though the exact nature of P188's function cannot be decoupled from the additional therapeutic measures employed.[69]

It is outside the scope of this thesis to elaborate on the details of experiments beyond a summary of findings reported by Bartos, et al.,[69] however, one particularly pressing question about the nature of the effect was raised, that is, whether the observed effect came about by specific interactions by P188 with vasculature, bulk changes to blood rheology, or otherwise. To probe this, parallel investigations were conducted comparing the rheological and bundled post-conditioning therapy efficacy of P188 to a comparable molecular weight PEO homopolymer, PEO-8k. In doing so, it was expected that the role of amphiphilicity in the mechanism of improved outcomes *in vivo* would be confirmed or denied.

Blood rheology is an extremely complicated problem, and the field of hemodynamics is vast.[237–239] The following experiments were performed in an effort to determine whether amphiphilicity has a unique effect on blood viscosity that might facilitate injury-free reperfusion post-ischemic event. To investigate this, Couette flow rheology was performed on aqueous solutions of P188 and PEO-8k at varied concentrations and shear rates to determine the shear-dependent viscosities. Following those studies, post-ischemic blood samples supplemented with both polymers were studied. Parallel *in vivo* tests involving STEMI (ST segment elevation myocardial infarction) were performed by Yannopoulos and

coworkers with either P188 or PEO-8k to determine whether the physiological improvement seen by P188 was a function of bulk-polymer addition or specifically related to molecular characteristics (i.e. amphiphilicity).

*6.2.1 Concentration and shear rate dependence of P188 and PEO solution viscosity*

Aqueous solutions of PEO-8k and P188 were first prepared at varying concentrations ranging from 50 mg/mL to 350 (P188) or 400 (PEO-8k) mg/mL. A concentric cylinder Couette flow fixture (cup and bob) was used on an AR-G2 rheometer to measure viscosity as a function of shear rate, ranging from 1 to 1,000 $s^{-1}$. Sample sizes of 10-15 mL were used to ensure the bob was covered. Shear rate sweeps were performed at 25 °C and 37 °C, and data are shown in Figure 6.10 for both PEO-8k and P188. At low concentrations, secondary flows contributed to viscosity measurements at high shear rates.

Within the flat region of shear rates, concentration dependence of viscosity could be compared directly. Viscosity as a function of concentration is plotted at 25 and 37 °C for PEO-8k and P188 at 1, 10, and 100 $s^{-1}$ shear rates in Figure 6.11. Note that data at low concentrations of PEO-8k show start-up effects at the slowest shear rate (1 $s^{-1}$).

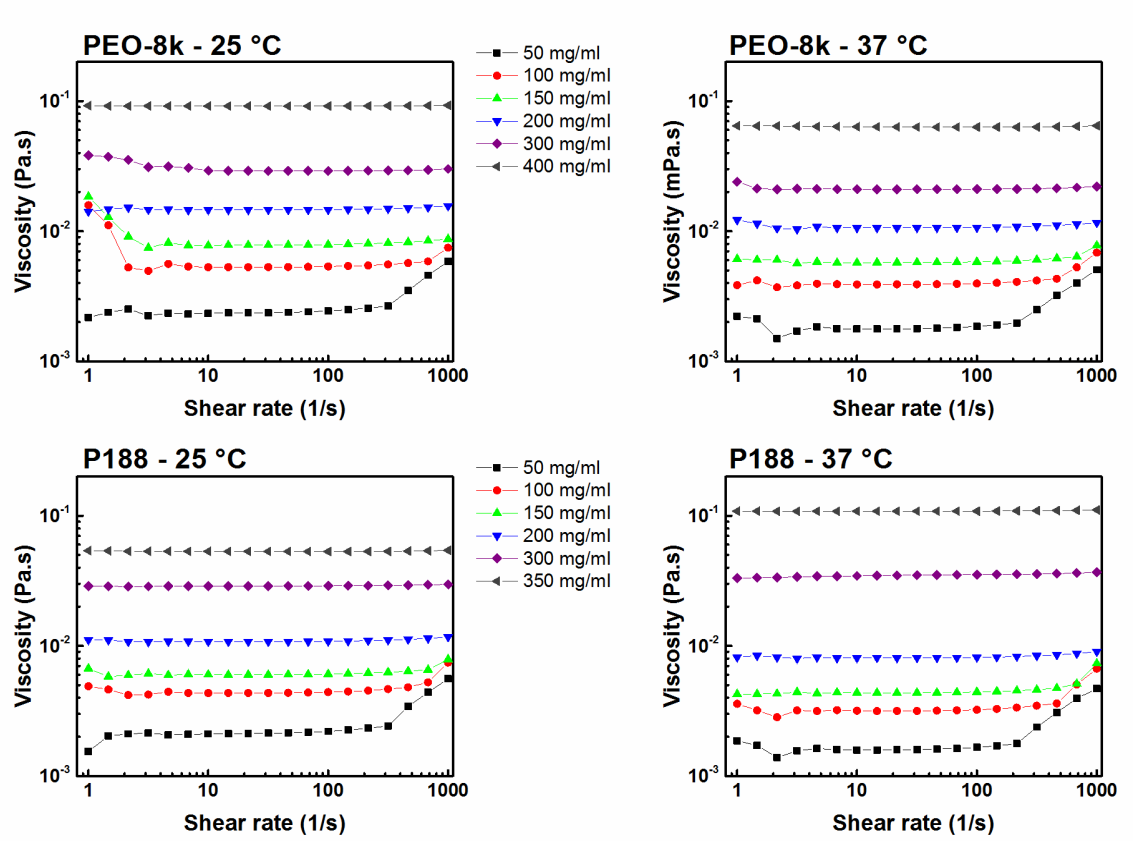


**Figure 6.10:** Shear-rate dependent viscosities measured for aqueous solutions of PEO-8k and P188 at 25 and 37 °C at varying concentrations.

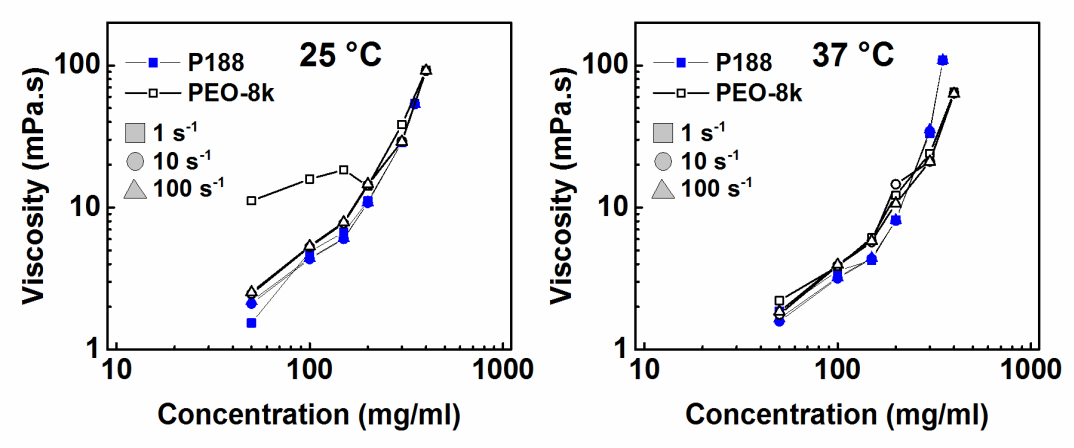


**Figure 6.11** Concentration dependence of viscosity shows good agreement between PEO-8k and P188.

*6.2.2 Polymer effects on post-ischemic blood viscosity*

Because no apparent difference in viscosity was observed between PEO-8k and P188 in aqueous solutions, the next logical step was to consider how polymers would affect blood viscosity. This returns to the origins of P188 use in medical applications. Besides serving as a rheological modifier in artificial blood development,[59,62,64] P188 was used to treat blood circulating through cardiopulmonary bypass;[45] and its reported effect was to protect blood from damage associated with shear (hemolysis) and reduce blood viscosity, the latter being confirmed by additional reports.[44,49,60,239,240] Though results were positive, FDA approval was never sought for the procedure.[1,31] Other studies focusing on sickle cell disease have also capitalized on the rheological modifying properties of P188. It is believed that hydrophobic interactions between PPO and rough, malformed red blood cells help to bind the polymers at the surface and prevent the clumping that leads to highly painful episodes of vaso-occlusive crisis.[47,48,241] Because PEO covalently bonded to surfaces of red blood cells has been found to similarly inhibit aggregation and reduce low shear blood viscosity, it was hypothesized that specific interactions by PPO and red blood cells were necessary to reduce blood viscosity.[68]

Viscosity was measured as a function of shear rate at physiological temperature (37 °C) in the Couette attachment on the AR-G2 rheometer. Steady shear rate (peak hold) experiments were first performed on non-ischemic blood at shear rates of 1 and 10 $s^{-1}$, to determine time to steady state (data not shown). From peak hold experiments, stepped shear rate experiments were designed: 15 seconds constant shear rate, with data averaged over 8 seconds, for logarithmically spaced shear rates ranging from 1 to 500 $s^{-1}$. Initial shear rate experiments were stepped up and back down to check for hemolysis, or mechanical damage to red blood cells (hysteresis would be expected if hemolysis occurred). Two samples of porcine blood were used: baseline (non-ischemic blood drawn before cardiac event) and post-ischemic blood removed after a 17 minute cardiac arrest and 2 minutes of mechanized CPR.[238] Blood was stabilized with Heparin, an anti-clotting agent, and hematocrit values

[1] Interestingly, Hunter, et al. went on to say that US marshals raided a cardiac surgery facility and confiscated equipment associated with the procedure, but no reference was given and no corroborating account could be found.[31]

(volume percent of whole blood volume which is red blood cells) were 27 and 31 for non-ischemic and ischemic blood, respectively. Higher hematocrit is expected to yield higher viscosity, which from Figure 6.12, showing shear rate sweeps from 1 to 500 $s^{-1}$ and back down to 1 $s^{-1}$, it clearly does.

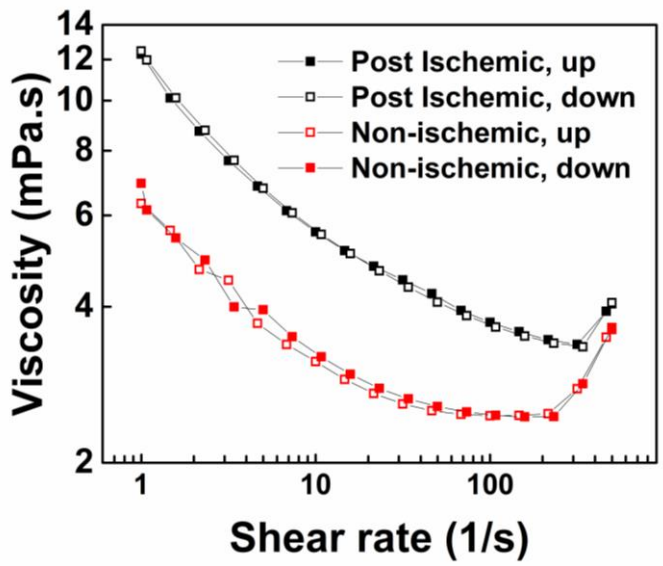


**Figure 6.12:** Shear rate sweeps of blood viscosity for post-ischemic and non-ischemic blood.

Next, post-ischemic blood was supplemented with polymers PEO-8k or P188. Initial bolus injection of P188 in saline is delivered at 250 mg/kg in animal model cardiac resuscitation, which corresponds to about 3.8 mg/ml in the blood. Note that this is significantly lower concentration than was studied in aqueous polymer solutions. Shear-rate sweeps are shown with post-ischemic blood for both P188 and PEO-8k in Figure 6.13. From the data, it is evident that a slight drop (~10%) in viscosity is induced at low shear rates by low concentration of P188 (12.3 to 11.2 mPa·s) and PEO-8k (12.3 to 10.6 mPa·s), but data converge onto the same curve at higher shear rates from about 10 $s^{-1}$ on.

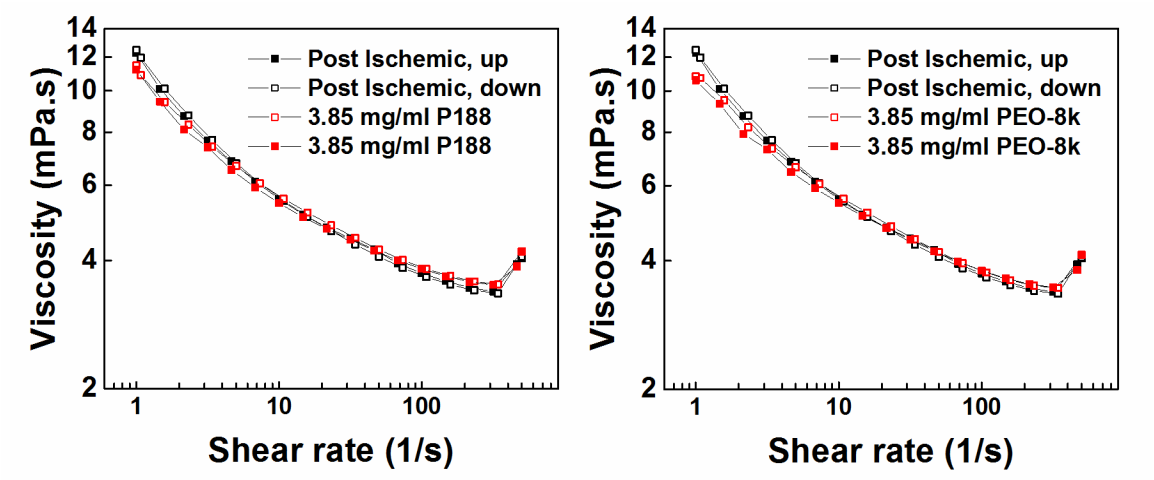


**Figure 6.13:** Viscosity as a function of shear rate for post-ischemic blood with 3.85 mg/mL polymer. Both P188 and PEO-8k show slight reductions of viscosity at low shear rates as compared to post-ischemic blood.

### *6.2.3 Polymer effects on non-ischemic blood viscosity*

Following the post-ischemic study showing little change in blood viscosity due to polymer addition and little to no difference between P188 or PEO-8k treated blood, a more detailed study was performed on baseline (non-ischemic) blood over a lower range of shear rates, 0.1-100 $s^{-1}$, which were expected to better exemplify viscosity changes induced by polymer addition. Blood in this study was freshly drawn hours prior to viscosity measurements and treated with a lower dose of heparin than above, corresponding to the slightly higher baseline blood viscosity (heparin, an antithrombolytic, is known to reduce blood viscosity in a dose-dependent manner[242]). For each polymer concentration considered (1.13, 2.25, 4.5, and 9 mg/mL), four stepped shear rate protocols were taken logarithmically from 0.1 to 100 $s^{-1}$ in succession with a 75 s low-shear (0.1 $s^{-1}$) equilibration step to reduce secondary velocity effects. Constant time was increased to 30 s, with data averaging over 8 s.

The shear-rate dependence of mean blood viscosities are shown for each polymer concentration in Figure 6.14, with error bars indicating standard error of the mean for $N$ = 4. As can be seen in the plots, error bars are very tight to the data points, and some are indiscernible from data symbols; larger errors appearing at low shear rates are attributable to some polymer-mixing effects in early measurements. Slight differences in baseline blood viscosities were observed between the two samples (i.e. Figure 6.14a versus Figure

6.14b), but the blood viscosity changes imposed by P188 and PEO-8k were nearly identical between the two.

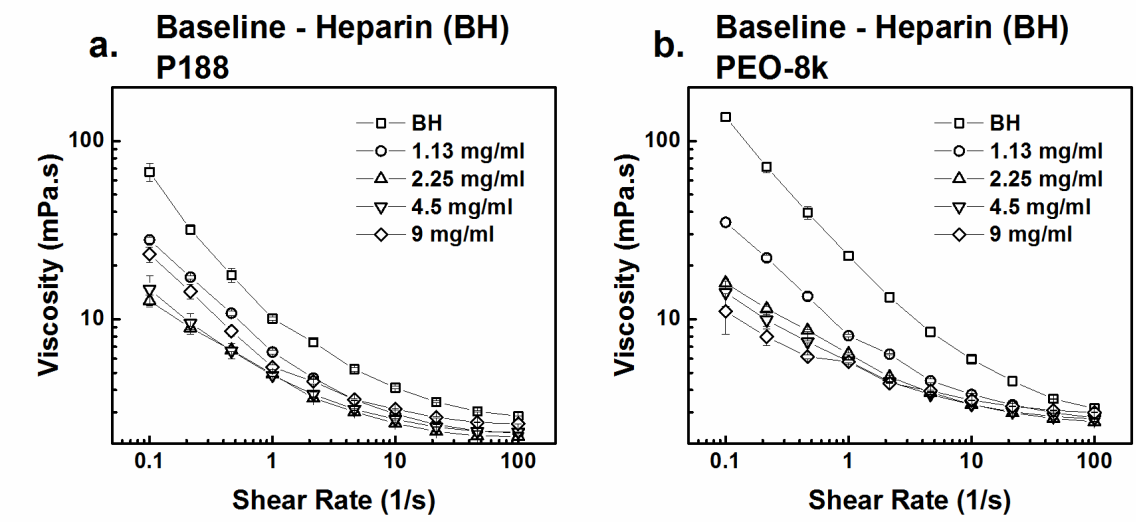


**Figure 6.14:** Shear-rate dependence of mean blood viscosity for non-ischemic blood. Measurements were performed at various P188 (**a**) and PEO-8k (**b**) loadings in baseline (non-ischemic) blood treated with Heparin, with error bars representing the S.E.M. for $N$ = 4 measurements.

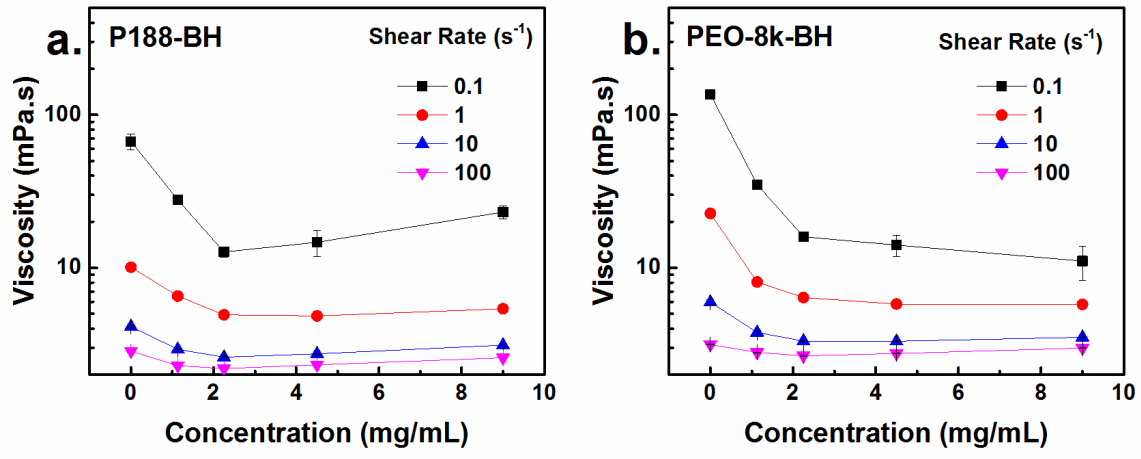


**Figure 6.15:** Polymer concentration dependence of mean blood viscosity. Data shown for P188 (**a**) and PEO-8k (**b**) for $N$ = 4 measurements at four shear rates.

To elucidate the concentration-dependence of polymers on blood viscosity, mean blood viscosities are plotted as functions of polymer concentration in Figure 6.15. The most striking feature of viscosity-concentration plots in Figure 6.15 is the leveling of blood viscosity above 2.25 mg/mL concentration. The slight rise in blood viscosity at the 9 mg/mL concentration of P188 suggests a bulk effect of polymer solution on blood viscosity. Because the viscosity change by polymer addition levels off for both P188 and PEO-8k, the effect is likely due to non-specific interactions by polymers with blood component interfaces at low concentrations.

### *6.2.4 In vivo implications and future directions*

The results of polymer-blood viscosity experiments did not reveal any dramatic differences between the two polymer species considered. This was in contrast to in vivo STEMI (ST segment elevation myocardial infarction) experiments performed using PEO-8k in place of P188 in post-conditioning therapy (preliminary results, data not shown). In these preliminary studies, the hydrophilic homopolymer PEO showed no benefit over control, suggesting that the amphiphilicity of P188 is a necessary condition of therapeutic benefit. Future experiments performed on blood which has been perfused with P188 would be interesting as well. *In situ* mixing of P188 may change the rheological profile of post-ischemic blood, or perhaps instead it serves to lubricate smooth muscle vasculature to mitigate reperfusion injury.

# Chapter 7

# Summary and future outlook

The primary objective of this work was to develop a model system to employ in the mechanistic investigation of membrane stabilization by block copolymer surfactants. This model system, consisting of synthetically prepared block copolymers and model membranes, was intended to bridge a decades-old gap in the membrane stabilization literature: mechanistic investigations have almost exclusively considered commercially available poloxamers to the exception of all other block copolymer formulations and architectures accessible by polymer synthesis techniques. Although countless studies featuring poloxamer interactions with model membranes have been carried out, no definitive mechanism of therapeutic membrane association by block copolymer surfactants has yet been reported. A shift toward a synthetic approach to mechanistic investigations was identified as an opportunistic path through the broad and multidisciplinary field of block copolymer membrane stabilization. The following pages summarize significant contributions toward that end and recaps the recommended pathways for future investigations presented in preceding chapters.

## 7.1 Consideration of a diblock architecture

Prior to this work, nearly all of the investigations of PEO-PPO cell membrane interactions leading to cell membrane stabilization or sealing were performed within a subset of poloxamer formulations. The two relevant exceptions considered specially-produced diblock copolymers of PEO-PPO[1] and PEO-PBO,[2] but given the breadth and depth of the field, it is surprising that no further studies were pursued. The diblock

architecture was identified as a candidate model polymer system for its ease of preparation and simplified route to tuning molecular properties, i.e., removal of the redundant PEO block.

*7.1.1 Confirmation of membrane protection by a diblock architecture*

The work described in Chapter 3: "Role of block copolymer architecture in model membrane protection against peroxidation" presented a diblock copolymer analog to Poloxamer 188 as a candidate membrane stabilizer. Direct comparisons of capacity for membrane protection were made between the diblock architecture and the standard triblock architecture, using a synthetic model membrane (liposomes) and a chemically induced membrane stress model (liposome peroxidation). The work showed that a diblock architecture was indeed protective of the membrane against the destructive chemical reaction, and more so, it was possible using a lower mass concentration (dose) of polymer. The exposed hydrophobic block of the diblock architecture was hypothesized to promote stronger attraction to the membrane, as compared to the triblock architecture, and the absence of the redundant PEO block was determined to improve the efficiency of polymer packing at the interface (i.e. an expected "perpendicular" diblock configuration, versus the "flattened" triblock configuration at the membrane).

*7.1.2 Future prospects for a diblock architecture*

Besides the pharmacological advantages (i.e. efficacy at a lower dose) offered by the diblock architecture, the pronounced difference observed between P188 and the Diblock P188 in liposome protection from peroxidation suggests there exists a significant difference in membrane interaction by the two architectures. Past work has indicated that the dynamics of chain insertion and ejection from block copolymer micelles is strongly dependent on architecture,[3] which could have tremendous implications in the model cell membrane interactions studied here.

Recognizing that polymer association with a membrane is unlikely an equilibrium process, kinetic considerations of polymer association and dissociation could still differ by orders of magnitude between the triblock and diblock architectures. Small angle neutron scattering experiments should be used to locate polymer blocks in the membrane (e.g. liposome dispersions with contrast matching or neutron reflectometry on supported lipid-

polymer films), and dynamic techniques (e.g. neutron spin-echo) should be used to differentiate dynamics of association between architectures, including the reversed B-A-B triblock architecture, synthesized to appropriate molecular weight and hydrophobic/hydrophilic balance. These characterization techniques should be combined with newly synthesized block copolymers to elucidate the structure-function relationship driving interactions, as will be highlighted in the following sections.

Preliminary SAXS measurements performed on multilamellar dispersions had also indicated that interactions by diblock architectures differ from those of triblock architectures. A more rigorous pursuit of diblock interactions with membranes should include varying molecular properties (i.e. block lengths and relative hydrophobic:hydrophilic balance) in order to better explain the "flattened" (i.e. triblock) or "perpendicular" (i.e. diblock) configurations hypothesized here.

## 7.2 Molecular design and chemical synthesis to study membrane interactions

Because the majority of the existing membrane stabilization literature has involved the same collection of commercially available poloxamers, the prospect of intentionally designing new molecules to study offers significant opportunity for the advancement of the field. Given the known subtleties of the structure-function relationship for this class of block copolymers, as well as the presumed mechanism of cell membrane stabilization, careful control of molecular properties afforded by chemical synthesis was unarguably the clearest path forward in a well-saturated field of research

### *7.2.1 Synthesis of new diblock copolymer membrane stabilizers*

Having established that a diblock architecture could beneficially interact with the model membrane, a series of diblock copolymers with varied molecular properties were prepared and tabulated in Chapter 2: "Materials and Methods." Although the crown ether strategy employed to prepare monodisperse PPO is well-recorded in the literature,[4–7] it was apparent that no prior studies had combined a synthetic strategy with membrane stabilization investigations. Polymers were prepared by living anionic polymerization in two steps, and products gave low dispersities, as measured by SEC.

*7.2.2 Significance of end-group functionalities on hydrophobic block*

Noting once again the membrane protection exhibited by Diblock P188 in Chapter 3, it was hypothesized that it was not only the "free" or "exposed" nature of the hydrophobic PPO block that facilitated membrane association, but also the end-functionality of the diblock copolymers. A series of diblock copolymers were prepared featuring two different end-group functionalities: a hydrophobic tert-butoxy group (t-PPO-PEO) and a hydrophilic hydroxyl group (OH-PPO-PEO). Liposome peroxidation experiments confirmed the importance of the end group: tert-butoxy functionalized diblock copolymers showed no protection against membrane peroxidation, despite equivalent PPO block lengths to the previously beneficial Diblock P188 and both shorter and longer PEO chains. In contrast, molecular properties played a more obvious role in hydroxyl-terminated PPO, for which molecular weights of both the PPO and PEO blocks dictated membrane protection.

*7.2.3 Future synthetic directions*

Having developed both the synthetic and purification methods necessary to make possible molecular design for the mechanistic investigation of cell membrane stabilization, future work should delve into the molecular parameter space described throughout this work. Following the findings reported in Chapter 4, "Effect of diblock copolymer end groups on membrane interactions," first priority should be placed on synthesizing polymers featuring a PEO block length sufficiently long for membrane stabilization ($M_{n,PEO} \geq 4{,}000$ g/mol) and varied hydrophobic PPO block lengths. It is recommended that hydrophilic (hydroxyl) end group functionalities be employed on PPO, or perhaps instead a methoxy terminus (i.e. termination of living anionic polymerization by $CH_3I$), in order to diminish end-group interference in membrane interactions for direct molecular property comparisons.

Beyond tuning block properties, a significant synthetic effort should be made to understand the end group effect of membrane association by block copolymer surfactants. This strategy should include diblock copolymer architectures previously discussed, as well as end-functionalized PEO homopolymers (i.e. $N_{hydrophobe} = 1$) and even reverse triblock architectures (e.g. B-A-B). Studies on synthesized polymers should involve liposome and

*in vivo* techniques already presented, in addition to other model membranes, simulated damage, and characterization.

## 7.3 Adaptation of a model membrane and membrane stress

As part of the model system developed in this work, a model membrane was required that could strike a balance between controlled properties and physiological relevance. The selected model consisted of large unilamellar vesicles (i.e., liposomes) comprised of a mixture of synthetic phospholipids with one to two degrees of unsaturation in the acyl tails. Reactivity by unsaturated lipids to free radicals is a naturally occurring phenomenon *in vivo*, and support for the relevance of a chemically induced lipid peroxidation event to cell membrane damage by permeabilization was offered. Most compelling to the choice of liposomes and membrane stress by lipid peroxidation, however, was found in a report of successful protection against peroxidation by P188.[8] In the model, liposomes incubated with candidate membrane stabilizers were subjected to peroxidation conditions before characterization by dynamic light scattering.

### *7.3.1 New interpretation to dynamic light scattering results*

Traditionally, DLS is used to determine and characterize particle size distributions for a given sample. As was discussed in Chapter 3, this technique alone is unsuitable for characterization of liposomes following the lipid peroxidation reaction, since peroxidized liposomes are expected to rupture as a result of propagation. The normalized average scattered intensity was presented as a quantifiable metric of the overall condition of the liposome population before and after peroxidation. A normalized scattered intensity near 1 indicated insignificant changes to the total population of liposomes in a sample, whereas a value near background (~0.2) indicated destruction of the population. Values in between, as were obtained from liposomes first incubated with various polymers prior to peroxidation, could therefore be attributed to partial protection by polymer association with the membrane. The development of scattered intensity as a metric of protection or peroxidation made possible direct comparisons between experiments performed on different liposome batches, as well as statistical analyses to determine significance of findings.

*7.3.2 Connections to in vivo work*

It was desirous to develop a connection between the findings of the liposome peroxidation experiments to collaborative experiments performed *in vivo*. The primary motivation for such a connection was to facilitate systematic investigations *in vivo* by informing the strategic selection of model compounds by a rapid, low cost screening method. Although a directly relatable link between the two methods was not established, the importance of diblock end functionality to membrane stabilization was independently drawn from each. Additionally, *in vivo* experiments presented in Chapter 4 showed that a diblock architecture could confer protection against a muscle lengthening contraction injury,

*7.3.3 Model membrane recommendations*

Selection of a relevant model membrane is a critical challenge in the pursuit of the membrane stabilization mechanism. This work has presented model membranes in the form of synthetic monolayers and liposomes, as well as monolayers of naturally derived membrane materials (Chapter 5), none of which are close physical representations of the confined spaces, heterogeneity, and function of cell membranes *in vivo*. In keeping with the current liposome peroxidation and monolayer models of membrane stress, further efforts should be made to quantify and clarify underlying mechanisms of damage, polymer association, and protection. Continued collaboration and *in vivo* work will also be required, in order to address concerns of physiological relevancy.

While continuing to work with existing model membranes, it is also recommended that efforts should be made to mimic the physiochemical properties of cell membranes by considering additional forms of model membranes. In addition to complementing ongoing live cell models *in vitro*,[9] several model systems described in the literature, which include giant unilamellar vesicles,[10–12] bicelles,[13–15] and supported bilayers,[16–18] are worth consideration. Each of these alternative membranes offers additional modes of membrane stress and characterization from which information about polymer interactions may be obtained.

## 7.4 Monolayered studies

### *7.4.1 Naturally derived membrane monolayers*

Although monolayered model membranes are functionally unlike native cell membranes, they have been used throughout the literature to investigate surface activity and adsorptive properties of soluble additives to the interface. Chapter 5: "Block copolymer interactions with model membrane monolayers" has presented monoalyered model membranes comprised of isolated sarcolemmal membranes which offer a better representation of *in vivo* membrane heterogeneity than can be accessed by synthetic means. Triblock and diblock copolymer interactions with synthetic and naturally derived membrane lipids showed similar, but not identical adsorption behavior, as well asdifferences in adsorbed and squeeze-out surface pressures, all of which were attributed to molecular weight differences. Fluorescence microscopy performed on monolayers of each polymer revealed substantial changes to lipid morphology induced by both architectures, but only qualitative arguments could be made.

### *7.4.2 Further monolayered studies*

By combining the newly isolated and naturally derived membrane materials with fluorescence tagging methods described in Chapter 6, "Collaborative support activities," confocal microscopy could be used to qualitatively locate block copolymer surfactants laterally or into the depth of the monolayer.[19,20] Furthermore, controlled studies of polymer effects on membrane fluidity could be investigated by analysis of the compressibility modulus.[21] Additionally, scattering techniques found in the literature to study lipid ordering and the influence of block copolymer association on lipid ordering in synthetic phospholipid monolayers could be applied to investigate newly synthesized block copolymer membrane stabilizers.[2,22]

## 7.5 Collaborative support and final comments

The fluorescent tagging and blood viscosity work described in Chapter 6: "Collaborative support activities" were important elements contributed to ongoing work in physiological experiments. Presumably, fluorescently tagged P188 or diblock copolymers could be used in model membrane systems in future work, in addition to the histology and

biodistribution purposes they were initially designed for. Blood viscosity experiments revealed insignificant differences in blood viscosity changes induced by either P188 or a homopolymer PEO of a similar molecular weight. The corresponding *in vivo* experiments in a porcine model indicated significant differences between the two, highlighting the importance of the hydrophobic PPO block in P188 as the critical component driving beneficial interactions, rather than bulk blood viscosity effects which would be similar for P188 and PEO-8k.

While a prediction of the path these collaborative activities will take is difficult to make, the importance of the cross-disciplinary exchange of ideas and findings to the advancement of the field cannot be understated. Each historical example of translation from one medical application of P188 to the next demonstrates the power of drawing connections between seemingly unrelated systems, and the multi-disciplinary approach driving this work stands to benefit both the physiochemical and physiological understandings of cell membrane interactions by block copolymer surfactants.

# Bibliography


(1) Pacifico, C. R.; Lundsted, L. G.; Vaughn, T. H. Flake form nonionic detergents. *Soap Sanit. Chem.* **1950**, *26*, 40–43,73,90.

(2) Vaughn, T.; Suter, H.; Lundsted, L.; Kramer, M. Properties of some newly developed nonionic detergents. *J. Am. Oil Chem. Soc.* **1951**, *28*, 294–299.

(3) Lundsted, L. G. Polyoxyalkylene Compounds. 2,674,619, 1954.

(4) Alexandridis, P. Poly(ethylene oxide)/poly(propylene oxide) block copolymer surfactants. *Curr. Opin. Colloid Interface Sci.* **1997**, *2*, 478–489.

(5) Alexandridis, P.; Lindman, B. Amphiphilic Block Copolymers, 2000.

(6) Mortensen, K. PEO-related block copolymer surfactants. *Colloids Surfaces A Physiochemical Eng. Asp.* **2001**, *183-185*, 277–292.

(7) Bates, F. S.; Fredrickson, G. H. Block copolymers-designer soft materials. *Phys. Today* **1999**, *52*, 32–38.

(8) Leibler, L. Theory of Microphase Separation in Block Copolymers. *Macromolecules* **1980**, *13*, 1602–1617.

(9) Bates, F. S.; Fredrickson, G. H. Block copolymer thermodynamics: theory and experiment. *Annu. Rev. Phys. Chem.* **1990**, *41*, 525–557.

(10) Lodge, T. P. Block Copolymers: Past Successes and Future Challenges. *Macromol. Chem. Phys.* **2003**, *204*, 265–273.

(11) Jain, S.; Bates, F. S. Consequences of nonergodicity in aqueous binary PEO-PB micellar dispersions. *Macromolecules* **2004**, *37*, 1511–1523.

(12) Discher, B. M.; Won, Y.-Y.; Ege, D. S.; Lee, J. C.-M.; Bates, F. S.; Discher, D. E.; Hammer, D. A. Polymersomes: tough vesicles made from diblock copolymers. *Science (80-. ).* **1999**, *284*, 1143–1146.

(13) Jain, S.; Bates, F. S. On the origins of morphological complexity in block copolymer surfactants. *Science (80-. ).* **2003**, *300*, 460–464.

(14) Davis, K. P.; Bates, F. S. Role of molecular architecture in amphiphilic dispersions, University of Minnesota: Minneapolis, 2009, Vol. Ph.D.

(15) Gohy, J.-F. Block Copolymer Micelles. In *Block Copolymers II SE - 48*; Abetz, V., Ed.; Advances in Polymer Science; Springer Berlin Heidelberg, 2005; Vol. 190, pp 65–136.

(16) Israelachvili, J. N. 20 - Soft and Biological Structures. In *Intermolecular and Surface Forces*; Elsevier, 2011; pp 535–576.

(17) Riess, G. Micellization of block copolymers. *Prog. Polym. Sci.* **2003**, *28*, 1107–1170.

(18) Israelachvili, J. N. 19 - Thermodynamic Principles of Self-Assembly. In; Israelachvili, J. N. B. T.-I. and S. F. (Third E., Ed.; Academic Press: San Diego, 2011; pp 503–534.

(19) Hiemenz, P. C.; Rajagopalan, R. *Principles of colloid and surface chemistry*; Marcel Dekker, 1997.

(20) Alexandridis, P.; Athanassiou, V.; Fukuda, S.; Hatton, T. A. Surface activity of poly(ethylene oxide)-block-poly(propylene oxide)-block-poly(ethylene oxide) copolymers. *Langmuir* **1994**, *10*, 2604–2612.

(21) Alexandridis, P.; Holzwarth, J. F.; Hatton, T. A. Micellization of poly(ethylene oxide)-poly(propylene oxide)-poly(ethylene oxide) triblock copolymers in aqueous solutions: thermodynamics of compolymer association. *Macromolecules* **1994**, *27*, 2414–2425.

(22) Zhou, Z.; Chu, B. Light-scattering study on the association behavior of triblock polymers of ethylene oxide and propylene oxide in aqueous solution. *J. Colloid Interface Sci.* **1988**, *126*, 171–180.

(23) Altinok, H.; Nixon, S. K.; Gorry, P. A.; Attwood, D.; Booth, C.; Kelarakis, A.; Havredaki, V. Micellisation and gelation of diblock copolymers of ethylene oxide and propylene oxide in aqueous solution, the effect of P-block length. *Colloids Surfaces B Biointerfaces* **1999**, *16*, 73–91.

(24) Holland, R. J.; Parker, E. J.; Guiney, K.; Zeld, F. R. Fluorescence Probe Studies of Ethylene Oxide/Propylene Oxide Block Copolymers in Aqueous Solution. *J. Phys. Chem.* **1995**, *99*, 11981–11988.

(25) Borbély, S.; Pedersen, J. S. Temperature-induced aggregation in aqueous solutions of pluronic F68 triblock copolymer containing small amount of o-xylene. *Phys. B Condens. Matter* **2000**, *276–278*, 363–364.

(26) Carraher, C. E. *Polymer Chemistry*, 8th ed.; CRC Press, 2010.

(27) Pembouong, G.; Morellet, N.; Kral, T.; Hof, M.; Scherman, D.; Bureau, M.-F.; Mignet, N. A comprehensive study in triblock copolymer membrane interaction. *J. Control. Release* **2011**, *151*, 57–64.

(28) Collins, J. M.; Despa, F.; Lee, R. C. Structural and functional recovery of electropermeabilized skeletal muscle in-vivo after treatment with surfactant poloxamer 188. *Biochim. Biophys. Acta - Biomembr.* **2007**, *1768*, 1238–1246.

(29) Yasuda, S.; Townsend, D.; Michele, D. E.; Favre, E. G.; Day, S. M.; Metzger, J. M. Dystrophic heart failure blocked by membrane sealant poloxamer. *Nature* **2005**, *436*, 1025–1029.

(30) Padanilam, J. T.; Bischof, J. C.; Lee, R. C.; Cravalho, E. G.; Tompkins, R. G.; Yarmush, M. L.; Toner, M. Effectiveness of poloxamer 188 in arresting calcein leakage from thermally damaged isolated skeletal muscle cells. *Ann. N. Y. Acad. Sci.* **1994**, *720*, 111–123.

(31) Hunter, R. L.; Luo, A. Z.; Zhang, R.; Kozar, R. a.; Moore, F. a. Poloxamer 188 inhibition of ischemia/reperfusion injury: Evidence for a novel anti-adhesive mechanism. *Ann. Clin. Lab. Sci.* **2010**, *40*, 115–125.

(32) Moloughney, J.; Weisleder, N. Poloxamer 188 (P188) as a Membrane Resealing Reagent in Biomedical Applications. *Recent Pat. Biotechnol.* **2013**, *6*, 200–211.

(33) Wang, J.-Y.; Chin, J.; Marks, J. D.; Lee, K. Y. C. Effects of PEO-PPO-PEO triblock copolymers on phospholipid membrane integrity under osmotic stress. *Langmuir* **2010**, *26*, 12953–12961.

(34) Steinhardt, R. A. The mechanisms of cell membrane repair: a tutorial guide to key experiments. *Ann. New York Acad. Sci.* **2005**, *1066*, 152–165.

(35) Maskarinec, S. A.; Wu, G.; Lee, K. Y. C. Membrane sealing by polymers. *Ann. New York Acad. Sci.* **2005**, *1066*, 310–320.

(36) Kim, D.; Gao, Z. G.; Lee, E. S.; Bae, Y. H. In vivo evaluation of doxorubicin-loaded polymeric micelles targeting folate receptors and early endosomal pH in drug-resistant ovarian cancer. *Mol. Pharm.* **2009**, *6*, 1353–1362.

(37) Batrakova, E. V; Lee, S.; Li, S.; Venne, A.; Alakhov, V. Y.; Kabanov, A. V. Fundamental relationships between the composition of Pluronic block copolymers and their hypersensitization effect in MDR cancer cells. *Pharm. Res.* **1999**, *19*, 1373–1379.

(38) Kabanov, A. V; Nazarova, I. R.; Astafieva, I. V; Batrakova, E. V; Alakhov, V. Y.; Yaroslavov, A. A.; Kabanov, V. A. Micelle formation and solubilization of fluorescent probes in poly(oxyethylene-b-oxypropylene-b-oxyethylene) solutions. *Macromolecules* **1995**, *28*, 2303–2314.

(39) Frey, S. L.; Lee, K. Y. C. Temperature dependence of poloxamer insertion into and squeeze-out from lipid monolayers. *Langmuir* **2007**, *23*, 2631–2637.

(40) Prasad, K. N.; Luong, T. T.; Florence, A. T.; Paris, J.; Vaution, C.; Seiller, M.; Puisieux, F. Surface activity and association of ABA polyoxyethylene-polyoxypropylene block copolymers in aqueous solution. *J. Colloid Interface Sci.* **1979**, *69*, 225–232.

(41) Nakashima, K.; Anzai, T.; Fujimoto, Y. Fluorescence studies on the properties of Pluronic F68 micelle. *Langmuir* **1994**, *10*, 658–661.

(42) Lopes, J. R.; Loh, W. Investigation of Self-Assembly and Micelle Polarity for a Wide Range of Ethylene Oxide - Propylene Oxide - Ethylene Oxide Block Copolymers in Water. *Langmuir* **1998**, *14*, 750–756.

(43) Maskarinec, S. A.; Hannig, J.; Lee, R. C.; Lee, K. Y. C. Direct observation of poloxamer 188 insertion into lipid monolayers. *Biophys. J.* **2002**, *82*, 1453–1459.

(44) Grover, F. L.; Heron, M. W.; Newman, M. M.; Paton, B. C. Effect of a Nonionic Surface-Active Agent on Blood Viscosity and Platelet Adhesiveness. *Circulation* **1969**, *39*, I – 249–252.

(45) Adams, J. E.; Owens, G.; Mann, G.; Headrick, J. R.; Munoz, A.; Scott, H. W. J. Experimental evaluation of pluronic F68 (A non-ionic detergent) as a method of diminishing systemic fat emboli resulting from prolonged cardiopulmonary bypass. *Surg. Forum* **1960**, *10*, 585–589.

(46) Schaer, G. L.; Spaccavento, L. J.; Browne, K. F.; Krueger, K. A.; Krichbaum, D.; Phelan, J. M.; Fletcher, W. O.; Grines, C. L.; Edwards, S.; Jolly, M. K.; et al. Beneficial Effects of RheothRx Injection in Patients Receiving Thrombolytic Therapy for Acute Myocardial Infarction: Results of a Randomized, Double-Blind, Placebo-Controlled Trial. *Circulation* **1996**, *94*, 298–307.

(47) Orringer, E. P.; Casella, J. F.; Ataga, K. I.; Koshy, M.; Adams-Graves, P.; Luchtman-Jones, L.; Wun, T.; Watanabe, M.; Shafer, F.; Kutlar, A.; et al. Purified poloxamer 188 for treatment of acute vaso-occlusive crisis of sickle cell disease: A randomized controlled trial. *J. Am. Med. Assoc.* **2001**, *286*, 2099–2106.

(48) Adams-Graves, P.; Kedar, A.; Koshy, M.; Steinberg, M.; Veith, R.; Ward, D.; Crawford, R.; Edwards, S.; Bustrack, J.; Emanuele, M. RheothRx (poloxamer 188) injection for the acute painful episode of sickle cell disease: a pilot study. *Blood* **1997**, *90*, 2041–2046.

(49) Emanuele, R. M. FLOCOR: a new anti-adhesive, rheologic agent. *Expert Opin. Investig. Drugs* **1998**, *7*, 1193–1200.

(50) Gu, J.-H.; Ge, J.-B.; Li, M.; Xu, H.-D.; Wu, F.; Qin, Z.-H. Poloxamer 188 Protects Neurons against Ischemia/Reperfusion Injury through Preserving Integrity of Cell Membranes and Blood Brain Barrier. *PLoS One* **2013**, *8*, e61641.

(51) Murphy, A. D.; McCormack, M. C.; Bichara, D. A.; Nguyen, J. T.; Randolph, M. A.; Watkins, M. T.; Lee, R. C.; Austen, W. G. J. Poloxamer 188 protects against ischemia-reperfusion injury in a murine hind-limb model. *Plast. Reconstr. Surg.* **2010**, *125*, 1651–1660.

(52) Shelat, P. B.; Plant, L. D.; Wang, J. C.; Lee, E.; Marks, J. D. The membrane-active tri-block copolymer pluronic F-68 profoundly rescues rat hippocampal neurons from oxygen-glucose deprivation-induced death through early inhibition of apoptosis. *J. Neurosci.* **2013**, *33*, 12287–12299.

(53) Lee, R. C.; River, L. P.; Pan, F. S.; Ji, L.; Wollmann, R. L. Surfactant-induced sealing of electropermeabilized skeletal muscle membranes in vivo. *Proc. Natl. Acad. Sci.* **1992**, *89*, 4524–4528.

(54) Townsend, D.; Turner, I.; Yasuda, S.; Martindale, J.; Davis, J.; Shillingford, M.; Kornegay, J. N.; Metzger, J. M. Chronic administration of membrane sealant prevents severe cardiac injury and ventricular dilation in dystrophic dogs. *J. Clin. Invest.* **2010**, *120*, 1140–1150.

(55) Alexandridis, P.; Hatton, T. A. Poly(ethylene oxide)-poly(propylene oxide)-poly(ethylene oxide) block copolymer surfactants in aqueous solutions and at interfaces: thermodynamics, structure, dynamics, and modeling. *Colloids Surfaces A Physiochemical Eng. Asp.* **1995**, *96*, 1–46.

(56) Johnsson, M.; Silvander, M.; Karlsson, G.; Edwards, K. Effect of PEO−PPO−PEO triblock copolymers on structure and stability of phosphatidylcholine liposomes. *Langmuir* **1999**, *15*, 6314–6325.

(57) Houang, E. M.; Haman, K. J.; Filareto, A.; Perlingeiro, R. C.; Bates, F. S.; Lowe, D. A.; Metzger, J. M. Membrane-stabilizing copolymers confer marked protection to dystrophic skeletal muscle in vivo. *Submitted* **2015**.

(58) Hymes, A. C.; Safavian, M. H.; Gunther, T.; Forsman, J. The influence of an industrial surfactant pluronic F-68, in the treatment of hemorrhagic shock. *J. Surg. Res.* **1971**, *11*, 191–197.

(59) Geyer, R. P. "Bloodless" rats through the use of artificial blood substitutes. *Fed. Proc.* **1975**, *34*, 1499–1505.

(60) Grover, F. L.; Amundsen, D.; Warden, J. L.; Fosburg, R. G.; Paton, B. C. The effect of pluronic F-68 on circulatory dynamics and renal and carotid artery flow during hemorrhagic shock. *J. Surg. Res.* **1974**, *17*, 30–35.

(61) Altman, L. K. "Artificial Blood" Tests Expanding in U.S. Amid High Hopes. *New York Times*. February 9, 1982, p C1.

(62) Schmolka, I. R. Artificial blood emulsifiers. *Fed. Proc.* **1975**, *34*, 1449–1453.

(63) Keipert, P. E. Perfluorochemical emulsions: future alternatives to transfusion. In *Blood Substitutes: Principles, Methods, and Clinical Trials*; Chang, T. M. S., Ed.; Karger Landes Systems, 1998; pp 127–156.

(64) Spence, R. K.; Norcross, E. D.; Costabile, J.; McCoy, S.; Cernaianu, A. C.; Alexander, J. B.; Pello, M. J.; Atabek, U.; Camishion, R. C. Perfluorocarbons as blood substitutes: the early years. Experience with Fluosol DA-20% in the 1980s. *Artif. Cells. Blood Substit. Immobil. Biotechnol.* **1994**, *22*, 955–963.

(65) Marwick, C. FDA committee questions fluosol efficacy; us approval not imminent. *JAMA* **1983**, *250*, 2585–2586.

(66) Singh-Joy, S. D.; McLain, V. C. Safety assessment of poloxamers 101, 105, 108, 122, 123, 124, 181, 182, 183, 184, 185, 188, 212, 215, 217, 231, 234, 235, 237, 238, 282, 284, 288, 331, 333, 334, 335, 338, 401, 402, 403, and 407, poloxamer 105 benzoate, and poloxamer 182 dibenzoate as use. *Int. J. Toxicol.* **2008**, *27*, 93–128.

(67) Schmolka, I. A review of block polymer surfactants. *J. Am. Oil Chem. Soc.* **1977**, *54*, 110–116.

(68) Armstrong, J. K.; Meiselman, H. J.; Fisher, T. C. Covalent binding of poly(ethylene glycol) (PEG) to the surface of red blood cells inhibits aggregation and reduces low shear blood viscosity. *Am. J. Hematol.* **1997**, *56*, 26–28.

(69) Bartos, J. A.; Matsuura, T. R.; Sarraf, M.; Youngquist, S. T.; McKnite, S. H.; Rees, J. N.; Sloper, D. T.; Bates, F. S.; Segal, N.; Debaty, G.; et al. Bundled

postconditioning therapies improve hemodynamics and neurologic recovery after 17min of untreated cardiac arrest. *Resuscitation* **2015**, *87*, 7–13.

(70) Merchant, F. A.; Holmes, W. H.; Capelli-Schellpfeffer, M.; Lee, R. C.; Toner, M. Poloxamer 188 Enhances Functional Recovery of Lethally Heat-Shocked Fibroblasts. *J. Surg. Res.* **1998**, *74*, 131–140.

(71) Spurney, C. F.; Guerron, A. D.; Yu, Q.; Sali, A.; van der Meulen, J. H.; Hoffman, E. P.; Nagaraju, K. Membrane sealant Poloxamer P188 protects against isoproterenol induced cardiomyopathy in dystrophin deficient mice. *BMC Cardiovasc. Disord.* **2011**, *11*, 20.

(72) Townsend, D.; Yasuda, S.; Metzger, J. Cardiomyopathy of Duchenne muscular dystrophy: pathogenesis and prospect of membrane sealants as a new therapeutic approach. *Expert Rev. Cardiovasc. Ther.* **2007**, *5*, 99–109.

(73) Townsend, D.; Yasuda, S.; Chamberlain, J.; Metzger, J. M. Cardiac Consequences to Skeletal Muscle-Centric Therapeutics for Duchenne Muscular Dystrophy. *Trends Cardiovasc. Med.* **2009**, *19*, 49–54.

(74) Mitchell, T. W.; Buffenstein, R.; Hulbert, a J. Membrane phospholipid composition may contribute to exceptional longevity of the naked mole-rat (Heterocephalus glaber): a comparative study using shotgun lipidomics. *Exp. Gerontol.* **2007**, *42*, 1053–1062.

(75) Otten, W.; Iaizzo, P. A.; Eichinger, H. M. Effects of a high n-3 fatty acid diet on membrane lipid composition of heart and skeletal muscle in normal swine and in swine with the genetic mutation for malignant hyperthermia. *J. Lipid Res.* **1997**, *38*, 2023–2034.

(76) Barnett, V. A. Cellular Myocytes. In *Handbook of Cardiac Anatomy, Physiology, and Devices2*; Iaizzo, P. A., Ed.; 2009; pp 147–158.

(77) Walker, C. A.; Spinale, F. G. The structure and function of the cardiac myocyte: a review of fundamental concepts. *J. Thorac. Cardiovasc. Surg.* **1999**, *118*, 375–382.

(78) Bers, D. M. Cardiac excitation-contraction coupling. *Nature* **2002**, *415*, 198–205.

(79) Petrof, B. J.; Shrager, J. B.; Stedman, H. H.; Kelly, A. M.; Sweeney, H. L. Dystrophin protects the sarcolemma from stresses developed during muscle contraction. *Proc. Natl. Acad. Sci. U. S. A.* **1993**, *90*, 3710–3714.

(80) Sarkis, J.; Vié, V.; Winder, S. J.; Renault, A.; Le Rumeur, E.; Hubert, J.-F. Resisting sarcolemmal rupture: dystrophin repeats increase membrane-actin stiffness. *FASEB J.* **2013**, *27*, 359–367.

(81) Gissel, H. The role of Ca2+ in muscle cell damage. *Ann. New York Acad. Sci.* **2005**, *1066*, 166–180.

(82) Bushby, K.; Bourke, J.; Bullock, R.; Eagle, M.; Gibson, M.; Quinby, J. The multidisciplinary management of Duchenne muscular dystrophy. *Curr. Paediatr.* **2005**, *15*, 292–300.

(83) Eagle, M.; Bourke, J.; Bullock, R.; Gibson, M.; Mehta, J.; Giddings, D.; Straub, V.; Bushby, K. Managing Duchenne muscular dystrophy--the additive effect of spinal surgery and home nocturnal ventilation in improving survival. *Neuromuscul. Disord.* **2007**, *17*, 470–475.

(84) Jarvis, L. M. Help for Boys With Duchenne Muscular Dystrophy. *Chem. Eng. News* **2014**, *92*, 17–20.

(85) Quinlan, J. G.; Wong, B. L.; Niemeier, R. T.; McCullough, A. S.; Levin, L.; Emanuele, M. Poloxamer 188 failed to prevent exercise-induced membrane breakdown in mdx skeletal muscle fibers. *Neuromuscul. Disord.* **2006**, *16*, 855–864.

(86) Maskarinec, S. A.; Lee, K. Y. C. Comparative study of poloxamer insertion into lipid monolayers. *Langmuir* **2003**, *19*, 1809–1815.

(87) Wu, G.; Majewski, J.; Ege, C.; Kjaer, K.; Weygand, M.; Lee, K. Y. C. Lipid Corralling and Poloxamer Squeeze-Out in Membranes. *Phys. Rev. Lett.* **2004**, *93*, 028101.

(88) Wu, G.; Lee, K. Y. C. Interaction of poloxamers with liposomes: an isothermal titration calorimetry study. *J. Phys. Chem. B* **2009**, *113*, 15522–15531.

(89) Wang, J.-Y.; Marks, J.; Lee, K. Y. C. Nature of interactions between PEO-PPO-PEO triblock copolymers and lipid membranes: (I) effect of polymer hydrophobicity on its ability to protect liposomes from peroxidation. *Biomacromolecules* **2012**, *13*, 2616–2623.

(90) Firestone, M. A.; Wolf, A. C.; Seifert, S. Small-angle X-ray scattering study of the interaction of Poly(ethylene oxide)-b-Poly(propylene oxide)-b-Poly(ethylene oxide) triblock copolymers with lipid bilayers. *Biomacromolecules* **2003**, *4*, 1539–1549.

(91) Frey, S. L.; Zhang, D.; Carignano, M. A.; Szleifer, I.; Lee, K. Y. C. Effects of block copolymer's architecture on its association with lipid membranes: Experiments and simulations. *J. Chem. Phys.* **2007**, *127*, 114904.

(92) Wu, G.; Majewski, J.; Ege, C.; Kjaer, K.; Wegand, M. J.; Lee, K. Y. C. Interaction between lipid monolayers and Poloxamer 188: an X-Ray reflectivity and diffraction study. *Biophys. J.* **2005**, *89*, 3159–3173.

(93) Wu, G.; Lee, K. Y. C. Effects of Poloxamer 188 on phospholipid monolayer morphology: an atomic force microscopy study. *Langmuir* **2009**, *25*, 2133–2139.

(94) Olson, F.; Hunt, C. A.; Szoka, F. C.; Vail, W. J.; Papahadjopoulus, D. Preparation of liposomes of defined size distribution by extrustion through polycarbonate membranes. *Biochim. Biophys. Acta* **1979**, *557*, 9–23.

(95) Aldwinckle, T. J.; Ahkong, Q. F.; Bangham, A. D.; Fisher, D.; Lucy, J. A. Effects of poly(ethylene glycol) on liposomes and erythrocytes: Permeability changes and membrane fusion. *Biochim. Biophys. Acta - Biomembr.* **1982**, *689*, 548–560.

(96) Bergstrand, N.; Edwards, K. Effects of poly(ethylene oxide)-poly(propylene oxide)-poly(ethylene oxide) triblock copolymers on structure and stability of liposomal dioleoylphosphatidylethanolamine. *J. Colloid Interface Sci.* **2004**, *276*, 400–407.

(97) Cheng, C.-Y.; Wang, J.-Y.; Kausik, R.; Lee, K. Y. C.; Han, S. Nature of interactions between PEO-PPO-PEO triblock copolymers and lipid membranes: (II) role of hydration dynamics revealed by dynamic nuclear polarization. *Biomacromolecules* **2012**, *13*, 2624–2633.

(98) Satoh, H.; Delbridge, L. M.; Blatter, L. A.; Bers, D. M. Surface:volume relationship in cardiac myocytes studied with confocal microscopy and membrane capacitance measurements: species-dependence and developmental effects. *Biophys. J.* **1996**, *70*, 1494–1504.

(99) Cooper, G. Actin, Myosin, and Cell Movement. In *The Cell: A Molecular Approach*; Sinauer Associates, 2000.

(100) McNeil, P. L.; Terasaki, M. Coping with the inevitable: how cells repair a torn surface membrane. *Nat. Cell Biol.* **2001**, *3*, E124–E129.

(101) Lee, R. C.; Hannig, J.; Matthews, K. L.; Myerov, A.; Chen, C.-T. Pharmaceutical therapies for sealing of permeabilized cell membranes in electrical injuries. *Ann. New York Acad. Sci.* **1999**, *888*, 266–273.

(102) Agarwal, J.; Walsh, A.; Lee, R. C. Multimodal strategies for resuscitating injured cells. *Ann. New York Acad. Sci.* **2005**, *1066*, 295–309.

(103) Samuni, A. M.; Lipman, A.; Barenholz, Y. Damage to liposomal lipids: protection by antioxidants and cholesterol-mediated dehydration. *Chem. Phys. Lipids* **2000**, *105*, 121–134.

(104) Tirosh, O.; Kohen, R.; Katzhendler, J.; Gorodetsky, R.; Barenholz, Y. Novel synthetic phospholipid protects lipid bilayers against oxidation damage: role of hydration layer and bound water. *J. Chem. Soc. Perkin Trans. 2* **1997**, 383–390.

(105) Buettner, G. R. The Pecking Order of Free Radicals and Antioxidants: Lipid Peroxidation, a-Tocopherol, and Ascorbate. *Arch. Biochem. Biophys.* **1993**, *300*, 535–543.

(106) Vitrac, H.; Courregeiongue, M.; Couturier, M.; Collin, F.; Therond, P.; Remita, S.; Peretti, P.; Jore, D. Radiation-induced peroxidation of small unilamellar vesicles of phosphatidylcholine generated by sonication. *Can. J. Physiol. Pharmacol.* **2004**, *160*, 153–160.

(107) Reis, A.; Spickett, C. M. Chemistry of phospholipid oxidation. *Biochim. Biophys. Acta - Biomembr.* **2012**, *1818*, 2374–2387.

(108) Niki, E. Free Radical Initiators as Source of Water- or Lipid-Soluble Peroxyl Radicals. *Methods Enzymol.* **1990**, *186*, 100–108.

(109) Kalogeris, T.; Bao, Y.; Korthuis, R. J. Mitochondrial reactive oxygen species: A double edged sword in ischemia/reperfusion vs preconditioning. *Redox Biol.* **2014**, *2*, 702–714.

(110) Hannig, J.; Zhang, D.; Canaday, D. J.; Beckett, M. A.; Astumian, R. D.; Weichselbaum, R. R.; Lee, R. C.; Weichselbaum, R. R. Surfactant Sealing of Membranes Permeabilized by Ionizing Radiation. *Radiat. Res.* **2000**, *154*, 171–177.

(111) Greenebaum, B.; Blossfield, K.; Hannig, J.; Carrillo, C. S.; Beckett, M. A.; Weichselbaum, R. R.; Lee, R. C. Poloxamer 188 prevents acute necrosis of adult skeletal muscle cells following high-dose irradiation. *Burns* **2004**, *30*, 539–547.

(112) Spiteller, G. The Important Role of Lipid Peroxidation Processes in Aging and Age Dependent Diseases. *Mol. Biotechnol.* **2007**, *37*, 5–12.

(113) Fagali, N.; Catalá, A. Fe2+ and Fe3+ initiated peroxidation of sonicated and non-sonicated liposomes made of retinal lipids in different aqueous media. *Chem. Phys. Lipids* **2009**, *159*, 88–94.

(114) Culbertson, S. M.; Porter, N. a. Unsymmetrical azo initiators increase efficiency of radical generation in aqueous dispersions, liposomal membranes, and lipoproteins. *J. Am. Chem. Soc.* **2000**, *122*, 4032–4038.

(115) Heuvingh, J.; Bonneau, S. Asymmetric oxidation of giant vesicles triggers curvature-associated shape transition and permeabilization. *Biophys. J.* **2009**, *97*, 2904–2912.

(116) Lu, J.; Bates, F. S.; Lodge, T. P. Remarkable Effect of Molecular Architecture on Chain Exchange in Triblock Copolymer Micelles. *Macromolecules* **2015**, *48*, 2667–2676.

(117) Choi, S.-H.; Lodge, T. P.; Bates, F. S. Mechanism of Molecular Exchange in Diblock Copolymer Micelles: Hypersensitivity to Core Chain Length. *Phys. Rev. Lett.* **2010**, *104*, 047802.

(118) Choi, S.-H.; Bates, F. S.; Lodge, T. P. Molecular Exchange in Ordered Diblock Copolymer Micelles. *Macromolecules* **2011**, *44*, 3594–3604.

(119) Lu, J.; Choi, S.; Bates, F. S.; Lodge, T. P. Molecular Exchange in Diblock Copolymer Micelles: Bimodal Distribution in Core-Block Molecular Weights. *ACS Macro Lett.* **2012**, *1*, 982–985.

(120) Lu, J.; Bates, F. S.; Lodge, T. P. Chain Exchange in Binary Copolymer Micelles at Equilibrium: Confirmation of the Independent Chain Hypothesis. *Macro Lett.* **2013**.

(121) Kostarelos, K.; Luckham, P. F.; Tadros, T. F. Addition of Block Copolymers to Liposomes Prepared Using Soybean Lecithin. Effects on Formation, Stability and the Specific Localization of the Incorporated Surfactants Investigated. *J. Liposome Res.* **1995**, *5*, 443–452.

(122) Firestone, M. A.; Seifert, S. Interaction of nonionic PEO-PPO diblock copolymers with lipid bilayers. *Biomacromolecules* **2005**, *6*, 2678–2687.

(123) Leiske, D. L.; Meckes, B.; Miller, C. E.; Wu, C.; Walker, T. W.; Lin, B.; Meron, M.; Ketelson, H. A.; Toney, M. F.; Fuller, G. G. Insertion mechanism of a poly(ethylene oxide)-poly(butylene oxide) block copolymer into a DPPC monolayer. *Langmuir* **2011**, *27*, 11444–11450.

(124) Ding, J.; Price, C.; Booth, C.; Heatley, F.; Price, C.; Booth, C.; Attwood, D. Use of crown ether in the anionic polymerization of propylene oxide - 1. Rate of polymerization. *Eur. Polym. J.* **1991**, *27*, 891–894.

(125) Ding, J.; Heatley, F.; Price, C.; Booth, C. Use of crown ether in the anionic polymerization of propylene oxide - 2. Molecular weight and molecular weight distribution. *Eur. Polym. J.* **1991**, *27*, 895–899.

(126) Ding, J.; Attwood, D.; Price, C.; Booth, C. Use of crown ether in the anionic polymerization of propylene oxide - 3. Preparation and diblock-copoly(oxypropylene/oxyethylene). *Eur. Polym. J.* **1991**, *27*, 901–905.

(127) Heatley, F.; Yu, G.; Sun, W.-B.; Pywell, E. J.; Mobbs, R. H.; Booth, C. Triad sequence assignment of the 13C-NMR spectra of copolymers of ethylene oxide and 1,2-butylene oxide. *Eur. Polym. J.* **1990**, *26*, 583–592.

(128) Bedells, A. D.; Arafeh, R. M.; Yang, Z.; Attwood, D.; Heatley, F.; Padget, J. C.; Price, C.; Booth, C. Micellisation of diblock copoly(oxyethylene/oxybutylene) in aqueous solution. *J. Chem. Soc. Faraday Trans.* **1993**, *89*, 1235–1242.

(129) Ndoni, S.; Papadakis, C. M.; Bates, F. S.; Almdal, K. Laboratory-scale setup for anionic polymerization under inert atmosphere. *Rev. Sci. Instrum.* **1995**, *15*, 1090–1095.

(130) Repetto, M.; Semprine, J.; Boveris, A. Lipid Peroxidation: Chemical Mechanism, Biological Implications and Analytical Determination. In; Catala, A., Ed.; Intech, 2012.

(131) Hillmyer, M. A.; Bates, F. S. Synthesis and characterization of model polyalkane−poly(ethylene oxide) block copolymers. *Macromolecules* **1996**, *29*, 6994–7002.

(132) Allgaier, J.; Willbold, S.; Chang, T. Synthesis of Hydrophobic Poly(alkylene oxide)s and Amphiphilic Poly(alkylene oxide) Block Copolymers. *Macromolecules* **2007**, *40*, 518–525.

(133) Malik, M. I.; Trathnigg, B.; Oliver Kappe, C. Microwave-assisted polymerization of higher alkylene oxides. *Eur. Polym. J.* **2009**, *45*, 899–910.

(134) Stolarzewicz, A.; Neugebauer, D.; Grobelny, Z. Influence of the crown ether concentration and the addition of tert-butyl alcohol on anionic polymerization of (butoxymethyl)oxirane initiated by potassium tert-butoxide. *Macromol. Chem. Phys.* **1995**, *196*, 1295–1300.

(135) Caine, D. Potassium tert-Butoxide–18-Crown-6. In *Encyclopedia of Reagents for Organic Synthesis*; John Wiley & Sons, Ltd, 2001.

(136) Dow Chemical Company. Propylene oxide. *Propylene Oxide Storage and Handling Guidelines*, 2007.

(137) Sigma Aldrich. 1,2-Epoxybutane, 2015.

(138) Hadjichristidis, N.; Iatrou, H.; Pispas, S.; Pitsikalis, M. Anionic polymerization: High vacuum techniques. *J. Polym. Sci. Part A Polym. Chem.* **2000**, *38*, 3211–3234.

(139) Sigma Aldrich. Ethylene Oxide, 2014.

(140) Gottlieb, H. E.; Kotlyar, V.; Nudelman, A. NMR Chemical Shifts of Common Laboratory Solvents as Trace Impurities In the course of the routine use of NMR as an aid for organic chemistry , a day-to-day problem is the identifica- tion of signals deriving from common contaminants literature , but the. *J. Org. Chem.* **1997**, *62*, 7512–7515.

(141) Olson, F.; Hunt, C. A.; Szoka, F. C.; Vail, W. J.; Papahadjopoulos, D. Preparation of liposomes of defined size distribution by extrusion through polycarbonate membranes. *Biochim. Biophys. Acta - Biomembr.* **1979**, *557*, 9–23.

(142) MacDonald, R. C.; MacDonald, R. I.; Menco, B. P.; Takeshita, K.; Subbarao, N. K.; Hu, L. R. Small-volume extrusion apparatus for preparation of large, unilamellar vesicles. *Biochim. Biophys. Acta* **1991**, *1061*, 297–303.

(143) Hope, M. J.; Bally, M. B.; Webb, G.; Cullis, P. R. Production of large unilamellar vesicles by a rapid extrusion procedure. Characterization of size distribution, trapped volume and ability to maintain a membrane potential. *Biochim. Biophys. Acta - Biomembr.* **1985**, *812*, 55–65.

(144) Fiorentini, D.; Cipollone, M.; Galli, M. C.; Pugnaloni, A.; Biangini, G.; Landi, L. Characterization of Large Unilamellar Vesicles as Models for Studies of Lipid Peroxidation Initiated by Azocompounds. *Free Radic. Res.* **1994**, *21*, 329–339.

(145) Olsher, M.; Yoon, S.-I.; Chong, P. L.-G. Role of Sterol Superlattice in Free Radical-Induced Sterol Oxidation in Lipid Membranes†. *Biochemistry* **2005**, *44*, 2080–2087.

(146) Koppel, D. E. Analysis of Macromolecular Polydispersity in Intensity Correlation Spectroscopy: The Method of Cumulants. *J. Chem. Phys.* **1972**, *57*, 4814–4820.

(147) Frisken, B. J. Revisiting the method of cumulants for the analysis of dynamic light-scattering data. *Appl. Opt.* **2001**, *40*, 4087–4091.

(148) Lomakin, A.; Teplow, D. B.; Benedek, G. B. Quasielastic light scattering for protein assembly studies. *Methods Mol. Biol.* **2005**, *299*, 153–174.

(149) Schätzel, K. Single-photon correlation techniques. In *Dynamic Light Scattering: The Method and Some Applications*; Brown, W., Ed.; Oxford University Press: Oxford, 1993; pp 76–148.

(150) Hiemenz, P. C.; Lodge, T. *Polymer chemistry*; CRC Press, 2007.

(151) Brown, W.; Schillén, K.; Almgren, M.; Hvidt, S.; Bahadur, P. Micelle and gel formation in a poly(ethylene oxide)/poly(propylene oxide)/poly(ethylene oxide) triblock copolymer in water solution. Dynamic and static light scattering and oscillatory shear measurements. *J. Phys. Chem.* **1991**, *95*, 1850–1858.

(152) Kaganer, V. M.; Mohwald, H.; Dutta, P. Structure and phase transitions in Langmuir monolayers. *Rev. Mod. Phys.* **1999**, *71*, 779.

(153) Milic, I.; Fedorova, M.; Teuber, K.; Schiller, J.; Hoffmann, R. Characterization of oxidation products from 1-palmitoyl-2-linoleoyl-sn-glycerophosphatidylcholine in aqueous solutions and their reactions with cysteine, histidine and lysine residues. *Chem. Phys. Lipids* **2012**, *165*, 186–196.

(154) Abuja, P. M.; Albertini, R. Methods for monitoring oxidative stress, lipid peroxidation and oxidation resistance of lipoproteins. *Clin. Chim. Acta* **2001**, *306*, 1–17.

(155) Yamamoto, Y.; Niki, E.; Kamiya, Y.; Shimasaki, H. Oxidation of lipids: 7. Oxidation of phosphatidylcholines in homogeneous solution and in water dispersion. *Biochim. Biophys. Acta - Lipids Lipid Metab.* **1984**, *795*, 332–340.

(156) Niki, E.; Saito, M.; Yoshikawa, Y.; Yamamoto, Y.; Kamiya, Y. Oxidation of Lipids, XII. Inhibition of Oxidation of Soybean Phosphatidylcholine and Methyl Linoleate in Aqueous Dispersions by Uric Acid. *Bull. Chem. Soc. Jpn.* **1986**, *59*, 471–477.

(157) Friedlander, S. K. Light Scattering. In *Smoke, Dust, and Haze*; Oxford University Press, 2000.

(158) Berg, J. C. Colloidal systems: phenomenology and characterization. In *Interfaces and Colloids*; 2010; pp 345–454.

(159) Bryant, G.; Thomas, J. C. Improved Particle Size Distribution Measurements Using Multiangle Dynamic Light Scattering. *Langmuir* **1995**, *11*, 2480–2485.

(160) Hannig, J.; Zhang, D.; Canaday, D. J.; Beckett, M. A.; Astumian, R. D.; Weichselbaum, R. R.; Lee, R. C.; Weichselbaum, R. Surfactant Sealing of Membranes Permeabilized by Ionizing Radiation Surfactant Sealing of Membranes Permeabilized by Ionizing Radiation. *Radiat. Res.* **2000**, *154*, 171–177.

(161) Russ, C.; Heimburg, T.; von Grünberg, H. H. The Effect of Lipid Demixing on the Electrostatic Interaction of Planar Membranes across a Salt Solution. *Biophys. J.* **2003**, *84*, 3730–3742.

(162) Gohy, J.-F.; Varshney, S. K.; Jérôme, R. Water-Soluble Complexes Formed by Poly(2-vinylpyridinium)-block-poly(ethylene oxide) and Poly(sodium methacrylate)-block-poly(ethylene oxide) Copolymers. *Macromolecules* **2001**, *34*, 3361–3366.

(163) Lehtonen, J. Y.; Kinnunen, P. K. Poly(ethylene glycol)-induced and temperature-dependent phase separation in fluid binary phospholipid membranes. *Biophys. J.* **1995**, *68*, 525–535.

(164) McDaniel, J. R.; Bhattacharyya, J.; Vargo, K. B.; Hassouneh, W.; Hammer, D. A.; Chilkoti, A. Self-Assembly of Thermally Responsive Nanoparticles of a Genetically Encoded Peptide Polymer by Drug Conjugation. *Angew. Chemie Int. Ed.* **2013**, *52*, 1683–1687.

(165) Lopes, A.; Edwards, K.; Feitosa, E. Extruded vesicles of dioctadecyldimethylammonium bromide and chloride investigated by light scattering and cryogenic transmission electron microscopy. *J. Colloid Interface Sci.* **2008**, *322*, 582–588.

(166) Ng, R.; Metzger, J. M.; Reeve, L.; Markham, B. Compositions and methods for treating and preventing skeletal muscle deficiencies. US20150030559, January 29, 2015.

(167) Barclay, L. R. C.; Ingold, K. U. Autoxidation of Biological Molecules. 2. The Autoxidation. *J. Am. Chem. Soc.* **1981**, *103*, 6478–6485.

(168) Qian, S.; Heller, W. T. Peptide-Induced Asymmetric Distribution of Charged Lipids in a Vesicle Bilayer Revealed by Small-Angle Neutron Scattering. *J. Phys. Chem. B* **2011**, *115*, 9831–9837.

(169) Qian, S.; Rai, D.; Heller, W. T. Alamethicin Disrupts the Cholesterol Distribution in Dimyristoyl Phosphatidylcholine–Cholesterol Lipid Bilayers. *J. Phys. Chem. B* **2014**, *118*, 11200–11208.

(170) Baltgalvis, K. A.; Call, J. A.; Nikas, J. B.; Lowe, D. A. Effects of prednisolone on skeletal muscle contractility in mdx mice. *Muscle Nerve* **2009**, *40*, 443–454.

(171) Call, J. A.; Eckhoff, M. D.; Baltgalvis, K. A.; Warren, G. L.; Lowe, D. A. Adaptive strength gains in dystrophic muscle exposed to repeated bouts of eccentric contraction. *J. Appl. Physiol.* **2011**, *111*, 1768–1777.

(172) Lee, B.; Firestone, M. A. Electron density mapping of triblock copolymers associated with model biomembranes: insights into conformational states and effect on bilayer structure. *Biomacromolecules* **2008**, *9*, 1541–1550.

(173) Togo, T.; Krasieva, T. B.; Steinhardt, R. A. A decrease in membrane tension precedes successful cell-membrane repair. *Mol. Biol. Cell* **2000**, *11*, 4339–4346.

(174) Wang, J.; Segatori, L.; Biswal, S. L. Probing the association of triblock copolymers with supported lipid membranes using microcantilevers. *Soft Matter* **2014**, *10*, 6417–6424.

(175) Liu, G.; Fu, L.; Zhang, G. Role of hydrophobic interactions in the adsorption of poly(ethylene glycol) chains on phospholipid membranes investigated with a quartz crystal microbalance. *J. Phys. Chem. B* **2009**, *113*, 3365–3369.

(176) Soong, R.; Majonis, D.; Macdonald, P. M. Size of bicelle defects probed via diffusion nuclear magnetic resonance of PEG. *Biophys. J.* **2009**, *97*, 796–805.

(177) Soong, R.; Nieh, M.-P.; Nicholson, E.; Katsaras, J.; Macdonald, P. M. Bicellar Mixtures Containing Pluronic F68: Morphology and Lateral Diffusion from Combined SANS and PFG NMR Studies. *Langmuir* **2009**, *26*, 2630–2638.

(178) Soong, R.; Nieh, M.-P.; Nicholson, E.; Katsaras, J.; Macdonald, P. M. Bicellar mixtures containing Pluronic F68: Morphology and lateral diffusion from combined SANS and PFG NMR studies. *Langmuir* **2010**, *26*, 2630–2638.

(179) Nieh, M.-P.; Raghunathan, V. A.; Pabst, G.; Harroun, T.; Nagashima, K.; Morales, H.; Katsaras, J.; Macdonald, P. Temperature Driven Annealing of Perforations in Bicellar Model Membranes. *Langmuir* **2011**, *27*, 4838–4847.

(180) Nagao, M. Observation of local thickness fluctuations in surfactant membranes using neutron spin echo. *Phys. Rev. E* **2009**, *80*, 31606.

(181) Heijkamp, L. F. Van; Sevcenco, A.-M.; Abou, D.; Luik, R. Van; Krijger, G. C.; Hagedoorn, P.-L.; Schepper, I. M. De; Wolterbeek, B.; Koning, G. a; Bouwman, W. G. Spin-Echo Small Angle Neutron Scattering analysis of liposomes and bacteria. *J. Phys. Conf. Ser.* **2010**, *247*, 012016.

(182) Schmiedel, H.; Jörchel, P.; Kiselev, M.; Klose, G. Determination of Structural Parameters and Hydration of Unilamellar POPC/C12E4 Vesicles at High Water Excess from Neutron Scattering Curves Using a Novel Method of Evaluation. *J. Phys. Chem. B* **2000**, *105*, 111–117.

(183) Ng, R.; Metzger, J. M.; Claflin, D. R.; Faulkner, J. a. Poloxamer 188 reduces the contraction-induced force decline in lumbrical muscles from mdx mice. *Am. J. Physiol. Cell Physiol.* **2008**, *295*, C146–C150.

(184) Von Tscharner, V.; McConnell, H. M. An alternative view of phospholipid phase behavior at the air-water interface. Microscope and film balance studies. *Biophys. J.* **1981**, *36*, 409–419.

(185) Gröger, T.; Nathoo, S.; Ku, T.; Sikora, C.; Turner, R. J.; Prenner, E. J. Real-time imaging of lipid domains and distinct coexisting membrane protein clusters. *Chem. Phys. Lipids* **2012**, *165*, 216–224.

(186) Mohwald, H. Phospholipid and Phospholipid-Protein Monolayers at the Air/Water Interface. *Annu. Rev. Phys. Chem.* **1990**, *41*, 441–476.

(187) Smith, E. A.; Wang, W.; Dea, P. K. Effects of cholesterol on phospholipid membranes: Inhibition of the interdigitated gel phase of F-DPPC and F-DPPC/DPPC. *Chem. Phys. Lipids* **2012**, *165*, 151–159.

(188) Kim, K.; Kim, C.; Byun, Y. Preparation of a Dipalmitoylphosphatidylcholine/Cholesterol Langmuir−Blodgett Monolayer That Suppresses Protein Adsorption. *Langmuir* **2001**, *17*, 5066–5070.

(189) Savva, M.; Sivakumar, B.; Selvi, B. The Conventional Langmuir Trough Technique as a Convenient Means to Determine the Solubility of Sparingly Soluble Surface Active Molecules: Case Study Cholesterol. *Colloids Surf. A. Physicochem. Eng. Asp.* **2008**, *325*, 1–6.

(190) Brockman, H. Lipid monolayers: why use half a membrane to characterize protein-membrane interactions? *Curr. Opin. Struct. Biol.* **1999**, *9*, 438–443.

(191) Hifeda, Y. F.; Rayfield, G. W. Evidence for first-order phase transitions in lipid and fatty acid monolayers. *Langmuir* **1992**, *8*, 197–200.

(192) Duncan, S. L.; Larson, R. G. Comparing experimental and simulated pressure-area isotherms for DPPC. *Biophys. J.* **2008**, *94*, 2965–2986.

(193) Muñoz, M. G.; Monroy, F.; Ortega, F.; Rubio, R. G.; Langevin, D. Monolayers of Symmetric Triblock Copolymers at the Air−Water Interface. 2. Adsorption Kinetics. *Langmuir* **1999**, *16*, 1094–1101.

(194) Chang, L.-C.; Chang, Y.-Y.; Gau, C.-S. Interfacial properties of Pluronics and the interactions between Pluronics and cholesterol/DPPC mixed monolayers. *J. Colloid Interface Sci.* **2008**, *322*, 263–273.

(195) Muñoz, M. G.; Monroy, F.; Ortega, F.; Rubio, R. G.; Langevin, D.; Mun, M. G.; Monroy, F.; Ortega, F. Monolayers of Symmetric Triblock Copolymers at the Air−Water Interface. 1. Equilibrium Properties. *Langmuir* **2000**, *16*, 1083–1093.

(196) Myrvold, R.; Hansen, F. K.; Balinour, B. Monolayers of some ABA block-copolymers at the air□water interface. *Colloids Surfaces A Physicochem. Eng. Asp.* **1996**, *117*, 27–36.

(197) Barentin, C.; Muller, P.; Joanny, J. F. Polymer Brushes Formed by End-Capped Poly(ethylene oxide) (PEO) at the Air−Water Interface. *Macromolecules* **1998**, *31*, 2198–2211.

(198) Kuzmenka, D. J.; Granick, S. Collapse of poly(ethylene oxide) monolayers. *Macromolecules* **1988**, *21*, 779–782.

(199) Lyklema, J. Gibbs monolayers. *Liquid-Fluid Interface*, 2000, *Volume 3*, 1–101.

(200) Blomqvist, B. R.; Wärnheim, T.; Claesson, P. M. Surface rheology of PEO-PPO-PEO triblock copolymers at the air-water interface: comparison of spread and adsorbed layers. *Langmuir* **2005**, *21*, 6373–6384.

(201) Díez-Pascual, A. M.; Compostizo, A.; Crespo-Colín, A.; Rubio, R. G.; Miller, R. Adsorption of water-soluble polymers with surfactant character.: Adsorption kinetics and equilibrium properties. *J. Colloid Interface Sci.* **2007**, *307*, 398–404.

(202) Chang, L.-C.; Lin, C.-Y.; Kuo, M.-W.; Gau, C.-S. Interactions of Pluronics with phospholipid monolayers at the air-water interface. *J. Colloid Interface Sci.* **2005**, *285*, 640–652.

(203) Peters, R.; Beck, K. Translational diffusion in phospholipid monolayers measured by fluorescence microphotolysis. *Proc. Natl. Acad. Sci.* **1983**, *80*, 7183–7187.

(204) Lee, K. Y. C.; Lipp, M. M.; Takamoto, D. Y.; Ter-Ovanesyan, E.; Zasadzinski, J. A.; Waring, A. J. Apparatus for the Continuous Monitoring of Surface Morphology via Fluorescence Microscopy during Monolayer Transfer to Substrates. *Langmuir* **1998**, *14*, 2567–2572.

(205) Berring, E. E.; Borrenpohl, K.; Fliesler, S. J.; Serfis, A. B. A comparison of the behavior of cholesterol and selected derivatives in mixed sterol-phospholipid Langmuir monolayers: a fluorescence microscopy study. *Chem. Phys. Lipids* **2005**, *136*, 1–12.

(206) Lipp, M. M.; Lee, K. Y.; Waring, A.; Zasadzinski, J. A. Fluorescence, polarized fluorescence, and Brewster angle microscopy of palmitic acid and lung surfactant protein B monolayers. *Biophys. J.* **1997**, *72*, 2783–2804.

(207) Shieh, I. C.; Waring, A. J.; Zasadzinski, J. A. Visualizing the Analogy between Competitive Adsorption and Colloid Stability to Restore Lung Surfactant Function. *Biophys. J.* **2012**, *102*, 777–786.

(208) Stottrup, B. L.; Nguyen, A. H.; Tüzel, E. Taking another look with fluorescence microscopy: Image processing techniques in Langmuir monolayers for the twenty-first century. *Biochim. Biophys. Acta - Biomembr.* **2010**, *1798*, 1289–1300.

(209) Shieh, I. Three-Dimensional Visualization of Interfacial Phenomena Using Confocal Microscopy, University of California - Santa Barbara, 2012.

(210) Fernandez, J.; Rosemblatt, M.; Hidalgo, C. Highly purified sarcoplasmic reticulum vesicles are devoid of Ca2+-independent ("basal") ATPase activity. *Biochim. Biophys. Acta - Biomembr.* **1980**, *599*, 552–568.

(211) Birmachu, W.; Nisswandt, F. L.; Thomas, D. D. Conformational transitions in the calcium adenosine triphosphatase studied by time-resolved fluorescence resonance energy transfer. *Biochemistry* **1989**, *28*, 3940–3947.

(212) Dufrêne, Y. F.; Lee, G. U. Advances in the characterization of supported lipid films with the atomic force microscope. *Biochim. Biophys. Acta - Biomembr.* **2000**, *1509*, 14–41.

(213) Hu, Y.; Doudevski, I.; Wood, D.; Moscarello, M.; Husted, C.; Genain, C.; Zasadzinski, J. a; Israelachvili, J. Synergistic interactions of lipids and myelin basic protein. *Proc. Natl. Acad. Sci. U. S. A.* **2004**, *101*, 13466–13471.

(214) Cruz, A.; Pérez-Gil, J. Langmuir Films to Determine Lateral Surface Pressure on Lipid Segregation Methods in Membrane Lipids. In; Dopico, A. M., Ed.; Humana Press, 2007; Vol. 400, pp 439–457.

(215) El Kirat, K.; Burton, I.; Dupres, V.; Dufrene, Y. F. Sample preparation procedures for biological atomic force microscopy. *J. Microsc.* **2005**, *218*, 199–207.

(216) Haugstad, G. Probing Material Properties I: Phase Imaging. In *Atomic Force Microscopy*; John Wiley & Sons, Inc., 2012; pp 187–257.

(217) Friedrich, H.; Frederik, P. M.; de With, G.; Sommerdijk, N. A. J. M. Imaging of Self-Assembled Structures: Interpretation of TEM and Cryo-TEM Images. *Angew. Chemie Int. Ed.* **2010**, *49*, 7850–7858.

(218) Ahmed, F.; Alexandridis, P.; Neelamegham, S. Synthesis and Application of Fluorescein-Labeled Pluronic Block Copolymers to the Study of Polymer−Surface Interactions. *Langmuir* **2000**, *17*, 537–546.

(219) Sahay, G.; Batrakova, E. V; Kabanov, A. V. Different internalization pathways of polymeric micelles and unimers and their effects on vesicular transport. *Bioconjug. Chem.* **2008**, *19*, 2023–2029.

(220) Tan, J. S.; Butterfield, D. E.; Voycheck, C. L.; Caldwell, K. D.; Li, J. T. Surface modification of nanoparticles by PEO/PPO block copolymers to minimize interactions with blood components and prolong blood circulation in rats. *Biomaterials* **1993**, *14*, 823–833.

(221) Amiji, M. M.; Park, K. Analysis on the surface adsorption of PEO/PPO/PEO triblock copolymers by radiolabelling and fluorescence techniques. *J. Appl. Polym. Sci.* **1994**, *52*, 539–544.

(222) Neal, J. C.; Stolnik, S.; Schacht, E.; Kenawy, E. R.; Garnett, M. C.; Davis, S. S.; Illum, L. In vitro displacement by rat serum of adsorbed radiolabeled poloxamer and poloxamine copolymers from model and biodegradable nanospheres. *J. Pharm. Sci.* **1998**, *87*, 1242–1248.

(223) Neff, J. A.; Caldwell, K. D.; Tresco, P. A. A novel method for surface modification to promote cell attachment to hydrophobic substrates. *J. Biomed. Mater. Res.* **1998**, *40*, 511–519.

(224) Grindel, J. M.; Jaworski, T.; Piraner, O.; Emanuele, R. M.; Balasubramanian, M. Distribution, metabolism, and excretion of a novel surface-active agent, purified poloxamer 188, in rats, dogs, and humans. *J. Pharm. Sci.* **2002**, *90*, 1936–1947.

(225) Willcox, M. L.; Newman, M. M.; Paton, B. C. A study of labeled pluronic F-68 after intravenous injection into the dog. *J. Surg. Res.* **1978**, *25*, 349–356.

(226) Li, Z. L.; Xiong, X. Y.; Li, Y. P.; Gong, Y. C.; Gui, X. X.; Ou-Yang, X.; Lin, H. S.; Zhu, L. J.; Xie, J. L. Synthesis and self-assembling behaviors of biotinylated pluronic/poly(lactic acid) biocompatible block copolymers in aqueous solutions. *J. Appl. Polym. Sci.* **2010**, *115*, 1573–1580.

(227) Salem, A. K.; Cannizzaro, S. M.; Davies, M. C.; Tendler, S. J.; Roberts, C. J.; Williams, P. M.; Shakesheff, K. M. Synthesis and characterisation of a degradable poly(lactic acid)-poly(ethylene glycol) copolymer with biotinylated end groups. *Biomacromolecules* **2001**, *2*, 575–580.

(228) Baskin, J. M.; Prescher, J. A.; Laughlin, S. T.; Agard, N. J.; Chang, P. V; Miller, I. A.; Lo, A.; Codelli, J. A.; Bertozzi, C. R. Copper-free click chemistry for dynamic in vivo imaging. *Proc. Natl. Acad. Sci.* **2007**, *104*, 16793–16797.

(229) Chang, P. V; Prescher, J. A.; Sletten, E. M.; Baskin, J. M.; Miller, I. A.; Agard, N. J.; Lo, A.; Bertozzi, C. R. Copper-free click chemistry in living animals. *Proc. Natl. Acad. Sci.* **2010**, *107*, 1821–1826.

(230) Davis, F. F.; Van Es, T.; Palczuk, N. C. Non-immunogenic polypeptides. 4,179,337, 1979.

(231) Roeder, R. D.; Rungta, P.; Tsyalkovskyy, V.; Bandera, Y.; Foulger, S. H. Colloidal templating: seeded emulsion polymerization of a soluble shell with a controlled alkyne surface density. *Soft Matter* **2012**, *8*, 5493–5500.

(232) Mahou, R.; Wandrey, C. Versatile Route to Synthesize Heterobifunctional Poly(ethylene glycol) of Variable Functionality for Subsequent Pegylation. *Polymers (Basel).* **2012**, *4*, 561–589.

(233) Dujols, V.; Ford, F.; Czarnik, A. W. A Long-Wavelength Fluorescent Chemodosimeter Selective for Cu(II) Ion in Water. *J. Am. Chem. Soc.* **1997**, *119*, 7386–7387.

(234) Skloot, R. *The Immortal Life of Henrietta Lacks*, 1st ed.; Crown Publishers: New York, 2009.

(235) Walters, T. J.; Mase, V. J. J.; Roe, J. L.; Dubick, M. A.; Christy, R. J. Poloxamer-188 reduces muscular edema after tourniquet-induced ischemia-reperfusion injury in rats. *J. Trauma* **2011**, *70*, 1192–1197.

(236) Coles, J. A.; Sigg, D. C.; Iaizzo, P. A. Reversible and Irreversible Damage of the Myocardium: New Ischemic Syndromes, Ischemia/Reperfusion Injury, and Cardio Protection. In *Handbook of Cardiac Anatomy, Physiology, and Devices*; Iaizzo, P. A., Ed.; 2009; pp 219–229.

(237) Thurston, G. B. Viscoelasticity of Human Blood. *Biophys. J.* **1972**, *12*, 1205–1217.

(238) Antonova, N. Methods in blood rheology – from theoretical and experimental approach to clinical applications. *Ser. Biomech.* **2012**, *27*, 44–50.

(239) Armstrong, J. K.; Wenby, R. B.; Meiselman, H. J.; Fisher, T. C. The Hydrodynamic Radii of Macromolecules and Their Effect on Red Blood Cell Aggregation. *Biophys. J.* **2004**, *87*, 4259–4270.

(240) Baskaran, H.; Toner, M.; Yarmush, M. L.; Berthiaume, F. Poloxamer-188 Improves Capillary Blood Flow and Tissue Viability in a Cutaneous Burn Wound. *J. Surg. Res.* **2001**, *101*, 56–61.

(241) Armstrong, J. K.; Meiselman, H. J.; Wenby, R. B.; Fisher, T. C. Modulation of red blood cell aggregation and blood viscosity by the covalent attachment of Pluronic copolymers. *Biorheology* **2001**, *38*, 239–247.

(242) Hitosugi, M.; Niwa, M.; Takatsu, A. Changes in blood viscosity by heparin and argatroban. *Thromb. Res.* **2001**, *104*, 371–374.

# Appendix A: Liposome peroxidation protocol

Prepared by: Karen Haman
Last revised: 8/8/2015
Protocol based on Wang, et al.[89] and Olson, et al.[141]

**Supplies**

*Phospholipids* (www.avantilipids.com):

| Name | Full name | Avanti product number | Mass (mg) | C in $CHCl_3$ (mg/ml) | Price 6/1/2015 |
|---|---|---|---|---|---|
| POPC | 1-palmitoyl-2-oleoyl-*sn*-glycero-3-phosphocholine | 850457C | 25 | 10 | 43 |
| PLPC | 1-palmitoyl-2-linoleoyl-*sn*-glycero-3-phosphocholine | 850458C | 25 | 10 | 150 |
| POPG | 1-palmitoyl-2-oleoyl-*sn*-glycero-3-phospho-(1'-*rac*-glycerol) (sodium salt) | 840457C | 25 | 10 | 45 |

*Consumable goods*

(3) 4 mL National Scientific amber vials, (on UMarket, Fisher Scientific product number: 0339111B), pack of 100
(3) National Scientific PTFE lined caps, (on UMarket, Fisher Scientific product number: 0339112B), pack of 100
PTFE tape (stockroom)
20 mL scintillation vials and caps (stockroom) *or reusable DLS tubes from glass shop*
4 mL (1 dram) glas vials and caps (stockroom)
1000 µL pipet tips (stockroom)
200 µL pipet tips (stockroom)
10 mL pipets (stockroom)
Kimwipes (stockroom)
1.5 mL centrifuge tubes (stockroom)
1 mL monotuberculin syringes (stockroom)
0.2 µm GHP syringe filters (stockroom)
250 mL bottle filter, 0.22 µm pore size (stockroom)
(1) 5 ml "V" vial (UMarket, Sigma Z115118-12EA)
20 mL (24 mL) plastic syringe (stockroom, lab supply)

*Chemicals and reagents*

HPLC-grade Chloroform (On umarket, Chromasolv plus, Sigma product number 650471-1L)

AAPH, 2,2'-Azobis(2-methylpropionamidine) dihydrochloride, (on UMarket, Sigma product number 440914-25G)
1 L Millipore water (Zasadzinski or Kokkoli labs)
Acetone (stockroom)

**DAY BEFORE:**

*Lipid transfer to vials*

1. Remove lipid ampoules from freezer to thaw. Ampoules must not be opened until at room temperature.
2. Clean 3 amber vials and caps with HPLC-grade chloroform, three times each.
3. Transfer lipid sample to clean vial by breaking seal and carefully pouring into vial. Cap quickly, seal outside with PTFE tape, and label. Keep sticker on ampoule for later reference.
4. Lipids are "good" for at least 2 weeks, but they must be kept in the freezer, and minimize exposure to air.

*Liposome Preparation*

1. Create a clean surface in a fume hood using foil or a large kimwipe.
2. If haven't already done so, remove lipid vials from freezer and allow to come to room temperature before proceeding.
3. Clean "V" vial and cap with HPLC grade chloroform three times (reusable vial). Allow to dry.
4. Clean 500 µL syringe with HPLC grade chloroform, minimum 10 times. Pour chloroform down needle first to avoid contamination of clean chloroform.
5. Quickly open POPC vial, measure 456 µL of solution, cap vial, and carefully push lipid solution into V vial. Close V vial, and seal POPC vial with Teflon tape. (Wrap in direction of tightening cap to avoid leaks).
6. Clean 500 µL syringe immediately, pouring chloroform down needle first to avoid contaminating clean chloroform.
7. Repeat steps 3-5 for PLPC and POPG, respectively to achieve a 6:3:1 molar ratio of lipids in solution in the V vial. Lipid recipe follows:

| **Sample Name** | | **6:3:1 Liposomes** | | | |
|---|---|---|---|---|---|
| **Total moles of Lipid (µmol)** | | **10** | | | |
| **Compound** | **MW (g)** | **Mole %** | **c (mg/ml)** | **Weight (mg)** | **Volume (µl)** |
| POPC | 760.08 | 60 | 10.00 | 4.56 | **456** |
| PLPC | 758.06 | 30 | 10.00 | 2.27 | **227** |
| POPG | 770.99 | 10 | 10.00 | 0.77 | **77** |

8. Next, prepare a thin film on the conical surface of the V vial containing the lipid mixture. Attach a clean tip (1 mL syringe exterior works well, just cut off the large end and insert into the tygon) to an air or Ar line and open valve so that a faint stream of air or Ar comes out.
9. Remove cap from lipid mixture vial and rotate slowly while drying with air stream. Continue rotating until all chloroform is removed, 5-10 minutes.
10. Complete drying by putting in dessicator hooked up to a small vacuum pump for about 30 minutes.
11. While lipids continue drying, prepare a small dish of water 40-45 °C on a hot plate. The hot plates without a temperature probe heat up VERY quickly, so monitor temperature with a thermometer and make adjustments accordingly. You don't want to overheat. Also put the extruder heating block on the hotplate, but not the extruder.
12. Hydrate lipid film with 1 mL (use a P1000 micropipettor set to 1000 µL) Millipore water. Cap vial and vortex to mix. Put in water bath to heat, and vortex periodically.
13. Assemble the mini-extruder and test the seals by extruding 1 mL of Millipore water in both directions. This also pre-wets the syringes, which should make extrusion a little easier (it will be hard as long as the extruder is still new). If the extruder leaks (e.g. puddle in the heating block, reduced volume in syringes), tighten the bolts on the extruder, tighten screws on syringes, dry the heating block, and try with a fresh 1 mL of water.
14. When lipids are warm and vortexed, and extruder is ready to go, use the "in" syringe to pull up the 1 mL of lipid/water suspension. Put into extruder and extrude **19** times. (Actual number is not as important as the fact that it's an **odd** number, ensuring that large particulates will not end up in final sample).
15. After extruding, *carefully* remove "out" syringe and slowly push liposomes into 1.5 mL centrifuge tube. Label (10 mM Liposomes, date, initials) and store in refrigerator. The Bates group refrigerators are not trustworthy (i.e. liposomes cannot be frozen and thawed), so another refrigerator, such as in Room 12, is recommended.
16. Put lipids (sealed with PTFE tape) back in freezer.
17. Clean extruder parts with Millipore water, allow to dry completely, put away. Clean V vial with chloroform, let it dry, and cap to store. Put away all components clean and dry to make them ready for the next user.

*Peroxidation prep (at least the day before):*

1. Clean 20 mL scintillation vials (if using reusable DLS tubes from the glass shop, clean in the same manner, but know that sample volumes and concentrations may need to be adjusted later on). A clean vial is needed for each sample; to save time, it is recommended that an entire flat (100 vials) is cleaned at once. Also, due to

manufacturing inconsistencies, note that more vials than are required by experiments will likely be needed. To clean, draw fresh acetone from a clean beaker into a 20 mL syringe, attach a 1" diameter GHP 0.2 μm syringe filter, and push about 3-4 mL into each vial. Repeat until a rack of 21 vials is full. Then cap vials, one at a time, shaking well, and discarding spent acetone into waste beaker (or bottle). When empty, turn vials upside down to dry (to prevent dust from getting in). The process may be repeated, but once is usually enough. After about 10 minutes, vials are dry enough to cap with fresh caps.

2. Collect 2-3 500 mL glass media bottles of Millipore water (room 12 or 216) and filter using the same 250 mL 0.22 μm bottle filter.
3. Prepare 2.5 mM polymer solutions in 8 mL glass vials using disposable syringes to measure water. For sufficient replicates, aim for about 2 mL of polymer solution. More than 2 mL is fine, but you should only save extra polymer solution if you will use it in the next day or so, or if caps have a water-tight seal (i.e. not stockroom vials with cardboard-lined caps). Use Millipore water. For example, a 2.5 mM solution of P188 requires about 40 mg of polymer for a 2 mL sample. Concentrations are dilute enough that final volume is very close to volume of water added. For larger copolymers, consider preparing solutions in the usual way, with a graduated cylinder and an appropriate volume to accurately measure.

**DAY OF**

*Preparatory steps*

1. Pull AAPH out of freezer, allow to fully thaw. Do this at least half an hour before planning to open it to avoid condensing moisture onto pellets. Replace AAPH every couple of months, or if reactivity with lipids is diminished (e.g. no loss of DLS scattering following liposome peroxidation). It decomposes in water and air, so store it in the freezer, sealed with parafilm to slow that.
2. When AAPH has warmed to RT, weigh 2 quantities of about 0.5 g each into clean 20 mL scintillation vials. Cap quickly. AAPH has a molecular weight of 271.2 g/mol, and a stock solution of 0.3 M will be mixed at a later time. The 2$^{nd}$ quantity is for back-up; mixing errors or noticeable inactivity during a long session can cause substantial delays and problems later on. You may wish to store it AAPH at the Lodge lab to avoid this step. Remember to wrap cap with parafilm and return to freezer when finished.
3. Gather all supplies, including water, liposomes, a flash drive, and notebook.

*At the Lodge Lab*

1. Prepare DLS as trained.
2. Turn on hot plate with sand bath. Set to 30 degrees (they overshoot a lot if you set it right to 40 deg, so start small and work up from there).

3. Using a 1.5 mL centrifuge tube, make a diluted liposome sample (20x dilution: 950 µL filtered Millipore water and 50 µL 10 mM liposome solution), final liposome concentration, 0.5 mM.
4. Prepare some vials with 8 mL of filtered Millipore water per vial, using 10 mL pipets and green 10 mL hand-pump. If desired, water can be measured and filtered once more with a 10 mL syringe and syringe filter.
5. Prepare 3 liposome controls. These are the basis of your normalization, so accurate concentration is important. To each of 3 prepared DLS vials, add 1.9 mL of filtered Millipore water (2x950 µL). Then add 100 µL of the 0.5 mM liposome sample to each. The final concentration of liposomes in DLS vials is 5 µM
6. Clean outsides of DLS vials with 2 fresh kimwipes and a healthy amount of acetone, turning vial in direction of tightening cap (or it will likely open).
7. Run each sample in DLS for 10 minutes, laser power 20 mW, 90 ° angle, temperature 25 °C, 1 to $10^6$ µs delay times. At these concentrations, count rates will be in the 20-24 kcps range, and apparent diameters should be in the 120-140 nm range. If you have drastic inconsistencies between samples, double check methodology. Measurements should give clean autocorrelation functions with low pdi (less than 0.2, ideally).
8. To save data, use the file menu to export data. Using the "Save autocorrelation function data as" command gives you access to save both the autocorrelation function and count rate history. You will need to save these at the conclusion of the experiment, autocorrelation function with *.dat extension, and count rate history with *.crh extension. Keep file names the same for the same sample; different extensions will prevent the files from overwriting each other.

**AAPH reactions**

*Negative control: liposome/AAPH without polymer (run at least 3 negative controls to check reactivity of AAPH and lipids)*

1. Total reaction volume is 2 mL. Prepare in 4 mL vial, since air will be needed for peroxidation, but cannot remain open since heating and UV illumination will need to happen with vials turned on their sides. Open cuvettes could be used if a better heat/light system were devised.
2. For Lipo/AAPH reaction, you'll need:
    a. 1800 µL filtered Millipore water (2x900 µL)
    b. 100 µL 0.5 mM liposome (final concentration in reaction 25 µM)
    c. 100 µL 0.3 M AAPH (final concentration in reaction 15 mM)
3. Cap vial and swirl contents to mix, label, and put into 40 °C (technically 37 °C) sand bath under 254 nm UV light. Cover bath with foil to maintain temperature and block other light. Set timer for 30 minutes. Consistency in heating and time is critical.

4. When timer is done, swiftly transfer vial contents to waiting 20 mL vial (which should already contain 8 mL of filtered water) using a *fresh* disposable 1 mL syringe. Do not pour, or sample will be lost to the walls of the vial, altering final concentration, intensity, etc.
5. Clean outside of vial with acetone/kimwipes as before and promptly put in DLS. If timing is performed carefully, continuous samples may be run. This timing takes practice and planning, however. For negative controls, expect to see count rates from about 1-4 kcps. Much higher than that, and there is something wrong – either temperature in bath is off, time was off, or reagents/lipids are inactive (worst case). Run negative controls until any issue is worked out and three consistent results with satisfactory (low) scattering are obtained consecutively.
6. Save data as stated above.

*With Polymer*

1. Total reaction volume is 2 mL. Prepare in 4 mL vial, since air is needed for peroxidation.
2. For Polymer/Lipo/AAPH reaction, the following volumes are required for 5:1 polymer:lipid molar ratios (use fresh tips for each component):
    a. 1700 µL filtered Millipore water (2x850µL)
    b. 100 µL 0.5 mM liposome (final concentration in reaction 25 µM)
    c. 100 µL 2.5 mM polymer (final concentration in reaction is 125 µM)
    d. 100 µL 0.3 M AAPH (final concentration in reaction 15 mM)
3. For liposome/polymer incubation samples, e.g. incubating liposomes and polymers together for 4 hours before reaction, it's helpful to prepare one large incubation volume and then pull out an appropriate volume for each reaction later. For example, to make 3 replicates of a 4 hour incubation sample, make one stock mixture at a slightly higher volume (since it's very difficult to get the last drops out of the vial):
    a. (*For the example of 3 replicates*) Multiply all the reaction volumes (above) by 4, except for AAPH, and put those volumes together in a 20 mL vial:
        i. 1700x4 = 6800 µL = 6.8 mL water (use the pipette/hand pump)
        ii. 100x4 = 400 µL 0.5 mM liposome
        iii. 100x4 = 400 µL 2.5 mM polymer
    b. After incubation time, transfer the following to a 4 mL reaction vial:
        i. 1900 µL stock liposome/polymer incubation mixture
        ii. 100 µL 0.3 mM AAPH
4. React as before, transfer to DLS vials, and immediately measure in DLS. Save data, as previously described.

**Liposome/polymer incubation only, no reaction**

1. Incubate polymer and liposome together and measure in DLS to verify that polymers are not detrimental to liposome integrity. Follow the same temperature conditions as would be used for liposomes incubated for reaction. Incubation is easiest at room temperature, but it could also be useful to try incubating at reaction temperature.
2. Incubation samples are as follows (stock solutions can be prepared as described previously, just keep track of whether the 100 µL AAPH volume is accounted for or not to maintain final concentration).
    a. 1800 µL water
    b. 100 µL 0.5 mM liposomes
    c. 100 µL 2.5 mM polymer
3. Prior to DLS, transfer incubation sample, either from vial (2 mL) or from stock solution (volume depends on stock prepared; 1.9 or 2.0 mL). If drawing from a stock solution also used for peroxidation samples, 1.9 mL of the stock (2x950 µL) plus 100 µL water should be added to the DLS vial with 8 mL of water. Otherwise, 2 mL (2x1000µL) should be used.
4. Clean vial, run DLS, and save data.